Analysis of Two Phase Transient Pressure from Permanent Down-Hole Gauges (PDG)

Wenbin Xu

Submitted for the
Degree of Doctor of Philosophy
Institute of Petroleum Engineering
Heriot-Watt University
June 2010

Abstract

Currently many of the world's mature fields have entered the middle-high water-cut period. At this stage, reservoir numerical simulation (RNS) becomes a powerful tool for reservoir management which allows the reservoir engineer to plan and evaluate future development options for the reservoir to carry out the ultimate goal of minimizing costs and maximizing economic returns. So the precision of RNS is crucial to the success of any development plan. A precise reservoir model, including a geological model and a fluid model, is the foundation of RNS. Hence, how to use all available history data (such as permanent down-hole gauges (PDG) data, production data, etc.) to calibrate a reservoir model is a huge challenge for reservoir management.

In this thesis, the multiphase flow well testing problems encountered in reservoir management are studied. Based on analytical solutions, traditional multiphase flow well testing approaches are modified to make them suitable for special reservoirs.

For non-uniform saturation reservoirs, some improved understandings of transient well testing have been synthetically developed. Before water breaks through, the transient pressure response in the transition zone of two phase flow systems is theoretically studied, and the results show that the pressure response in the transition zone is a function of the total effective mobility of the fluid. After water breaks through, the derivative of the bottom-hole pressure is a function of the integral of total mobility, which can be approximately replaced by the average total effective mobility. The trend of the BHP curve is controlled by the total mobility.

For layered commingled reservoirs, the type curves of transient pressure data are obtained. According to these type curves, some improved understandings are developed. At the same time, the practicality of selective inflow performance methods (SIP) on field scale reservoir models is also discussed.

Because of the limitation of analytical solutions, not all existing multiphase flow well testing approaches are fit for evaluating mature field cases. So based on numerical solutions, a new multiphase flow well testing procedure is developed.

The overall conclusion to the work is that transient well test data or PDG data with multiphase flow effects should be used to improve the degree of accuracy of reservoir model and fulfill the ultimate goal of well testing of dynamic reservoir monitoring and management.

To my great parents,

who gave me their endless love and examples of absolute integrity.

To my family and my lovely daughter.

Acknowledgements

I would like to express my sincere thanks to my supervisor Dr. Shiyi Zheng who has provided me with the opportunity to work on this PhD at the Institute of Petroleum Engineering of Heriot-Watt University. His guidance, help, and encouragement throughout my research time are wealth of my lifetime.

I would also like to thank Conoco-Philips, BG group and Wintershall Holding AG for their financial support. Schlumberger and Edinburgh Petroleum Services (EPS) Ltd. are gratefully thanked for providing with the simulation and well testing analysis software.

I am thankful to the academics, research staff, secretaries, librarian and those who helped during the course of this study in the Institute of Petroleum Engineering at Heriot-Watt University. Many thanks to the PRIME project group, and to my colleagues Fei Wang, Xiaogang Li, Ludovic Ricard, Fuyong Wang and Lili Xue.

Finally, special thanks would like to be given to my friend Dr. Zeyun Jiang, Dr. Kejian Wu, Dr. Jingsheng Ma, Dr. Min Jin, Dr. Jinhai Yang, Dr. Weisheng He, Dr. Qing Yang, and Dr. Eric Mackay during the course of this study. Their advice, suggestions, and help are gratefully appreciated.

Table of Contents

Table of Figures

List of Tables

Nomenclature

$A(r)$: Cross-section area, m^2, ft^2

B_o : Oil formation volume factor, reservoir volume/ standard volume

B_w : Oil formation volume factor, reservoir volume/ standard volume

B_g : Oil formation volume factor, reservoir volume/ standard volume

c_o : Oil compressibility, Bar^{-1}, psi^{-1}

c_w : Oil compressibility, Bar^{-1}, psi^{-1}

c_f : Rock compressibility, Bar^{-1}, psi^{-1}

c_t : Total compressibility, Bar^{-1}, psi^{-1}

f_w : Water fractional flow, fraction

h : Formation thickness, m, ft

h_o : Oil formation thickness, m, ft

h_w : Water formation thickness, m, ft

H : Distance of movement for saturation front with time, m, ft

K : Absolute reservoir permeability, mD

K_o : Oil phase effective permeability, mD

K_w : Water phase effective permeability, mD

K_g : Gas phase effective permeability, mD

K_{ro} : Oil relative permeability

K_{rw} : Water relative permeability

K_{rg} : Gas relative permeability

m : Slope of semi-log straight line

$m(p)$: Pseudo pressure, Bar, psi

P_c : Capillary pressure, Bar, psi

P_o : Oil phase pressure, Bar, psi

P_w : Water phase pressure, Bar, psi

P_i : Initial pressure, Bar, psi

P_e : Outer pressure, Bar, psi

P_{wf} : Flowing bottom-hole pressure, Bar, psi

∇p : Pressure gradient

q_t : Total rate for all systems, stb/day, m^3/day

q_o : Oil rate for all systems, stb/day, m^3/day

q_w : Water rate for all systems, stb/day, m^3/day

R_{inv} : Investigation radius, m, ft

r : Radius, m, ft

r_w : Wellbore radius, m, ft

r_e : Radial extent of reservoir, m, ft

S : Skin factoe

S_w : Water saturation, fraction

S_o : Oil saturation, fraction

S_{wi} : Connate water saturation, fraction

t : Time, hour

t_{sss} : Pseudo stead state time, hour

GOR : Producing gas-oil ratio, Mscf/stb

WOR : Water-oil ratio, bbl/stb

R_s : Solution gas-gas ratio, Mscf/stb

R_{sw} : Gas-water ratio, Mscf/stb

Z : Normalized total mobility

C_1 C_2 C_3 C_4 : Constant values

Greek

μ_0 : Oil phase viscosity, cp

μ_w : Water phase viscosity, cp

μ_g : Gas phase viscosity, cp

∇ : Vector operator

α : The angle of bedding, $^\circ$

α : Empirical slope, constant

r_{f^-} : Radius to downstream saturation front, ft

r_{f^+} : Radius to upstream saturation front, ft

λ_o : Oil phase effective mobility

λ_w : Water phase effective mobility

λ_t : Total effective mobility

$\overline{\lambda_t}$: Average total effective mobility

ϕ : Porosity

π : Constant

Subscripts

c: capillary

g: gas phase

o: oil phase

w: water phase

t: total

w: wellbore

l : phase

Name

BHP: Bottom-hole Pressure

BU: Buildup test

DD: Drawdown test

IPR: Inflow Performance Relationship

LGR: Local Grid Refinement

MLT: Multilayer Transient Test

MRMZ: Multi-Rate Multi-Zone test

NWT: Numerical well testing

OWC: Oil water contact

PDG: Permanent down-hole pressure gauges

P-M: Perrine- Martin approach

P.I: Productivity Index

PL: Production logging

RNS: Reservoir numerical simulation

STOIIP: The Stock Tank Oil Initially in Place

SIP: Selective inflow performance method

VOI: Volume of Interest Model

PUBLICATIONS

Zheng, S.Y., **Xu, Wenbin**., " New Approaches for Analyzing Transient Pressure from Oil and Water Two-phase Flowing Reservoir ", SPE127615, presented at the 2009 Kuwait International Petroleum Conference and Exhibition held in Kuwait City, Kuwait, 14–16 December 2009.

Zheng, S.Y., **Xu, Wenbin**., " New Understanding of Transient Pressure Response in the Transition Zone of Oil-water and Gas-water Systems ", in press for publication in Transport In Porous Media , 2010.

Chapter 1
Introduction

1.1 Background

Petroleum is not only a precious commodity but also an important strategic supply. As a result, in the modern world economics, politics and the military all have a multi-faceted and close relationship with petroleum.

Recoverable reserves in the world have continued to decrease in the last few years, whilst at the same time oil prices have increased continuously. As a reservoir engineer, an important objective is to make a viable field development plan, so as to improve recovery factors and fulfill the ultimate goal of minimizing costs and maximizing economic returns.

Currently many of the world's mature fields have entered the middle-high water-cut period. At this stage, reservoir numerical simulation (RNS) becomes a tool for reservoir management which allows the reservoir engineer to plan and evaluate future development options for the reservoir. So the precision of RNS is crucial to the success of any development plan. A precise reservoir model, including a geological model and a fluid model, is the foundation of RNS.

There is much field-production history-data in this stage, such as pressures (some fields have permanent down-hole gauge data), cumulative oil, water-cuts and GORs (both for field-wide and for individual wells), in addition to having some understandings of which wells are in communication, and possibly some production logs. This data can be used to history-match and continually update reservoir models. Commonly, the initial reservoir simulation model for a field may have been found to be "incorrect", in that it

fails in some aspects of its predictions of reservoir performance. For example, it may fail to predict water breakthroughs during floods, or forecast the productivity of new infill wells. Furthermore, if the original model has been proved to be wrong, it cannot be used to do reservoir simulation in the first place. So during history matching, it is very important to integrate all the available pressure data, PVT data, petrophysical data, and geological data, etc. By using these data, the reservoir model can be adjusted again and again to improve the precision of the numerical model. (Heriot-watt University, "Reservoir Simulation", [1])

Particularly at this stage, with permanent down-hole pressure gauges (PDG) increasingly being installed in mature fields around the world, these gauges have high reliability and can be operated for several years. They provide a record of everything that is happening to the well. So a large amount of the dynamic monitor data measured can be used to analyze and obtain reservoir information, and according to the interpretation of this information, the reservoir model can be updated dynamically.

However for all reservoir engineers, the challenge is how to process and analyze PDG data according to the influences of multiphase flow and interference.

1.1.1 Development of Permanent Down-hole Gauge (PDG) in Mature Fields

The earliest mention of permanent down-hole gauges in the literature was by Nestlerode in 1963[W.A. Nestlerode, 1963 [126]]. Using eight field cases, he described how pressure data from permanent down-hole gauges was being used. ExxonMobil's first permanent down-hole gauge was installed in 1978 in the Beryl field area. The first subsea satellite wells with permanent gauge systems were completed in the UK sector of the North Sea in 1979 (Liang-Biao Ouyang, *et al*., 2002[15]).

Long-term data from permanent gauges have the potential to provide more information about a reservoir than data from traditional pressure transient tests that last for a relatively small duration. Besides reducing ambiguity and uncertainties in the interpretation, long-term data also provide an insight into how reservoir properties may change as the reservoir is produced. This type of long-term surveillance provides the opportunity to understand reservoir information in four dimensions rather than obtaining a mere glimpse or snapshot in time.

For operational purposes, bottom-hole pressure data has been be used to study petroleum engineering problems by a number of researchers.

• determine when production or injection rates in wells can be adjusted;

• indicate instantaneous declines in well performance or influences from other wells' production or injection;

• evaluate completion performance such as gravel-pack efficiency;

• evaluate the performance of stimulation or workover jobs of well;

• monitor skin, permeability, pressure drawdown over time;

• calculate reservoir characteristics such as permeability, thickness and distance to boundaries/contacts through traditional well test analysis on unscheduled buildups;

• reduce ambiguity and uncertainties in interpretations;

• recover the true down-hole flow rate;

• monitor the performance of the aquifer;

• assist reservoir simulation through history matching and updating of the simulation model. (Athichanagorn, Suwat, *et al.*, 1999[14]; Chorneyko, D.M., *et al*., 2006[18]; McCracken, M., *et al*., 2006[19]; Tibold, M.P., *et al*., 2000[20]; Queipo, N.V., *et al*., 2002[21]; Gringarten,A.C., *et al*., 2003[22]; Zheng, S.Y., *et al*., 2007[89])

Due to test behavioral aberration, missing data and noise, etc, the PDG data requires processing and interpretation:

• Extremely large volume of data. In some cases, pressure is measured at 10-second or 15-second interval for a period of several years. One year of data consists of over three million measurements. It is impossible to include the entire body of data in one processing or interpretation, due to limited computer resources.

•Compared to data from pressure transient tests, PDG data are prone to different types of errors. In the case of long-term monitoring via PDG, fluid, wells and reservoirs may undergo dynamic changes throughout their lives. The well may be stimulated, worked-over due to failure in the well-bore, etc. Reservoir pressure may fall below the bubble point because of oil and/or gas production, resulting in two-phase or even three-phase flow in the reservoir. Because of these changes the PDG data may contain extraneous measurements. Abrupt changes in flowing temperature can also cause erroneous recordings.

• Aberrant pressure behavior during a transient test may lead to large uncertainties in parameter estimates or even an unreasonable interpretation**. (Figure1.1)**

- The instability of in-situ permanent data acquisition systems.
- Incomplete flow rate history caused by unmeasured and uncertain rate changes.

In these situations, it is challenging to interpret PDG data and use the results to carry out reservoir management.

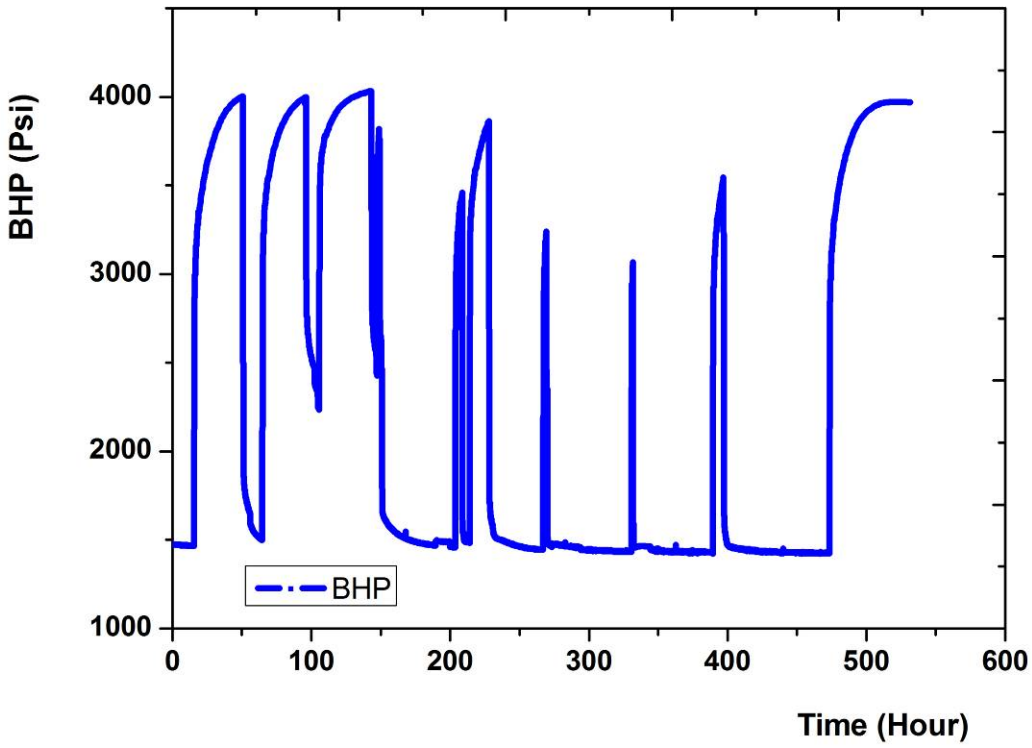

Figure1.1 An example of a curve of initial PDG data

1.1.2 Challenges in Management of Mature Fields

With the rapid development of computer technology, RNS is widely used in the management of mature fields. According to the reservoir model the oilfield development process can be repeated, performance in the future can be predicted, and corresponding adjustments can be guided and made (Kamal, M.M., 1979[88]; Ayan, C., *et al*., 1988[121]; Kamal, M.M., *et al*., 1995[103]; He, Nanqun., *et al*., 1999[70]; Kamal, M.M., 2004[108]; Freddy, H.E., 2004[74]; Sinha, S.P., *et al*., 2005[106]; Zheng, S.Y., *et al*., 2005[107]; Babadagli, T., 2005[114]; Bui, T., *et al*., 2006[111]; Zakirov, S.N., 2006[75]). But all to be successful, the precision of RNS is vital. A precise reservoir model is the foundation of RNS.

Hence there are two challenges for RNS. One is how to obtain a precise geological model and fluid model. The other is how to ensure the quality of dynamic data and

integrate all the available pressure data, production data, PVT data, petrophysical data, and geological data, etc. to update the reservoir model.

For 3D geological models, because the model is built up with seismic data, well-logging data, coring data and sedimentary facies data, etc. the model is a static one. But there are some limitations to the data. For example, seismic data covers a more extensive region, but the resolution is poor **(Figure1.2);** the data of well-logging and coring is very reliable, but the size of measurement is only around the well-bore; The sedimentary facies only stand for an area of deposition background; they cannot characterize formation heterogeneity **(Figure1.3).** Hence, geological models are not accurate, and the formation parameters from a stochastic model have big uncertainties, which need to be corrected continuously. For fluid models there are the same uncertainties, due to the influence of different sample locations and different laboratory conditions. These results of sample tests cannot stand for fluid heterogeneity in a full field model.

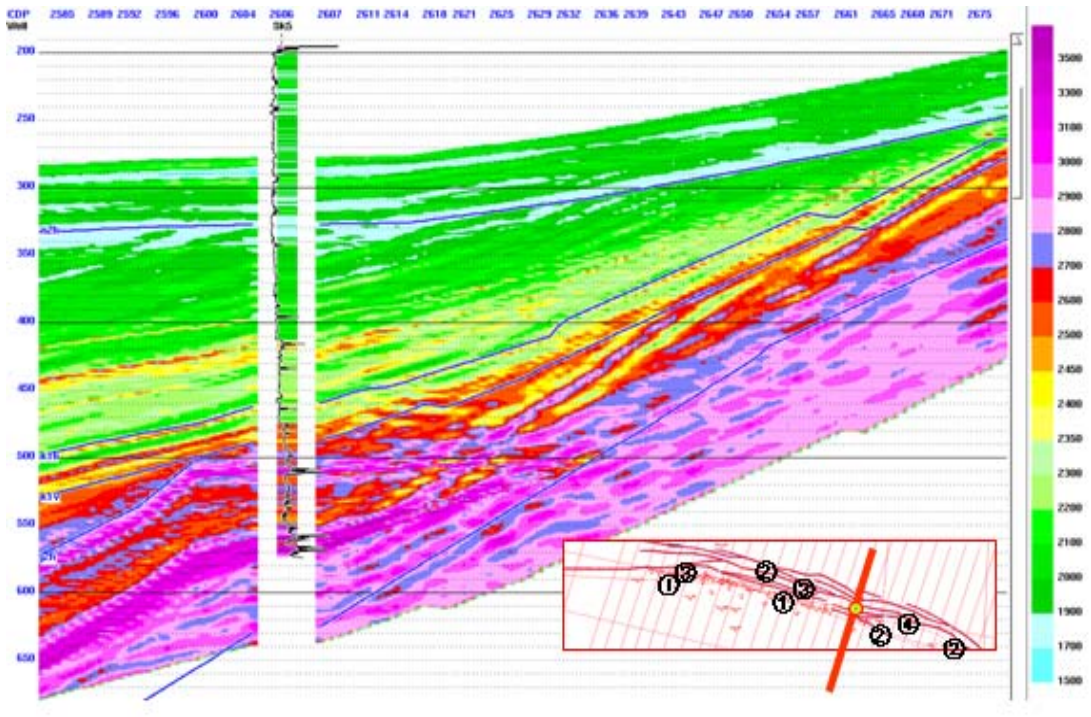

Figure1.2 Seismic section of some in-line (adapted from a project by author in Kazakstan)

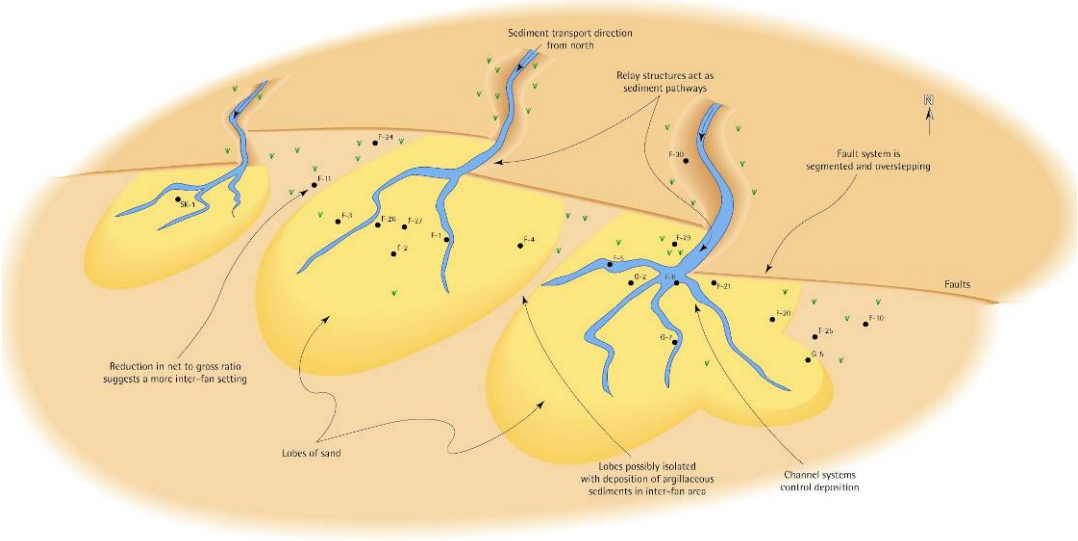

Figure1.3 The sedimentary facies for deltaic fan (adapted from a project by author in Kazakstan)

In comparison with the static data of reservoirs, well test data is the only dynamic measurement at the reservoir scale, and the interpretation results of well testing can generally be used to represent dynamic situations. According to the analysis of these results, the pressure system of a reservoir may be identified. Also, well testing can derive physical properties of the formation, well productivity, reservoir outer boundaries, effects of stimulation, reservoir performance and reserve, etc. However, the formation parameters from conventional well testing have a generally average value, which cannot couple to a 3D model or a flow simulation model. In particular, under multiphase flow conditions, traditional well testing approaches are only applicable to ideal reservoirs, such as uniform saturation reservoirs, low water-cut or very high water-cut reservoirs, etc. Because many wells for mature fields have plenty of PDG data, understanding the rules of multiphase flow and applying them to an updated reservoir model, is a big challenge for reservoir engineers.

As with the description above, when an oil field enters the middle-high water-cut stage, the wells and the field have a large amount of history-data, such as production data, and monitoring data. In particular, with current trends favoring permanent down-hole instrumentation, continuous bottom-hole well pressure monitoring is becoming more common. These instrumentations can now operate for several years and provide a record of everything that is happening to the well and, in the long term, they will

replace production tests for well and conventional reservoir monitoring. It is very difficult to utilize all the available data to update reservoir models over time. This is another challenge for mature field management.

1.2 Main Conflicts in Multiphase Flow Well Testing

Currently the analysis approach of well testing is used under conditions of single phase flow (Horne, R.N., Modern Well Test Analysis [28]; Lee, J., Rollins, J.B., and Spivey, J.P., Pressure Transient Testing [29]; Sabet, M.A., Well Test Analysis [125]). It is applicable when the formation pressure is more than bubble point pressure at the early development stage. In this situation, solution gas does not come out of oil, and there is no multiphase flow in the formation. But in fact, single phase flowing conditions in the formation stage are rare. Usually there are several multiphase flow types as follows:

(1) If the reservoir pressure is higher than the bubble point pressure, bottom hole flowing pressure is lower than bubble point pressure, and there is no water flooding or active aquifer, the energy comes from the expansion of the fluids in the reservoir and its associated pore space. In the oil formation only oil phase is flowing, but in the near borehole region, free gas comes out of solution from the oil, so two phase flow exists.

(2) If the reservoir pressure and bottom hole flowing pressure are less than the bubble point pressure, and there is no water drive or active aquifer, this depletion drive mechanism is the solution gas drive. As bottom hole flowing pressure is reduced to the bubble point pressure of the fluid, there exist two phases in the near well-bore region. As reservoir pressure decreases gradually to below bubble point pressure, the two phase area will be extended. When the saturation of solution gas reaches critical saturation, then two phases of oil/gas will flow in the long-range area of the formation.

(3) If formation pressure is more than bubble point pressure, no free gas exists in the formation. This drive mechanism is water drive (water injection, edge water and bottom water). If the bottom hole flowing pressure is less than the bubble point pressure, then the solution gas will come out of oil in the near well region. At the same time, if water has invaded the oil formation and has broken through, then there is a three-phase flow in the near-well region, but only oil/water phase flow in the formation.

Hence, multiphase flow is the common in petroleum reservoirs. But relative to the

single phase, the equations describing multiphase flow are highly nonlinear and do not have simple analytical solutions. Up to the present day, many works have been done in multiphase well testing to estimate reservoir properties. These publications can be divided into two main categories. The first category includes traditional multiphase flow well testing approaches, which contain three kinds of approach (Perrine, R.L, 1956[2]; Martin, J.C., 1959[3]; Brons, F., *et al*, 1961[4]; Fetkovich, M.J., 1973[6]; Raghavan, R., 1976[7]; Raghavan, R., 1989[8]; Al-Khalifa, A.J., *et al*, 1987[9][10]; Al-Khalifa, A.J., *et al*, 1989[11][13]; Chu, Wei-Chun, *et al*., 1986[25]; Dyung, T.Vo., *et al*., 1991[26]; Evinger,H.H., *et al*., 1942[24]). The first is the pressure approach [P-M approach [2] [3]], the second is the pseudo-pressure approach [Raghavan[7][8]], and the third is the pressure-squared approach [Al-Khalifah[9][10][11][12][13]]. The common characteristic of these approaches is the consideration of many assumptions and the simplification of the black oil model to derive an analytical solution. The other category is the numerical well testing approach. According to the numerical solution, some problems of multiphase flow well testing can be solved. Because gravitational effects, heterogeneity effects, capillary pressure and relative permeability, etc can be considered in a numerical well testing model, this model is closer to the real reservoir model and the results of numerical well testing are consistent with the actual reservoir parameters.

1.2.1 Review of Traditional Multiphase Flow Well Testing Approaches

1.2.1.1 Mathematical Model

It is assumed that gravitational effects and capillary pressure can be neglected. The equations governing the simultaneous flow of gas, oil and water in porous media are:

For oil:

$$\nabla\left[\frac{kk_{ro}}{\mu_o B_o}\nabla p\right]=\frac{\partial}{\partial t}\left[\frac{\phi S_o}{B_o}\right] \tag{1.1}$$

For gas:

$$\nabla\left[\left[\frac{kk_{rg}}{\mu_g B_g}+\frac{R_s kk_{ro}}{\mu_o B_o}\right]\nabla p\right]=\frac{\partial}{\partial t}\left[\frac{\phi S_g}{B_g}+\frac{\phi R_s S_o}{B_o}\right] \tag{1.2}$$

For water:

$$\nabla\left[\frac{kk_{rw}}{\mu_w B_w}\nabla p\right]=\frac{\partial}{\partial t}\left[\frac{\phi S_w}{B_w}\right] \tag{1.3}$$

Where: ∇ is a vector operator.

It is also assumed that oil does not evaporate into the gas phase, and that gas does not dissolve in the water phase.

If **Equation 1.1** is multiplied by (Bo-BgRs), **Equation 1.2** by Bg and **Equation 1.3** by Bw and the three equations are expanded as:

$$\frac{KK_{ro}}{\mu_o}\nabla^2 p-\frac{B_g R_s KK_{ro}}{\mu_o B_o}\nabla^2 p+\left(B_o-B_g R_s\right)\nabla p\nabla\left(\frac{KK_{ro}}{\mu_o B_o}\right)$$
$$=(B_o-B_g R_s)S_o\left[-\frac{\phi}{B_o{}^2}\frac{\partial B_o}{\partial p}+\frac{1}{B_o}\frac{\partial\phi}{\partial p}\right]\frac{\partial p}{\partial t}+\phi\frac{\partial S_o}{\partial t}-\frac{\phi B_g R_s}{B_o}\frac{\partial S_o}{\partial t} \tag{1.4}$$

$$\frac{KK_{rg}}{\mu_g}\nabla^2 p+B_g\nabla p\nabla\left(\frac{KK_{rg}}{\mu_g B_g}\right)+\frac{B_g R_s KK_{ro}}{\mu_o B_o}\nabla^2 p+B_g\nabla p\nabla\left(\frac{R_s KK_{ro}}{\mu_o B_o}\right)$$
$$=\left[(-\frac{\phi}{B_g{}^2}\frac{\partial B_g}{\partial p}+\frac{1}{B_g}\frac{\partial\phi}{\partial p})+B_g S_o(-\frac{\phi R_s}{B_o{}^2}\frac{\partial B_o}{\partial p}+\frac{\phi}{B_o}\frac{\partial R_s}{\partial p}+\frac{R_s}{B_o}\frac{\partial\phi}{\partial p})\right]\frac{\partial p}{\partial t} \tag{1.5}$$
$$+\phi\frac{\partial S_g}{\partial t}+\frac{\phi B_g R_s}{B_o}\frac{\partial S_o}{\partial t}$$

$$\frac{KK_{rw}}{\mu_w}\nabla^2 p+B_w\nabla p\nabla\left(\frac{KK_{rw}}{\mu_w B_w}\right)$$
$$=B_w S_w\left[-\frac{\phi}{B_w{}^2}\frac{\partial B_w}{\partial p}+\frac{1}{B_w}\frac{\partial\phi}{\partial p}\right]\frac{\partial p}{\partial t}+\phi\frac{\partial S_w}{\partial t} \tag{1.6}$$

Equation 1.4, **Equation 1.5** and **Equation 1.6** are rearranged as:

$$\phi(\frac{1}{\phi}\frac{\partial\phi}{\partial p}-\frac{S_o}{B_o}\frac{\partial B_o}{\partial p}+\frac{B_g S_o}{B_o}\frac{\partial R_s}{\partial p}-\frac{S_g}{B_g}\frac{\partial B_g}{\partial p}-\frac{S_w}{B_w}\frac{\partial B_w}{\partial p})\frac{\partial p}{\partial t}$$
$$=(\frac{KK_{ro}}{\mu_o}+\frac{KK_{rg}}{\mu_g}+\frac{KK_{rw}}{\mu_w})\nabla^2 p$$
$$+\left[B_o-B_g R_s+B_g GOR+B_w WOR\right]\nabla p\nabla\frac{KK_{ro}}{\mu_o B_o} \tag{1.7}$$
$$+B_g\frac{KK_{ro}}{\mu_o B_o}\nabla p\nabla GOR+B_w\frac{KK_{ro}}{\mu_o B_o}\nabla p\nabla WOR$$

Therefore

$$\begin{aligned}&\phi c_t \frac{\partial p}{\partial t}\\&= \lambda_t \nabla^2 p + \underbrace{\left[B_o - B_g R_s + B_g GOR + B_w WOR \right] \nabla p \nabla \frac{KK_{ro}}{\mu_o B_o}}_{A1}\\&+ \underbrace{B_g \frac{KK_{ro}}{\mu_o B_o} \nabla p \nabla GOR}_{A2} + \underbrace{B_w \frac{KK_{ro}}{\mu_o B_o} \nabla p \nabla WOR}_{A3}\end{aligned} \tag{1.8}$$

Where c_t is the total system compressibility, defined as:

$$c_t = \frac{1}{\phi}\frac{\partial \phi}{\partial p} - \frac{S_o}{B_o}\frac{\partial B_o}{\partial p} + \frac{B_g S_o}{B_o}\frac{\partial R_s}{\partial p} - \frac{S_g}{B_g}\frac{\partial B_g}{\partial p} - \frac{S_w}{B_w}\frac{\partial B_w}{\partial p}$$

λ_t is the total mobility, defined as:

$$\lambda_t = \frac{KK_{ro}}{\mu_o} + \frac{KK_{rg}}{\mu_g} + \frac{KK_{rw}}{\mu_w}$$

GOR is the producing gas-oil ratio, MSCF/STB, defined as:

$$GOR = R_s + \frac{K_{rg}}{K_{ro}}\frac{B_o \mu_o}{B_g \mu_g}$$

WOR is the water-oil ratio, bbl/STB, defined as:

$$WOR = \frac{K_{rw}}{K_{ro}}\frac{B_o \mu_o}{B_w \mu_w}$$

Equation 1.8 is the equation governing of multiphase flow. Through considering many assumptions, the black oil mathematical model will be simplified to obtain an analytical solution. Then the single phase well testing theory can be used to analyze multiphase flow well test data, as explained below.

1.2.1.2 P-M Approach

According to **Equation 1.8**, it is assumed that $\nabla GOR \nabla p$ and $\nabla WOR \nabla p$ are very small. Neglecting terms A1, A2, A3, and then pressure equation is noted:

$$\phi c_t \frac{\partial p}{\partial t} = \lambda_t \nabla^2 p \tag{1.9}$$

This method was introduced by Perrine [Perrine, R.L, 1956[2]), by using total mobility ($k_o / \mu_o + k_w / \mu_w + k_g / \mu_g$) to replace mobility（$k_o / \mu_o$） of the single phase, using

multiphase compressibility instead of single phase compressibility. In this way, the approach of single-phase well testing is now modified for multiphase flow well testing. Martin [Martin, J.C., 1959[3]] proved the validity of the pressure method from theory, e.g. the pressure gradient and liquid saturation gradient must be neglected in the pressure diffusivity equation. So this method is called the P-M approach.

According to the P-M approach [Perrine, R.L, 1956[2]; Martin, J.C., 1959[3]], the effective phase permeability, skin factor and the total mobility can be estimated as (field units):

$$K_l = \frac{162.6 q_l \mu_l B_l}{mh} \tag{1.10}$$

$$\begin{aligned}\lambda_t &= (k_o/\mu_o + k_w/\mu_w + k_g/\mu_g) \\ &= \frac{162.6}{mh}\left\{Q_o B_o + 1000\left[Q_g - 0.001\left(Q_o R_s + Q_w R_{sw}\right)\right]B_g + Q_w B_w\right\}\end{aligned} \tag{1.11}$$

Where:

q_l (l = o, g, w) is flow rate of phase l, STB/D;

μ_l (l = o, g, w) is viscosity of phase l, cp;

B_l (l = o, g, w) is formation volume factor of phase l, RB/STB;

m is slope of semi-log straight line on Horner plot；

R_s is solution gas-oil ratio, MSCF/STB;

R_{sw} is gas-water ratio, MSCF/STB.

The skin factor is given by

$$S = 1.151\left\{\frac{\Delta P_{1hour}}{m} - \log\left(\frac{\lambda_t}{\phi c_t r_w^2}\right) + 3.23\right\} \tag{1.12}$$

However through numerical study, Weller [Weller, W.T., 1966[5]] had proved that the P-M equation was right when the changes of liquid saturation were very small. If the well was in production for a long time, the changes of liquid saturation were very big, and then P-M equation wasn't valid.

1.2.1.3 Pressure-Squared Approach

According to **Equation 1.8**, it is assumed that the $\nabla GOR \nabla p$ and $\nabla WOR \nabla p$ is very

small, and we can neglect terms A2, A3, and then pressure-squared approach is noted,

$$\phi c_t \frac{\partial p}{\partial t} = \lambda_t \nabla^2 p + \underbrace{\left[B_o - B_g R_s + B_g GOR + B_w WOR \right] \nabla p \nabla \left[\frac{KK_{ro}}{\mu_o B_o} \right]}_{A1} \tag{1.13}$$

Equation 1.13 reduces to:

$$\phi c_t \frac{\partial p}{\partial t} = \lambda_t \left[\nabla^2 p + \nabla p \nabla \left[\ln \frac{KK_{ro}}{\mu_o B_o} \right] \right] \tag{1.14}$$

Fetkovich considered the $\frac{KK_{ro}}{\mu_o B_o}$ term can be assumed to vary linearly with pressure; the linear relation can be expressed as:

$$\frac{KK_{ro}}{\mu_o B_o} = \alpha p \tag{1.15}$$

Where α is the empirical slope (constant).

Utilizing **Equation 1.15** to reduce **Equation 1.14** the following diffusivity equation is obtained in terms of p^2 :

$$\frac{\phi c_t}{\lambda_t} \frac{\partial p^2}{\partial t} = \nabla^2 p^2 \tag{1.16}$$

For **Equation 1.16**, initial and boundary conditions are defined as:

Initial:

$$\text{At } t \to 0 \text{ , for all r, } \quad p^2 = p^2_i \tag{1.17}$$

Outer boundary:

$$\text{At } r \to \infty \text{ , for all t, } \quad p^2 = p^2_i \tag{1.18}$$

Initial boundary:

$$\lim_{r \to 0} \left[r \left[\frac{KK_{ro}}{\mu_o B_o} \right] \frac{\partial p}{\partial r} \right] = \frac{q_o}{2\pi h} \tag{1.19}$$

Using **Equation 1.15**, the **Equation 1.19** can be written as:

$$\lim_{r \to 0} \left[r \frac{\partial p^2}{\partial r} \right] = \frac{q_o}{\pi \alpha h} \tag{1.20}$$

The following line source solution is obtained:

$$p^2{}_i - p^2(r,t) = \frac{q_o}{2\pi\alpha h}\left[-E_i\left[-\frac{\phi r^2}{4t}\frac{c_t}{\lambda_t}\right]\right] \tag{1.21}$$

Here E_i represents the exponential integral function.

When the logarithmic approximation applies, using field units, **Equation 1.20** can be expressed as:

$$p^2{}_{wf} - p^2(r,t) = -\frac{325.2q_o}{\alpha h}\left[\log t + \log\left[-\frac{\lambda_t}{\phi c_t r^2{}_w}\right] - 3.23 + 0.869s\right] \tag{1.22}$$

The skin factor is given by:

$$s = 1.1513\left\{\left[\frac{p^2{}_{1hr} - p^2{}_i}{m}\right] - \log\left[\frac{\lambda_t}{\phi c_t r^2{}_w}\right] + 3.23\right\} \tag{1.23}$$

Where: m is the slope of the straight line in semi-log plot ($p^2{}_{wf}$ versus $\log t$).

$$m = \frac{325.2q_o}{\alpha h} \tag{1.24}$$

According to **Equation 1.15**, **Equation 1.24** can be written as:

$$KK_{ro} = \frac{325.2q_o\mu_o B_o p}{mh} \tag{1.25}$$

Equation 1.15 can be used to linearize both the diffusivity equation and inner boundary condition. In fact, for highly nonlinear PVT relationships and relative permeability data, **Equation 1.15** is only approximately linear. So the empirical slope α needs to be estimated. Al-Khalifah gave three rules to evaluate the slope, α .

The first, using average pressure to evaluate the slope, α , for semi-log cycle, one cycle is chosen(e.g. t=1hour to t=10hour), the slope of p^2 vs log t is:

$$m = \left(p^2{}_{1hr} - p^2{}_{10hr}\right) \tag{1.26}$$

Hence the empirical slope, α can be evaluated at $p = \frac{p_{1hr} + p_{10hr}}{2}$,

$$\alpha = \left(\frac{KK_{ro}}{\mu_o B_o}\right)\frac{2}{\left(p_{1hr} + p_{10hr}\right)} \tag{1.27}$$

Reducing **Equation 1.25** and **Equation 1.27**, the oil effective permeability can be

obtained:

$$K_o = KK_{ro} = \frac{162.6 q_o \left(\mu_o B_o\right)_{\frac{p_{1hr}+p_{10hr}}{2}}}{\left(p_{1hr} - p_{10hr}\right) h} \tag{1.28}$$

The second, for highly volatile oil at all ranges of drawdowns and low volatile oil at low drawdowns, the empirical slope, α, can be estimated at the initial pressure,

$$\alpha = \left(\frac{KK_{ro}}{\mu_o B_o}\right)_i \frac{1}{p_i} \tag{1.29}$$

This slope is substituted to **Equation 1.24** and results in,

$$K_o = KK_{ro} = \frac{325.2 q_o p_i \left(\mu_o B_o\right)_i}{mh} \tag{1.30}$$

The third, for low volatile oil at high drawdowns, the empirical slope, α, can be estimated at $p = p_{wf}(t = 0.1hr)$, hence, the following relation is obtained:

$$K_o = KK_{ro} = \frac{325.2 q_o p_{0.1hr} \left(\mu_o B_o\right)_{o.1hr}}{mh} \tag{1.31}$$

1.2.1.4 Pseudo-pressure Approach

Fetkovich (1973 [6]) introduced the pseudo pressure method to calculate the productivity of a well from a solution gas drive reservoir. Raghavan (1976 [7]) developed the calculation method of pseudo pressure for the oil-gas phase.

Evinger and Muskat (1942[24]) gave the production relation under conditions of steady radial flow:

$$q_o = \frac{Kh}{142.2 \ln r_e / r} \int_p^{P_e} \frac{K_{ro}\left(s_o\right)}{\mu_o B_o} dp \tag{1.32}$$

Definition of pseudo pressure:

$$m\left(p\right) = \int_0^P \frac{K_{ro}}{\mu_o B_o} dp \tag{1.33}$$

The **Equation 1.33** is substituted into **Equation 1.32** to obtain:

$$q_o = \frac{Kh}{142.2 \ln r_e / r} \left[m\left(p_e\right) - m\left(p\right)\right] \tag{1.34}$$

Raghavan found that the curvse of P_{wf} vs Log t and m (p) vs Log t are very similar; at

early times, and they form a straight line. This theory is the basis of pseudo-pressure analysis. Using pseudo-pressure, we can obtain absolute permeability and skin factor:

$$K = \frac{162.6 q_o}{mh} \tag{1.35}$$

$$s = 1.1513\left[\frac{m(p)_{t-1} - m(p)_i}{m} - \log\frac{K}{\phi\mu_o c_t r^2{}_w} + 3.23\right] \tag{1.36}$$

Raghavan gave the procedure for calculating the m(p) vs p relation by producing GOR. The following procedure is provided for drawdown:

(1) Using production data, tabulate t, p and GOR;

(2) Use $GOR = R_s + \frac{K_{rg}}{K_{ro}}\frac{B_o\mu_o}{B_g\mu_g}$ and the relation of P vs GOR to calculate K_{rg}/K_{ro};

(3) From the relative permeability curve calculate the ratio of K_{rg}/K_{ro} vs S_o;

(4) Use step (2) and step (3) to obtain the relation of P vs S_o;

(5) From the relation P vs S_o and relative permeability cure calculate the relation of K_{ro} vs P;

(6) Using **Equation 1.33** and PVT data, calculate pseudo-pressure, m(p).

1.2.1.5 Discussion

In order to validate the practicality of traditional multiphase flow well testing approaches, a 3D model was set up using Eclipse to simulate the pressure responses due to multiphase flow. The oil-water and oil-gas systems were studied. Capillary effect is assumed to be negligible and initial pressure is assumed to be constant everywhere.

1.2.1.5.1 Basic Reservoir Model

Two models, an oil-water model and a gas-water model were studied, and different properties were used in the simulations. Data for the simulation model are summarized in **Table 1.1**.

Table 1.1 Reservoir model characteristics

Parameter	Oil-Water	Oil-Gas
Porosity Φ,%	30	30
Absolute permeability K, mD	500	500
Wellbore radius r_w, ft	0.15	0.15
Total reservoir thickness, ft	30	30
Initial reservoir pressure, Pi, psi	2401	2401
Top depth, ft	4000	4000
Skin factor	0	0

Simulation Grid

In the constructed numerical model, the basic simulation grid consists of 51 cells in the I-direction, 51 in the J-direction, with 1 layer in anticline model (**Figure 1.4**). Because the bottom hole pressure is sensitive to the size of grid, if the size of cells near the well bore are large, then the numerical dispersion will appear **(Figure 1.5)**, so a nested grid technique will be used in the model **(Figure 1.6)**. This not only makes the wellbore better connected to grid to avoid numerical dispersion **(Figure 1.7)**, but also reduces the number of local refinement grids and improves the simulation speed.

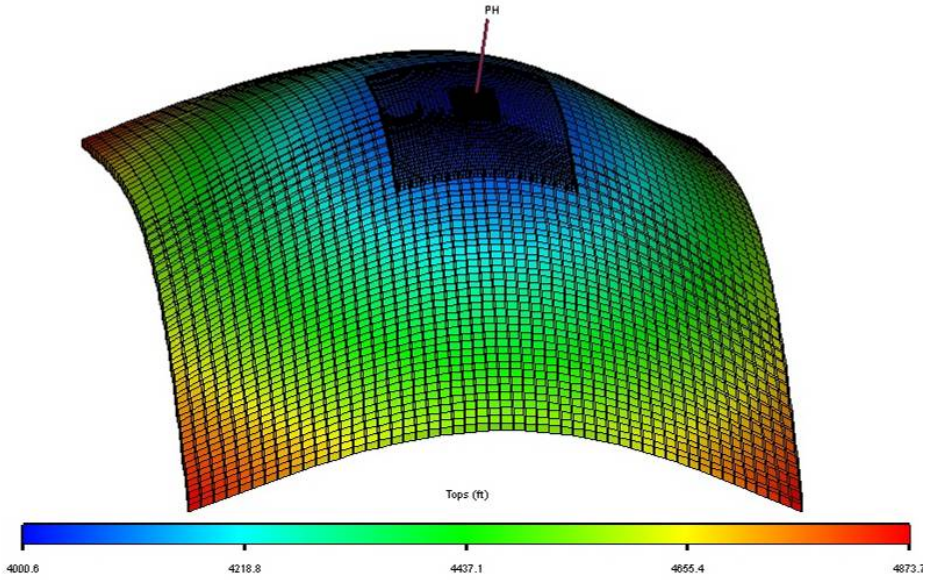

Figure 1.4 Anticline model for oil-water system or gas-oil system

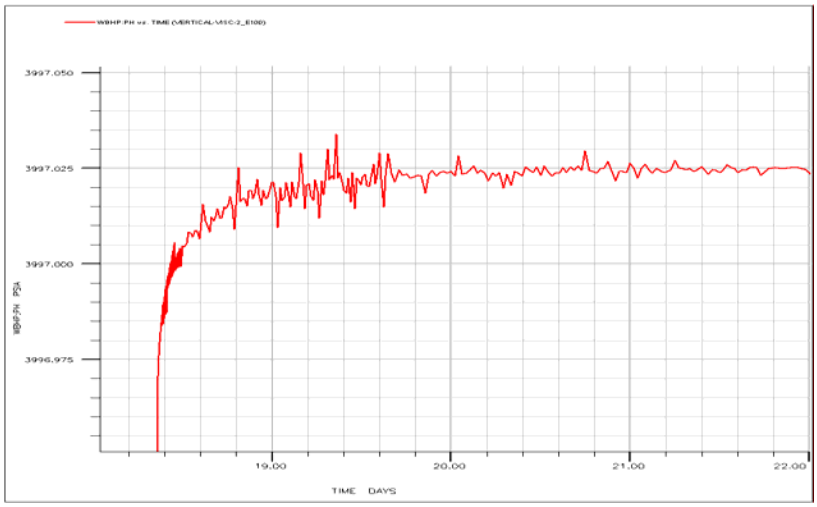

Figure 1.5 Curve showing effect of numerical dispersion. The reason for the dispersion is that the coarse-scale model produces a large change in the pressure gradient.

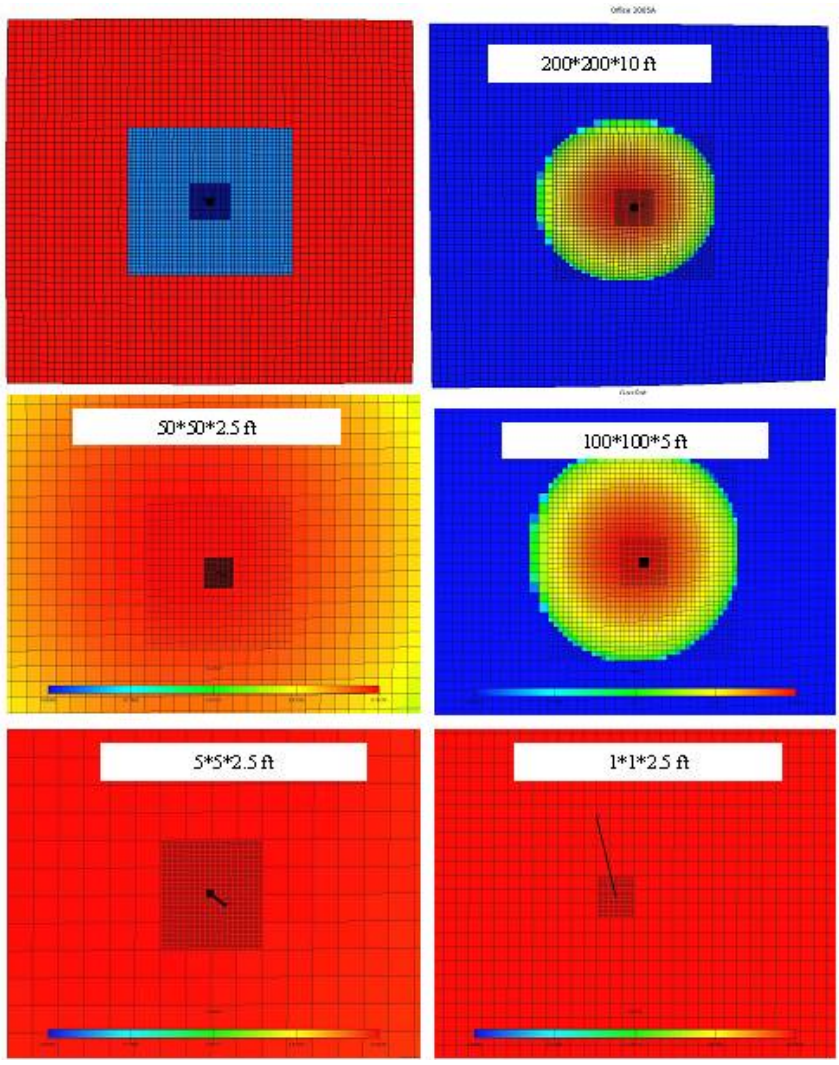

Figure 1.6 Nested grid systems show that the size of the grid cells in each direction can be reduced step by step until the size of the near wellbore grid cells is close to the radius of the wellbore.

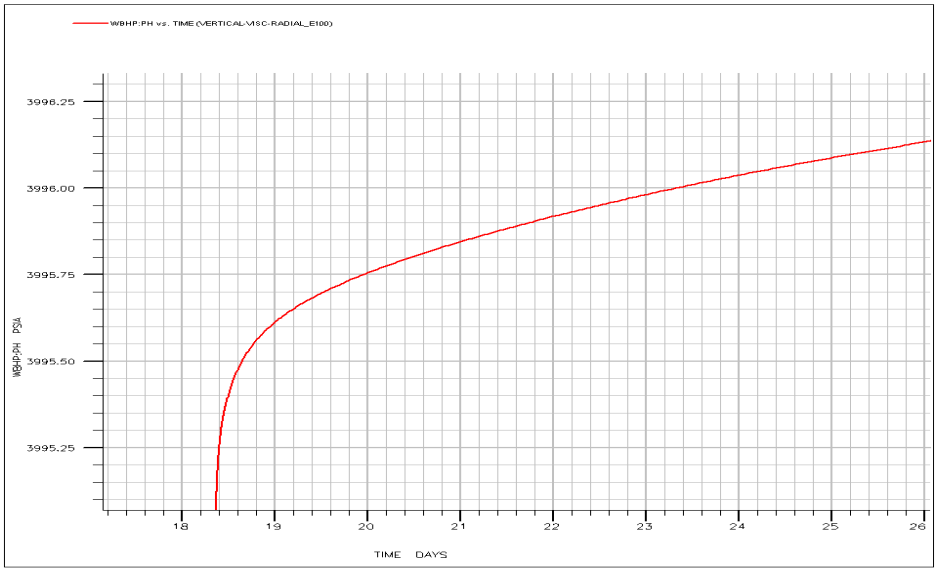

Figure 1.7 The curve of BHP is very smooth for nested grid systems condition.

Fluid Characterization

The variation of the fluid properties in the lateral and the vertical directions has been taken into account. Under reference pressure, for an oil-water system, the viscosity of oil and water are 10cp and 0.5cp. But for an oil-gas system, the PVT data of oil and gas change with reservoir pressure. (**Figure 1.8** and **Figure 1.9**)

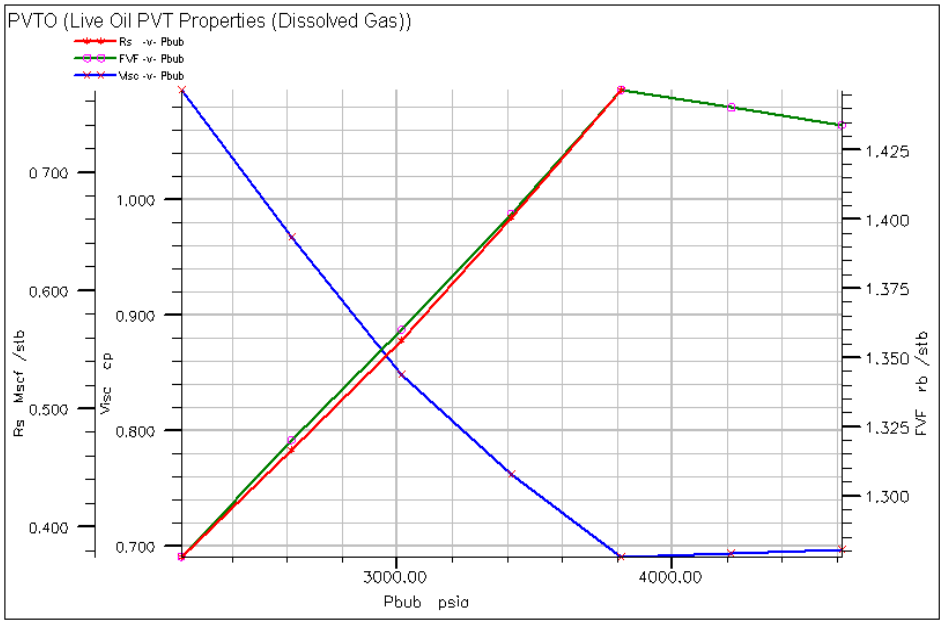

Figure 1.8 PVT Data of Oil for oil-gas system

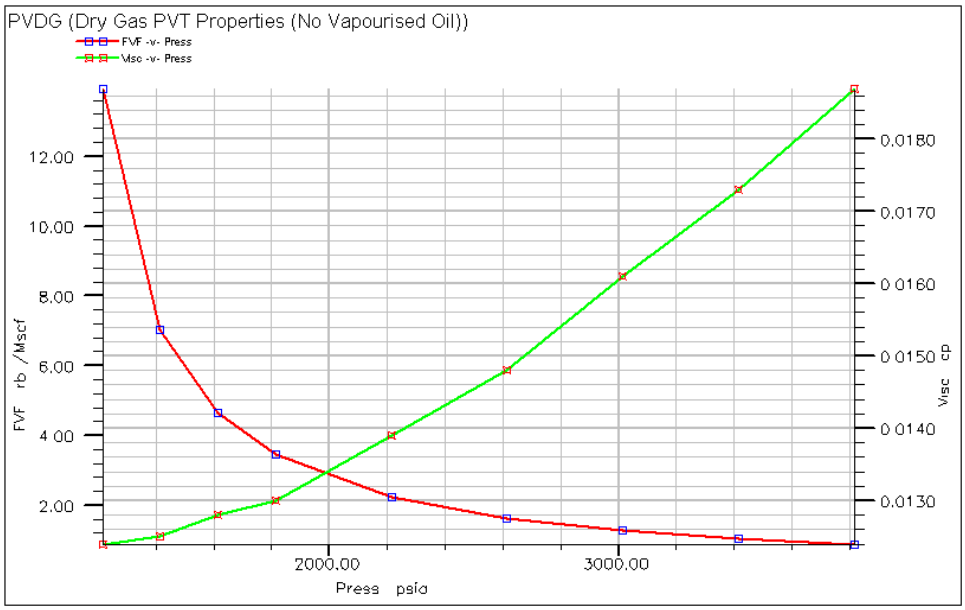

Figure 1.9 PVT Data of Gas for oil-gas system

Relative Permeability Modeling

Two sets of relative permeability data for an oil-water model (**Figure 1.10**) and an oil-gas model (**Figure1.11**) were used. **Figure 1.10** shows that when Kro equals Krw, the corresponding water saturation is more than 0.5.This denotes that the rock is water wetting property.

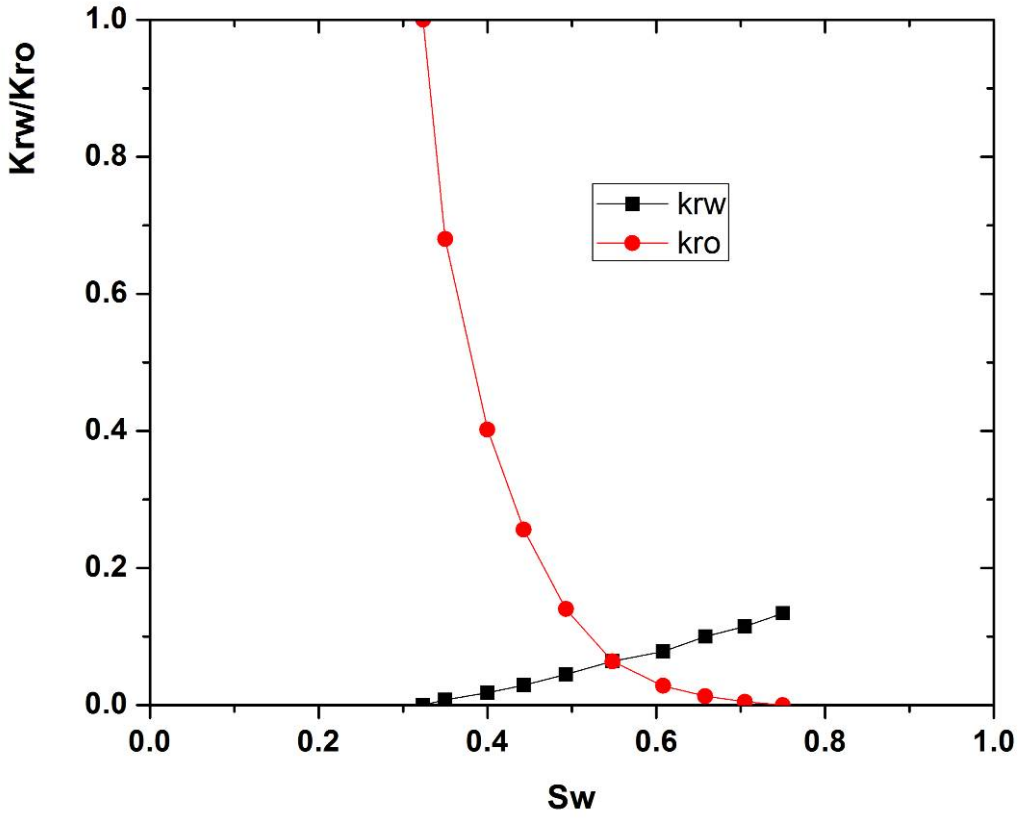

Figure 1.10 The Oil/water Relative Permeability Curve

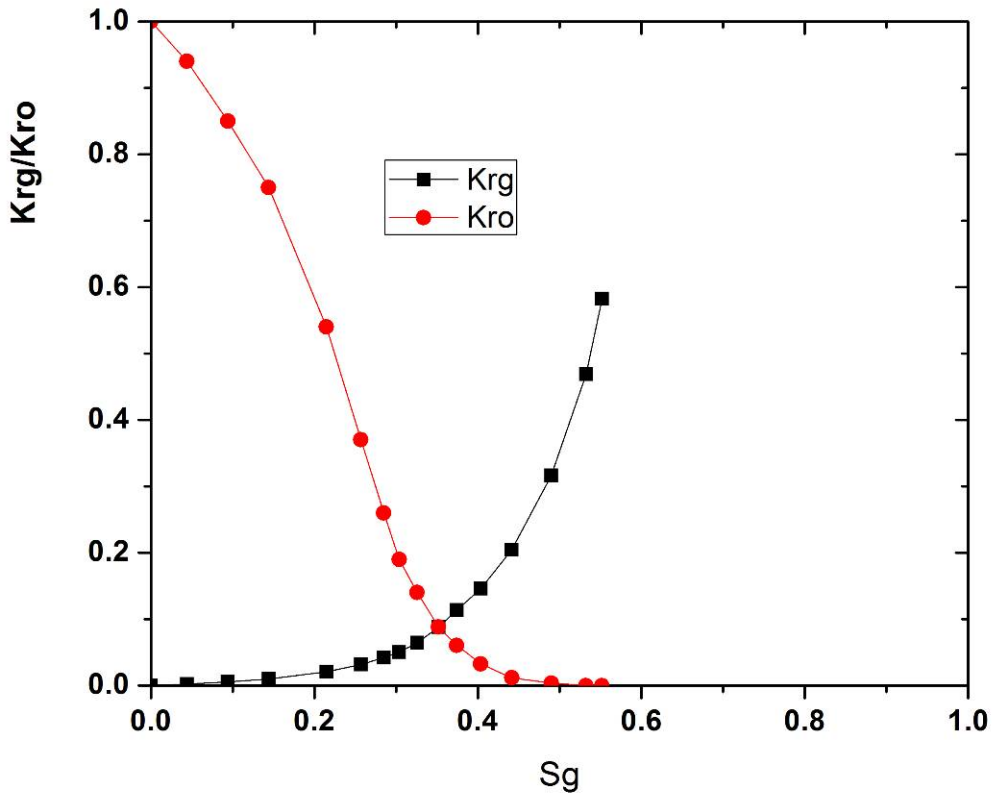

Figure 1.11 The Oil/gas Relative Permeability Curve

Model Initialization

The model uses unified oil water contact (OWC) and oil gas contact (OGC).

Case Design

The studies were designed to test the impact of different flowing rates on the pressure response. These key parameters are listed in **Table 1.2**.

Table 1.2 The designs of different flow rates

Fluid	Case	Liquid Rate Under Surface Condition(Stb/Day)	Liquid Rate Under Reservoir Condition(RB/Day)	Oil Rate Under Surface Condition(Stb/Day)	Oil Rate Under Reservoir Condition(RB/Day)
Oil-Water System	Case1	100	/	96.617	/
	Case2	1000	/	968.677	/
	Case3	2000	/	1938.059	/
Oil-Gas System	Case4	/	1000	757	/
	Case5	/	6000	4297	/
	Case6	/	12000	8177	/
	Case7	/	1325	/	1000
	Case8	/	4112	/	3000
	Case9	/	7042	/	5000

1.2.1.5.2 Oil-Water System

1.2.1.5.2.1 P-M Approach

In order to verify the practicability of the P-M method for oil/water systems, a drawdown test to analyze multiphase flow has been designed, assuming $K_{ro}/\mu_o B_o$ is very small and its change can be negligible (**Figure 1.12**), three drawdown tests were simulated at 100, 1000 and 2000 stb/day, **Figure 1.13, Figure 1.14** and **Figure 1.15** show the semi-log plot of pressure vs time. According to simulation and analysis of the results (**Table 1.3**), the oil effective permeability thickness is underestimated and skin factor is overestimated.

Table 1.3 Comparison results for drawdown in the oil-water system at different production rates

Test No.	liquid rate (stb/day)	Oil rate (stb/day)	Water rate (stb/day)	Input Koh (md-ft)	Slope,m (psi/hr)	Koh (md-ft)		λt	s	
						calculation	error(%)		Input	Caclulation
case1	100	96.61	3.39	15000	14122.4	14122.425	5.85	48.45	0	0.040
case2	1000	968.67	31.33	15000	14276.53	14276.535	4.82	48.87	0	0.065
case3	2000	1938.05	61.96	15000	14279.74	14279.743	4.80	48.87	0	0.052

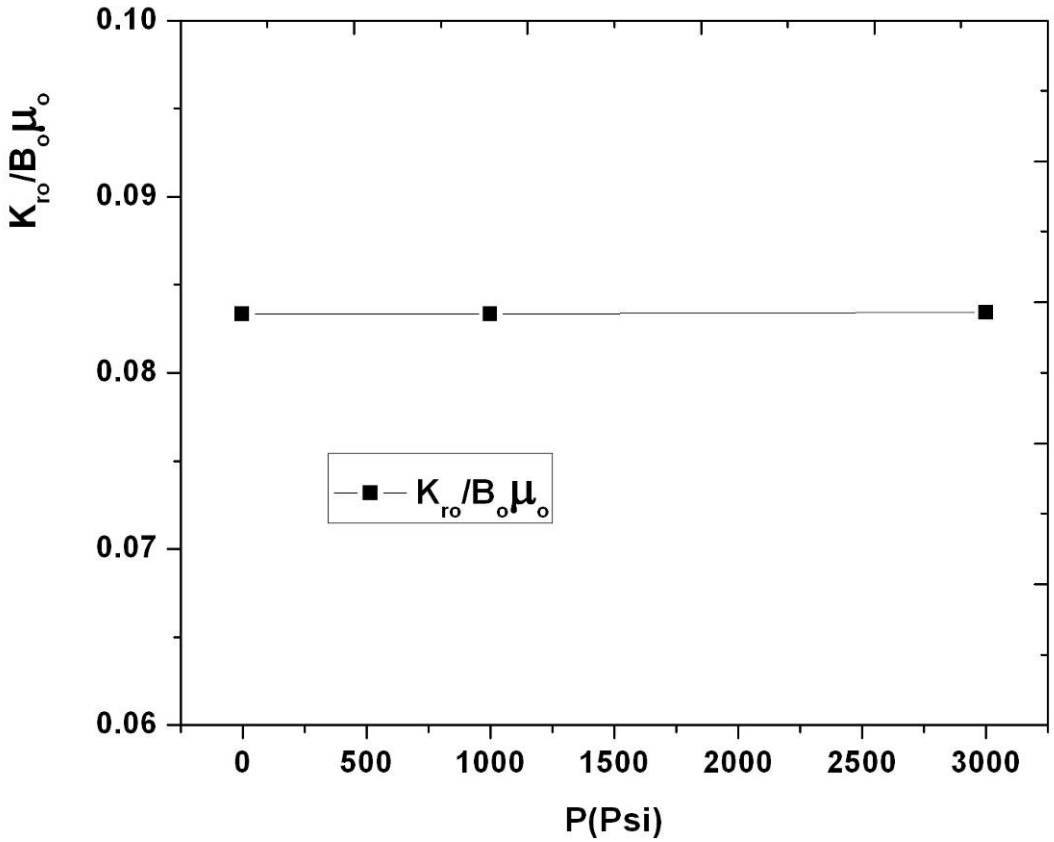

Figure 1.12 Data of drawdown test for oil-water system

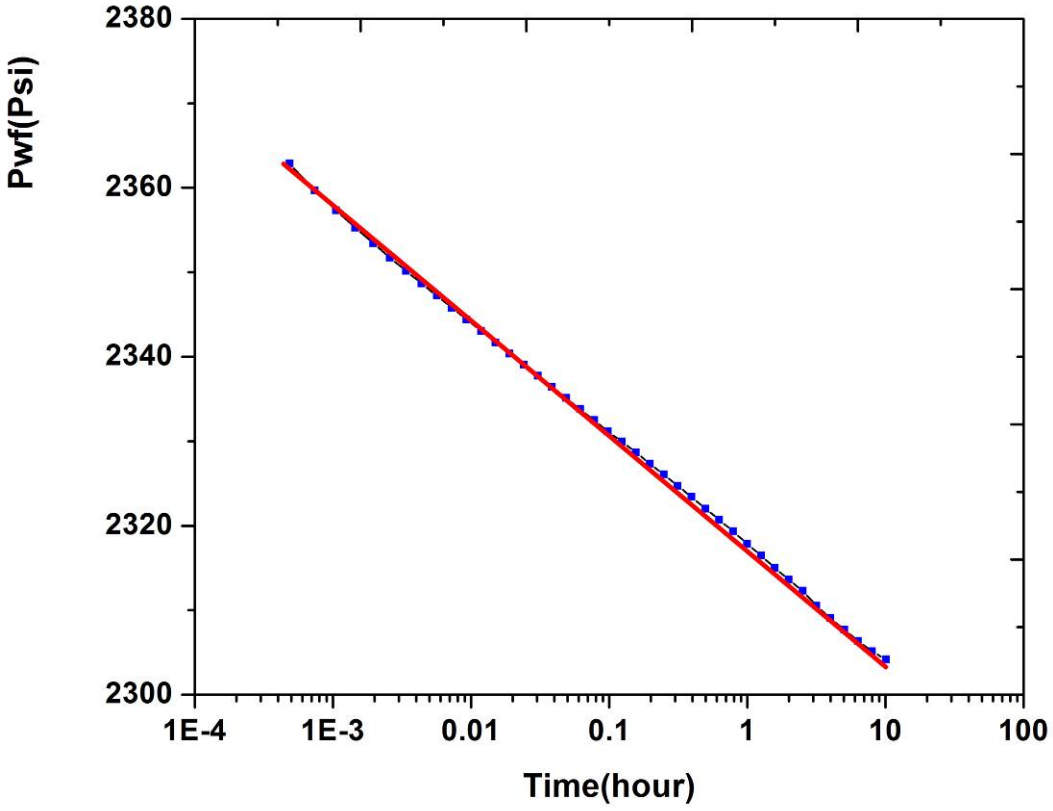

Figure 1.13 A drawdown test at 100 stb/day for oil-water system, pressure approach

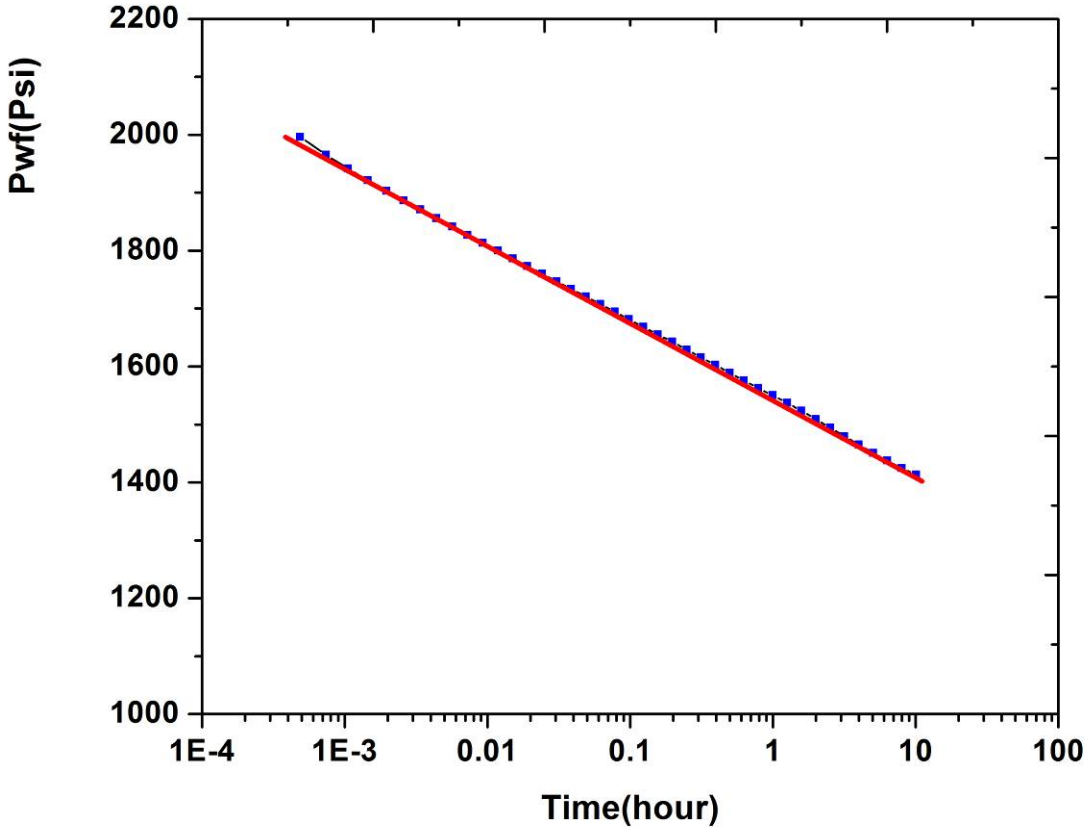

Figure 1.14 A drawdown test at 1000 stb/day for oil-water system, pressure approach

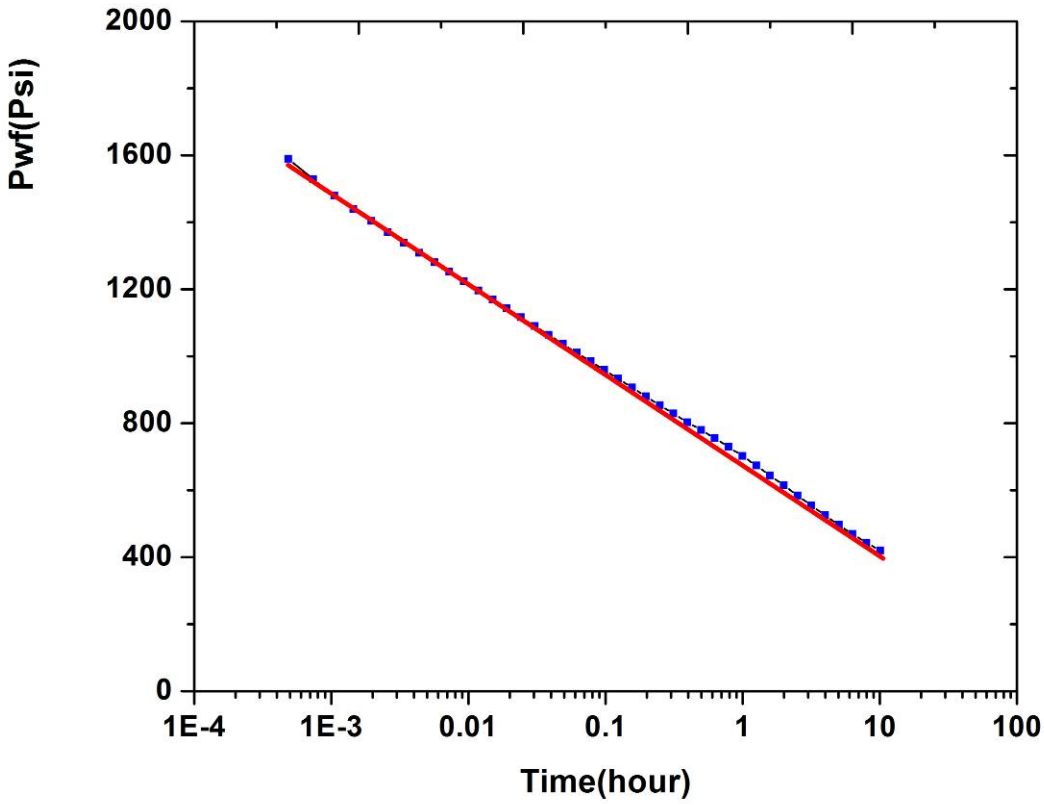

Figure 1.15 A drawdown test at 2000 stb/day for oil-water system, pressure approach

1.2.1.5.2.2 Pressure-squared Approach

Using **Equation 1.22** and **Equation 1.23** to analyze the oil-water system, **Figure 1.16, Figure 1.17** and **Figure 1.18** show that when low production rate or low drawdown was considered, the slope of the semi-log will appear straight. With an increased rate or drawdown, two or more straight lines, or even no straight line will occur. So the pressure-squared approach applies to oil-water system under low rate or low drawdown conditions.

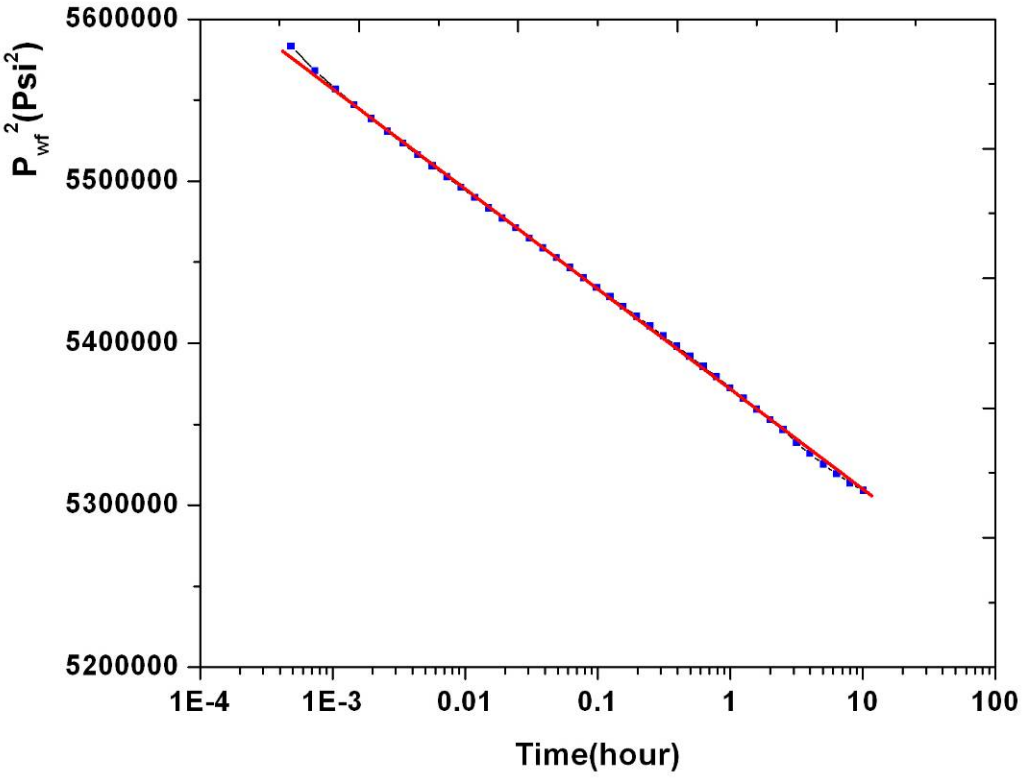

Figure 1.16 A drawdown test at100 stb/day for an oil-water system, pressure-squared approach

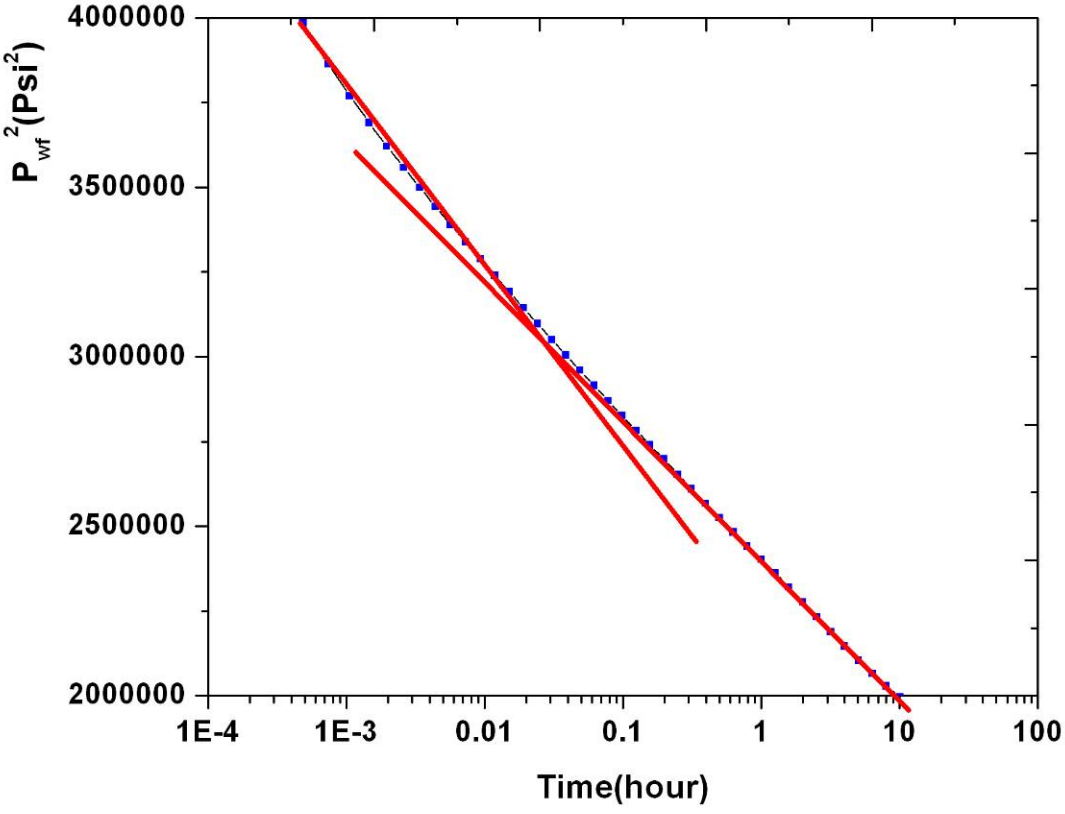

Figure 1.17 A drawdown test at 1000 stb/day for an oil-water system, pressure-squared approach

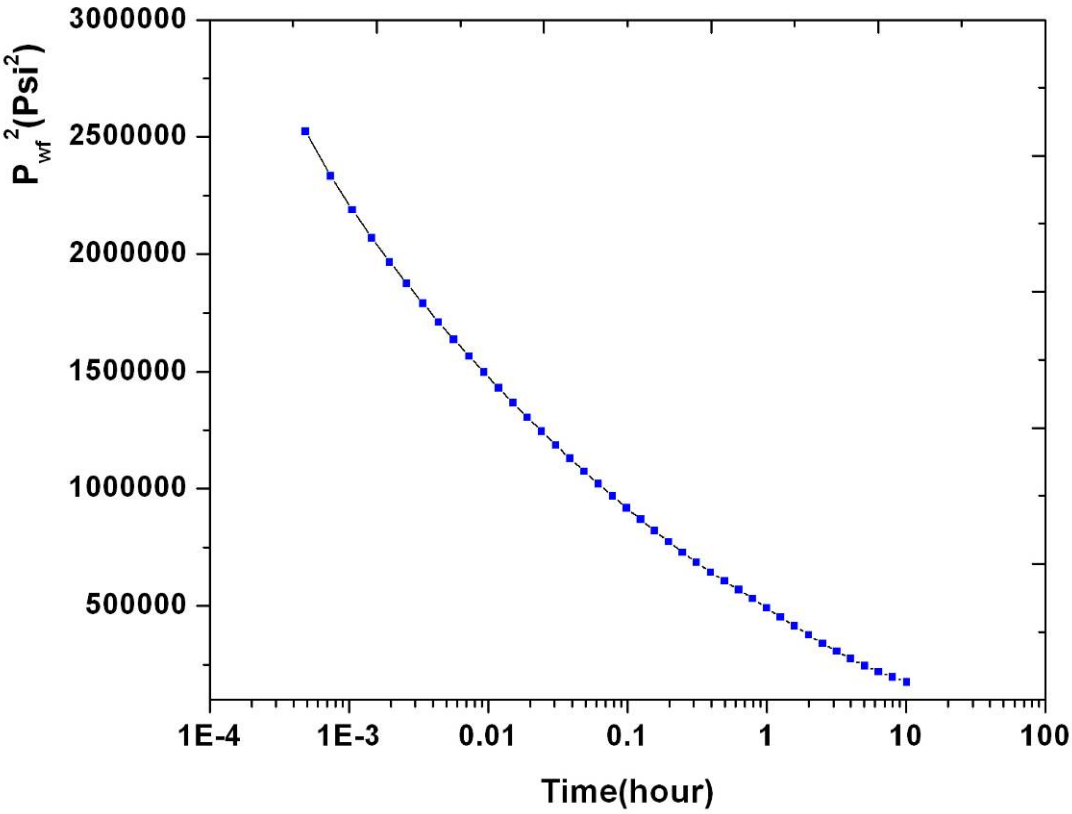

Figure 1.18 A drawdown test at 2000 stb/day for an oil-water system, pressure-squared approach

Comparing the pressure approach and the pressure-squared approach at low production rate in an oil-water system, (**Table 1.4)**, a pressure-squared approach can get a more accurate effective oil permeability. For skin factor, pressure and pressure-squared are overestimated, but pressure-squared method may be higher.

Table 1.4 Comparison results for drawdown in oil-water system with different analysis methods

Test No.	Liquid rate (stb/day)	Oil rate (stb/day)	Water rate (stb/day)	Input Koh (md-ft)	K_oh (P-M) (md-ft)		K_oh (Pressure-squared) (md-ft)		S (P-M)	S (Pressure-squared)
					calculation	Error (%)	calculation	Error (%)		
case1	100	96.61	3.39	15000	14122.4	5.85	14554.96	2.97	0.040	0.991
case2	1000	968.67	31.33	15000	14276.53	4.82	/	/	0.065	/
case3	2000	1938.05	61.96	15000	14279.74	4.80	/	/	0.052	/

1.2.1.5.3 Oil-Gas System

For the Oil-Gas system, the geological parameters were the same as for the oil-water model, changing only the PVT data and the relative permeability curve. The initial pressure has set to the bubble point pressure.

1.2.1.5.3.1 P-M Approach

When Al-Khalifa and Horne R.N. [Al-Khalifah[9][10][11][12][13]] introduced the pressure-squared approach, they used new normalization methods for pressure-rate data in transient test at the same time, plot $\Delta p / q_t \rightarrow \log t$ or $\Delta p / q_o \rightarrow \log t$, using these semi-log slopes to estimate formation parameters. So two sets of drawdown tests were simulated; one set was run at 1000, 6000 and 12000 RB/day total liquid rate (the corresponding surface oil rates were 757, 4297 and 8177 STB/day), and another set was 1000, 3000 and 5000 STB/day total oil rates (the corresponding reservoir liquid rates were 1325, 4112 and 7042 RB/day).

Figure 1.19 and **Figure 1.20** show that the P-M approach was sensitive to the flow rates in gas-oil system, when the rates were increasing, then the straight line shifted more.

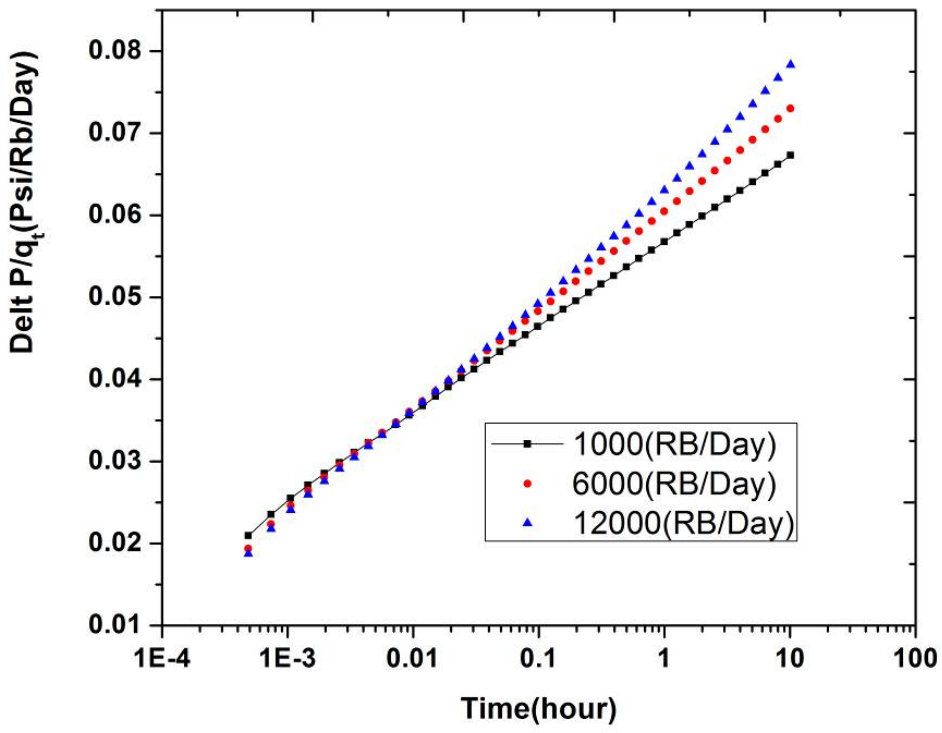

Figure 1.19 The normalized response of three drawdown tests for different liquid rates, pressure method (P-M approach)

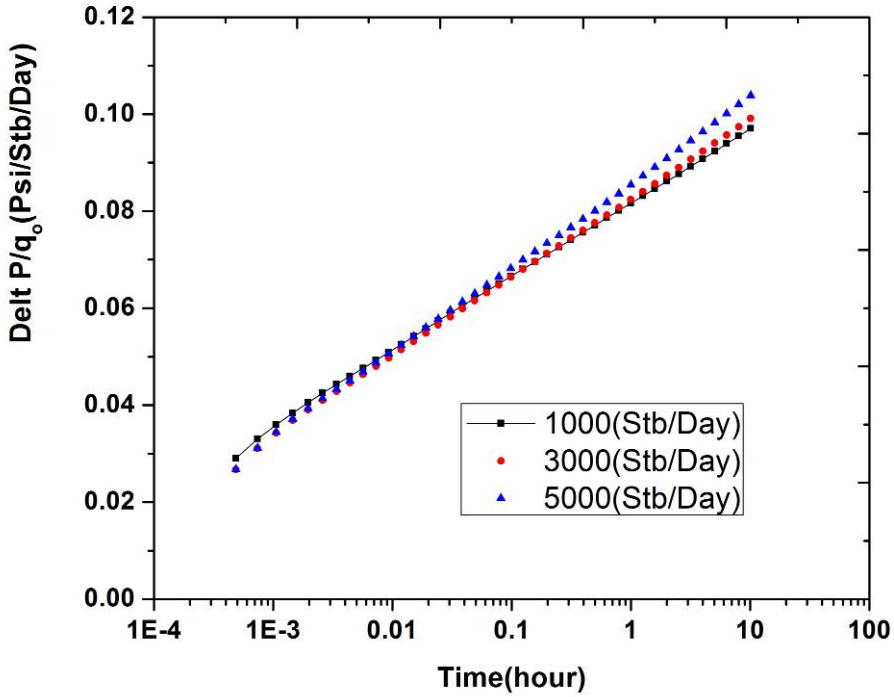

Figure 1.20 The normalized response of three drawdown tests for different oil rates, pressure method (P-M approach)

Table 1.5 and **Table 1.6** indicate that the pressure method only applies at low rates, and the total mobilities are underestimated. At high rates, the error is very large. If we use the reservoir rate in the analysis, the error is lower than for the surface oil rate. However, for the gas-oil system, it is very difficult to get reservoir rates.

For the gas-oil system, because the gas saturation has a large variation, the pressure method does not apply to high rate wells, if using low rate figures, accuracy is not good.

Table 1.5 Comparison results for drawdown in gas-oil system at reservoir conditions

Test No.	Liquid rate (RB/day)	Oil rate (stb/day)	Input λt (md/cp)	Input Koh (md-ft)	Input S	Slope,m (psi/hr)	λt	s
case4	1000	757	520	15000	0	11.53	469.70	0.532
case5	6000	4297	520	15000	0	72.78	446.79	0.066
case6	12000	8177	520	15000	0	161.85	401.84	-0.243

Table 1.6 Comparison results for drawdown in gas-oil system at surface conditions

Test No.	Oil rate (stb/day)	Liquid rate (RB/day)	Input Koh (md-ft)	Input S	Slope,m (psi/hr)	K_oh (md-ft)	λt	s
case7	1000	1325	15000	0	15.312	10194.35	353.97	0.582
case8	3000	4112	15000	0	48.771	9601.771	333.39	0.307
case9	5000	7042	15000	0	86.87	8984.459	311.96	0.166

1.2.1.5.3.2 Pressure-squared Approach

For the gas-oil system, if we use the pressure-squared method to analyze, plot $\left(p_i^2 - p_{wf}^2\right)/q_o$ vs logt, **Figure 1.21** and **Figure 1.22** show that the pressure-squared method is insensitive to rates and applies to all rates for the gas-oil system. Using **Equation 1.25**, the effective permeability can be estimated by the following equation:

$$K_o = \frac{325.2 B_o \mu_o P_i}{mh} \qquad (1.37)$$

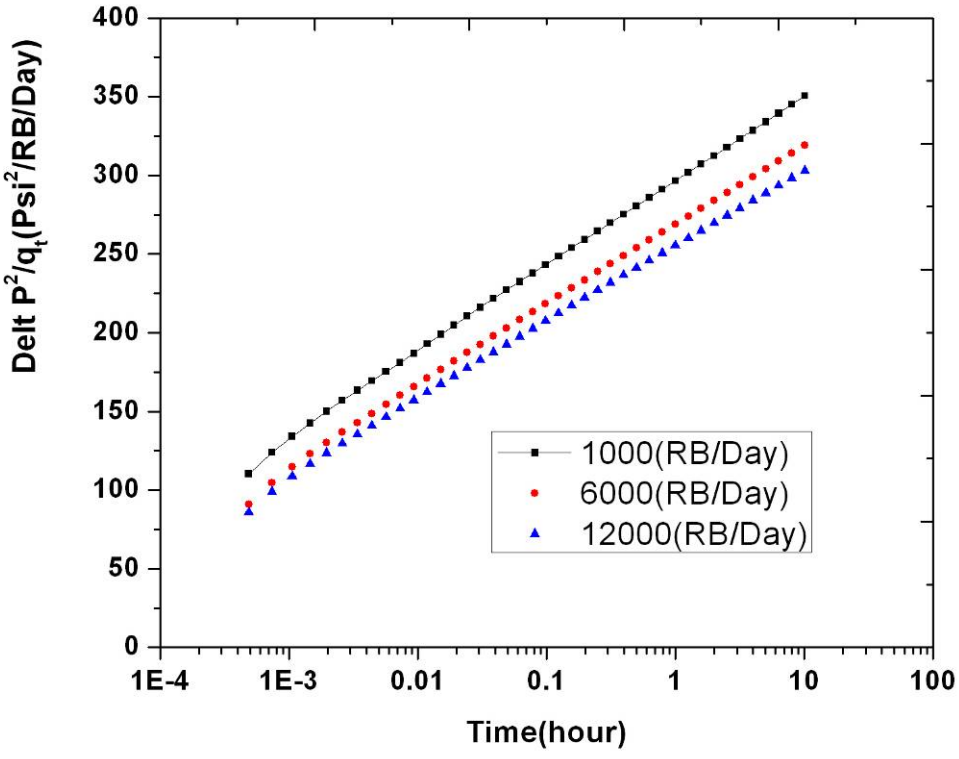

Figure 1.21 The normalized response of three drawdown tests for different liquid rates, pressure-squared method

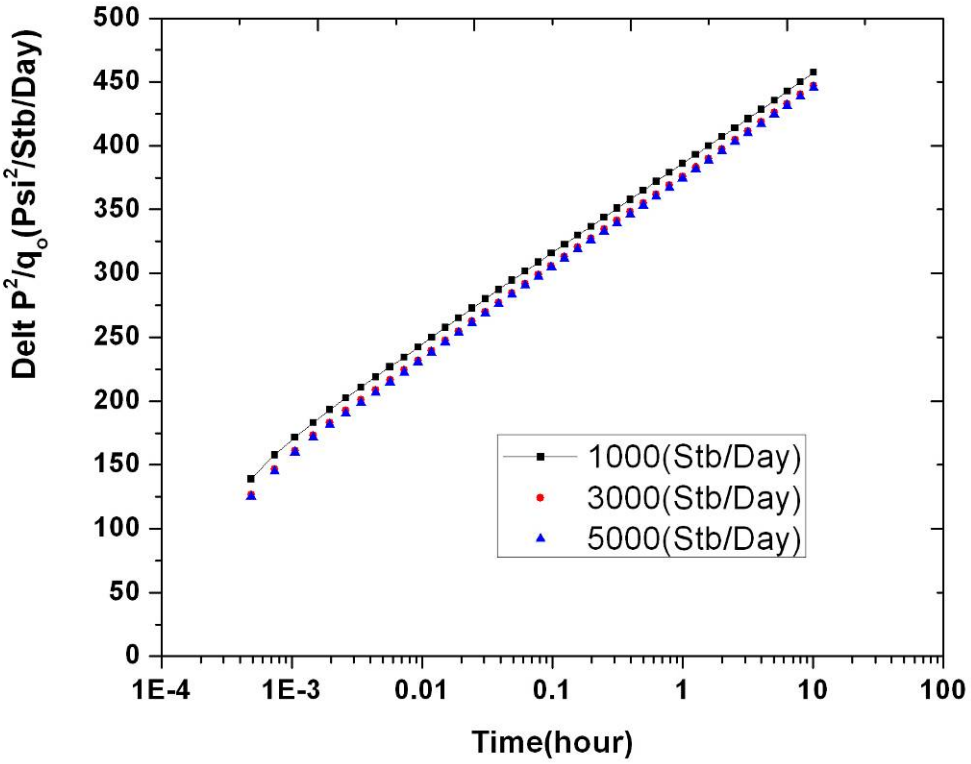

Figure 1.22 The normalized response of three drawdown tests for different oil rates, pressure-squared method

Hence, the rate-normalization method based on the pressure-squared approach can be applied at all rates for the gas-oil system, and the estimated results are more reasonable (**Table 1.7**). When comparing monitoring of the surface production rate and reservoir rate, the surface rate is easier to realize.

Table 1.7 Comparison results for drawdown for gas-oil system at surface conditions

Test No.	Oil rate (stb/day)	Liquid rate (RB/day)	Input Koh (md-ft)	Slope,m (psi/hr)	K_oh (md-ft)
case7	1000	1325	15000	71.663	13619.89
case8	3000	4112	15000	71.898	13575.37
case9	5000	7042	15000	71.937	13568.01

1.2.1.5.3.3 Pseudo-pressure Approach

According to the calculating procedure of pseudo-pressure, we can obtain the relation between pressure and pseudo-pressure for the gas-oil system. (**Table 1.8**)

Table 1.8 Drawdown pseudo-pressure vs. flowing pressure

P_{wf}(psi)	pseudo-pressure (psi/cp)
30	0
50	7.7344
75	13.212
100	18.7058
200	40.9372
300	63.6676
400	87.2404
500	112.182
600	138.3099
700	165.5834
800	193.8816
900	223.6484
1000	255.6897
1100	290.0688
1200	326.6344
1300	365.9913
1400	411.6447
1500	463.5327
1600	518.0379
1700	574.8553
1800	634.0301

According to the relation between pressure and pseudo-pressure **(Figure 1.23, Figure 1.24, Figure 1.25),** from **Equation 1.35**, the absolute permeability at different rates can be obtained. (**Table 1.9**) The estimated results of absolute permeability are very satisfactory.

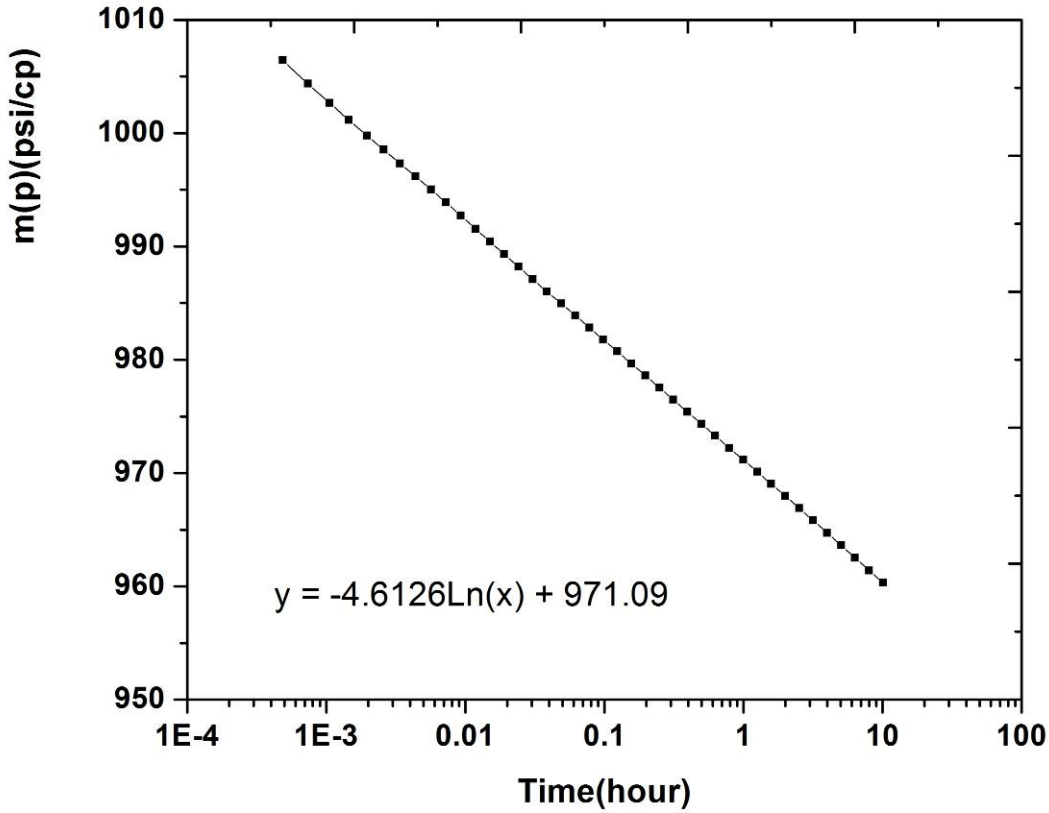

Figure 1.23 A drawdown test at 1000 stb/day for an oil-water system, pseudo-pressure approach

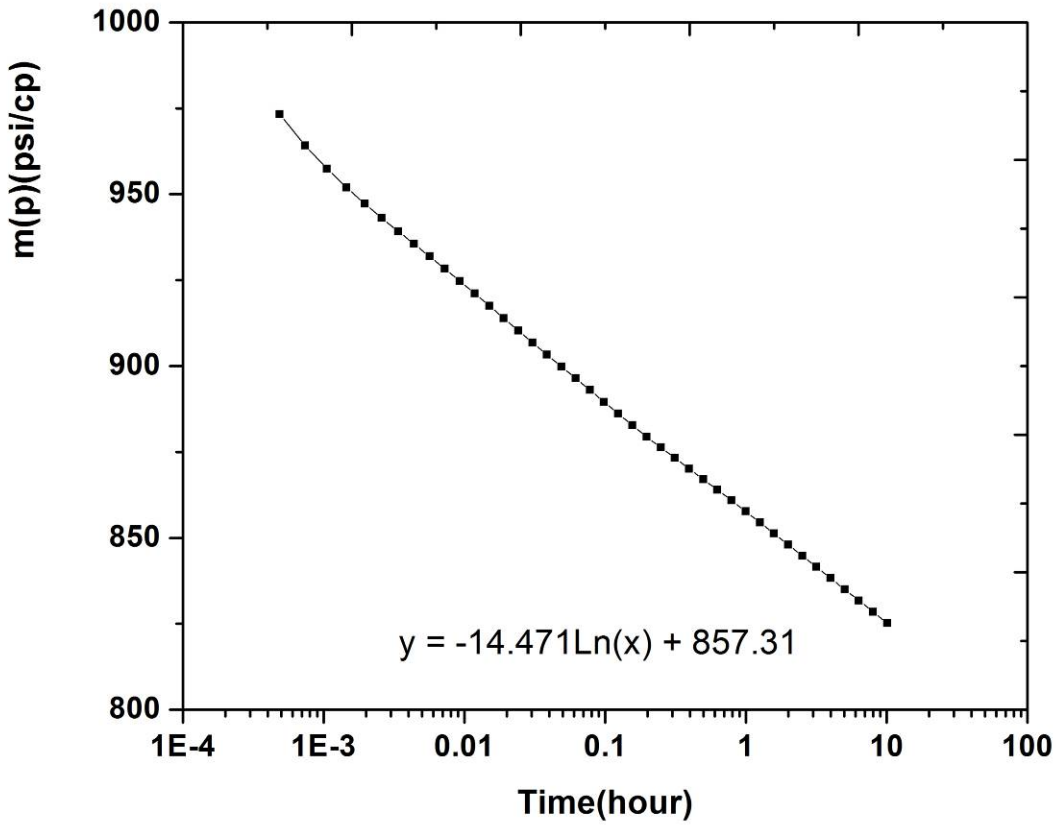

Figure 1.24 A drawdown test at 3000 stb/day for an oil-water system, pseudo-pressure approach

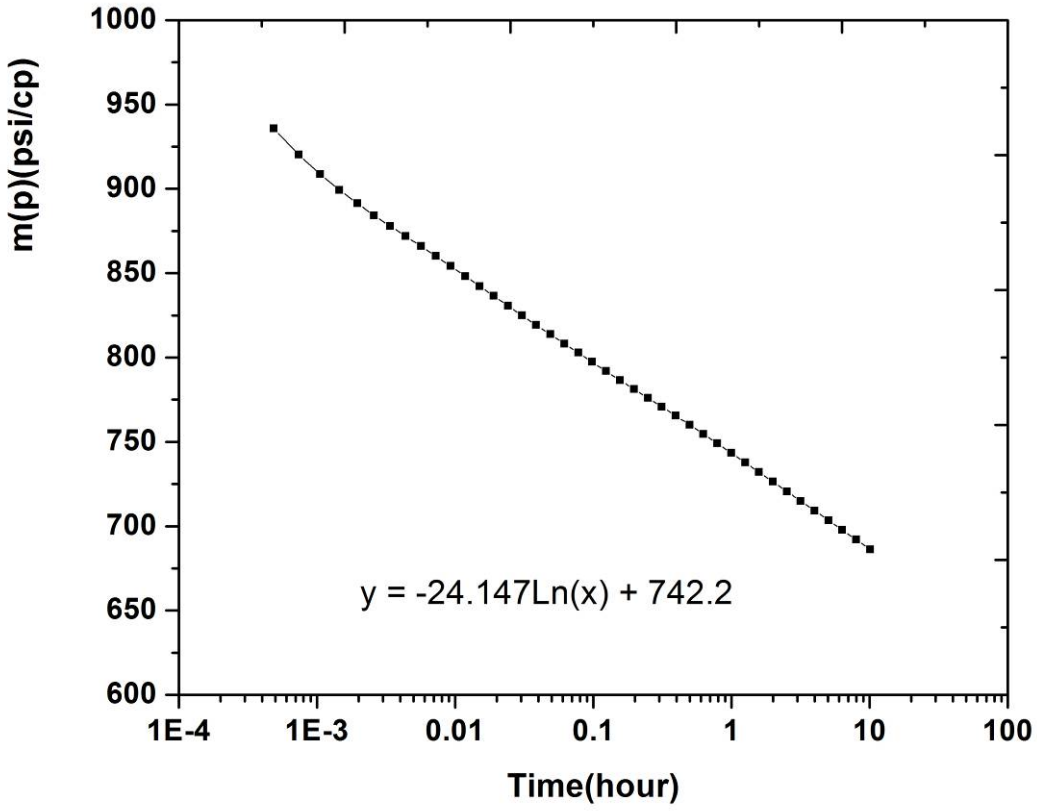

Figure 1.25 A drawdown test at 5000 stb/day for an oil-water system, pseudo-pressure approach

Table 1.9 Comparison of the interpretation results for drawdown in a gas-oil system under different surface rates with the pseudo-pressure approach

Test No.	Oil rate (stb/day)	Liquid rate (RB/day)	Input Koh (md-ft)	Input S	Slope,m (psi/hr)	Kh (md-ft)	s
case7	1000	1325	15000	0	10.608	15328.05	0.587
case8	3000	4112	15000	0	33.745	14455.47	0.135
case9	5000	7042	15000	0	56.31	14437.93	0.122

Hence, applying the three approaches to a gas-oil system and comparing the results, (**Table 1.10**) the estimated results with pseudo-pressure and pressure-squared have good accuracy. The P-M approach is sensitive to production rates, and only applies to low rate or low drawdown, but the pressure-squared approach has no effect on rates. So the pressure-squared and the pseudo-pressure approach have good applicability to a gas-oil system.

Table 1.10 Comparison of results for drawdown in a gas-oil system with different approaches

Test No.	Oil rate (stb/day)	Liquid rate (RB/day)	Input Koh (md-ft)	P-M koh(md-ft)	Pressure-squared koh(md-ft)	Pseudo-pressure kh(md-ft)
case7	1000	1325	15000	10194.36	13619.89	15328.05
case8	3000	4112	15000	9601.77	13575.37	14455.47
case9	5000	7042	15000	8984.46	13568.01	14437.93

1.2.1.6 Summary

According to the previous analysis, the three approaches have different applicability for oil-water systems and gas-oil systems.

1.2.1.6.1 Application Scope

The P-M approach can be used in all reservoir systems, but it is limited by the saturation gradient. If saturation gradients are large, the P-M approach has a large error, as with the gas-oil system. With increasing gas saturation, pressure is sensitive to production rates, so the approach only has good accuracy in low rate or low drawdown.

The pressure-squared approach only applies at low rate for an oil-water system. Under high well rate conditions for an oil-water system, it is invalid. However for a gas-oil system, it has better application than the P-M approach, because it is insensitive to rate.

The pseudo-pressure approach can be used effectively in a gas-oil system.

1.2.1.6.2 Analysis Precision and Parameter

When treating the inner boundary conditions, $\frac{K_{ro}}{\mu_o B_o}$ is considered to be constant for the P-M approach. However, this assumption is not correct, so it results in an-under-estimated phase permeability and an overestimated skin factor. However for the pressure-squared approach, using $\frac{K_{ro}}{\mu_o B_o} = \alpha p$ reduces the error of the P-M approach, and so it has a more accuracy.

The P-M and pressure-squared approaches only estimate phase permeability, not absolute permeability.

Pseudo-pressure must use relative permeability to estimate absolute permeability. Furthermore, Bφe[Bφe. A., *et al*., 1989[27]] proves that when the well reached pseudo steady state (PSS) or the pressure reached its boundary, the pseudo-pressure approach is invalid.

1.2.1.6.3 Application Practicality

Comparing the difficulty of application for the three approaches, the P-M approach is the most simple. It can be used directly to convert single phases, and, using single-phase theory, to interpret well tests. The pressure-squared approach has a similar analysis procedure to P-M, but it is necessary to choose suitable α values, so it is somewhat difficult to apply. For the pseudo-pressure approach, the calculating procedure for pseudo-pressures is very complex, because it requires relative permeability data to obtain pseudo-pressure, but the relative permeability curve has a large uncertainty in laboratory, so the estimated results have greater error.

1.2.1.6.4 Analysis Method

At present, all analysis methods for multiphase well testing are semi-log plots, which belong to traditional well test methods, and these approaches only were used in early time and middle time in simple reservoir models, but for complex reservoirs, they do not work.

1.2.2 Review of Numerical Well Testing Approach

Because traditional multiphase well testing approaches are suitable for ideal reservoirs, which are restricted by the assumptions of homogeneous formation, uniform saturation, infinite boundary and single layer, etc, if each condition of these assumptions changes with time, then the numerical solution or numerical well testing must be used. According to the numerical well testing model, reservoir geological factors (for example, reservoir heterogeneities, complicated boundary, reservoir types such as fracture reservoir or carbonatite reservoir, et al.), the reservoir fluid factors (for example, fluid heterogeneities, multiphase flow, size of aquifer, et al.) and the development factors (for example, production history, partial completion, multi-well interference, multi-layer interference, drive mechanism such as injection water, depletion or polymer flooding, et al.) can all be considered, so the numerical well testing model is closer to the real reservoir model (Lee, W.J., *et al*., 1998[61];.Landa, J.L., *et al*., 1996[76]; Archer, R.A., *et al*., 2001[78];Dubost,F.X., *et al*., 2004[86]; Yin, Hongjun., *et al*., 1999[87]; Kamal,

M.M., *et al*., 1979[88];).

Since Puchyr [Puchyr, P.J., 1991[69]] first proposed the numerical well testing concept in 1991, almost twenty years have passed. Based on a single phase numerical solution, Puchyr studied three aspects. Firstly, the new external radius concept was inducted. If the tested reservoir has a boundary, it is very important to confirm this boundary. According to this boundary, the change of pressure must be less than constant value among the simulation course. Secondly, the method of wellbore-reservoir interaction was studied. Though Peaceman used a special transmissibility to treat the relation of the bottom-hole pressure and the grid block pressure, this method was not going to work. Puchyr came up with a new idea. For positive skin, the infinitesimal skin concept is introduced; for negative skin, the usual analytic technique is to replace the well radius and negative skin by an equivalent well radius. But Puchyr introduced the composite model to describe the skin area, in which the porosity is retained while the permeability increases. Compared with usual method, the match between radial simulation and radial analytic solutions is more accurate. Thirdly, initial grid block near-wellbore and time step sizes are selected. The limit of pressure change near-wellbore is first determined, and then according to this limit, the limit of pressure change per time step can be determined. Further, the size of time step can be calculated, and finally the size of near-wellbore grid blocks can be obtained through the time step. Although Puchyr focuses on single phase flow, his work provided many good references for the problems of heterogeneous formation and multiphase flow. In recent years, with the progress of numerical reservoir simulation and computer technique, there has been an increase in the use of numerical well testing. But these studies focus on the numerical models and their solving methods. Corbett [Corbett, P.W.M., *et al*., 1996[92]] used a numerical model of braided fluvial reservoirs to calculate well test response, and introduced the geo-skin concept from these simulation data. Zheng [Zheng, S.Y., *et al*., 1996[93]] used a model of meandering channels to study the effects of well location within the channel, channel shape, and completions ratios. Landa [Landa *et al*., 2000[72]] used a field example to present a method to integrate well test, production rate, log, core and geological data to obtain a heterogeneous model. Through a comparison with the measured well test data and calculated data from a numerical model, the spatial distributions of permeability and porosity can be obtained. Raghavan [Raghavan, R., *et al*., 2001[68]] reviewed the progress of numerical well testing. They found that the numerical well testing technique is growing quickly in three areas of petroleum industry:

"the use of the numerical model to predict the geological model's effect upon the well test response; the conditioning of geo-statistically generated geologic models to the well test response; and the history matching of the numerical model to observed well test data." Faisal M. Al-Thawad [Al-Thawad, F.M., *et al*., 2003[67]] built a numerical model of a complex well with fracture to study the importance of near well bore grid setup. Magnus Nnadi [Nnadi, M., *et al*., 2004[73]] contrasted the numerical method with the analytical method, and the results showed that the numerical solution is more applicable than analytical solution in real complex geology. Kamal [Kamal et al., 2005 [64]] reviewed the limitation of traditional well testing, and present the workflow of numerical well testing. Yao Jun [Yao Jun., *et al*., 2009[79]] introduced streamline simulation techniques and further improved the precision and speed for numerical well testing interpretations.

As can be seen from the description above, numerical well testing has grown quickly, but the studies were focused on the geological model. Few papers referred to multiphase flow problems. In fact, much PDG data or well testing data from mature fields are influenced by multiphase flow. Currently, the numerical well testing approach is a very useful way to study the rules of multiphase flow and to achieve the ultimate goal of well testing-real time reservoir monitoring, model calibration and mature field management.

1.2.3 Impracticability of Multiphase Flow Well Testing

As described in the previous section, when some assumptions were considered, the governing equations of multiphase flow have analytical solutions. So the traditional multiphase flow well testing approach is only applicable to an ideal system or special reservoir, such as a uniform saturation reservoir, segregated flow reservoir, etc. due to the limitations of multiphase governing equations. Unfortunately, few actual reservoirs satisfy these assumptions. Furthermore, traditional multiphase flow well testing approaches are limited to the application scope, analysis precision and parameters, application practicality, and interpretation method. So the traditional multiphase flow well testing interpretation methods based on analytical solutions do not work for most practical cases and cannot be widely popularized.

For reservoirs with complex heterogeneity, numerical well testing has been used for several years. But relating to the rule of multiphase flow well testing interpretation, few papers were published. In particular, many permanent down-hole gauges have been

installed in mature fields. The importance of dynamic reservoir monitoring and analysis of results obtained using dynamical up-to-date information has been recognized as a vital element in modern reservoir management. With regard to PDG data, including multiphase flow effects, because of the particularity of PDG data, such as behavioral aberration, missing data, extremely large volume and noise, etc., it cannot be conveniently applied by reservoir engineers in mature field management.

1.3 Motivation and objective

It has been noted that the current traditional multiphase flow well testing interpretation methods and numerical well testing method are not satisfactory, e.g. the traditional multiphase flow well testing approaches and numerical well testing approach are not practical in field cases. Frequently, the modern reservoir model is a highly heterogeneous geological model and fluid model. Some rules of multiphase flow and some accurate and practical multiphase flow well testing methods are demanded so that the geological and fluid understanding can be fully assimilated in the reservoir simulation in real time. It is this requirement that motivated the work of this thesis.

The main objective of this thesis is to find some rules and improved methods (based on analytical solutions and numerical solutions) for multiphase flow well testing interpretation which are suitable for PDG data analysis in mature field management. In order to achieve these objectives, the main considerations are as follows:

- To analyse the advantages and disadvantages of multiphase flow well testing approaches which are based on analytical solutions, and then to develop a more accurate and efficient approach which will be practical for field cases.
- To gain a thorough understanding of multiphase flow well testing through qualitative comparison between the analytical solutions and numerical solutions for real reservoirs which can be used to guide reservoir management.
- To find a practical procedure for multiphase flow numerical well testing that can be easily used to update the reservoir model in real time according to transient data or PDG data.
- To test the accuracy of the improved method, the validity of understanding and the practicality of procedure, some field examples will be confirmed by these approaches.

1.4 Study workflow and outline of the thesis

1.4.1 Study workflow

In this study, I will be using numerical well testing model to generate multiphase flow well testing data (such as, PDG data, transient data, stabilized well testing data, et al.), According to these data, multiphase flow well testing analysis methods are studied. The detail is summarized in **Figure 1.26**.

Firstly, I will build up ideal multiphase flow reservoir models (such as, uniform saturation reservoir, et al.) and use analytical solutions to study traditional multiphase flow well testing methods and further improved them to obtain methods which are more accurate and practical.

Secondly, I consider real reservoirs (such as non-uniform saturation reservoirs, layered commingled reservoirs, etc) to obtain new understanding and analysis procedures for multiphase flow well testing interpretation, based on numerical solutions. These new understandings and analysis procedure can be used to guide mature field management.

Thirdly, in order to confirm these improved approaches, new understandings and new analysis procedure, two examples were studied. Through these researches, a new multiphase flow numerical well testing approach was developed which can be used to study multiphase transient pressure from permanent down-hole gauges (PDG) in mature fields.

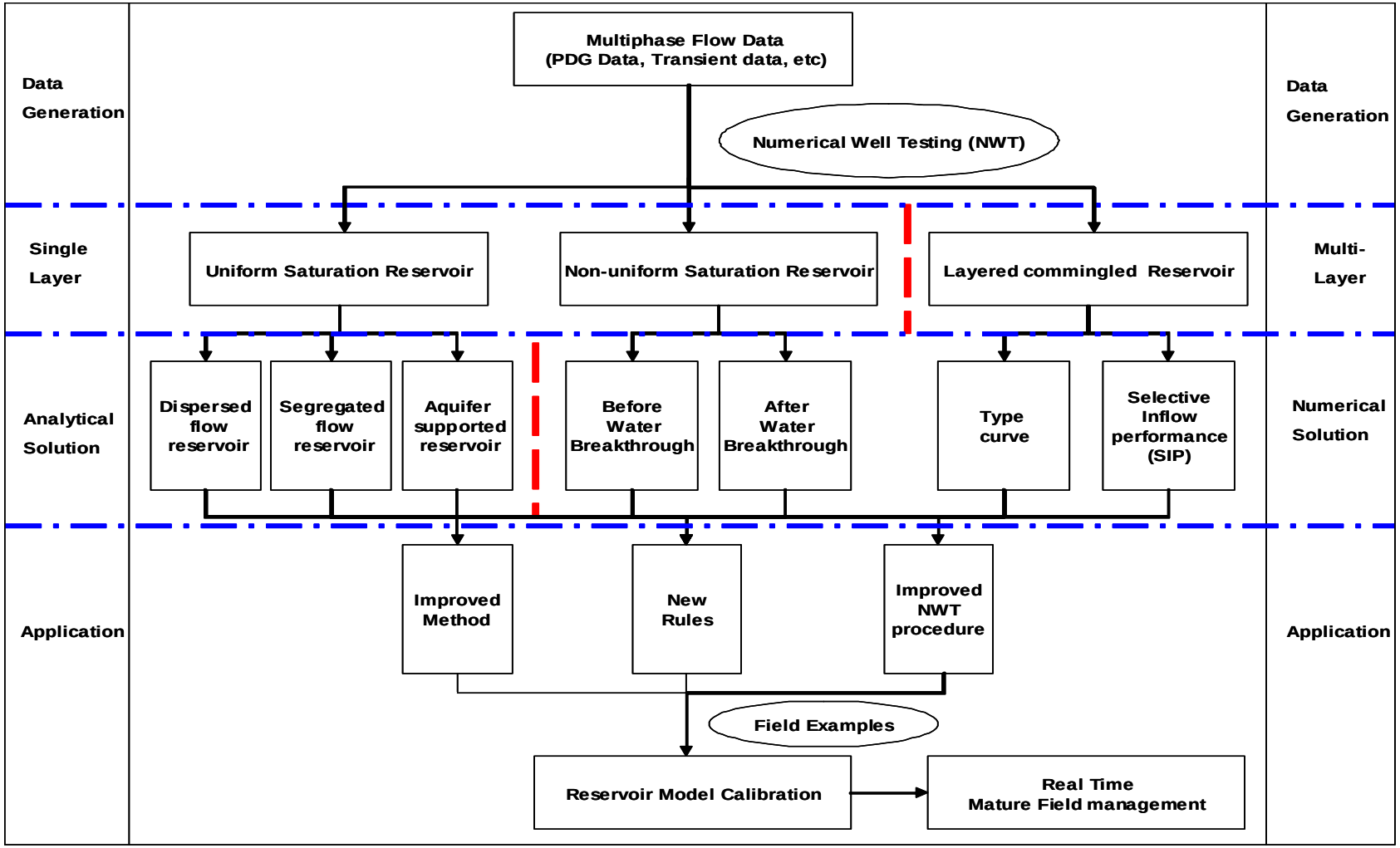

Figure 1.26 Workflow of Multiphase flow Study

1.4.2 Outline of the thesis

This thesis is structured as follows:

Chapter 1 has given a brief background to PDG data applications and challenges of the mature field management process and reviews and discusses the advantages and disadvantages of the multiphase flow well testing analysis methods. As a result, the development of new understandings and improved approaches to multiphase flow well testing interpretations which are suitable for calibrating mature field models will be the focus of this thesis.

Chapter 2 contains a description of improved methods of two phase flow well testing for uniform saturation reservoirs. The traditional P-M approach is only suitable for dispersed flow with uniform saturation, oil-water segregated flow and oil reservoir with aquifer-support. But due to the limitation of analytical solutions, P-M approach is not practical. In this chapter, modified P-M is developed and used to interpret the practical cases.

Chapter 3 contains new understandings of non-ideal reservoirs, which are set out in two parts.

In Part I, the transient pressure response in the transition zone of two phase flow systems before water break through, is studied. Following theoretical development, a new expression is derived, which shows that pressure response in the transition zone is a function of total effective mobility. For oil-water systems, the total effective mobility increases with an increase in the radius of the transition zone, while for gas-water systems, the effect is opposite.

In Part II, the well test data are studied after water breaks through. As shown by the results of this study, it is normal that bottom-hole pressure increases with time due to the changing of the total mobility of the fluid.

Chapter 4 contains a description of synthetic studies for layered commingled reservoir. The multiphase multi-layer systems are surveyed and classified. Under different system conditions, the type curves of transient pressure data are obtained. According to these type curves, some new understandings are developed. At the same time, the practicality of selective inflow performance methods (SIP) on field scale reservoir models is also discussed.

Chapter 5 contains a description of new multiphase flow numerical well testing procedures. Conventional numerical well testing procedure, which is suitable for studying complex heterogeneous reservoir, is reviewed in detail. But for new procedures, considering the multiphase effect, the PDG data can be used easily to update reservoir model in real time through the history-matching approach.

Chapter 6 takes the knowledge described in the previous chapters and applies it to two real field examples. Cases studies are developed to demonstrate the key issues of multiphase flow well testing interpretation. These practical applications confirm that the new numerical well testing procedure can successfully handle PDG data to calibrate reservoir models and carry out dynamic management in mature fields.

Chapter 7 concludes by summarizing the thesis and its major findings and its possible contributions to industry. It also outlines some ideas for future work.

Chapter 2
Analysis of Two Phase Flow Well Testing for Uniform Saturation Reservoir

2.1 Introduction

Well testing has been used for many years in the oil industry, to evaluate well conditions and obtain reservoir parameters such as permeability, skin factor, average pressure and well productivity. With the advent of PDG becoming available to the industry, continuous reservoir monitoring and dynamic reservoir management in a mature field becomes possible. As many oil fields reach the middle to high water-cut stage, the influence of multiphase flow, due to the long-term nature of PDG data, is significant.

Traditionally, the well test interpretation approach is used for single phase and uniform reservoirs. Well test interpretation in multiphase flow reservoirs is difficult due to the fact that well test equations describing multiphase flow are highly non-linear. In order to get simple analytical solutions and use single phase theory to analyze the data from multiphase flow reservoir, many assumptions have to be made. In the literature, many articles on this subject were published. In summary, these publications can be divided into three main categories. The first is the pressure approach (P-M approach, Perrine, 1956[2]; Martin, 1959[3]), the second is the pseudo-pressure approach (Fetkovich, 1973[6]; Raghavan, 1976[7]), and the third is the pressure-squared approach

(Al-Khalifah, 1987[9]).

In these multiphase flow approaches, only the P-M method is applicable in strictly oil-water systems. The essence of this method is the definition of total flow properties to replace the individual phase properties. This method is simple and has been widely used in practice, but it has restrictions that limit its applicability or accuracy due to the changing of phase saturation, viscosity and formation volume factor during the time period of a test. The greatest disadvantage of the method is that some of the estimated results from the P-M approach, for example the phase effective permeability, can not be applied directly as the input to the reservoir simulation model for performance management.

This chapter focuses on the oil-water two-phase flow system and presents in depth the problem of well testing. Three types of ideal flow mechanisms are modelled and studies are conducted through numerical simulations (**Figure 2.1**). These are dispersed flow with uniform saturation, oil-water segregated flow and oil reservoir with aquifer-support. Dispersed flow with uniform saturation is an ideal case, where oil and water is assumed to be fully dispersed across the entire reservoir thickness. But in practice, this system does not exist. Segregated flow occurs when gravity forces are dominant, leading to complete segregation of oil overlying water. Such situations can also be due to early water breakthrough with high permeability formation in layered reservoirs. The last flow mechanism is the aquifer supported reservoir, where the well is completed quite apart from the water formation to prevent water coning.

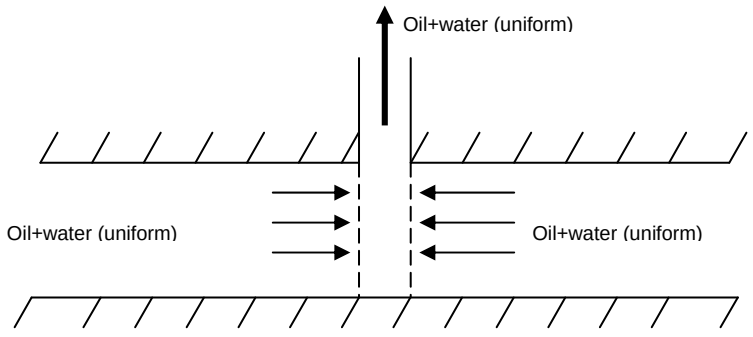

(a) Dispersed flow with uniform saturation

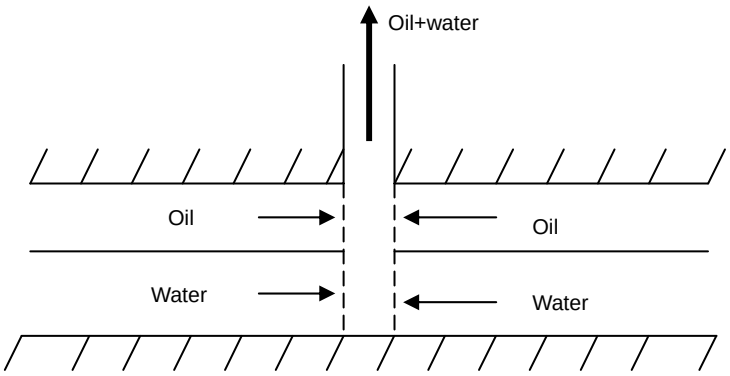

(b) Segregated flow

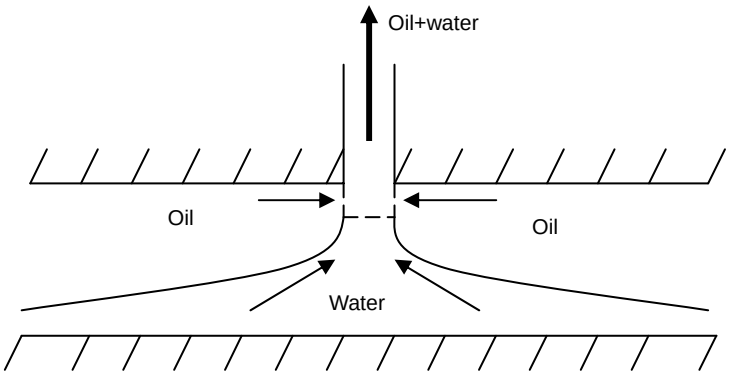

(c) Aquifer-supported reservoir

Figure 2.1 Three types of ideal flow mechanisms

Several simulation models have been developed for these numerical experiments. With these models, different kinds of transient data were generated for each defined flow mechanism. Considering the relative permeability curve, the traditional P-M method has been further modified to obtain the absolute permeability. This result can be used to update the reservoir model for management.

2.2 Problem of multiphase flow and P-M approach

According to the Buckley-Leverett theory [Buckley, S.E., 1941[94]; 1943[95]], oil-water simultaneous flow is linear, immiscible, one dimension flow, in every cross section the total flow rate $q_t = q_o + q_w$ is constant. The ratio of the flow of water under different water saturation conditions is termed the fractional flow, f_w where:

$$f_w = \frac{q_w}{q_o + q_w} = \frac{1}{1 + \frac{\mu_w k_{ro}}{\mu_o k_{rw}}} \tag{2.1}$$

Because the relative permeability is a function of saturation and time, so in a multiphase flow system, the permeability of each phase varies with time. According to the relative permeability curve (**Figure 2.2**), the total mobility curve versus water cut can be generated (**Figure 2.3**). Under low oil viscosity conditions, the total mobility decreases firstly with water-cut and then increases at high water-cut, but for middle-high oil viscosity, the total mobility increases constantly.

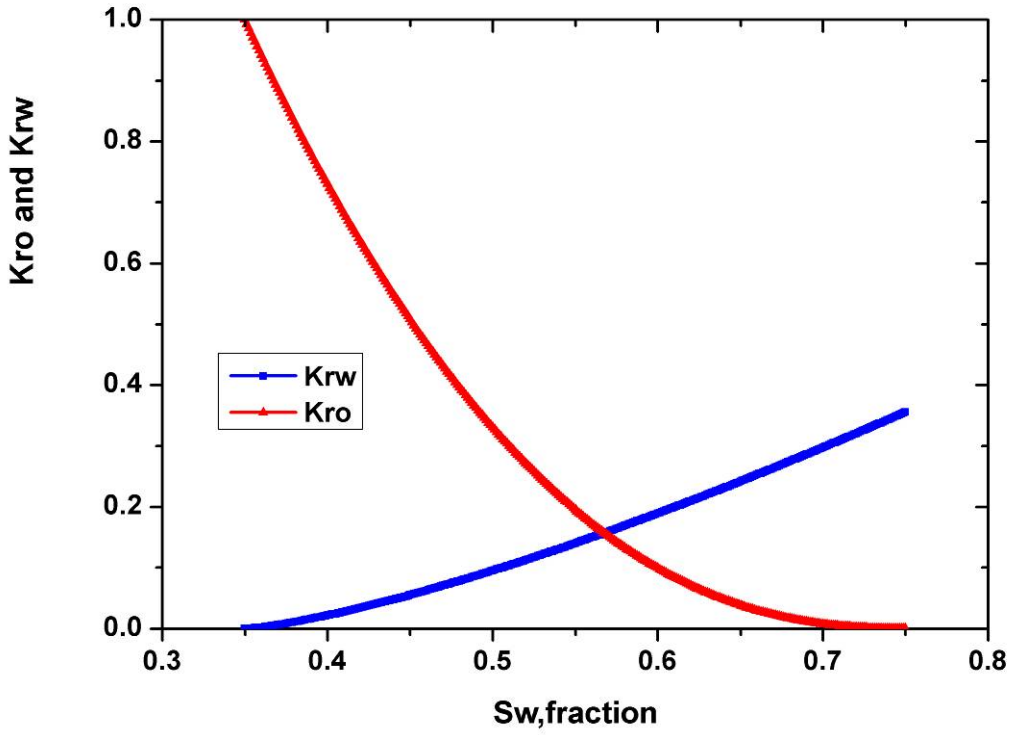

Figure 2.2 The Oil/water Relative Permeability Curve

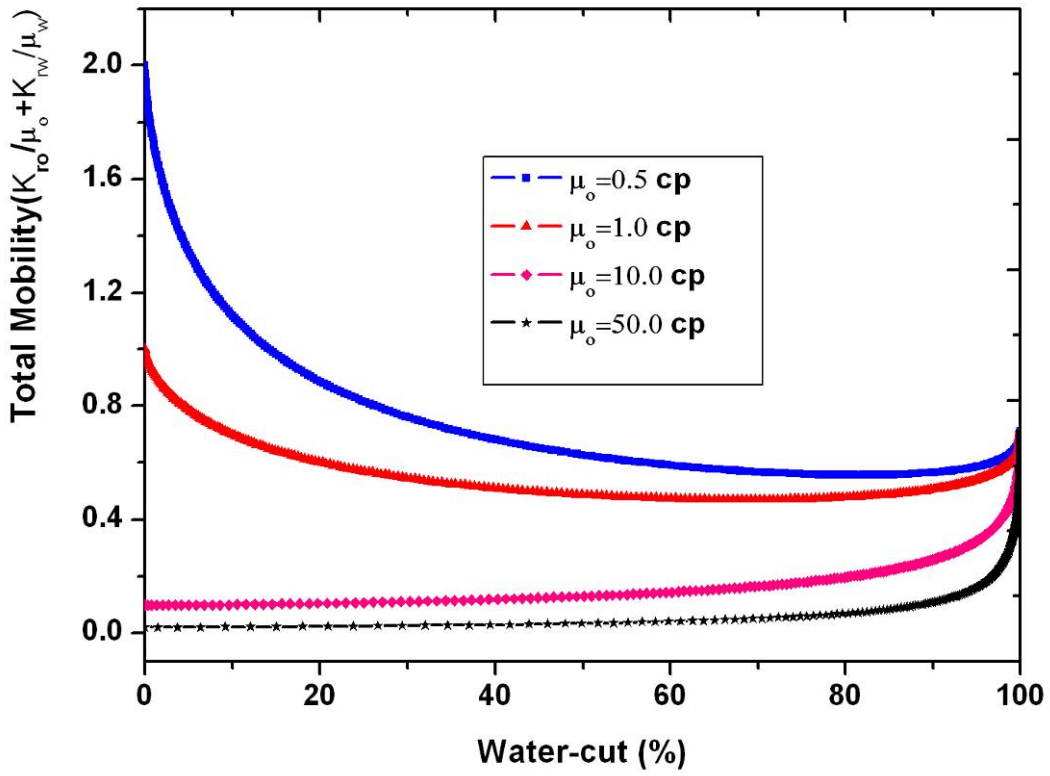

Figure 2.3 This figure shows the total mobility curve under different water-cut conditions.

Figure 2.3 shows that the total mobility curve decreases at first and then increases as the water-cut increases with low oil viscosity conditions. However, for high oil viscosity conditions, the total mobility increases with increased water-cut.

For well test analysis, the major difference between single phase and multiphase flow is the evaluation of Kh/μ and the total compressibility (C_t). For single phase, Kh/μ and C_t are constant, but for multiphase flow, it is difficult to determine these values under some water saturation conditions, because Kh/μ and C_t of each fluid phase changes with water saturation and production time.

According to **Equation 1.9**, if the pressure gradient, liquid saturation gradient and capillary pressures are ignored, the P-M approach can be used to interpret multiphase flow well tests. But from the results of the P-M method, only phase effective permeability can be obtained. This result cannot be used directly to update the

reservoir simulation model, where total mobility of fluid changes with production time and water-cut. If the absolute permeability can be obtained, the relative permeability needs to be derived. This is a challenging task for engineers. However, numerical well testing can help to address the problem.

2.3 Numerical Simulation model

In this section, a 3D model was built to simulate multiphase flow in order to derive a numerical solution. At the same time, the well test data generated by reservoir simulations in oil-water reservoirs with different flow mechanisms conditions was used to verify qualitatively the accuracy and the practicality of the P-M approach.

Data used for the simulation model are summarized in **Table 2.1**. **Figure 2.4** and **Figure 2.2** are the basic radial flat model and the relative permeability curve.

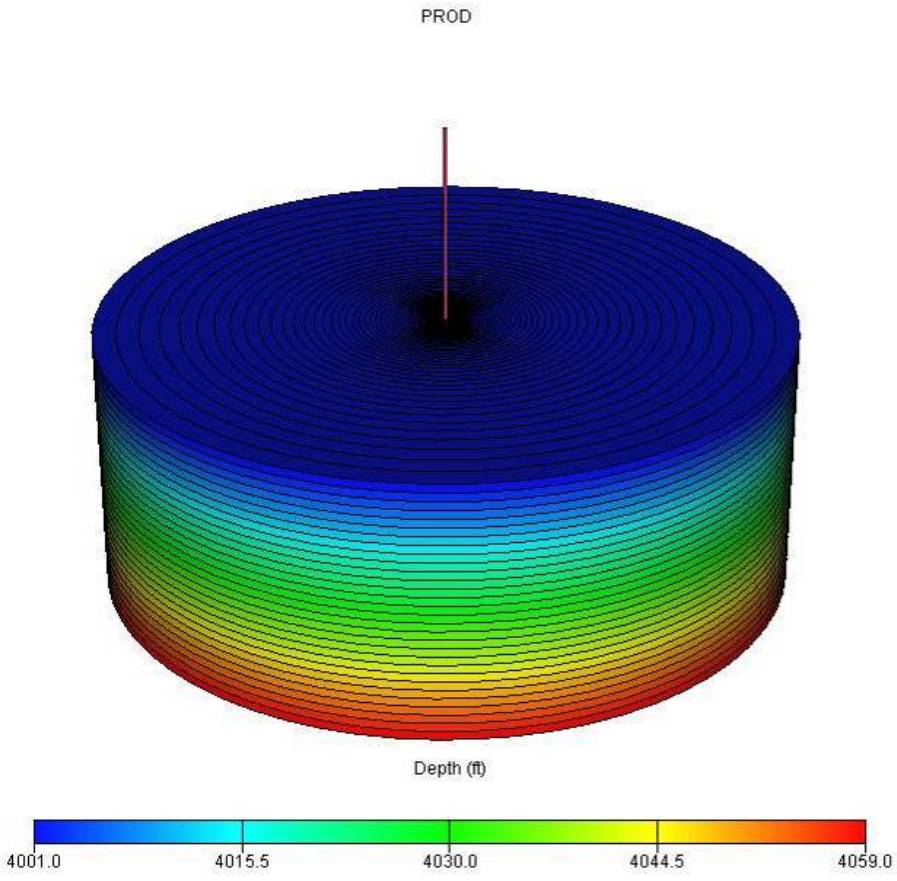

Figure 2.4 The basic top structure model

Table 2.1 Parameters of base model

Radial grid cells	100
Theta grid cells	1
Z grid cells	30
Well radius, ft	0.5
External Radius, ft	5000
Porosity, %	25
Thickness, ft	60
Permeability, mD	200
Kv/Kh ratio	1
Oil viscosity	1cp
Oil volume factor	1.05
Water viscosity, cp	0.5
Water volume factor,	1
Oil compressibility, 1/psi	6.5e-6
Water compressibility, 1/psi	3e-6
Rock compressibility, 1/psi	3e-6
Connate water saturation	0.35
Residual oil saturation	0.25
Well location	Centre
Perforation	Full penetration

2.4 Analysis of Dispersed Flow with Uniform Saturation

Currently, the P-M approach is applied widely to oil-water reservoirs, but it is difficult to obtain the absolute permeability under different water-cuts. In this situation, the total mobility normalization is introduced to dispersed flow reservoirs with uniform

saturation. The idea of total mobility normalization is that the multiphase total mobility from the P-M method at current water-cut can be normalized to the effective oil permeability at connate water saturation with the help of the total mobility curve.

According to normalized total mobility, the term, Z is introduced.

$$Z = \left(\frac{K_o}{\mu_o}\right)_{S_{wi}} \Big/ \left(\frac{K}{\mu}\right)_t \tag{2.2}$$

Where, $\left(\frac{K}{\mu}\right)_t = \frac{162.6 q_t B_t}{m} = k_{Abs}\left(\frac{K_{ro-S_w}}{\mu_o} + \frac{K_{rw-S_w}}{\mu_w}\right)$, is the total mobility under a current water-cut condition.

$\left(\frac{K_o}{\mu_o}\right)_{S_{wi}}$, is oil mobility under a connate water condition.

According to **Equation 2.2**, under a connate water saturation condition, the effective oil permeability may be obtained. This result can be used to update the simulation model.

$$K_{abs} \approx K_{eff\_S_{wi}} = Z\left(\frac{K}{\mu}\right)_t \mu_{oil} \tag{2.3}$$

According to relative permeability and fluid viscosity, the theoretical Z curve can be generated (**Figure 2.5**).

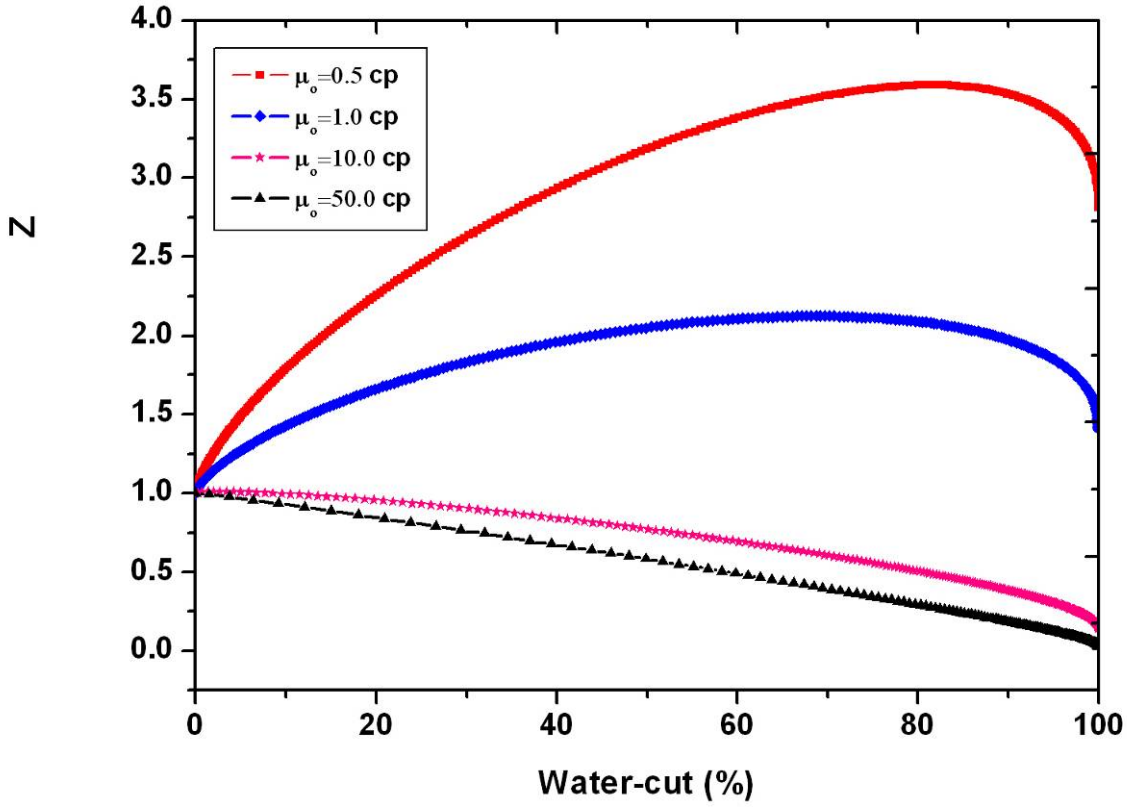

Figure 2.5 This figure shows the normalized total mobility curves for different oil viscosities. It shows that the normalized total mobility curve goes up firstly and then goes down with the water-cut increasing for the low oil viscosity condition, but for the high oil viscosity condition, the normalized total mobility decreases with the water-cut increasing.

2.4.1 Well test Analysis

In order to evaluate the error of normalized total mobility, sensitivities on different oil viscosity cases (0.5cp, 1cp, 10cp, 50cp), with changing model initial water saturation were carried out. Pressure draw down (DD) was obtained in each case and analyzed using the PanSystem software.

The radial flow was determined from a log-log plot, and then the slope of the straight line from the semi-log plot and the total mobility ($\left(\frac{K}{\mu}\right)_t = \frac{162.6 q_t B_t}{m}$) were obtained

using the current water-cut. Finally, using $\left(\frac{K_o}{\mu_o}\right)_{S_{wi}}$, the Z value can be obtained.

Compared to theoretical the Z values, the error is very small (**Figure 2.6**). So this normalized total mobility approach can be applied for multiphase well test analysis.

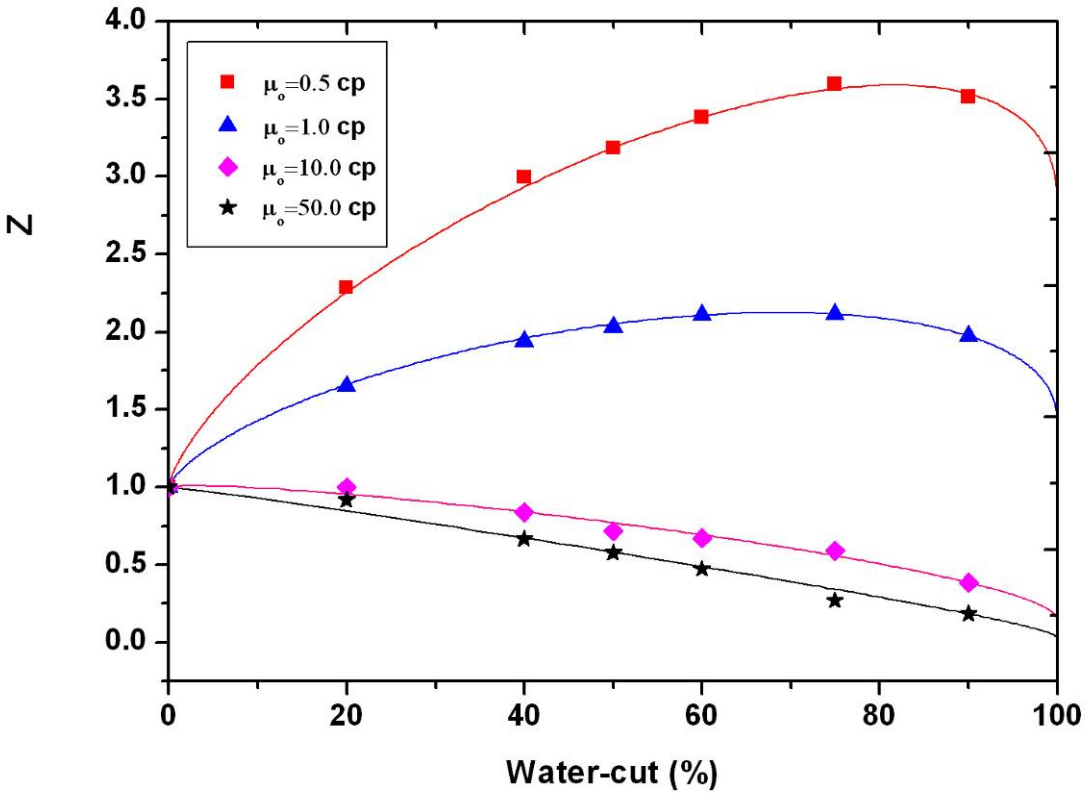

Figure 2.6 This figure is the comparison between Z theoretical curves (solid line) and simulated results (points) under different oil viscosity conditions. It shows that the simulated results are close to theoretical curves.

2.4.2 Sensitivity studies on reservoir parameters

2.4.2.1 Impact of permeability

In order to test the influence of permeability, three cases were designed, keeping the homogeneous nature of model, and changing the permeability of model from 20md to 2000md. The plot of mobility ratio (Z) versus water-cut was derived. **Figure 2.7** shows that the influence of the permeability is very small.

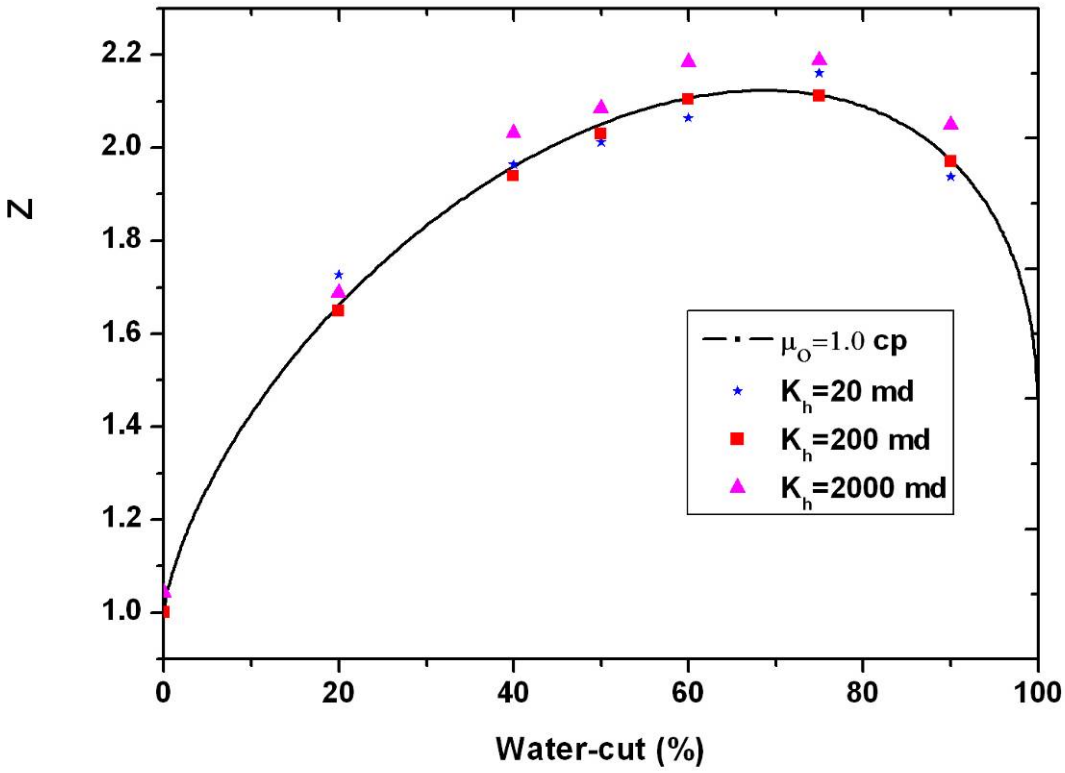

Figure 2.7 This figure is the comparison between Z theoretical curves and simulated results under different absolute permeability conditions. It shows that the simulated results are close to those theoretical curves.

2.4.2.2 Impact of reservoir heterogeneity

A radial, layered model was built, which has homogeneous in horizontal directions and heterogeneous in the vertical direction. The layer permeability varied from 20 mD to 2000 mD. According to the simulation results under a different water-cut, a Z curve was generated. **Figure 2.8** shows that in such complex reservoirs, the mobility ratio (Z) corresponds closely to the theoretical mobility ratio curve. This also means that vertical permeability has a very small impact on the reservoir mobility ratio, due to the domination of the radial flow.

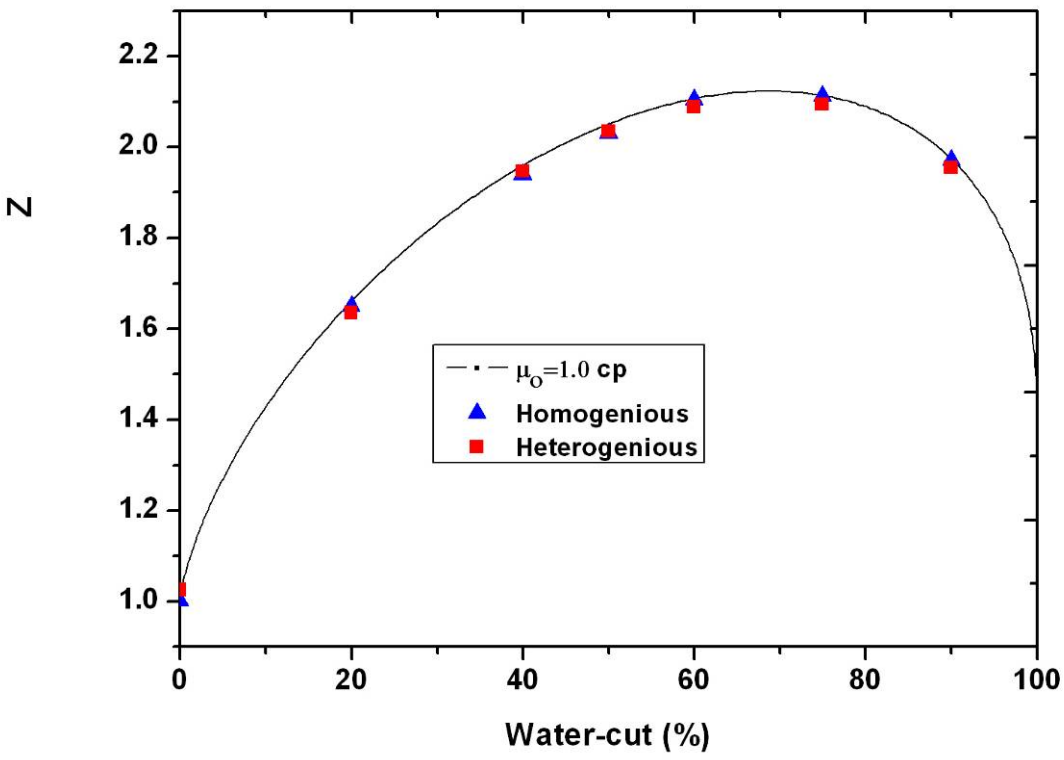

Figure 2.8 This figure is the comparison between the Z theoretical curves and the simulated results under different reservoir heterogeneities. It shows that the simulated results are close to the theoretical curves.

2.4.2.3 Impact of relative permeability

As the trend of the Z curve depends on the relative permeability and viscosity of fluids, the accuracy of relative permeability curves is very important for this method.

Three cases with different relative permeability curves were designed. **Figure 2.9** shows case 1 as base case. The oil relative permeability of case 2 is less than that in the base case, and the water relative permeability of case 3 is less than that in the base case. Z curves for all cases are presented in **Figure 2.10**. According to the Z curves, it can be seen that small changes of water relative permeability had a large effect on the mobility ratio, but for the oil relative permeability, they just led to a small variation in the mobility ratio. (**Table 2.2**)

Table 2.2 Average errors in Z calculation in cases of incorrect relative permeability (According to the Z values for Case1, Case2 and Case3 under different oil viscosity and water-cut conditions, the relative errors ($\frac{V_{case2}-V_{case1}}{V_{case1}}$ or $\frac{V_{case3}-V_{case1}}{V_{case1}}$) can be obtained under different water-cut conditions, then the average errors can be obtained.)

Cases	Underestimation of water relative permeability (case3)	Underestimation of oil relative permeability (case2)
Oil viscosity 0.5 cp	36.1%	22.9%
Oil viscosity 1.0 cp	33.4%	17.7%
Oil viscosity 10 cp	38.5%	13.3%
Oil viscosity 50 cp	27.1%	22.3%

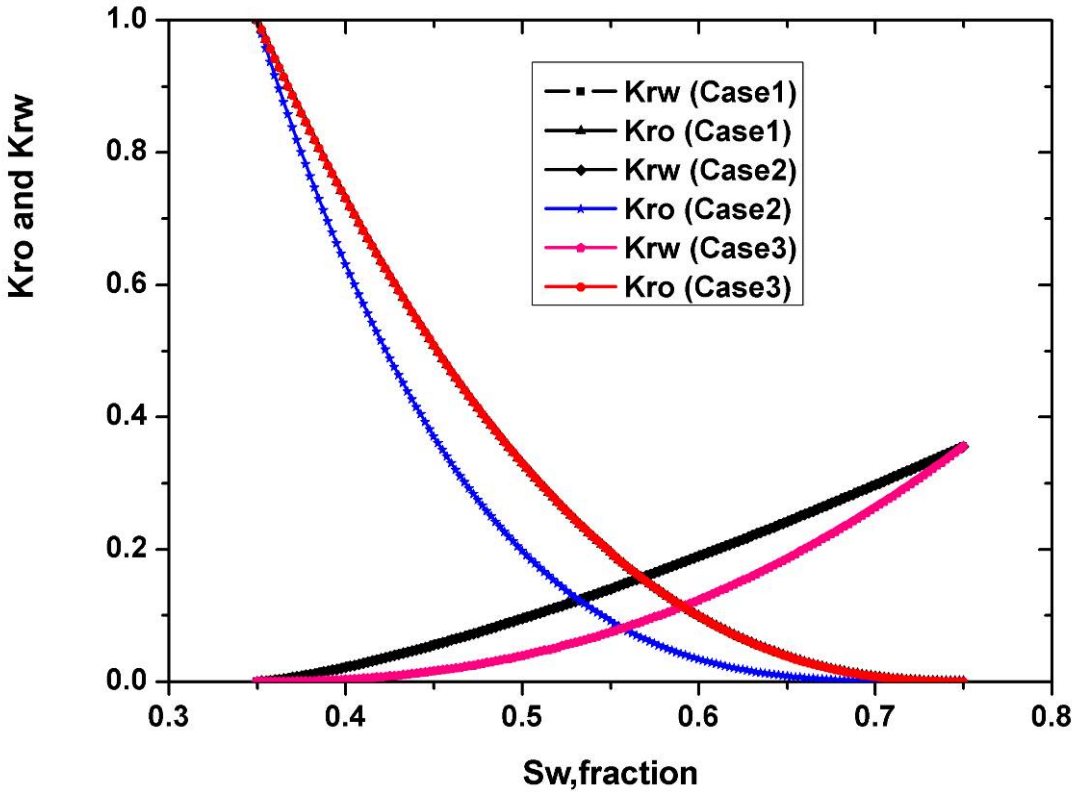

Figure 2.9 The oil/water relative permeability curves for three cases

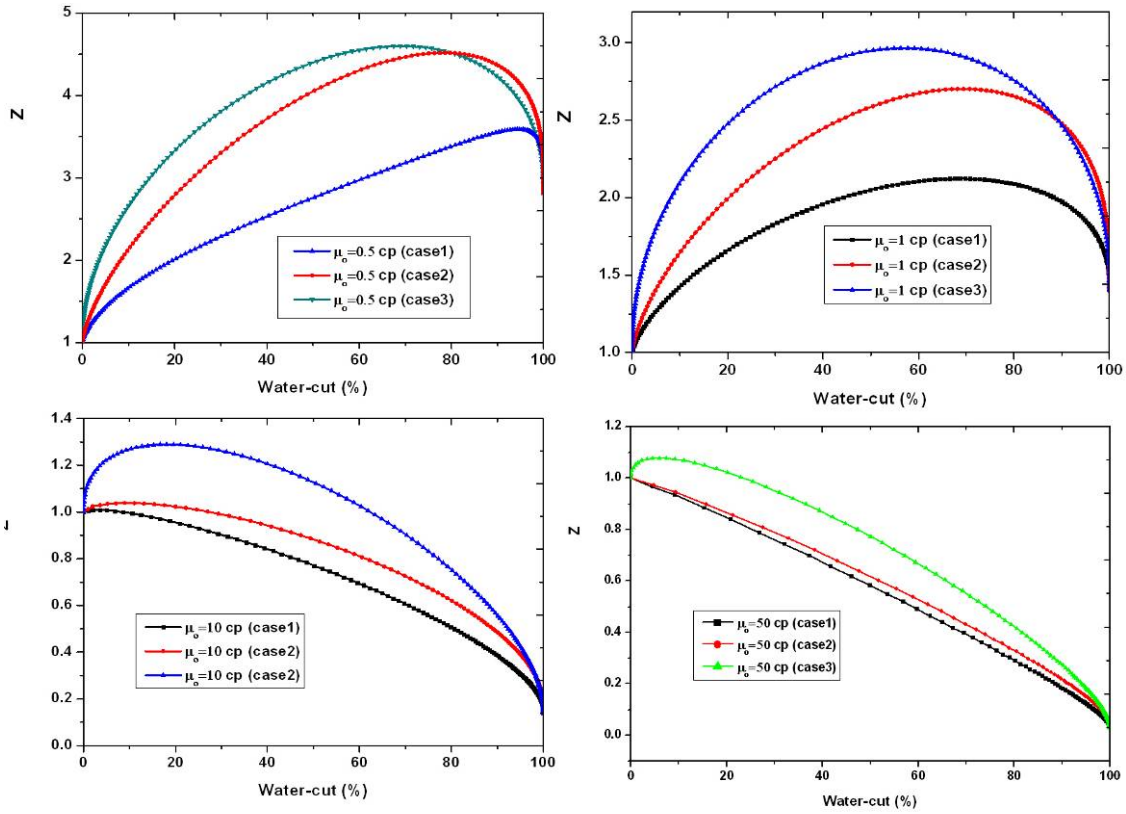

Figure 2.10 This figure shows the normalized total mobility curves with different relative permeability curves under different oil viscosities. It shows that there is a big difference in the normalized total mobility for different oil viscosities and different relative permeability curves.

2.4.3 Summary

According to the studies above, one can see that the mobility normalization approach yields good results for oil effective permeability at connate water saturation under a different water-cut, but this approach is quite sensitive to the accuracy of the relative permeability.

2.5 Analysis of Segregated Flow

The simplest reservoir with segregated flow is the homogeneous reservoir with aquifer at the bottom, or the layered reservoir with a high permeability layer, with perforations across all production formation thickness. The BHP under different water-cut conditions can be obtained through changing the oil water contact (OWC) location or water saturation of the high permeability layer. (**Figure 2.11**)

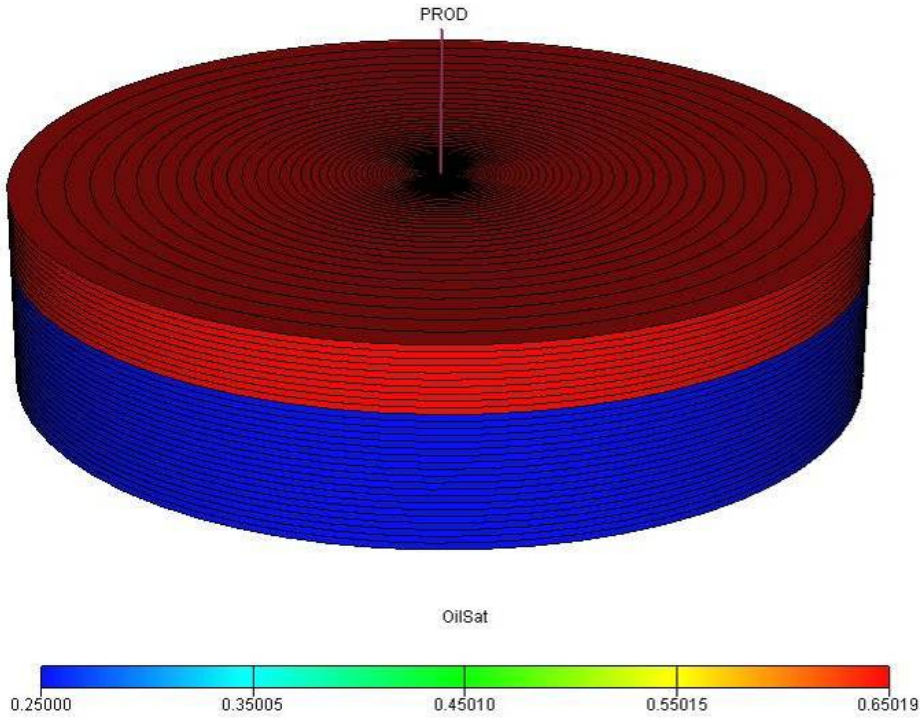

Figure 2.11 The segregated flow model

2.5.1 Modified P-M method

In this case, a modified P-M method is introduced first before presenting the study results.

It is known that there is an analytical solution of single phase for DD. The approximation equation is:

$$P_{wf} = P_i - \frac{162.6qB\mu}{Kh}\left[\log\frac{0.000264Kt}{\phi\mu C_t r_w{}^2} + 0.80908 + 2s\right] \qquad (2.4)$$

In the case of zero influence of capillary pressure, and oil /water flowing separately from the uniform formation, then for oil and water, **Equation 2.4** can be written:

$$P_{wf} = P_i - \frac{162.6 q_o B_o \mu_o}{K_{abs} K_{ro}(S_{wi}) h_o}\left[\log\frac{0.000264 K_{abs} K_{ro}(S_{wi}) t}{\phi \mu_o (C_t)_o r_w^{\,2}} + 0.80908 + 2s\right] \tag{2.5}$$

$$P_{wf} = P_i - \frac{162.6 q_w B_w \mu_w}{K_{abs} K_{rw}(S_w) h_w}\left[\log\frac{0.000264 K_{abs} K_{rw}(S_w) t}{\phi \mu_w (C_t)_w r_w^{\,2}} + 0.80908 + 2s\right] \tag{2.6}$$

Equation 2.5 and **Equation 2.6** are rearranged as:

$$\begin{aligned}(qB)_t &= q_o B_o + q_w B_w \\ &= \frac{K_{abs} K_{rw}(S_w) h_w}{162.6 \mu_w\left[\log\frac{0.000264 K_{abs} K_{rw}(S_w) t}{\phi \mu_w (C_t)_w r_w^{\,2}} + 0.80908 + 2s\right]}\left(P_i - P_{wf}\right) \\ &+ \frac{K_{abs} K_{ro}(S_{wi}) h_o}{162.6 \mu_o\left[\log\frac{0.000264 K_{abs} K_{ro}(S_{wi}) t}{\phi \mu_o (C_t)_o r_w^{\,2}} + 0.80908 + 2s\right]}\left(P_i - P_{wf}\right)\end{aligned} \tag{2.7}$$

For solution of P-M method:

$$(qB)_t = \frac{\lambda_t h}{162.6\left[\log\frac{0.000264 \lambda_t t}{\phi C_t r_w^{\,2}} + 0.80908 + 2s\right]}\left(P_i - P_{wf}\right) \tag{2.8}$$

Comparing with **Equation 2.7** and **Equation 2.8**, the following equation can be obtained:

$$\lambda_t = \frac{K_{abs} K_{ro}(S_{wi})}{\mu_o} \cdot \frac{h_o}{h} + \frac{K_{abs} K_{rw}(S_w)}{\mu_w} \cdot \frac{h_w}{h} \tag{2.9}$$

Through well test analysis, the total mobility can be determined, and absolute

permeability can be obtained:

$$K_{abs} = \frac{\lambda_t}{\frac{K_{ro}(S_{wi})}{\mu_o} \cdot \frac{h_o}{h} + \frac{K_{rw}(S_w)}{\mu_w} \cdot \frac{h_w}{h}} \tag{2.10}$$

According to **Equation 1.12**, the skin factor can be modified:

$$S = 1.151\left\{ \frac{\Delta P_{1hour}}{m} - \log\left(\frac{\left(\frac{Kh}{\mu}\right)_t}{\phi(c_t h)_o r_w^2 + \phi(c_t h)_w r_w^2} \right) + 3.23 \right\} \tag{2.11}$$

Where, $(c_t)_o$ and $(c_t)_w$ are oil total compressibility and water total compressibility, 1/Psi;

$$(C_t)_o = C_f + C_o(1-S_{wi}) + C_w S_{wi}; (C_t)_w = C_f + C_o(1-S_{wi}) + C_w S_w$$

For **Equation 2.10**, the key problem is how to determine $K_{ro}(S_{wi})$, $K_{rw}(S_w)$, h_o and h_w.

In order to determine these terms, the saturation logging and the relative permeability curve need to be used and analysis procedures are as following:

- Firstly, determine h_o and h_w from the saturation log,
- Secondly, determine S_{wi} of oil formation and S_w of water swept formation,
- Thirdly, using laboratory measured the relative permeability curve, $K_{ro}(S_{wi})$ and $K_{rw}(S_w)$ can be found, and the absolute permeability can be obtained.

2.5.2 Evaluation of modified P-M

If single-phase flow theory is used to interpret multiphase flow, **Figure 2.12** shows that when water cut is less than 20% or more than 80%, single phase oil or single phase water can be used respectively to interpret the well test and the error of the analysis is small.

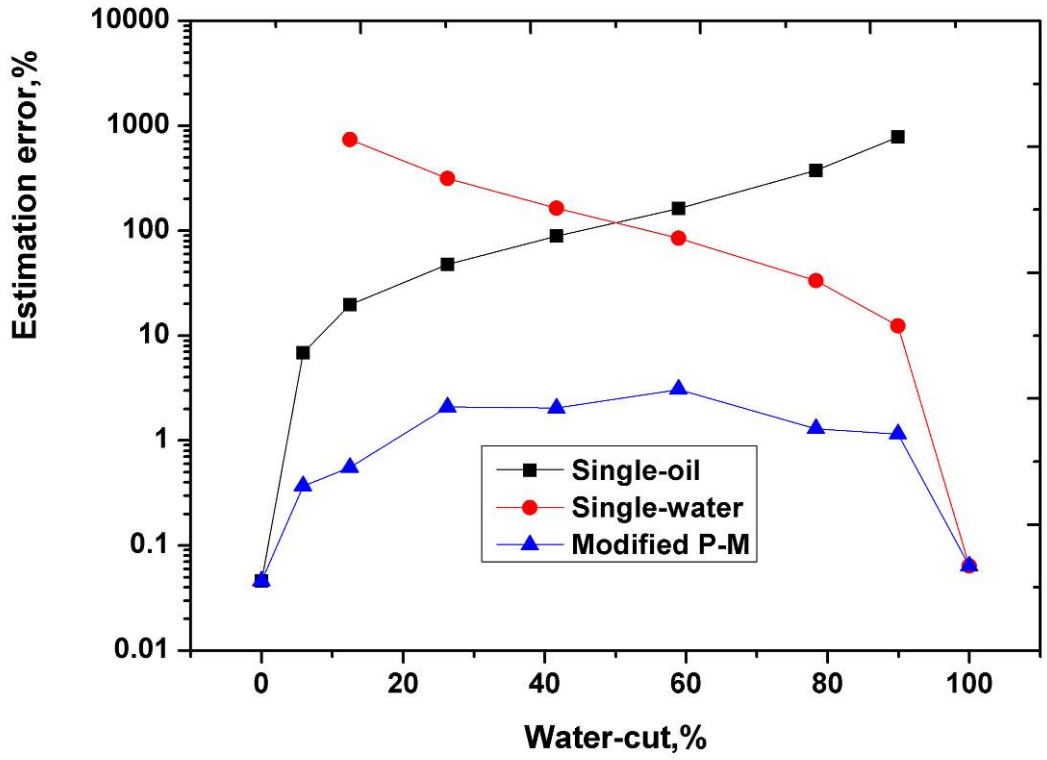

Figure 2.12 The errors of absolute permeability estimated by single phase and modified P-M method

If using tradition the P-M method to interpret and obtain the phase permeability of oil and water, then by considering the relative permeability curve, the absolute permeability can be obtained.

$$K_l = \frac{162.6 q_l \mu_l B_l}{m h_l} \tag{2.12}$$

Where, l stands for any phase.

In contrast to the traditional P-M method, a modified P-M approach can get more accurate results. (**Figure 2.13**)

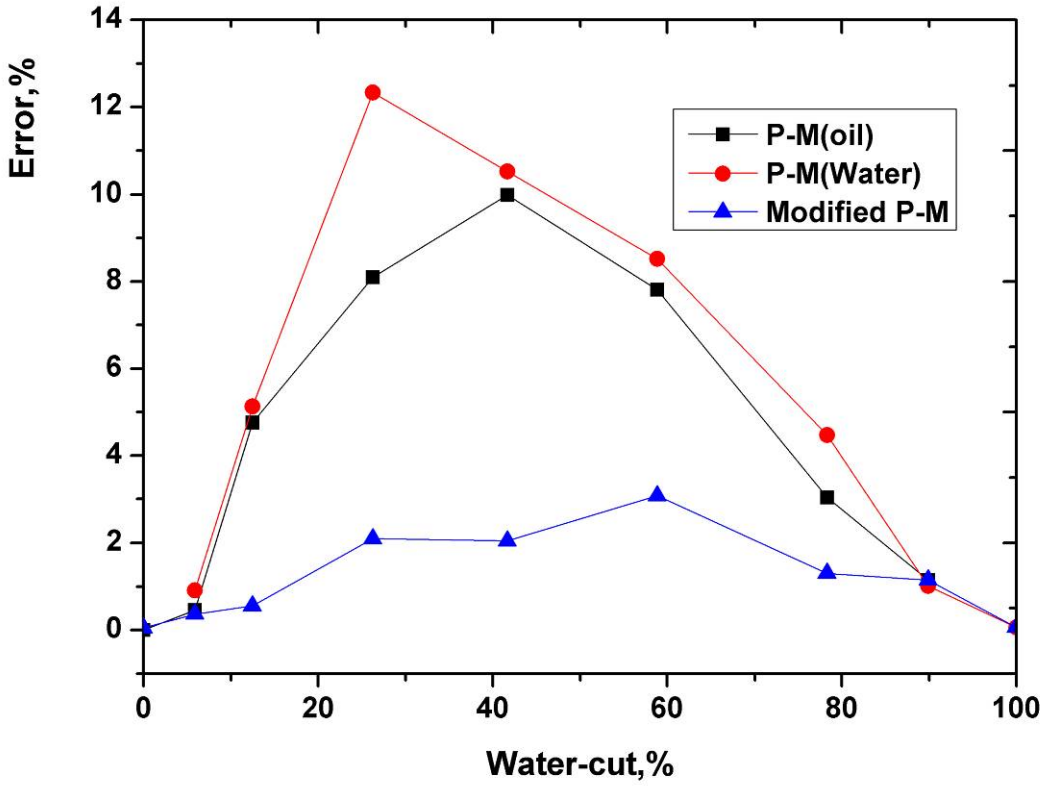

Figure 2.13 The errors of absolute permeability estimated by the traditional P-M and a modified P-M method.

But for the skin factor, the input value of the model was 0. Using **Equation 2.11** to interpret, **Figure 2.14** shows that the skin factor was overestimated. When the water-cut reached 45%, the error of the skin factor is very big.

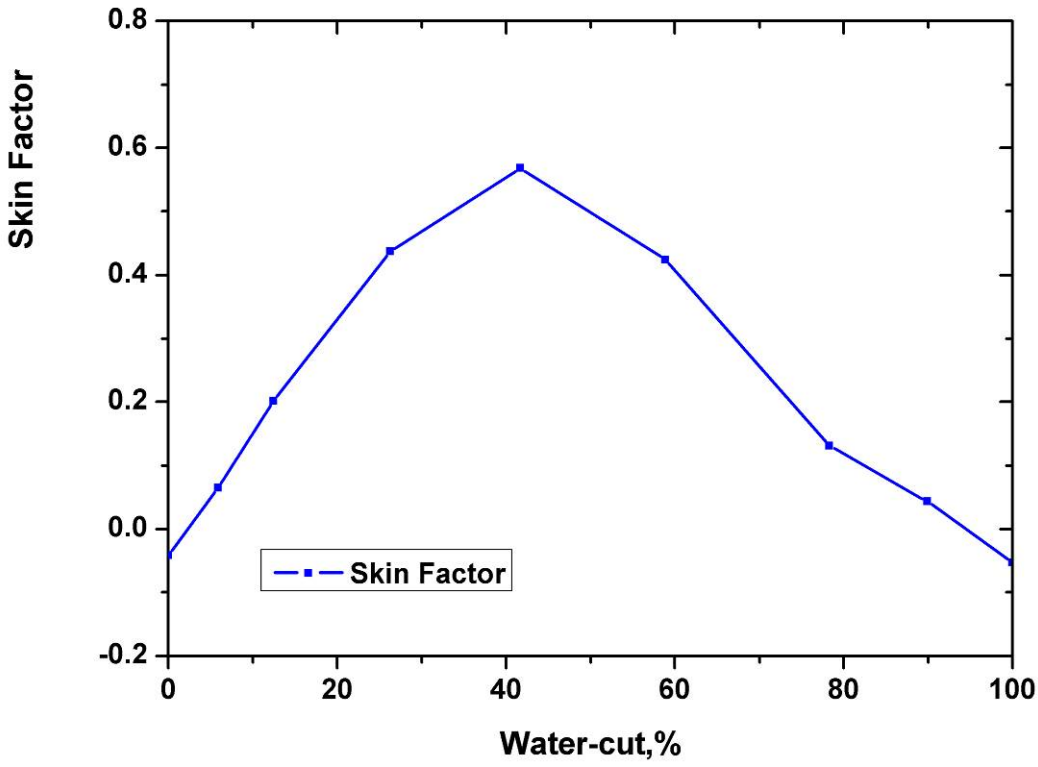

Figure 2.14 This figure shows the calculation results for the skin factor under different water-cut conditions by the modified P-M method.

2.6 Analysis of Oil Reservoir with Aquifer support

For pressure transient testing of a well partially penetrating a single-phase reservoir, two semi-log straight lines were developed. The slope of the first line represents the radial flow to the penetrated interval. Using this slope, the reservoir permeability can be obtained, but because of the well bore storage effect, this short semi-log straight line may not occur in most cases. After the first radial flow, spherical flow will appear due to partial penetration. Finally, the second slope in semi-log plot will occur, which stands for the pseudo-radial flow in the entire formation (Nabor, G.W., *et al*., 1964[122]; Miller, R.T., *et al*., 1973[124]; Gomas, E.E., 1975[123]; Al-Khalifa, A.J., *et al*., 1988[12]; Al-Khalifa, A.J., et al., 1989[13]). (**Figure 2.15**)

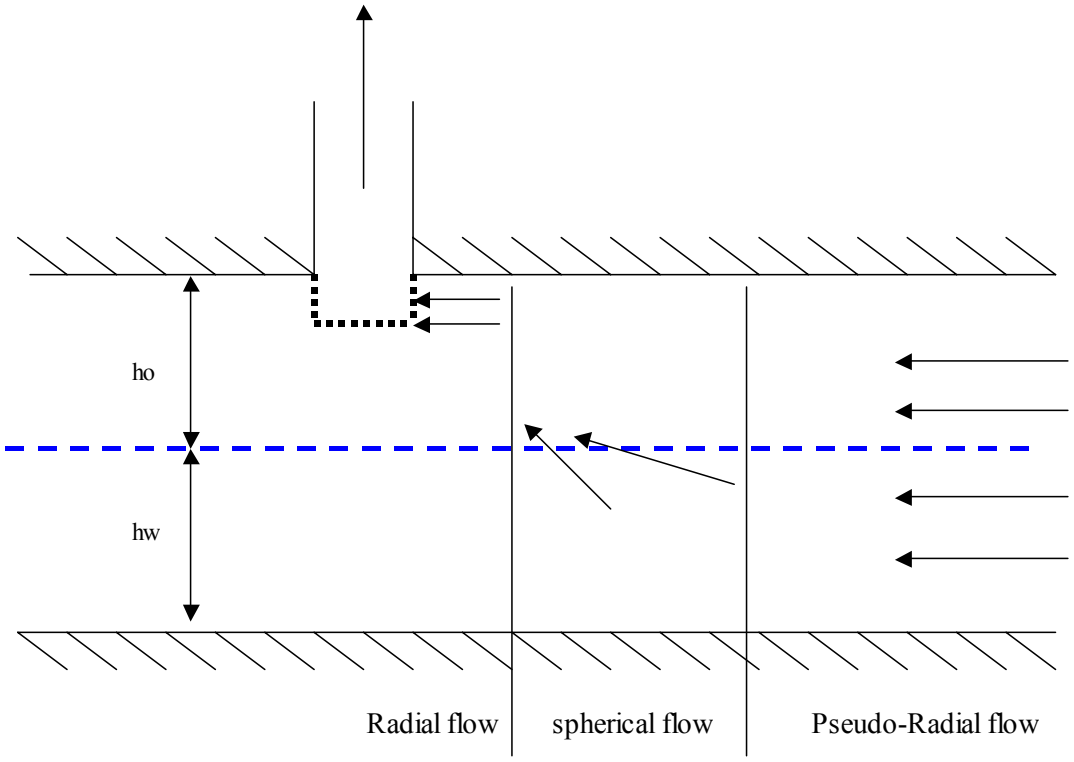

Figure 2.15 Schematic diagram of the multi-flow in aquifer-supported reservoir

2.6.1 Empirical solution

Unlike the single-phase system, in an aquifer-supported reservoir, the slope of the second semi-log straight line has some characteristics. The reason is that the fluids have different properties. Al-Khalifah (1989[13]) used many numerical models to study well test problems under different reservoir conditions and finally derived a semi-empirical analytical solution:

$$\left[\frac{kh}{\mu}\right]_o + \left[\frac{kh}{\mu}\right]_w \sqrt{\frac{(\mu c_t)_w}{(\mu c_t)_o}} = \frac{162.6 q_o B_o}{m_2} \qquad (2.13)$$

Assuming K to be the same in both oil and water formations and water formations with virgin aquifer, so $K_{ro(Swi)}$=1 and $K_{rw(Sw=100\%)}$=1, the **Equation 2.13** can be rearranged as:

$$K = \frac{\dfrac{162.6 q_o B_o}{m_2}}{\left[\dfrac{h}{\mu}\right]_o + \left[\dfrac{h}{\mu}\right]_w \sqrt{\dfrac{(\mu c_t)_w}{(\mu c_t)_o}}} \tag{2.14}$$

This permeability may approximately equal to reservoir absolute permeability. But if water formation is swept, using **Equation 2.14** to estimate reservoir permeability, it will result in a big error.

So **Equation 2.13** needs to be modified. Considering the relative permeability, **Equation 2.13** can be written as:

$$K_{abs}\left\{\left[\frac{k_{ro(S_{wi})} h}{\mu}\right]_o + \left[\frac{k_{rw(S_w)} h}{\mu}\right]_w \sqrt{\frac{(\mu c_t)_w}{(\mu c_t)_o}}\right\} = \frac{162.6 q_o B_o}{m_2} \tag{2.15}$$

In order to study the influence of water relative permeability, three cases were designed. The endpoints of water relative permeability were 1, 0.8 and 0.35 respectively.

According to **Figure 2.16**, the slope of pseudo-radial flow straight line can be obtained. Using **Equation 2.13** and **Equation 2.15**, the absolute permeability of formation may be obtained. (**Table 2.3**)

Comparing these results, when considering relative permeability, the absolute permeability may be more accurate.

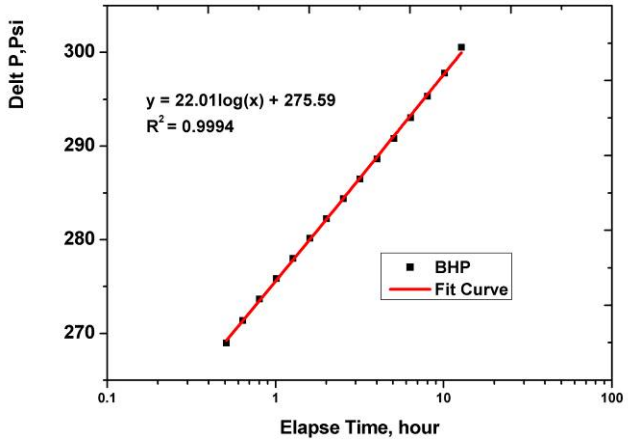

(a) The endpoint of water relative permeability is 1;

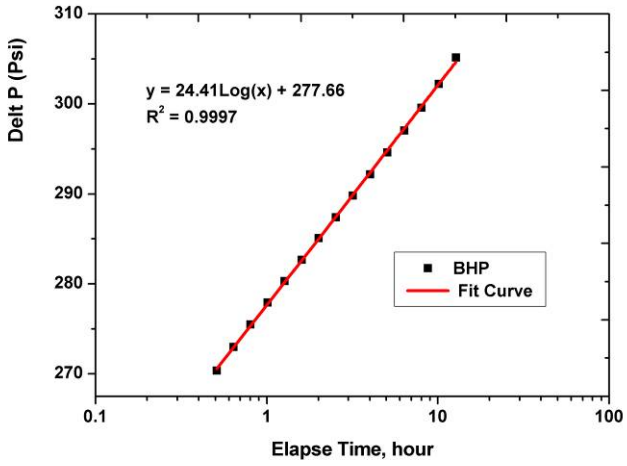

(b) The endpoint of water relative permeability is 0.8;

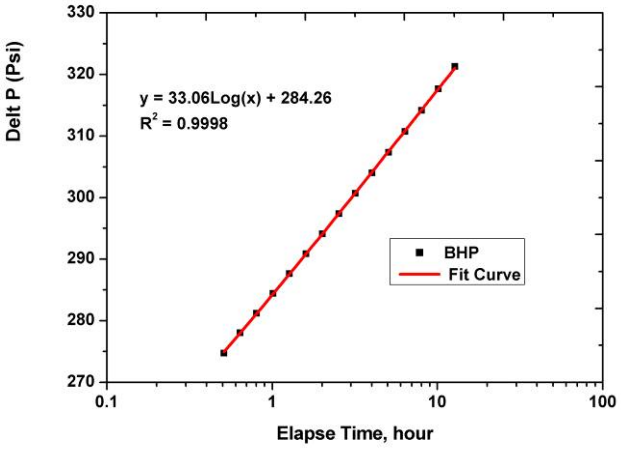

(c) The endpoint of water relative permeability is 0.35;

Figure 2.16 This figure shows the semi-log plots of DD under different endpoints of water relative permeability conditions.

Table 2.3 Segregated flow analysis results for aquifer-supported reservoir

	Input	K_{rw}=1		K_{rw}=0.8		K_{rw}=0.35	
Equation	K_{abs} (mD)	K_{abs} (mD)	Error (%)	K_{abs} (mD)	Error (%)	K_{abs} (mD)	Error (%)
2-13	20	20.57	2.85	18.55703	7.21	13.70	31.52
2-15		20.57	2.85	21.00254	5.01	22.04	10.18

2.6.2 Empirical equation application

According to the semi-empirical equation, the movement of oil-water contact can be monitored (Veeken,C.A.M., *et al*., 2000[85]; Chen,C.C., *et al*., 1996[119]). Long term data was generated through simulation, which included two DDs and two BUs (**Figure 2.17**). Selecting the first DD and the second DD for the analysis, the slope of the pseudo-radial flow straight line was obtained (**Figure 2.18**).

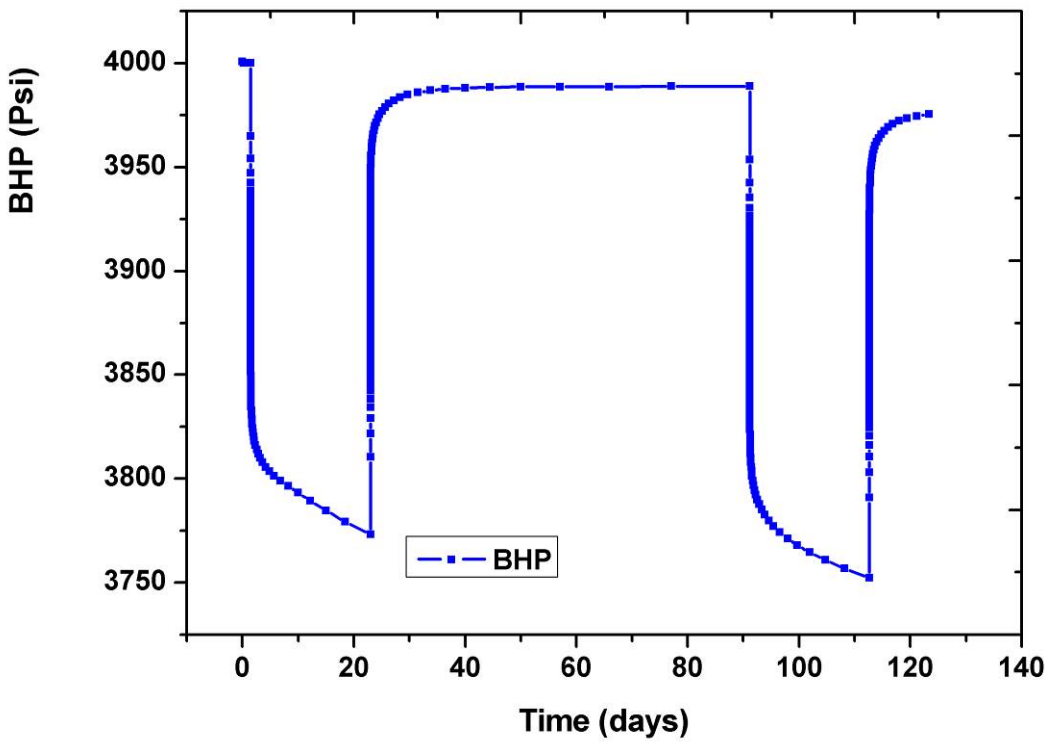

Figure 2.17 This figure shows the simulated long-term transient pressure data. The first DD and the last DD were selected for the analysis.

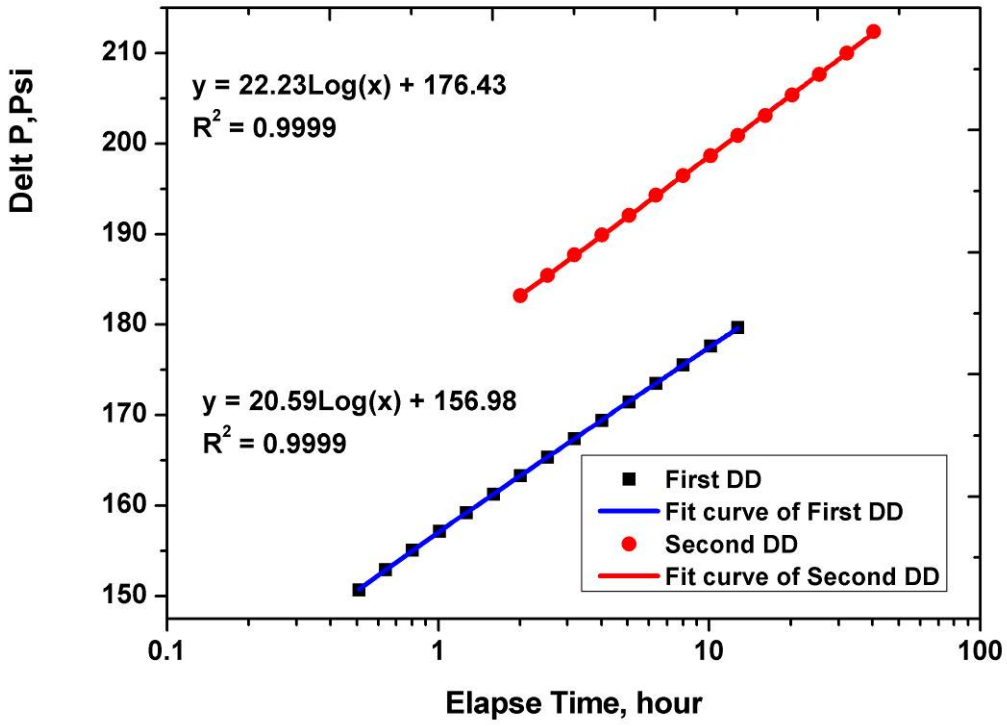

Figure 2.18 This figure shows the semi-log plots of two DDs. From these plots, the slope of pseudo-radial flow straight line can be obtained.

For the first DD, If h_o, h_w, $k_{ro(S_{wi})}$, and $k_{rw(S_w=100\%)}$ are known, **Equation 2.15** can be written as:

$$K_{abs}\left\{\frac{k_{ro(S_{wi})}h_o}{\mu_o}+\frac{k_{rw(S_w=100\%)}h_w}{\mu_w}\sqrt{\frac{(\mu c_t)_w}{(\mu c_t)_o}}\right\}=\frac{162.6q_oB_o}{m_2} \tag{2.16}$$

According to **Equation 2.16**, K_{abs} can be obtained. For the second DD, **Equation 2.16** can be written as:

$$K_{abs}\left\{\frac{k_{ro(S_{wi})}\left(h_o-\Delta h\right)}{\mu_o}+\left(\frac{k_{rw(S_w=100\%)}h_w}{\mu_w}+\frac{k_{rw(S_w)}\Delta h}{\mu_w}\right)\sqrt{\frac{\left(\mu c_t\right)_{w(S_w=100\%)}+\left(\mu c_t\right)_{w(S_w)}}{\left(\mu c_t\right)_o}}\right\}=\frac{162.6q_oB_o}{m_2} \quad (2.17)$$

According to **Equation 2.17**, if $k_{rw(S_w)}=k_{rw(S_w=100\%)}$, Δh=10.22ft, this swept zone thickness is maximal; If $k_{rw(S_w)}\neq k_{rw(S_w=100\%)}$, according to numerical solution, after the second DD, the average water saturation ($\overline{S_w}$) for the swept zone (Δh) can be obtained, using this average water saturation, from relative permeability curve, $k_{rw(S_w)}$ can be derived. From **Equation 2.17**, Δh=8.5ft, this swept zone thickness is minimal.

Hence, after producing for 112 days, the distance of movement for the oil-water contact over the entire drainage area is between 8.5ft and 10.22ft.

In the field, it is difficult to determine $k_{rw(S_w=100\%)}$ and $k_{rw(S_w)}$, so the saturation logging needs to be used to determine the saturation (S_w), then from the relative permeability curve, the water relative permeability can be obtained.

2.6.3 Well test analysis

As shown in **Figure 2.19**, before the point of 16.05 hours, the first radial flow for a penetrated interval occurs. The next is the spherical flow, and the last flow regime is the pseudo-radial flow. The 16.05 hours is the key point, after this point, the pressure derivative starts to increase. This situation does not mean that pseudo-radial flow has finished. In fact, from this point, the oil well is at water break through. The point at which the pseudo-radial flow ends is at 1031 hours. From this point, the pressure reaches its outer boundary.

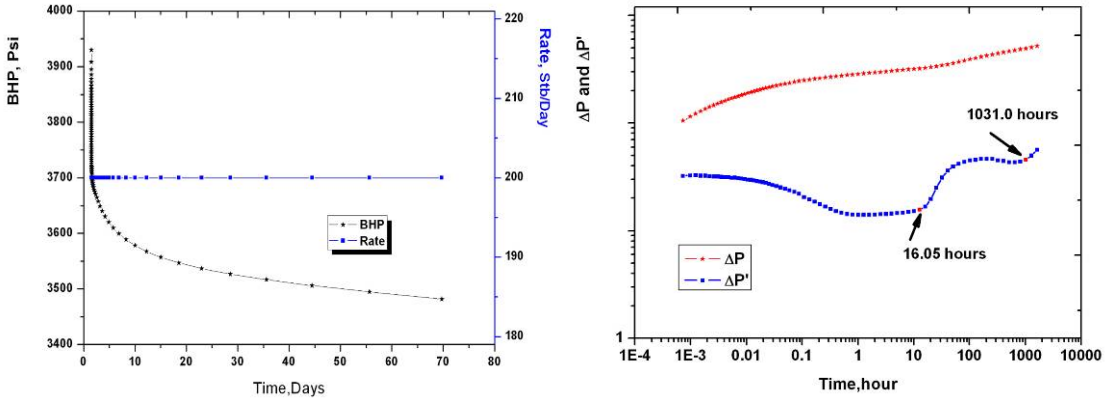

Figure 2.19 This figure shows the simulation results (Left) and the log-log plot (Right) of the DD test with partial perforation (hp=20ft). The log-log plot shows the first radial flow, the spherical flow and the pseudo-radial flow before 16.05 hours. After this point, the well is at water break through, until 1031 hours, when the pseudo-radial flow finishes and the pressure reaches its outer boundary.

But how can the changes from 16.05 hours to 1031 hours be explained? The total mobility of fluid was used to interpret the results of the well test. **Figure 2.20** shows that the total mobility of the point near the OWC starts to go up at 16.05 hours; it means that from this point the water starts to breakthrough. As shown in **Figure 2.21**, the overall average total mobility decreases, and as a result of this, the pressure derivative increases after 16.05 hours as shown on the log-log plot.

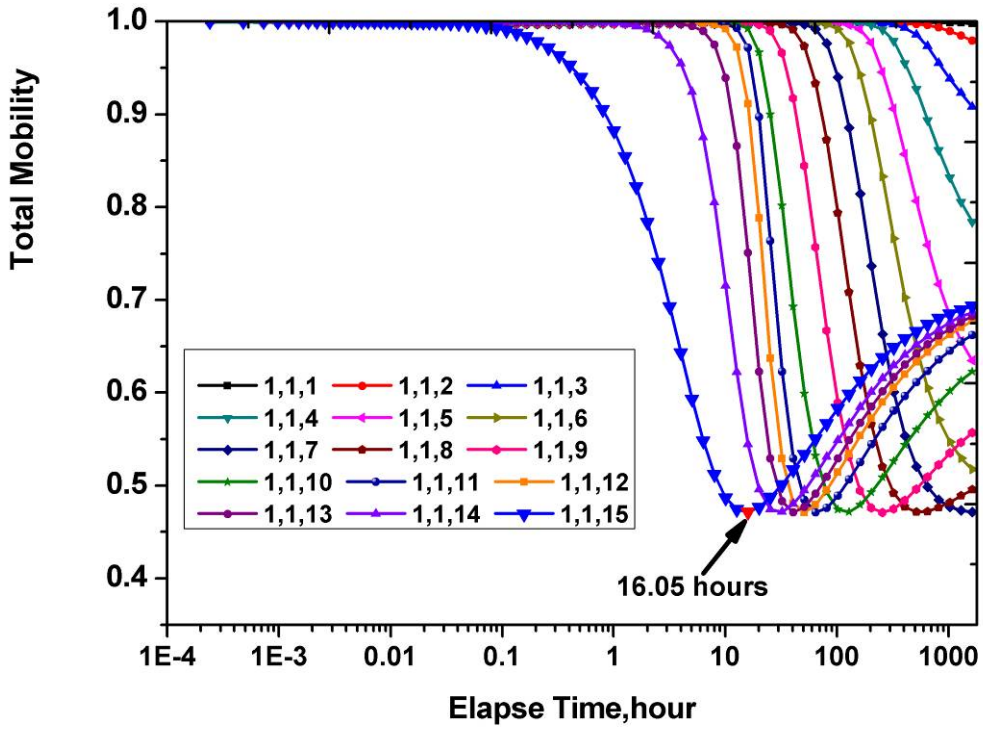

Figure 2.20 This figure is the total mobility of the fluid for every grid cell from OWC to the top of the oil formation. It shows that the kick point of total mobility for the grid to OWC is at about 16.05 hours. It represents for the point of water breakthrough.

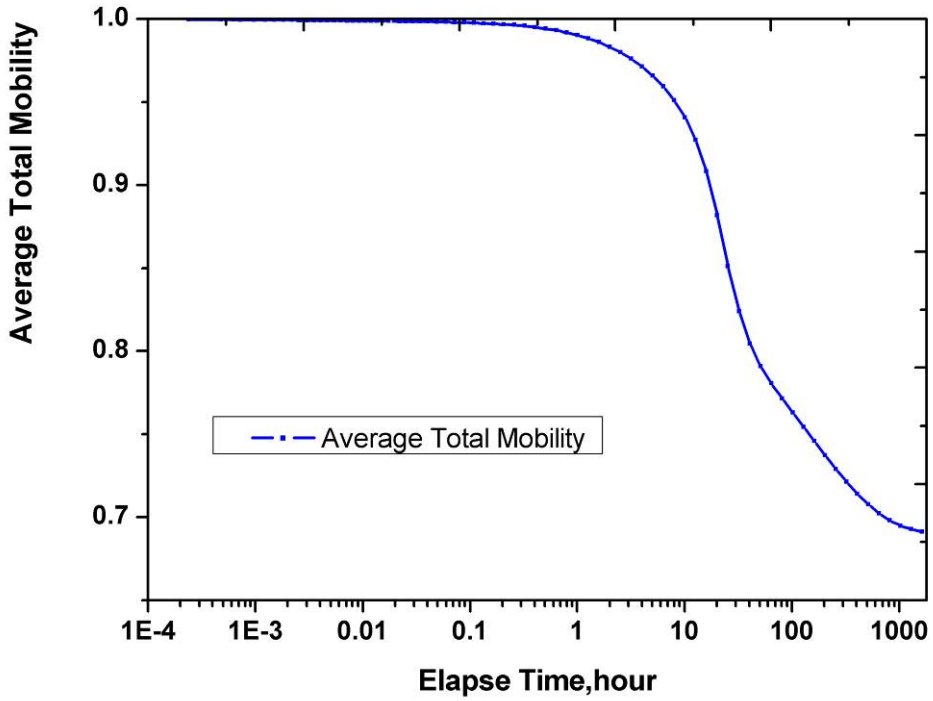

Figure 2.21 This figure is the average total mobility of the fluid for all cells from OWC to the top of the oil formation. It shows that the average total mobility decreases constantly.

2.6.4 Sensitivity studies on reservoir parameters

2.6.4.1 Influence of thickness of perforation

Three cases were designed, with perforation thickness changing from 4ft to 20ft, **Figure 2.22** shows that the perforation thickness has a big influence on pressure derivatives. If the thickness of perforation is bigger, then the first radial flow occurs easily, and the point of water breakthrough will be faster. But the change of perforation thickness did not affect the slope of the pseudo-radial flow straight line.

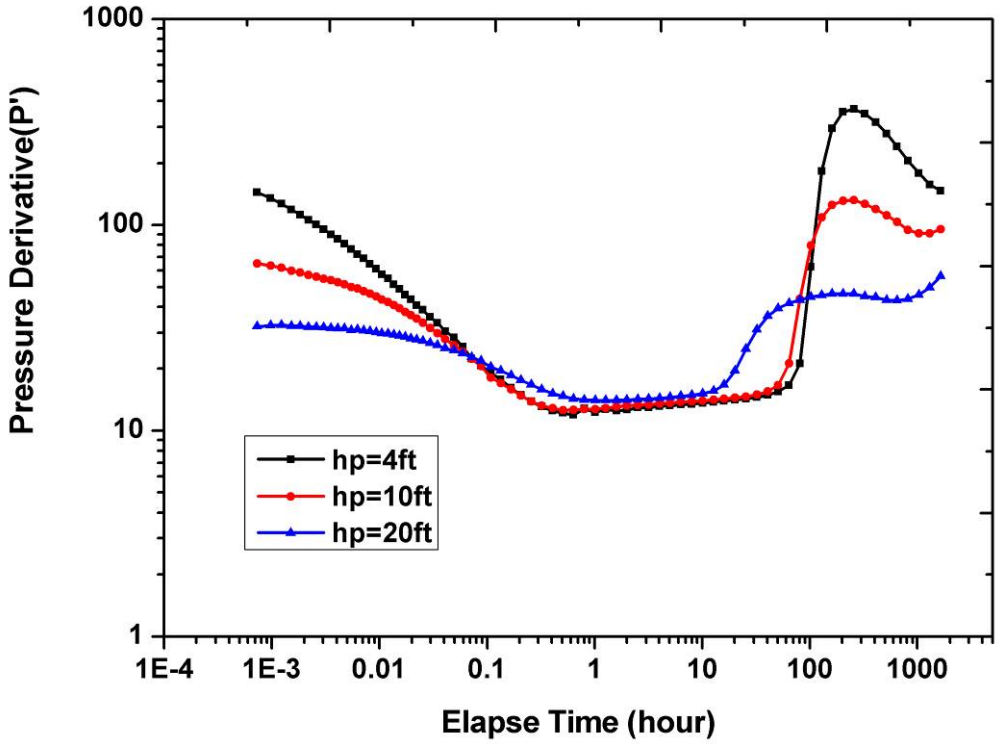

Figure 2.22 This figure shows the log-log plots of the DD tests with different partial perforation ratios (hp=20ft, hp=10ft and hp=4ft). It shows that the changing of perforation thickness does not affect the onset of pseudo-radial flow.

2.6.4.2 Influence of K_v/K_h

Considering different K_v/K_h ratios, three cases were designed (k_v/k_h=0.1, 0.5 and 1). **Figure 2.23** shows that the value of k_v/k_h affects the start or end time of the spherical flow and water breakthrough, but for the slope of pseudo-radial flow straight line, it only has a small influence.

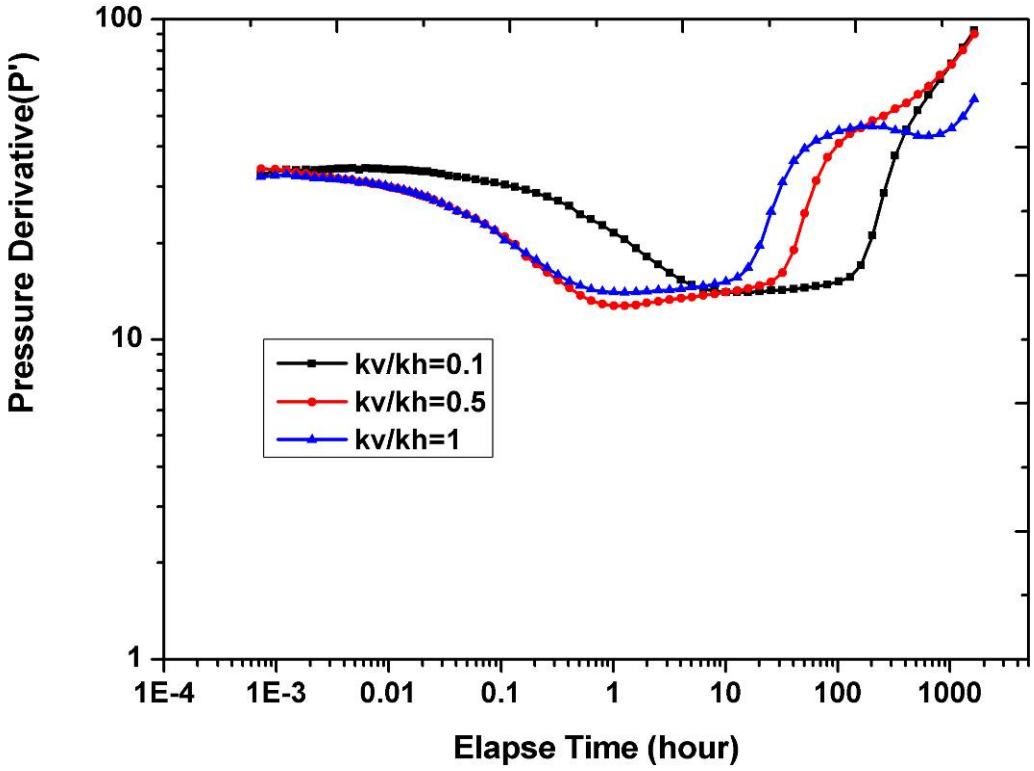

Figure 2.23 This figure shows the log-log plots of the DD tests with different Kv/Kh ratios. It shows that there is a small influence on the pseudo-radial flow due to the changing of the Kv/Kh ratio.

2.6.4.3 Influence of endpoints of the relative permeability

Changing the endpoint of relative permeability from 0.35 to 1, **Figure 2.24** shows that there is a large effect on the pseudo-radial flow, i.e. the endpoint relative permeability has a big influence on the slope of the semi-log straight line.

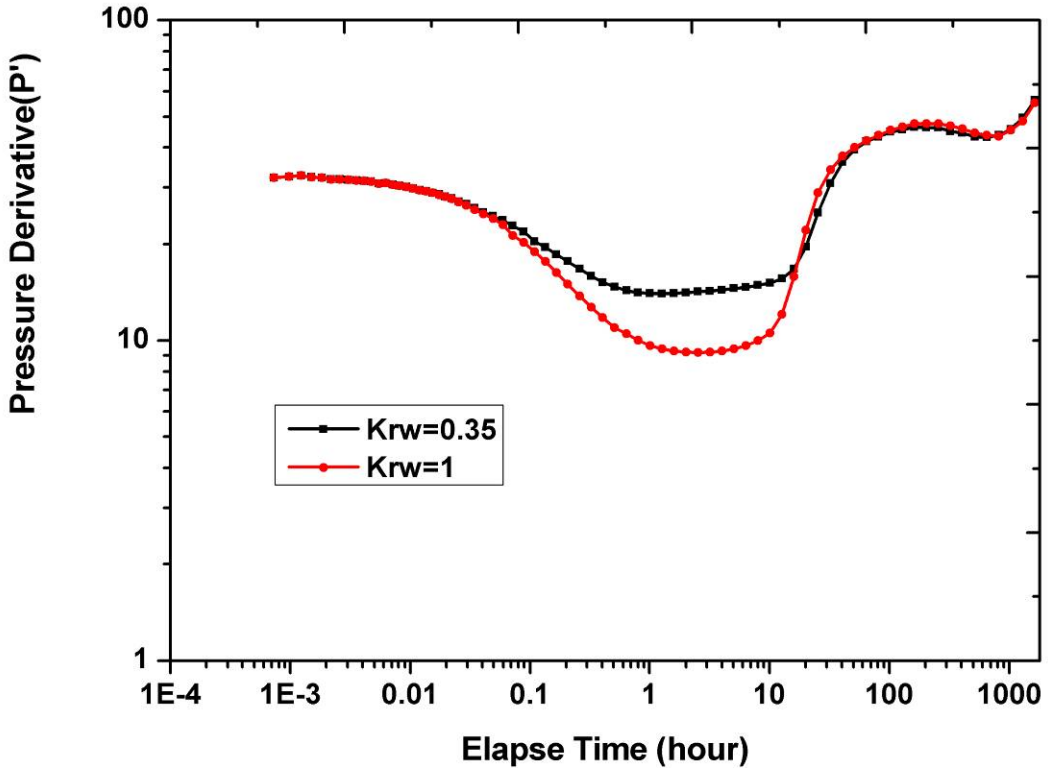

Figure 2.24 This figure shows the log-log plots of the DD tests with different endpoints of relative permeability. It shows that there is a big influence on pseudo-radial flow due to the changes of the endpoint of relative permeability.

2.6.4.4 Influence of water compressibility

The effect of changing water compressibility from 3e-7 1/psi to 3e-6 1/psi, is shown in **Figure 2.25**. The water compressibility has a big influence on spherical flow and pressure response of the outer boundary. But there is no influence on the slope of the pseudo-radial flow straight line.

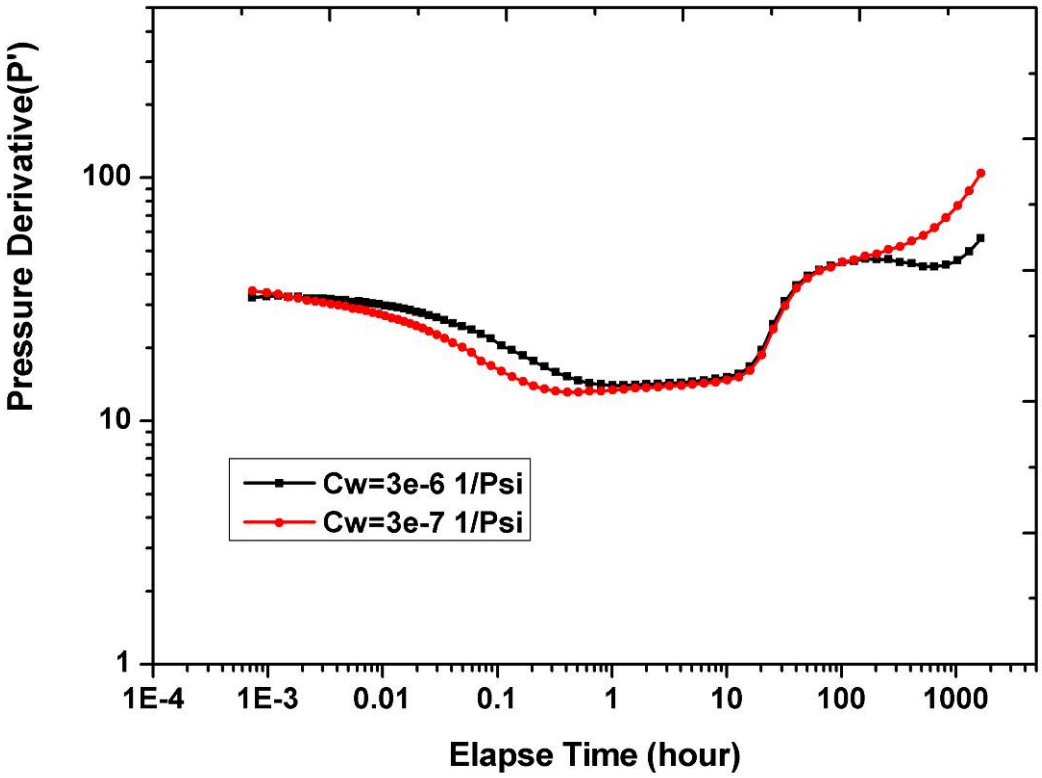

Figure 2.25 This figure shows the log-log plots of the DD tests with different water compressibility conditions. It shows that there is no influence on pseudo-radial flow due to the changes of the water compressibility.

2.6.4.5 Influence of thickness of water formation

Changing the water formation thickness from 30ft to 60ft, as show in **Figure 2.26**, there is a big influence on pseudo-radial flow.

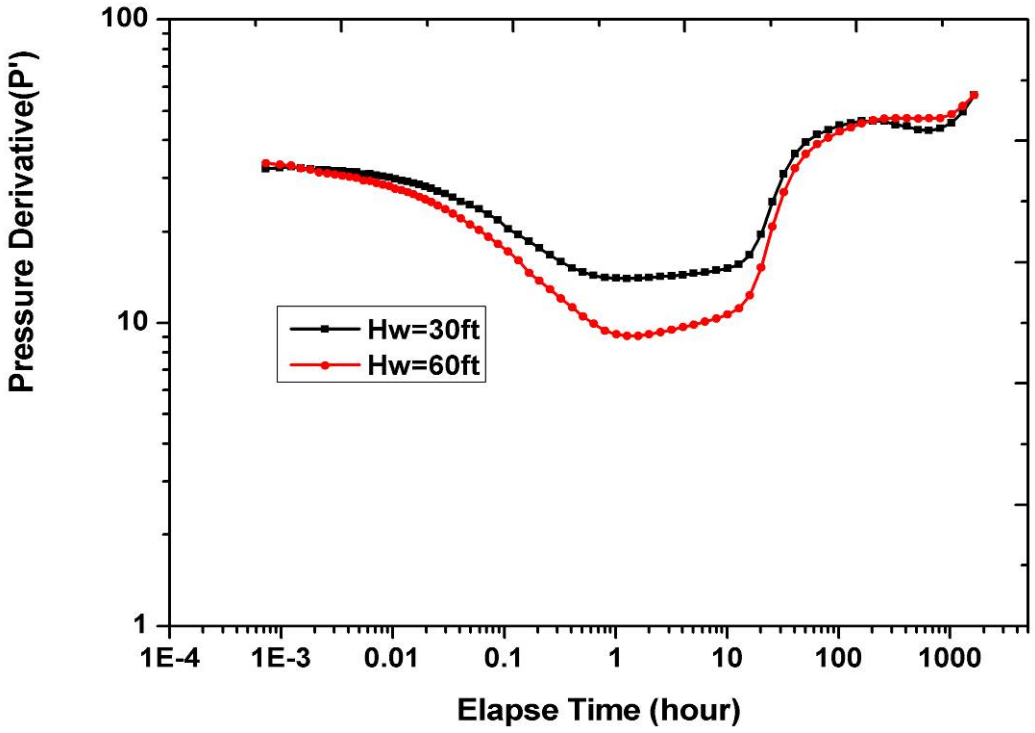

Figure 2.26 This figure shows the log-log plots of the DD tests with different thickness of water formation conditions. It shows that there is a large influence on pseudo-radial flow due to the changing of the thickness of the water formation.

2.6.4.6 Influence of oil/water viscosity ratio

For all previously studied cases, the oil viscosity was set to 1cp. If oil viscosity is increased to 5cp, **Figure 2.27** and **Figure 2.28** show that after water breaks through and the water-cut reaches a certain value, the bottom-hole pressure starts to go up. From this kick point, the DD data cannot be analyzed by using existing well testing methods.

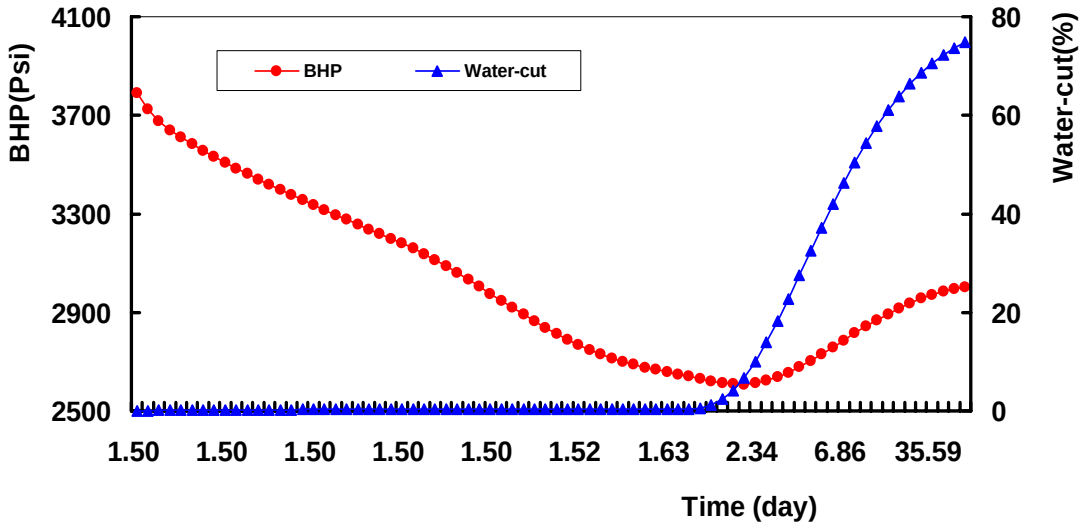

Figure 2.27 This figure shows the BHP curve and water-cut curve with high oil viscosity (5cp). It shows that the BHP curve starts to go up after water breaks through and reaches a value.

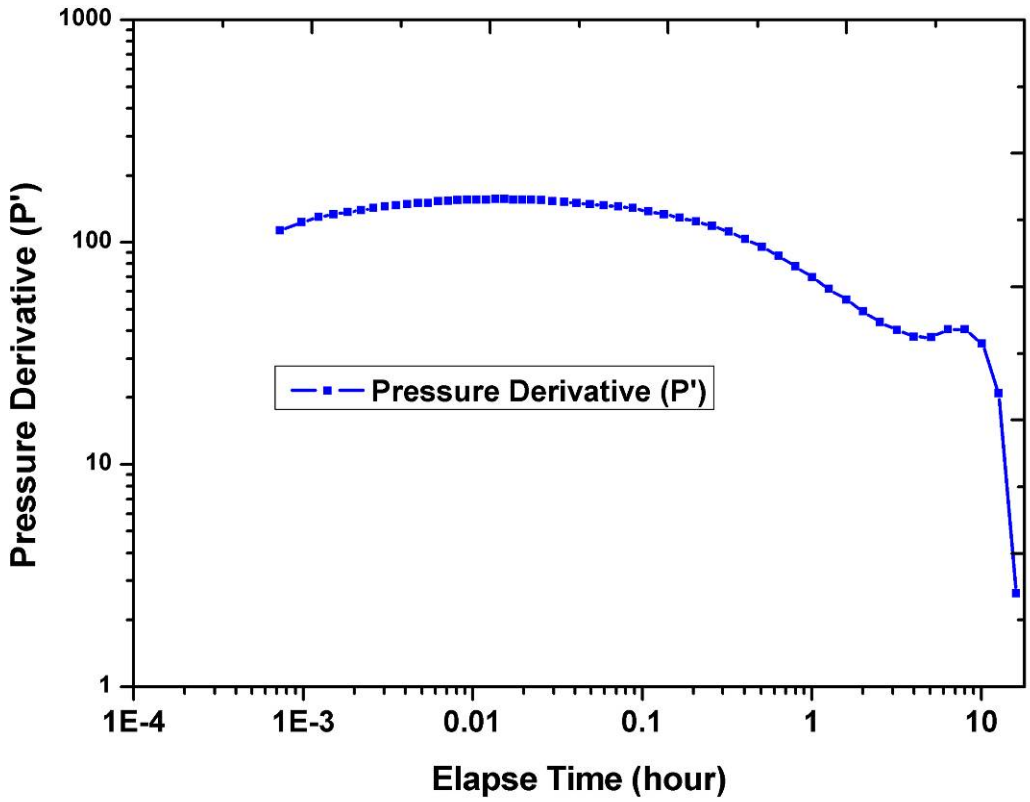

Figure 2.28 This figure shows the log-log plots of the DD test with high oil viscosity (5cp). It shows that after the BHP curve goes up, the DD data cannot be used for well testing analysis.

2.7 Chapter Conclusion

According to previous studies, the P-M approach only applies to several ideal reservoirs due to the limitation of the saturation gradient, and that the results of well test interpretation are phase permeability, which cannot be directly used to update reservoir model Hence, the P-M approach has been modified and several conclusions have been obtained, as follows:

- The modified P-M method involves using the total mobility at the current water-cut condition. The method assumes that the relative permeability curves for the reservoir are known, and that the relative permeability to oil at connate water saturation is approximately 1.

- The modified P-M shows good correlation with simulated data. The study also shows that the results from a modified P-M approach can be used directly to update a reservoir model for reservoir management. However, the modified P-M method is quite sensitive to the error of the relative permeability data. So it is very important to ensure the quality of relative permeability data in order to get representative results.

Because the equations governing multiphase flow have no analytical solution, numerical well testing is an effective way to address multiphase flow well testing problems.

Chapter 3
Analysis of Two Phase Flow Well Testing for a reservoir with Non-uniform saturation

3.1 Background

As described above in chapter 2, the traditional P-M approach and its modified approach are suitable for ideal reservoirs, such as a uniform saturation reservoir, segregated flow reservoir, and oil reservoirs with aquifer support, etc. The common feature is that the liquid saturation and geological properties in the horizontal direction are homogeneous. But in practice, the most fields are heterogeneous reservoirs. In this thesis, the emphasis of study is the multiphase flow problem. So the goal of research focuses on reservoirs with non-uniform saturation and homogenous geological properties. This chapter provides a systematic study of the effect of heterogeneous saturation on multiphase flow well testing.

In order to gain an in-depth understanding of the pressure response in non-uniformly saturated reservoirs, two kinds of numerical models are built up. One is used to analyze transient pressure response in the transient zone for a two phase flow system before water breakthrough, and the other is used to study the problems of multiphase flow well testing for two phase flow system after water breakthrough. According to the results of these studies, some new findings are derived and may be used to guide mature field management.

3.2 Analysis of Transient Pressure Response in the Transient Zone for Two Phase Flow System before Water Breakthrough

3.2.1 General Remarks

Well test analysis requires a pre-selected model, which relies on context input and diagnostic through the pressure logarithmic derivative curve. Transient pressure outer boundary response heavily impacts on the selection of such a model. Traditional boundary type curves used for such diagnostic purposes are only suitable for single-phase flow in a homogeneous reservoir, while practical situations, such as in multiphase flow well tests, are often much more complicated. There is a great influence on pressure derivatives due to the changes of fluid properties in the transition zone. For example, the logarithmic-derivative of bottom-hole pressure goes up and then goes down in late time for gas-water reservoir systems with an active aquifer underneath. If using a traditional boundary type curve for the model diagnostic, the wrong conclusions may be obtained.

In the literature, several articles have been published on multiphase flow, including those from Thompson [Thompson, L.G., 1997[31]] and Roadifer [Roadifer,R.D., 1995[48];1996[30]]. Thompson examined the behavior of transient pressure for single and multiphase flow in heterogeneous reservoirs. He used mass conservation equations and Darcy's law to derive the pressure derivatives, which can be used to interpret well test from single phase and multiphase flow. For single-phase gas reservoirs, the pressure derivative is a function of the changing of rates with time. But for multiphase flow, Thompson focused on gas-condensate reservoir and water injection in an oil reservoir. He found multiphase flow drawdown is heavily influenced by mobility in the region, where mobility is changing most rapidly with time. But for both oil-water and gas-water systems, Thompson did not consider the influence of the transition zone.

Roadifer (1995[48]) examined the pressure behavior in a multiphase reservoir with a constant pressure boundary. Buckley-Leverett theory was used to analyze multiphase well test at the same time. Some laws on water saturation front were derived

numerically. Roadifer used the Thompson equation to interpret the pressure derivative of oil-water and oil-gas system with a constant pressure boundary. But he did not consider the influence of capillary pressure.

In fact, for multiphase flow system, capillary pressure cannot be ignored. In this work, based on the Thompson equation, but also considering capillary pressure, a new theoretical equation is derived from Darcy's Law, which shows that pressure response in the transition zone is a function of total effective mobility.

In order to validate the new approach, a 3D model was set up using Eclipse to simulate the pressure responses due to multiphase flow. The oil-water and gas-water systems were studied. Capillary pressure was considered under closed reservoir or constant pressure outer boundaries. Numerical well testing results proved that this new approach can be used to interpret qualitatively well tests for these different multiphase reservoir systems. It is particularly useful for analyzing the transient pressure outer boundary response.

3.2.2 Mathematical Model

According to the law of conservation of matter for black oil systems, isothermal multiphase flow in radial homogeneous reservoir is described by a partial differential equation, i.e.; a diffusivity equation. When the mass of conservation equations are satisfied, Darcy's Law, which describes pressure losses in each flowing phase, is also satisfied.

First, in an oil-water system, capillary pressure is considered and the gravity effect is ignored. The production rate can be written at any radial location as (field units): (Eigestad et al., 2000[49]; Fanchi et al., 2002[50]; Dahroug et al., 2005[51])

$$q_t(r,t) = q_o(r,t) + q_w(r,t) \tag{3.1}$$

$$q_o(r,t) = \frac{KK_{ro}(S_w)}{\mu_0} A(r) \frac{\partial P_o}{\partial r} \tag{3.2}$$

$$q_w(r,t) = \frac{KK_{rw}(S_w)}{\mu_w} A(r) \frac{\partial P_w}{\partial r} \tag{3.3}$$

Where, A(r) is cross-section flow area, ft^2; i.e.,

$$A(r) = 2\pi rh \tag{3.4}$$

And Pc is capillary pressure, psi; i.e.,

$$P_c = P_o - P_w \tag{3.5}$$

Equation 3.1, **Equation 3.2** and **Equation 3.3** can be rearranged as:

$$q_t(r,t) = 2\pi rKh\left[\lambda_t(r,t)\frac{\partial P_o}{\partial r} - \frac{K_{rw}(S_w)}{\mu_w}\frac{\partial P_c}{\partial r}\right] \tag{3.6}$$

Where, $\lambda_t(r,t)$ is the total effective mobility; i.e.,

$$\lambda_t(r,t) = \frac{K_{ro}(S_w)}{\mu_o} + \frac{K_{rw}(S_w)}{\mu_w} \tag{3.7}$$

Combining **Equation 3.6 and Equation 3.7**, **Equation 3.8** can be written as:

$$\frac{\partial P_o}{\partial r} = \frac{q_t(r,t)}{2\pi rKh\lambda_t(r,t)} + \left[\frac{\lambda_w(r,t)}{\lambda_t(r,t)}\right]\frac{\partial P_c}{\partial r} \tag{3.8}$$

Where, $\lambda_o(r,t)$ and $\lambda_w(r,t)$ are phase effective mobility; i.e.,

$$\lambda_o(r,t) = \frac{K_{ro}(S_w)}{\mu_0} \tag{3.9}$$

$$\lambda_w(r,t) = \frac{K_{rw}(S_w)}{\mu_w} \tag{3.10}$$

Equation 3.8 obviously applies equally to bounded or infinite-acting reservoirs. Considering infinite-acting reservoirs, separating variables in **Equation 3.8** and taking integral along a radial direction:

$$\int_{r_w}^{\infty}\frac{\partial P_o}{\partial r}dr = \frac{1}{2\pi Kh}\int_{r_w}^{\infty}\frac{q_t(r',t)}{r'\lambda_t(r',t)}dr' + \int_{r_w}^{\infty}\left[\frac{\lambda_w(r',t)}{\lambda_t(r',t)}\right]\frac{\partial P_c}{\partial r'}dr' \tag{3.11}$$

Assuming:

$$\lambda_{\text{equivalent}}\left(r',t\right)=\frac{\lambda_w\left(r',t\right)}{\lambda_t\left(r',t\right)} \tag{3.12}$$

Equation 3.11 reduces to:

$$\int_{r_w}^{\infty}\frac{\partial P_o}{\partial r}dr=\frac{1}{2\pi Kh}\int_{r_w}^{\infty}\frac{q_t\left(r',t\right)}{r'\lambda_t\left(r',t\right)}dr'+\int_{r_w}^{\infty}\lambda_{\text{equivalent}}\left(r',t\right)\frac{\partial P_c}{\partial r'}dr' \tag{3.13}$$

For **Equation 3.8**, outer boundary condition is defined as:

$$\lim_{r\to\infty}P\left(r,t\right)=P_i \quad \text{i.e.; infinite acting reservoir} \tag{3.14}$$

According to **Equation 3.11** and **Equation 3.14**, we can get drawdown solution:

$$\Delta P_o\left(t\right)=P_i-P_{wf}\left(t\right)=\frac{1}{2\pi Kh}\int_{r_w}^{\infty}\frac{q_t\left(r',t\right)}{r'\lambda_t\left(r',t\right)}dr'+\int_{r_w}^{\infty}\lambda_{\text{equivalent}}\left(r',t\right)\frac{\partial P_c}{\partial r'}dr' \tag{3.15}$$

Finally, differentiating **Equation 3.15**, with respect to the natural logarithm of time, the pressure derivative is given by:

$$\frac{d\Delta P_o\left(t\right)}{d\ln t}=\frac{1}{2\pi Kh}\int_{r_w}^{\infty}\left\{\left[\frac{1}{r'\lambda_t\left(r',t\right)}\frac{\partial q_t\left(r',t\right)}{\partial\ln t}\right]-\frac{q_t\left(r',t\right)}{r'\lambda^2{}_t\left(r',t\right)}\frac{\partial\lambda_t\left(r',t\right)}{\partial\ln t}\right\}dr'$$
$$+\int_{r_w}^{\infty}\frac{\partial\lambda_{\text{equivalent}}\left(r',t\right)}{\partial\ln t}\frac{\partial P_c}{\partial r'}dr' \tag{3.16}$$

Because capillary pressure is a function of water saturation and water saturation is a function of radial distance, so **Equation 3.16** can be rearranged as:

$$\frac{d\Delta P_o\left(t\right)}{d\ln t}=\frac{1}{2\pi Kh}\int_{r_w}^{\infty}\left\{\left[\frac{1}{r'\lambda_t\left(r',t\right)}\frac{\partial q_t\left(r',t\right)}{\partial\ln t}\right]-\frac{q_t\left(r',t\right)}{r'\lambda^2{}_t\left(r',t\right)}\frac{\partial\lambda_t\left(r',t\right)}{\partial\ln t}\right\}dr'$$
$$+\int_{r_w}^{\infty}\frac{\partial\lambda_{\text{equivalent}}\left(r',t\right)}{\partial\ln t}\frac{\partial P_c}{\partial S_w}\frac{\partial S_w}{\partial r'}dr' \tag{3.17}$$

Equation 3.17 is the general equation, which applies to a radial flow system producing

under defined wellbore boundary conditions.

From this equation, it can be seen that the pressure logarithmic derivative is a function of the total effective mobility, capillary pressure, liquid rate and water saturation. Because this equation is highly non-linear, an analytic solution cannot be obtained, so the numerical well testing approach was used, considering phase effective permeability, capillary pressure, saturation gradient and complex formation properties.

3.2.3 Numerical Well Testing

In this section, a 3D model was built to simulate multiphase flow in order to derive a numerical solution. At the same time, **Equation 3.17** was used to verify qualitatively the accuracy of the numerical solution.

3.2.3.1 Numerical model

In the constructed numerical model, the basic simulation grid consisted of 51 cells in the I-direction, 51 cells in the J-direction, with 6 layers (in both the anticline model and the flat model) (**Figure 3.1**).Two systems, an oil-water model and a gas-water model, with different properties, were used in the simulations. Data for the simulation model are summarized in **Table 3.1.**

Table 3.1 Reservoir model characteristics

Parameter	Oil-water	Gas-water
Porosity Φ,%	30	30
Absolute permeability K, mD	500	10
Wellbore radius r_w, ft	0.15	0.15
Total reservoir thickness, ft	180	180
Initial reservoir pressure, Pi, psi	2555	2430
Top depth, ft	4500	4500

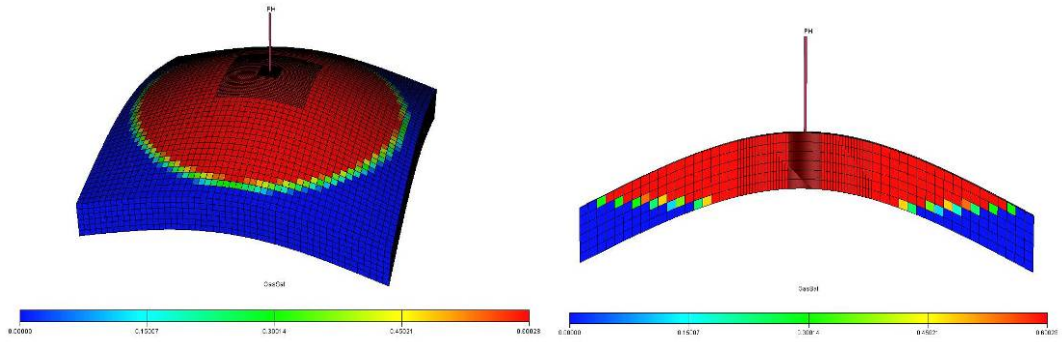

Figure 3.1 The anticline model: 3D (left), 2D cross-section profile (right)

Grid description

Corner point geometry grids were used with approximate dimension of 200*200*30ft. Because bottom-hole pressure is sensitive to the size of the grid, a nested grid technique was used in the model. This not only makes the well bore better connected to the grid thereby avoiding numerical dispersion, but also improves the simulation speed.

Fluid characterization

The variation of the fluid properties in the lateral and the vertical directions has been taken into account. Under reference pressure, the viscosity of gas, oil and water is 0.02cp, 10cp and 0.5cp, respectively.

Relative permeability modeling

Inputting two sets relative permeability data to oil-water and gas-water model, **Figure 3.2** and **Figure 3.3** show that when Kro equals to Krw, the corresponding water saturation is more than 0.5， which denotes that the rock has water wetting properties.

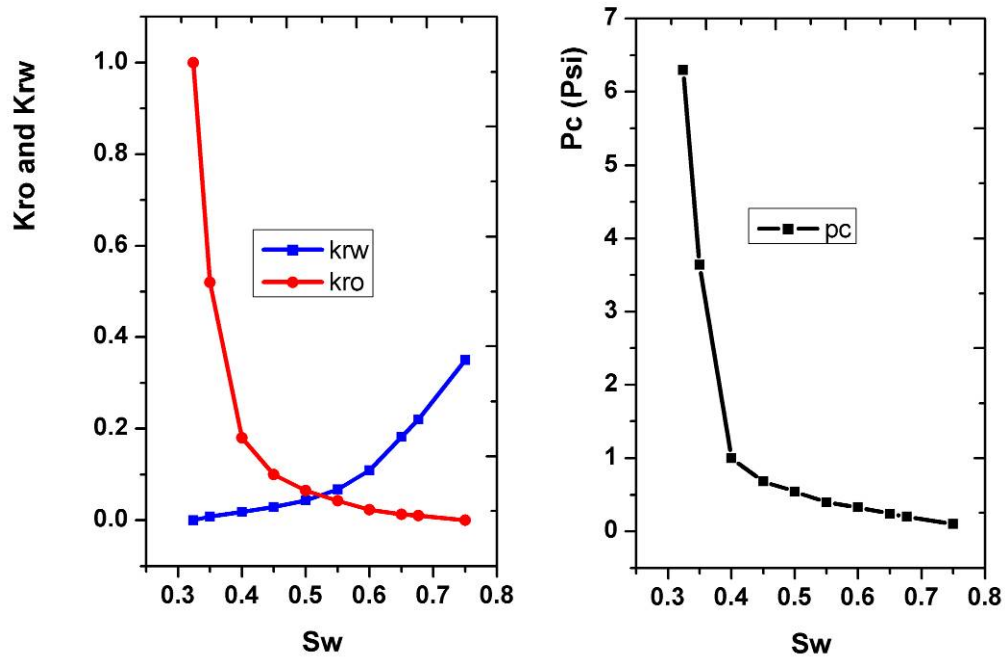

Figure 3.2 The Oil/water Relative Permeability Curve and Capillary Pressure

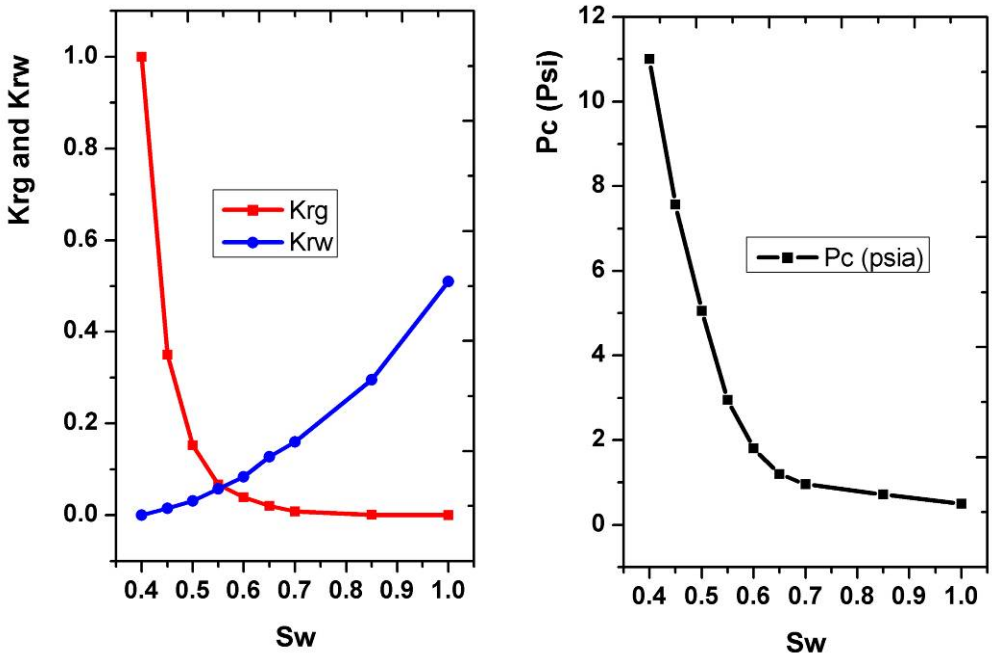

Figure 3.3 The Gas/water Relative Permeability Curve and Capillary Pressure

3.2.3.2 Case study 1: Oil-water system

The first case considered single-phase flow. The studies were designed to test the impact of reservoir and fluid properties on the pressure response. These key parameters are listed in **Table 3.2**.

Table 3.2 The designs of different flow conditions

Fluid	Case	Pc	Model	OWC (ft)	Well location	Aquifer	Viscosity (cp)
Single phase model	Flat	/	Flat	/	Center	closed system	10
	Anticline	/	Anticline	/	Center	closed system	10
Oil-water model	OW-1	No pc	Anticline	4735	Center	closed system	10
	OW-2	No pc	Anticline	4735	Center	closed system	1
	OW-3	No pc	Anticline	4735	Center	closed system	5
	OW-4	No pc	Anticline	4735	Center	closed system	25
	OW-5	Pc	Anticline	4735	Center	closed system	10
	OW-6	High-Pc	Anticline	4735	Center	closed system	10
	OW-7	Pc	Anticline	4735	Center	Aquifer	10
	OW-8	No pc	Anticline	4735	Center	Aquifer	10
	OW-8	High pc	Anticline	4735	Center	Aquifer	10
	OW-9	No pc	Anticline	4700	Center	closed system	10

3.2.3.2.1 Single-phase flow

As shown in **Figure 3.4**, the pressure derivatives for single phase flow with flat and anticline models are the same. It means that the shape of model does not affect the numerical solutions of models.

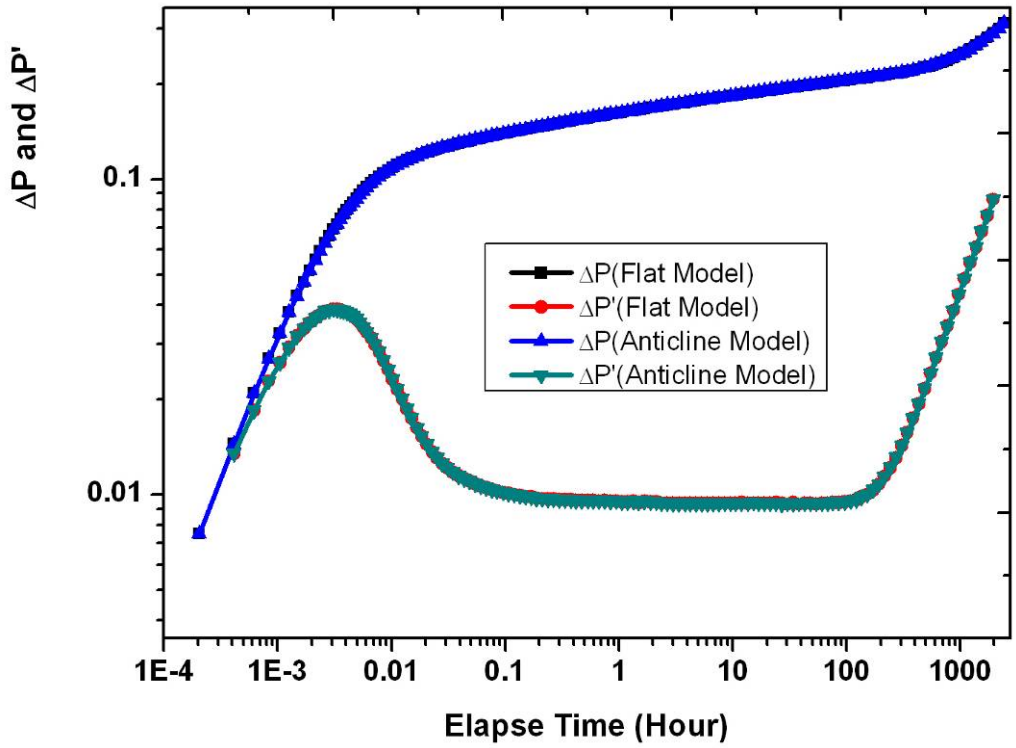

Figure 3.4 This figure shows the log-log plot of drawdown from a closed system. It shows that the pressure derivative responses for the anticline model and flat model under single-phase flow condition are the same.

For single-phase flow in these closed systems, mobility does not change and capillary pressure is not present, i.e., $\frac{\partial \lambda_t(r,t)}{\partial t}=0$ and $P_o=P_w; P_c=0$, therefore, **Equation 3.17** reduces to:

$$\frac{d\Delta P_o(t)}{d(\ln t)}=\frac{t}{2\pi Kh}\int_{r_w}^{\infty}\frac{1}{r'\lambda_t(r',t)}\frac{\partial q_t(r',t)}{\partial t}dr' \qquad (3.18)$$

Hence, the pressure derivative is a function of the flow rate changes with time in the reservoir.

Before semi-steady-state is reached, the flow rate in the reservoir will continue to increase, e.g. if $t<t_{sss}$, where t_{sss} is the time to reach the semi-steady-state, we can get:

$$\frac{\partial q_t\left(r',t\right)}{\partial t}>0, \tag{3.19}$$

The **Equation 3.19** shows that the pressure derivative will remain positive until the semi-steady-state is reached; i.e.:

$$\frac{d\Delta P_o\left(t\right)}{d\left(\ln t\right)}>0, \quad t<t_{sss} \tag{3.20}$$

At late time, when the pressure disturbance reaches a closed boundary, the formation pressure decreases with time, until the drawdown at wellbore equals to the drawdown at boundary, from then on, the pseudo-steady-state flow will start. At the same time, the changes of formation flow rate at any location will approach to zero, and the changes of formation pressure at any location will approach to constant.

$$q_t\left(r_e',t\right)\equiv 0, \Delta q_t\left(r',t\right)\to 0, \Delta P\left(r,t\right)\to C_1 \quad (C_1=\text{constant value}), \quad t\to t_{sss} \tag{3.21}$$

$$\frac{d\Delta P_o\left(t\right)}{d\left(\ln t\right)}\to C_1 * t, \quad t\to t_{sss}, \tag{3.22}$$

Equation 3.22 indicates that in late time the slope of derivative in Log-Log plot is unit 1. **Figure 3.4** shows that the numerical result is identical to that from **Equation 3.22**.

3.2.3.2.2 Two-phase flow

For two-phase flow in homogeneous reservoir, the capillary pressure was not considered at the beginning, i.e. $P_o=P_w, P_c=0$. According to the Buckley-Leverett theory, in oil-water transition zone, there exists saturation front, and the reservoir can be divided into three regions. (**Figure 3.5**) The first region is between the wellbore and the downstream side of saturation front, $r_w<r<r_f^-$; the second region is between the downstream side of saturation front and the upstream side of saturation front, $r_f^-<r<r_f^+$; and the third region is between the upstream side of saturation front and outer boundary of the reservoir, $r_f^+<r<r_e$. Because the change of

volumetric flow rate at any location in late time will approach zero, i.e. $\Delta q_t(r',t) \to 0$, the general pressure derivative equation (**Equation 3.17**) can be simplified as:

$$\frac{d\Delta P_o(t)}{d\ln t} = \frac{t}{2\pi Kh}\left\{\int_{r_w}^{r_f^-}\left[-\frac{q_t(r',t)}{r'\lambda^2{}_t(r',t)}\frac{\partial\lambda_t(r',t)}{\partial t}\right]dr'\right\} + \frac{t}{2\pi Kh}\left\{\int_{r_f^-}^{r_f^+}\left[-\frac{q_t(r',t)}{r'\lambda^2{}_t(r',t)}\frac{\partial\lambda_t(r',t)}{\partial t}\right]dr'\right\} + \frac{t}{2\pi Kh}\left\{\int_{r_f^+}^{r_e}\left[-\frac{q_t(r',t)}{r'\lambda^2{}_t(r',t)}\frac{\partial\lambda_t(r',t)}{\partial t}\right]dr'\right\} \tag{3.23}$$

Ahead of the saturation front, the flow is single-phase (oil) and the total effective mobility is unchanged, so $\frac{d\lambda_t(t)}{dt} = 0$, $r_w < r < r_f{}^-$, then **Equation 3.23** can be reduced to

$$\frac{d\Delta P_o(t)}{d(\ln t)} = \frac{t}{2\pi Kh}\left\{\int_{r_f^-}^{r_f^+}\left[-\frac{q_t(r',t)}{r'\lambda^2{}_t(r',t)}\frac{\partial\lambda_t(r',t)}{\partial t}\right]dr'\right\} + \frac{t}{2\pi Kh}\left\{\int_{r_f^+}^{r_e}\left[-\frac{q_t(r',t)}{r'\lambda^2{}_t(r',t)}\frac{\partial\lambda_t(r',t)}{\partial t}\right]dr'\right\} \tag{3.24}$$

Before water breakthrough, from upstream of saturation front to outer boundary, the total effective mobility increases and finally becomes constant, so at late time, $\frac{d\lambda_t(t)}{dt} \to 0$, $r_f{}^+ < r < r_e$, and then **Equation 3.24** can be rearranged as:

$$\frac{d\Delta P_o(t)}{d(\ln t)} = \frac{1}{2\pi Kh}\int_{r_f^-}^{r_f^+}\left[-\frac{q_t(r',t)}{r'\lambda^2{}_t(r',t)}\frac{\partial\lambda_t(r',t)}{\partial(\ln t)}\right]dr'$$
$$= \frac{t}{2\pi Kh}\int_{r_f^-}^{r_f^+}\left[-\frac{q_t(r',t)}{r'\lambda^2{}_t(r',t)}\frac{\partial\lambda_t(r',t)}{\partial t}\right]dr' \qquad (3.25)$$

Equation 3.25 is the generalized pressure derivative equation for transition zone. This was proved by the numerical simulation result shown in **Figure 3.6**. The pressure derivative starts to go down at 48.16 hours.

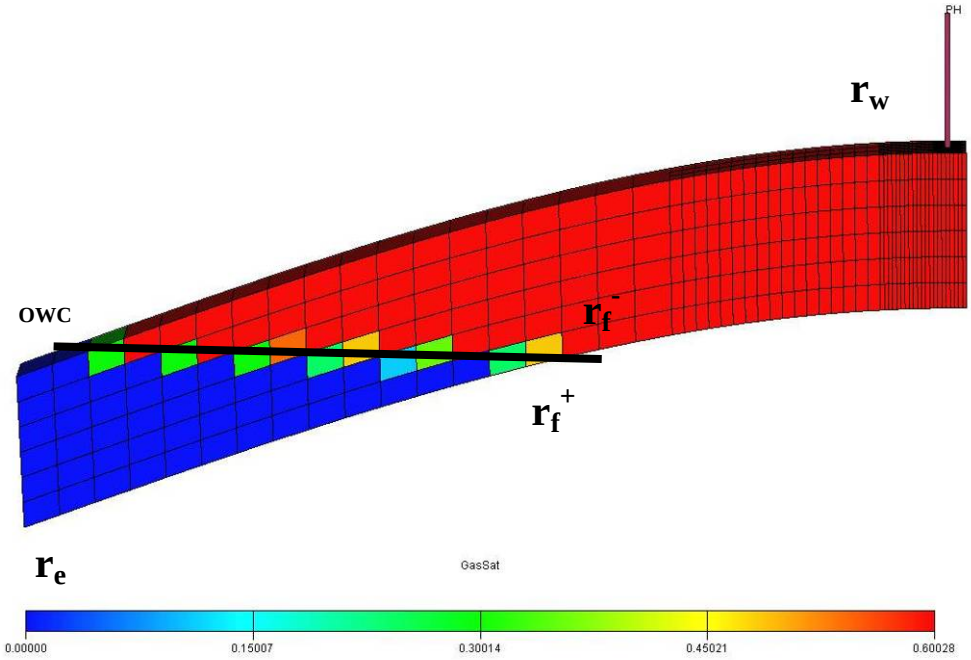

Figure 3.5 According to the Buckley-Leverett theory, using saturation front, reservoir can be divided to three regions. The first region is between the wellbore and the downstream side of saturation front, $r_w < r < r_f^-$; the second region is between the downstream side of saturation front and the upstream side of saturation front, $r_f^- < r < r_f^+$; the third region is between the upstream side of saturation front and outer boundary of the reservoir, $r_f^+ < r < r_e$.

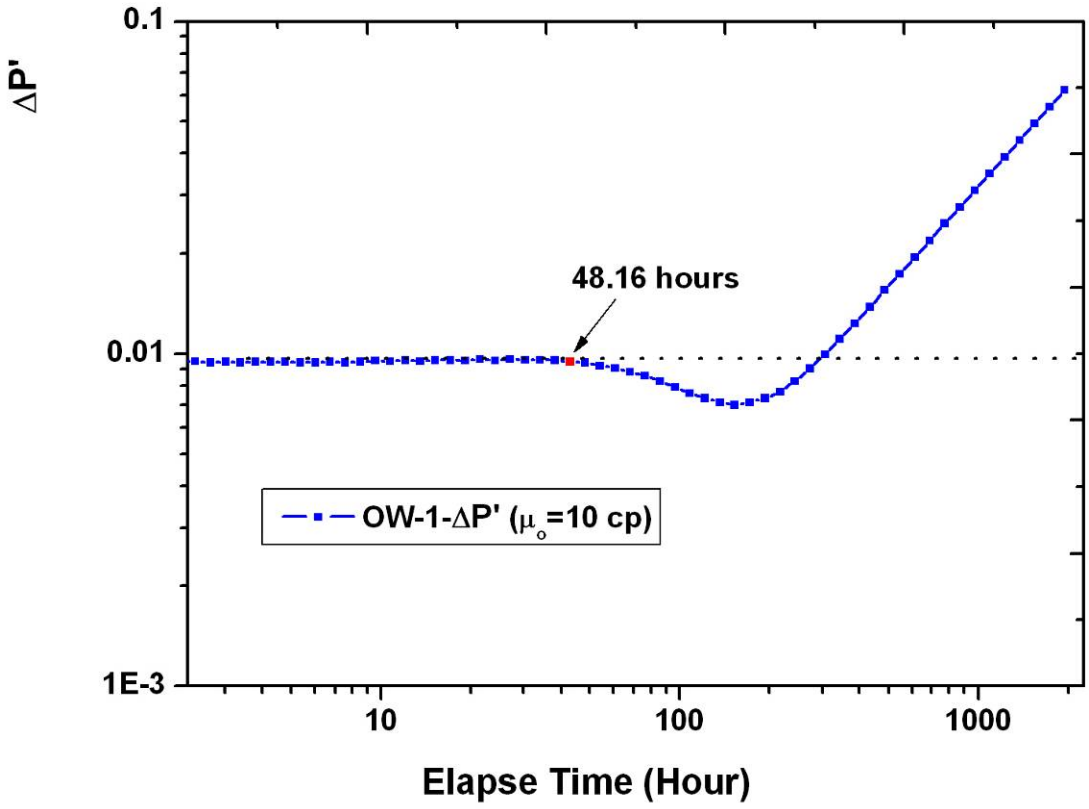

Figure 3.6 This figure is log-log plot of drawdown of a closed system. It shows that the pressure derivative starts to decrease at 48.16 hours. At this point, the pressure reached the transient zone.

Figure 3.7 shows that when the well produces by depletion, at the downstream saturation front, with oil produced, the combined water did not flow, and the oil mobility was decreased, so the total mobility was decreased, until to the point of 48.16 hours. At the upstream saturation front the combined water starts to flow, water encroachment will occur, and total mobility starts to increase rapidly.

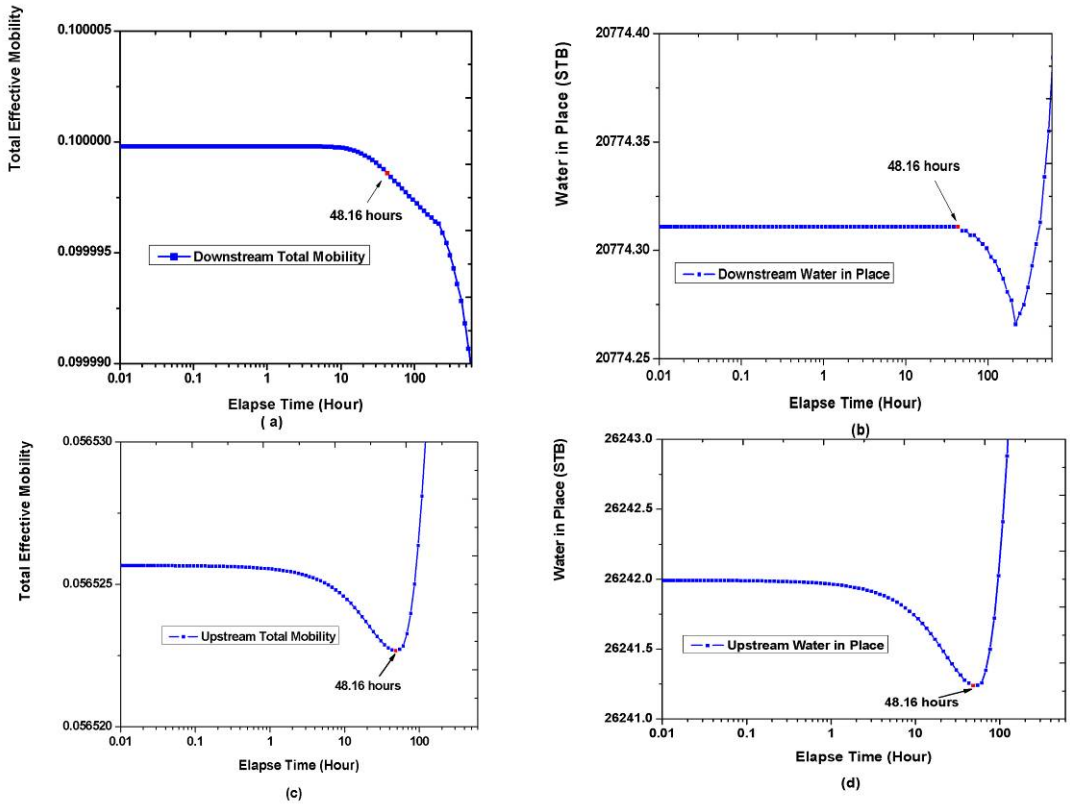

Figure 3.7 (a) is the total mobility curve and (b) is the volumetric of water curve just downstream of the saturation front ($r \to r_f^-$). Before 48.16hr, the combined water does not flow, but because the oil is moving, so the total mobility decreases. (c) is the total mobility curve and (d) is the volumetric of water curve at upstream saturation front ($r \to r_f^+$), from 48.16hr, water encroachment will occur, and the total mobility starts to increase rapidly.

According to **Equation 3.25**, from this moment, the $\lambda_t(r,t)$ increases, so $\frac{\partial \lambda_t(r,t)}{\partial t}$ increases and $\frac{\partial \lambda_t(r,t)}{\partial t}$>0, but $\frac{d\Delta P_o(t)}{d(\ln t)}$ is negative and decreases with time. (**Figure 3.8**)

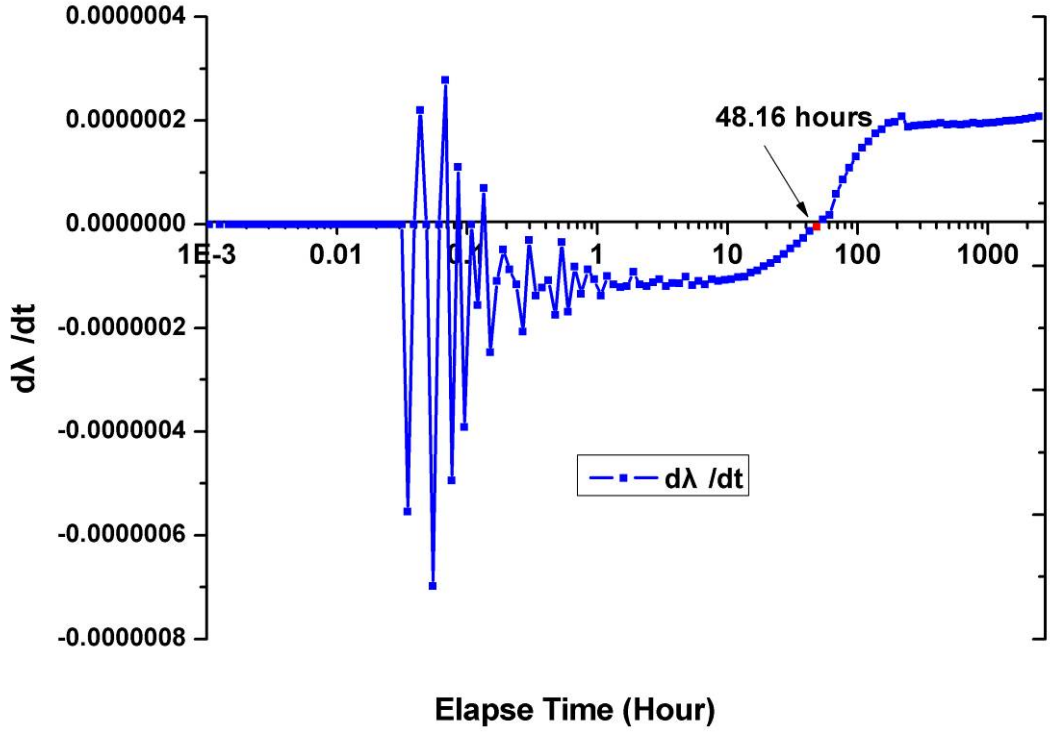

Figure 3.8 This figure shows the total mobility derivative curve just upstream of the saturation front ($r \to r_f^+$), the total mobility derivative is positive and increasing with time.

3.2.3.2.3 Sensitivity studies

Effect of different oil-water-contact (OWC)

Under different OWC conditions, there is a large variation in the pressure derivative. **Figure 3.9** shows that the pressure derivatives go down overall at the transition zone, but for high oil-water-contact, because the saturation front is much higher, the pressure disturbance reaches the saturation front quickly. Hence, the pressure derivative goes down earlier and much further.

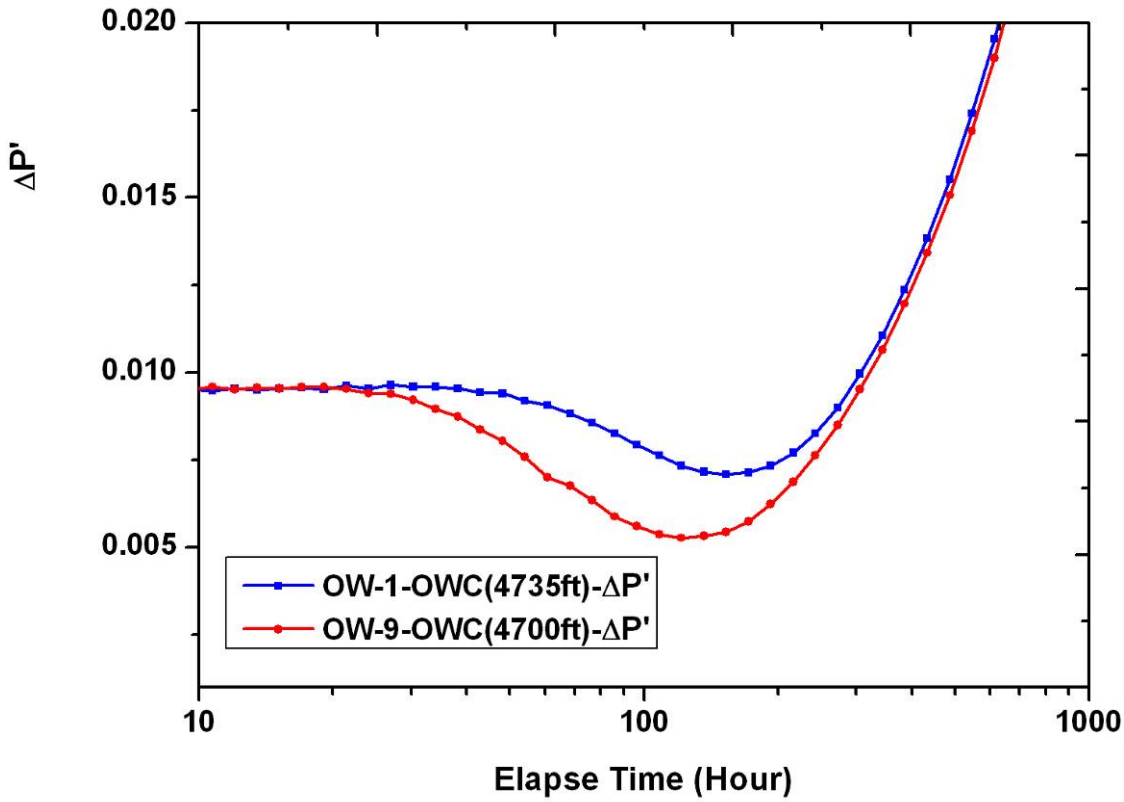

Figure 3.9 This figure shows log-log plot of drawdown for closed system. It shows that the pressure derivatives for different OWC case go down overall in the transition zone, but for high OWC cases, the pressure derivative goes down earlier and much further.

Effect of capillary pressure

In practice, capillary pressure exists everywhere in reservoirs with multi-phase flow as long as oil saturation is different from water saturation. This is reservoir's inherent nature. Under this condition, **Equation 3.17** can be rearranged for transition zone as:

$$\frac{d\Delta P_o(t)}{d(\ln t)} = \frac{t}{2\pi Kh}\int_{r_f^-}^{r_f^+}\left\{-\frac{q_t(r',t)}{r'\lambda^2{}_t(r',t)}\frac{\partial\lambda_t(r',t)}{\partial t}\right\}dr' + t\int_{r_f^-}^{r_f^+}\frac{\partial\lambda_{\text{equivalent}}(r',t)}{\partial t}\frac{\partial P_c}{\partial S_w}\frac{\partial S_w}{\partial r'}dr' \tag{3.26}$$

For $\lambda_{\text{equivalent}}(r',t)=\dfrac{\lambda_w(r',t)}{\lambda_t(r',t)}$, because from the upstream saturation front, $\lambda_w(r',t)$ increases and $\lambda_t(r',t)$ also increases, so $\lambda_{\text{equivalent}}(r',t)$ increases, and $\dfrac{\partial\lambda_{\text{equivalent}}(r',t)}{\partial t}>0$. But $\dfrac{\partial P_c}{\partial S_w}$ is negative as shown in **Figure 3.10**. However, **Figure 3.11** indicates that $\dfrac{\partial S_w}{\partial r'}$ is positive, so

$$\frac{\partial\lambda_{\text{equivalent}}(r',t)}{\partial t}\frac{\partial P_c}{\partial S_w}\frac{\partial S_w}{\partial r'}<0 \qquad (3.27)$$

Figure 3.12 shows that the transition zone pressure derivative of the reservoir with capillary pressure decreases more than that without capillary pressure.

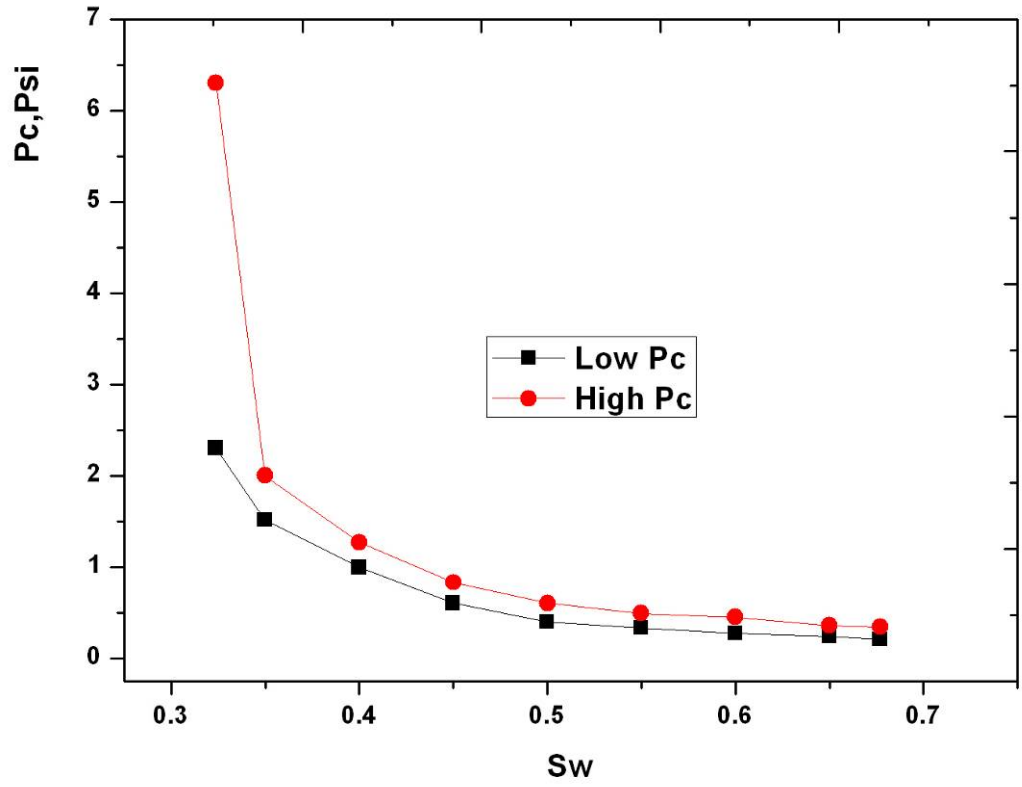

Figure 3.10 This figure shows different capillary pressure curves.

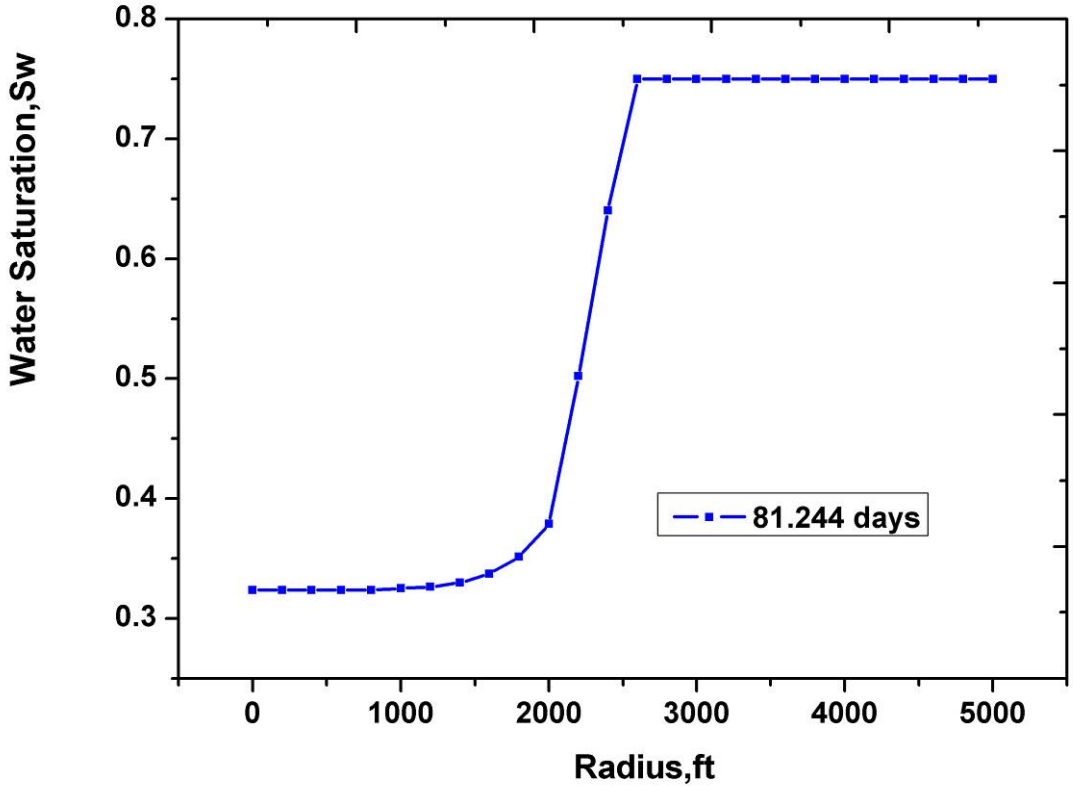

Figure 3.11 This figure shows water saturation profile changes with radial distance.

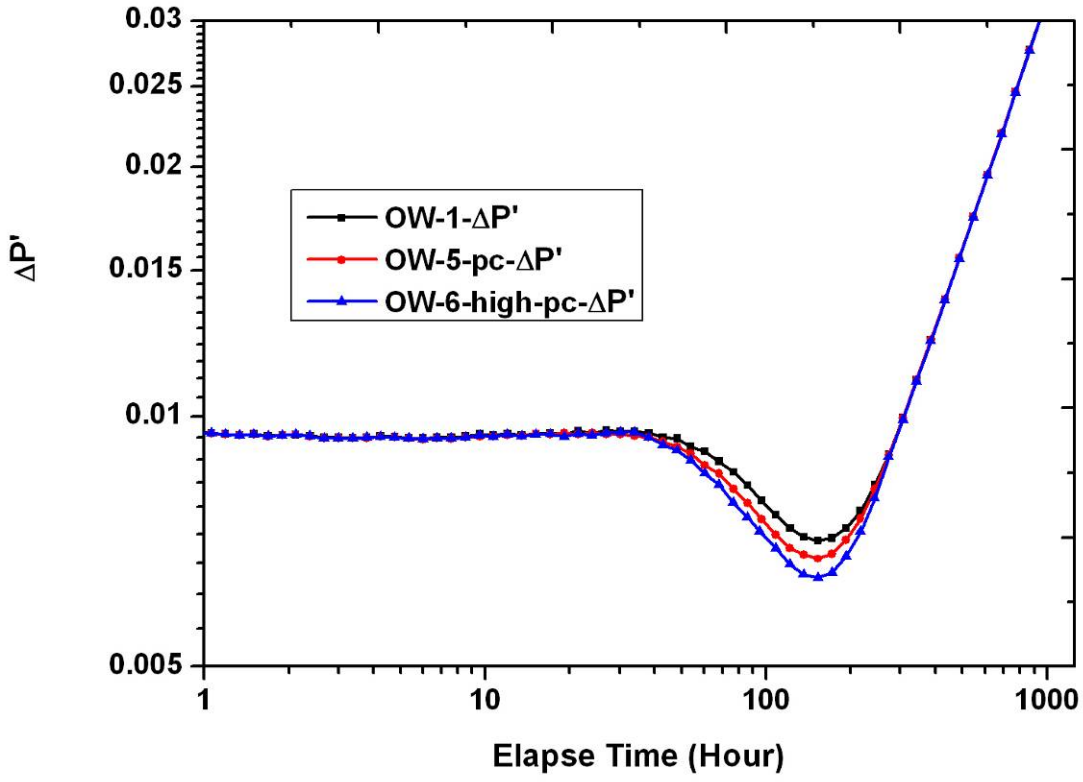

Figure 3.12 This figure shows log-log plot of drawdown of a closed system. It shows

that the transition zone pressure derivative of reservoir with capillary pressure goes down more than that without capillary pressure.

Effect of constant pressure outer boundary

As shown in **Figure 3.13**, with and without capillary pressure the pressure derivative follows nearly the same trend in reservoirs with constant pressure at outer boundary.

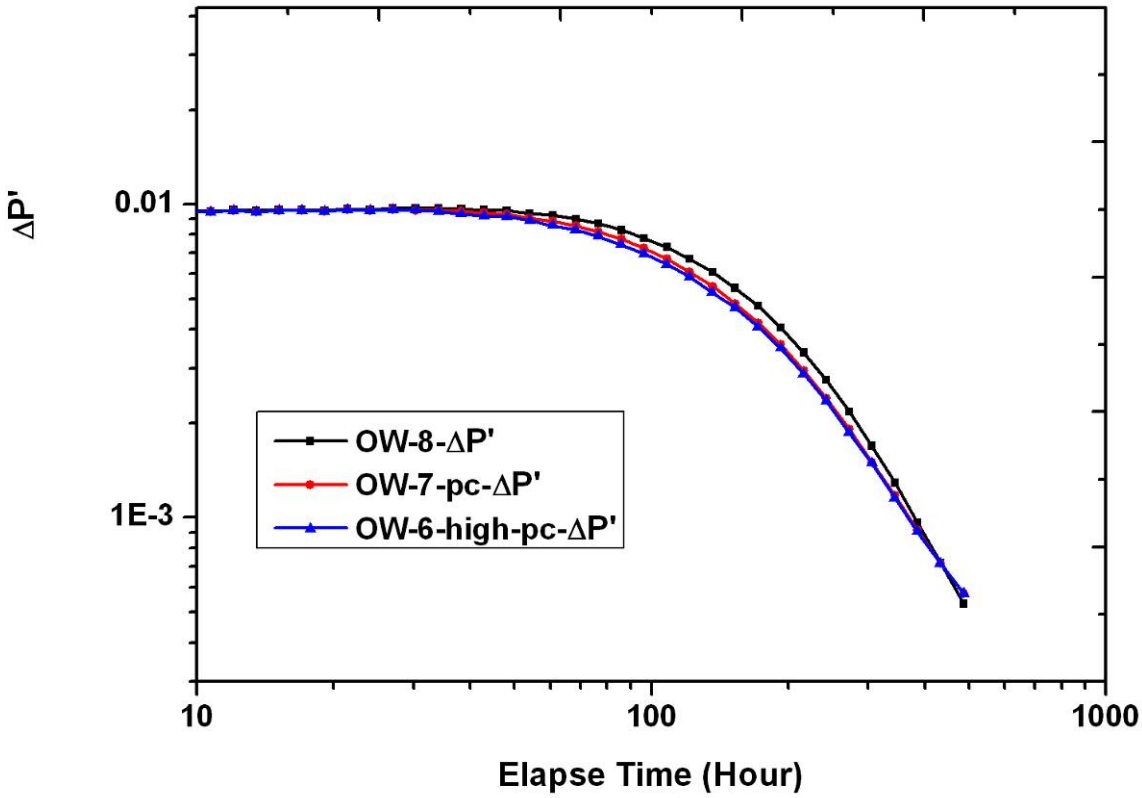

Figure 3.13 This figure shows a log-log plot of drawdown in a reservoir with constant pressure boundary. It shows that the transition zone pressure derivative of reservoir with capillary pressure goes down more than that without capillary pressure.

Effect of oil viscosity

In order to study the pressure behavior of a transition zone caused by varying oil viscosities, four cases were designed, in which oil viscosity is 1cp, 5cp, 10cp, and 25cp respectively.

According to the radius of investigation equation,

$$R_{inv} = 0.033\sqrt{\frac{kt}{\phi\mu c_t}} \tag{3.28}$$

If oil viscosity is greater, the time taken to reach transition zone is longer. This is consistent with the simulation results shown in **Figure 3.14.**

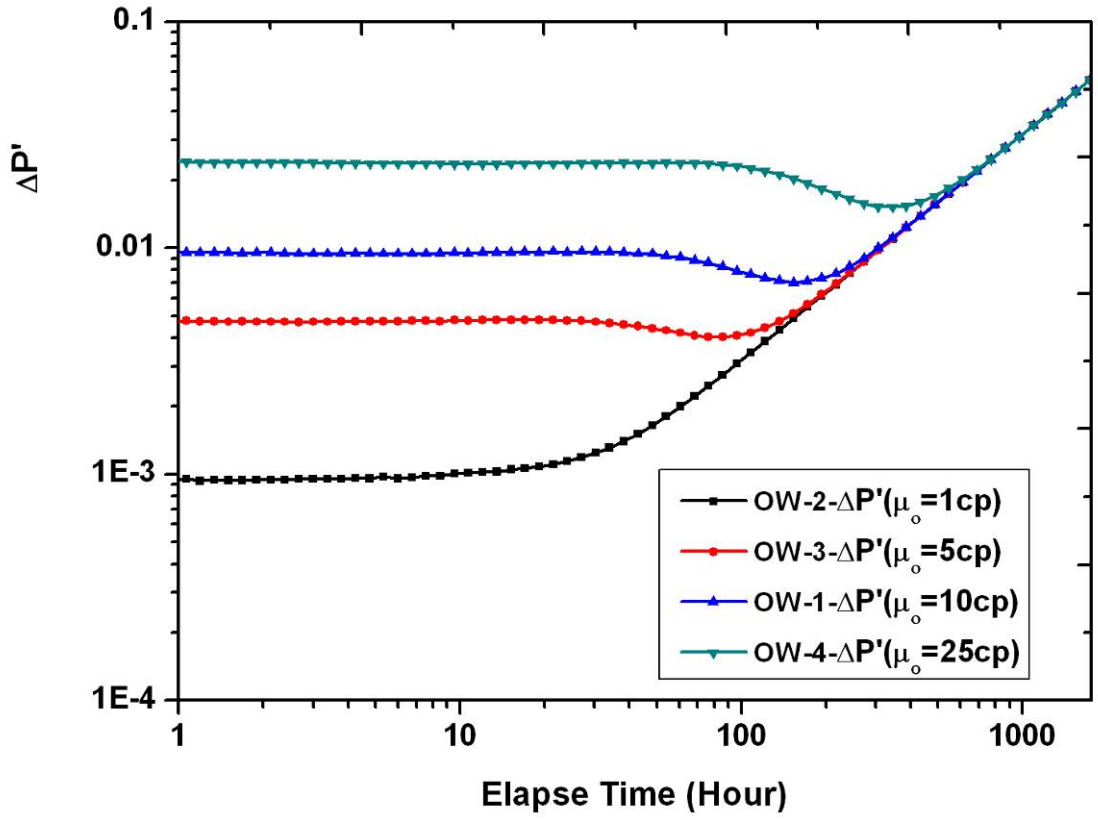

Figure 3.14 This figure shows the log-log plot of pressure response in a reservoir without Pc under different oil viscosities. If oil viscosity is greater, the time taken to reach the transition zone is longer.

But in the case of oil viscosity at 1cp, the pressure derivative does not decrease in the transition zone. As shown in **Figure 3.15**, although the total mobility has changed, the change in total mobility is very small, especially at late time, $\frac{\partial \lambda_t}{\partial t} \to C_2$ (C_2 = constant value).Hence, total effective mobility does not change quickly under low oil viscosity, so the phenomenon of the pressure derivative going down at the transition zone will not occur.

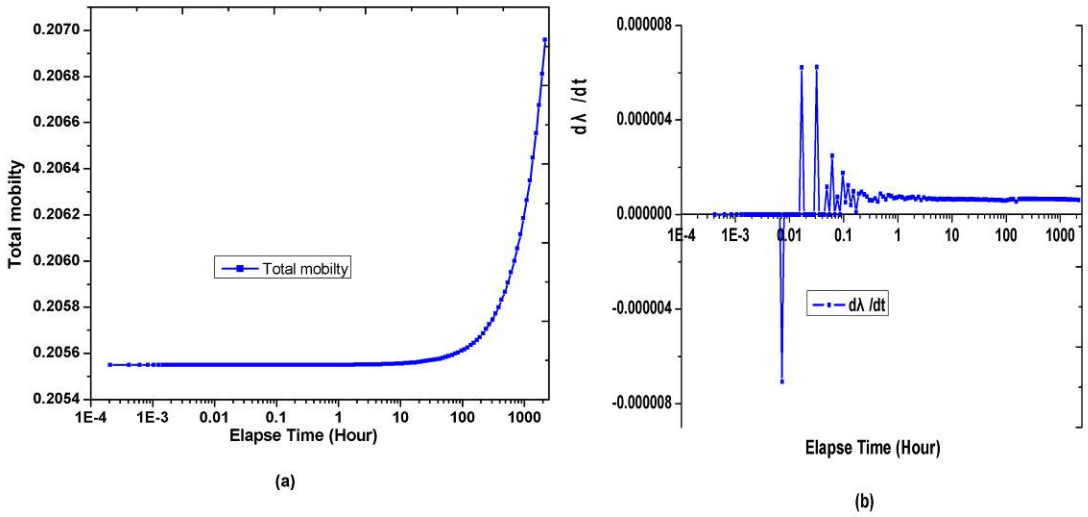

Figure 3.15 (a) The total mobility curve; and (b) the total mobility derivative curve at upstream saturation front with oil viscosity at 1 cp. Although the total mobility shows some changes, the total mobility derivative is very small and close to constant in late time.

3.2.3.3 Case study 2: Gas-water system

3.2.3.3.1 Two phase flow

For a gas-water reservoir system, there are two boundary system conditions: the closed boundary and the constant pressure boundary. Sensitivity studies were designed for these systems. The key parameters are listed in **Table 3.3**.

Table 3.3 The design of different flow conditions

Fluid	Case	Pc (Psi)	Model	OWC (ft)	Well location	Aquifer	Viscosity (cp)
Gas-water model	GW-1	No pc	Anticline	4735	Center	No	0.02
	GW-2	Pc	Anticline	4735	Center	No	0.02
	GW-3	Pc	Anticline	4735	Center	Aquifer	0.02
	GW-4	No Pc	Anticline	4735	Center	Aquifer	0.02
	GW-5	High Pc	Anticline	4735	Center	Aquifer	0.02

As with the studies of the oil-water system, capillary pressure was not considered at first. As shown in **Figure 3.16,** the pressure derivative starts to go up at 10.10 hours. This is due to the rapid decrease in total mobility (**Figure 3.17**). According to **Equation 3.25**, at 10.10 hours, the $\lambda_t(r,t)$ decreased, so the absolute value of $\frac{\partial \lambda_t(r,t)}{\partial t}$ increased and $\frac{\partial \lambda_t(r,t)}{\partial t} < 0$, but $\frac{d\Delta P_o(t)}{d\ln t}$ is positive and increasing with time.

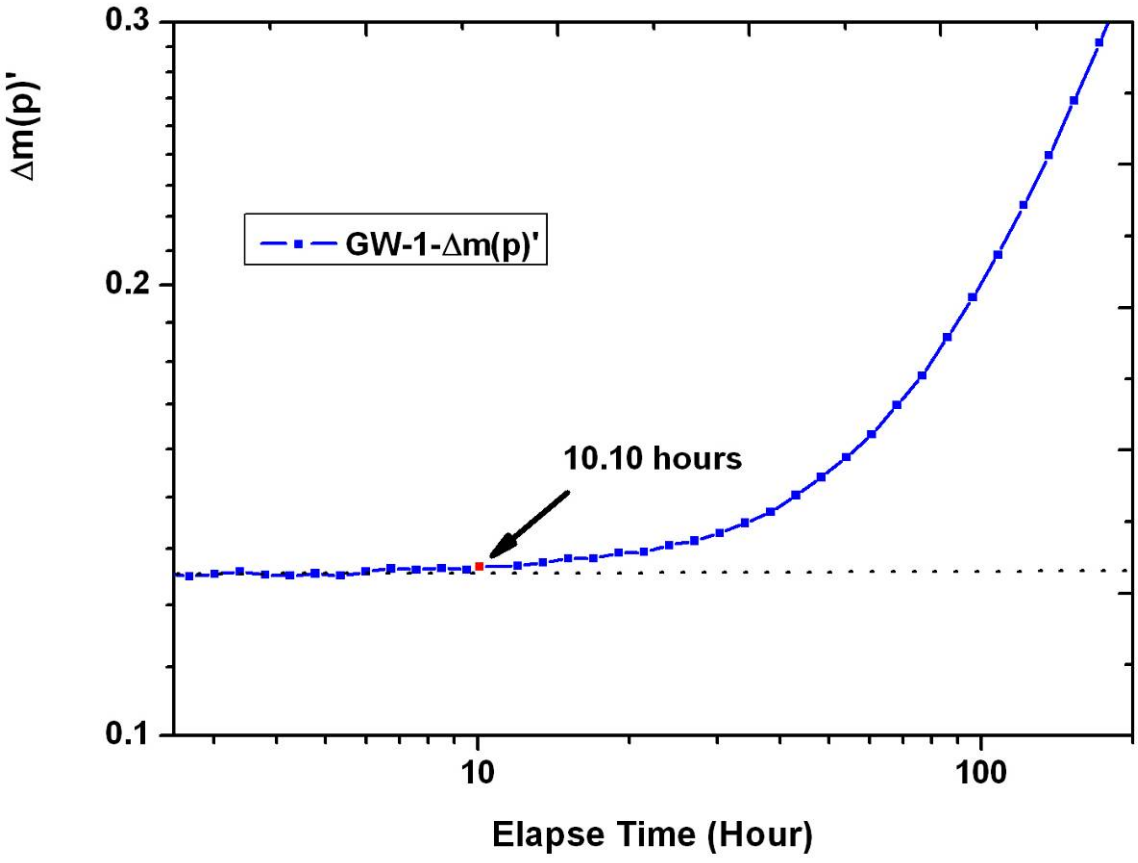

Figure 3.16 This figure shows the log-log plot of a gas-water reservoir with a closed boundary. The pressure derivative starts to increase from 10.10 hours.

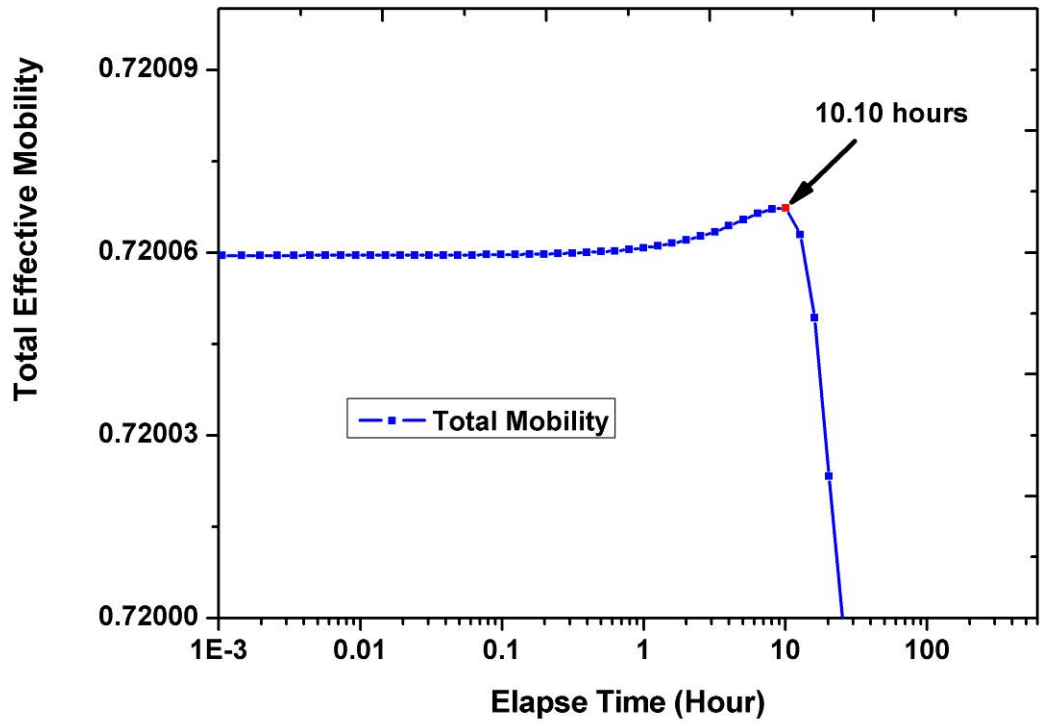

Figure 3.17 This figure shows the total mobility curve at the upstream saturation front ($r \to r_f^+$). From 10.10 hours, the total mobility starts to decrease rapidly.

3.2.3.3.2 Sensitivity studies

Effect of capillary pressure

According to **Equation 3.26**, because $-\frac{q_t(r',t)}{r'\lambda^2{}_t(r',t)}\frac{\partial\lambda_t(r',t)}{\partial t} > 0,$

The $\frac{\partial\lambda_{\text{equivalent}}(r',t)}{\partial t}\frac{\partial P_c}{\partial S_w}\frac{\partial S_w}{\partial r'} > 0$, so $\frac{d\Delta P_o(t)}{d\ln t} > 0,$

Figure 3.18 shows that the transition zone pressure derivative of a reservoir with capillary pressure goes up more than that without capillary pressure.

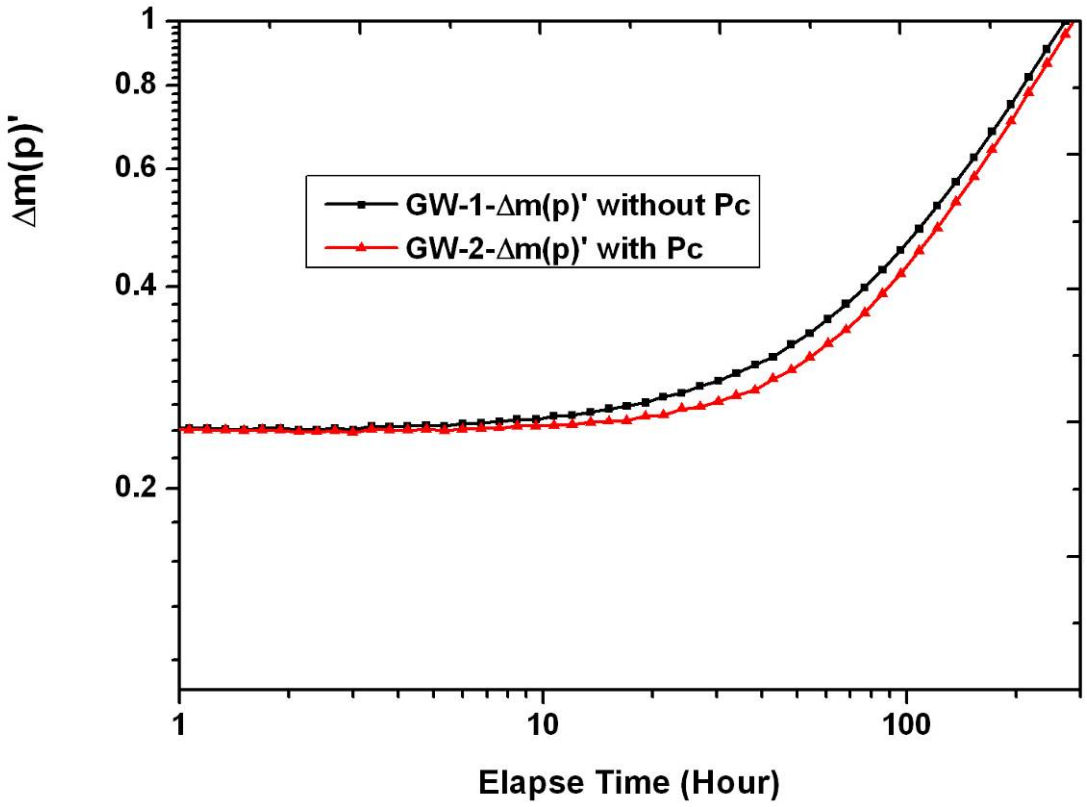

Figure 3.18 This figure shows the log-log plot of the pressure response in a gas-water reservoir with Pc and closed boundary; the pressure derivative with capillary pressure goes up more than that without capillary pressure.

Effect of constant pressure boundary

Considering constant pressure boundary, **Figure 3.19** shows that the pressure derivative of DD and BU goes up when the transition zone is reached, then goes down when the outer boundary is reached.

Figure 3.20 shows that the transition zone pressure derivative in a reservoir with capillary pressure goes up more than that without capillary pressure.

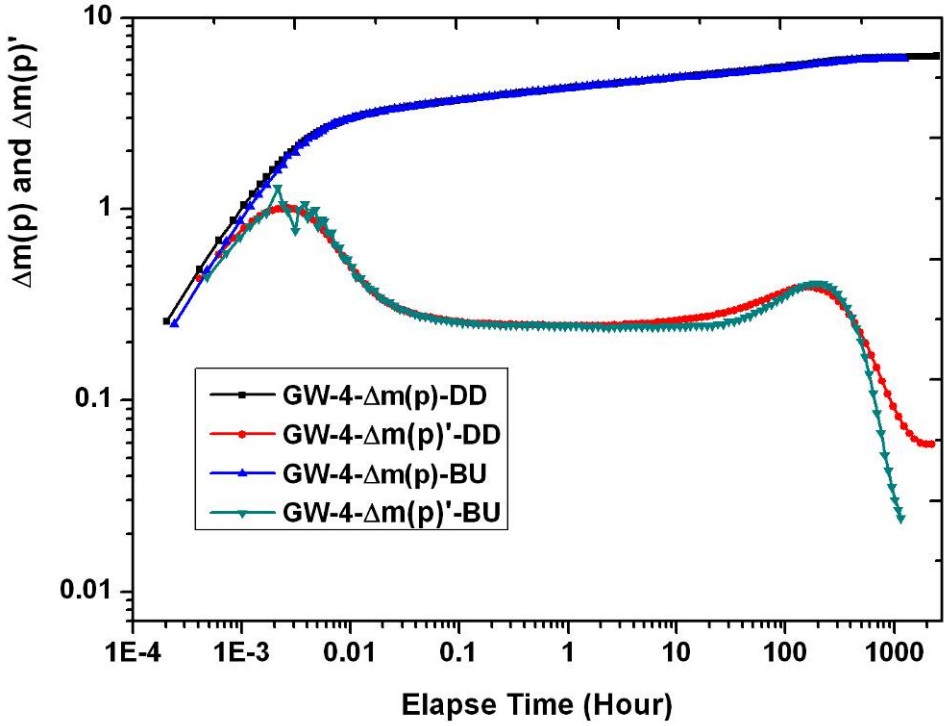

Figure 3.19 This figure shows the log-log plot of the pressure response in gas-water reservoir under constant pressure boundary. The pressure derivative of DD and BU goes up when the transition zone is reached, then goes down when the outer boundary is reached.

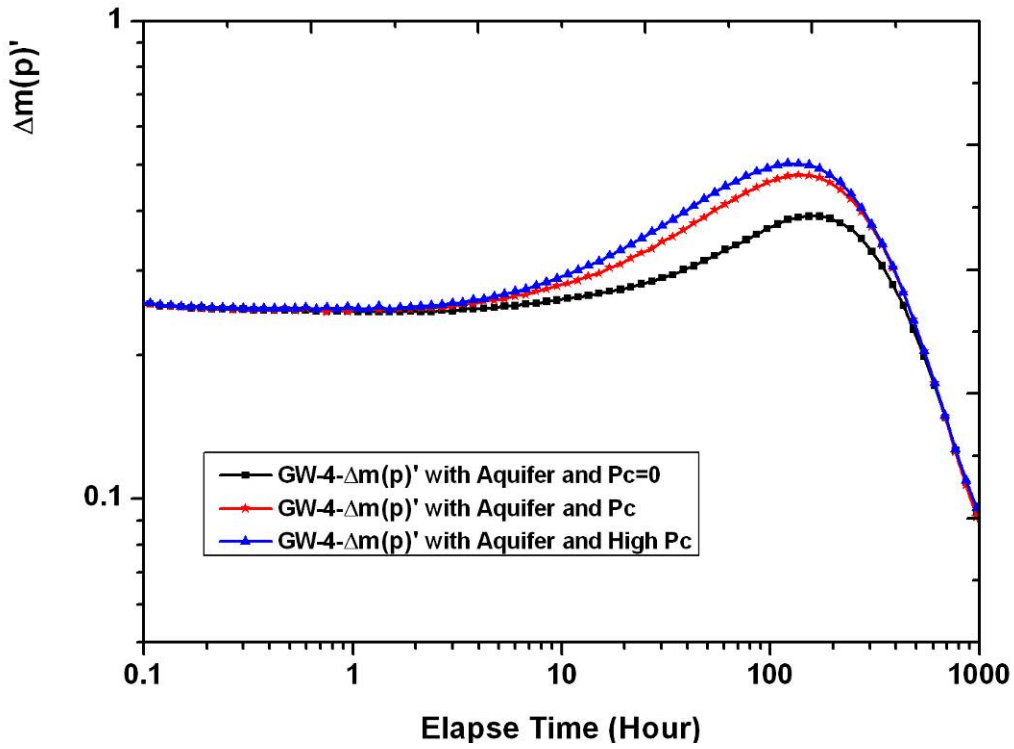

Figure 3.20 This figure shows the log-log plot of the pressure response in a gas-water reservoir with Pc and constant pressure boundary. It shows that the pressure derivative with capillary pressure goes up more than that without capillary pressure in the transition zone.

Distance of Movement for Saturation Front

In order to simulate the saturation front movement, PDG data were generated by simulation (**Figure 3.21).** The first DD and the last DD were selected for analysis. As shown in **Figure 3.22**, for the first DD, at 2.123hours, pressure reached the saturation front, but for the last DD, the time for pressure reaching the saturation front is about 1.190hours. Using **Equation 3.28**, for the first DD, the radius investigation of R1 is calculated as about 1712.237 ft; for the last DD, the radius investigation of R2 is calculated as about 2282.869 ft. The angle of formation bedding (α) is about 2.8^0, $H = \sin\alpha \times (R_2 - R_1)$, the height of saturation front can be obtained as about 27.87 ft.

Figure 3.23 shows that the height of saturation front is about 27.7 ft. In comparison with the well test and simulation results, the error is only 0.6%.

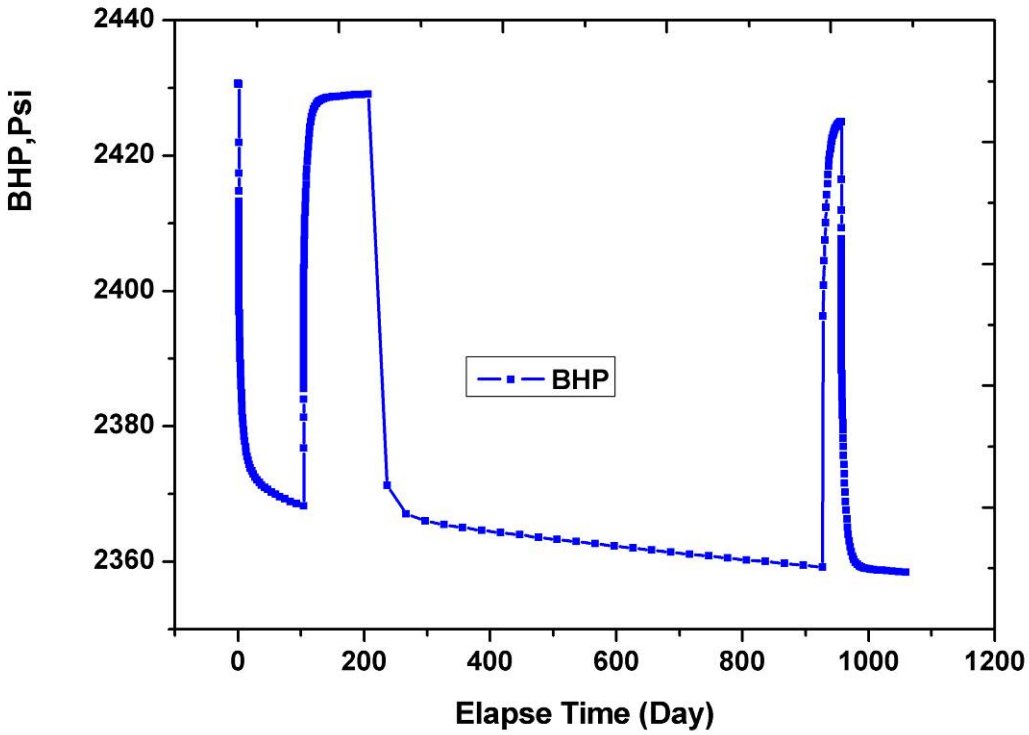

Figure 3.21 The bottom-hole pressure history. The first DD and last DD were selected for the analysis.

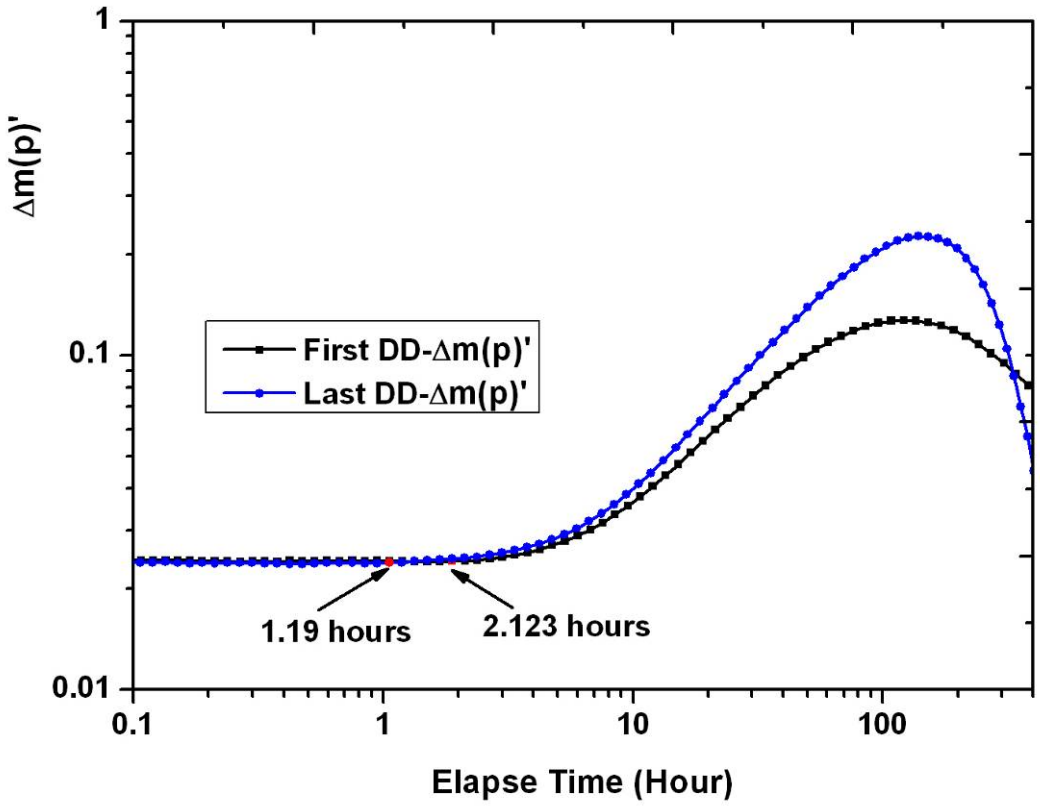

Figure 3.22 This figure shows interpretation results of the first and last DD. For the first DD, from 2.123 hours, pressure reaches the saturation front, but for the last DD, the time of pressure reaching the saturation front is about 1.190 hours.

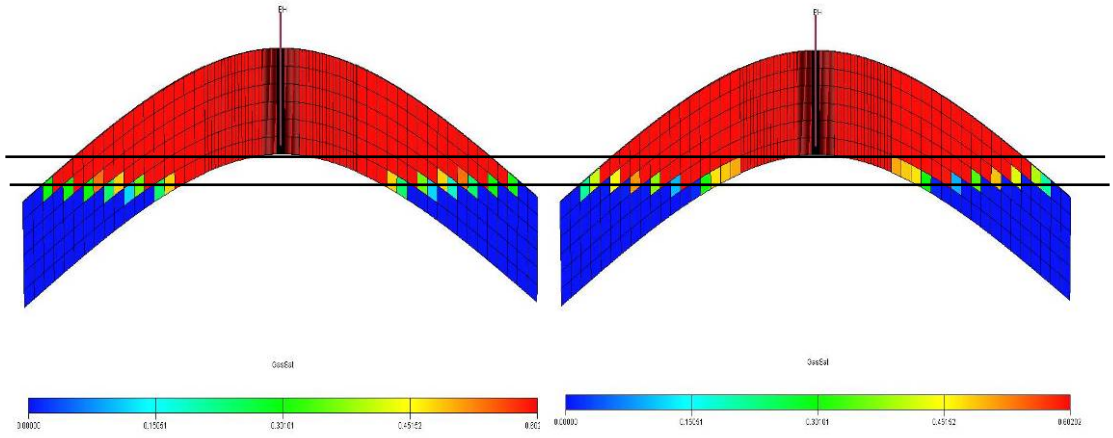

(a) (b)

Figure 3.23 (a) the initial oil water contact (OWC); (b) the oil water contact at 1060 days, according to the saturation profile, the distance of movement for the saturation front with time is about 27.7ft.

3.2.4 Field Application

In order to apply the pressure behavior of the study in practice, two field examples are examined a gas well test and an oil well test.

3.2.4.1 Well A-Gas Well Test

This well is located between two faults. The distances from the well to the faults are 2100ft and 3600ft (**Figure 3.24**). The average permeability of the gas reservoir is 1.8mD and the porosity is 11.5%. In order to test well productivity, a well test was performed (**Figure 3.25**). From the test data, the last build up data was analyzed. Because geologist engineers thought that the gas well did not encounter a water layer during the drilling, this gas reservoir is assumed to be a dry gas reservoir. Therefore, a single-phase theory was used to interpret the well test. From the log-log plot (**Figure 3.26**), at late time, the pressure derivative went up, using one fault model to match this test response, at 670 ft away from well A, there is a no-flow boundary. Combining the geological knowledge, reservoir engineers believed this no-flow boundary may be a sub-seismic fault. But after this well was put into production for two months, the water broke through.

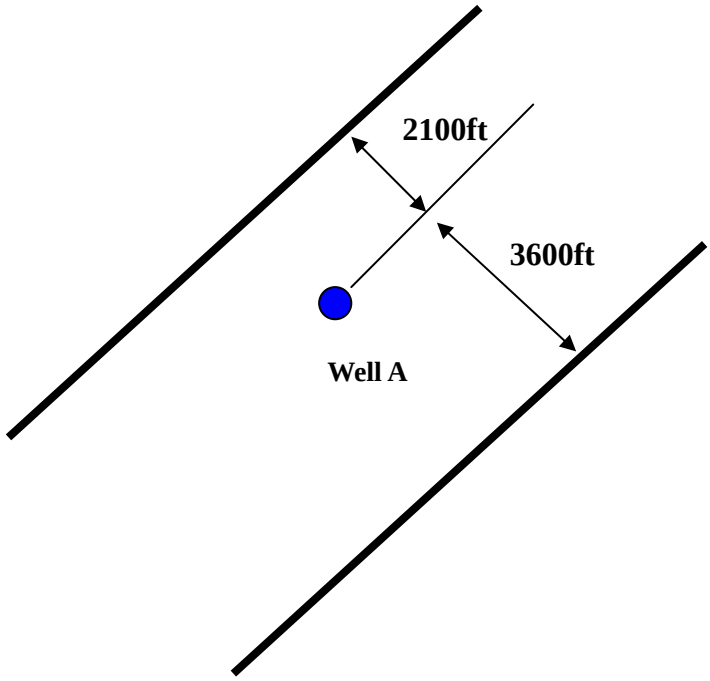

Figure 3.24 This figure shows the sketch map of Well A. This gas reservoir was controlled by two faults.

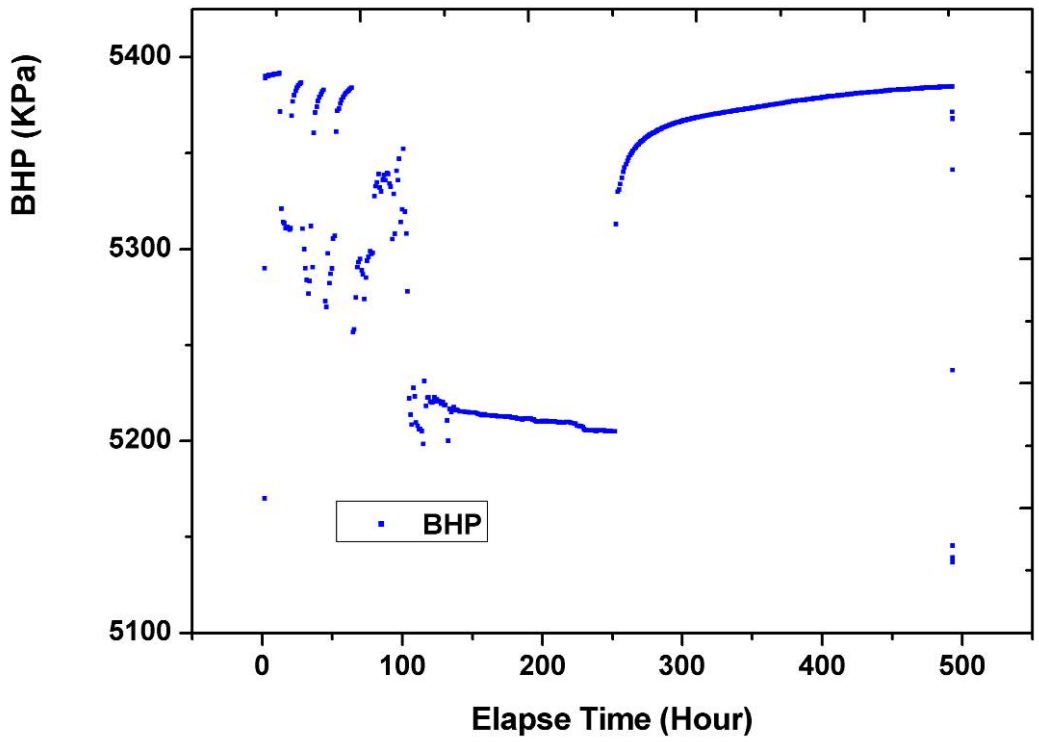

Figure 3.25 This is the test history of well A. The last BU was selected for the analysis.

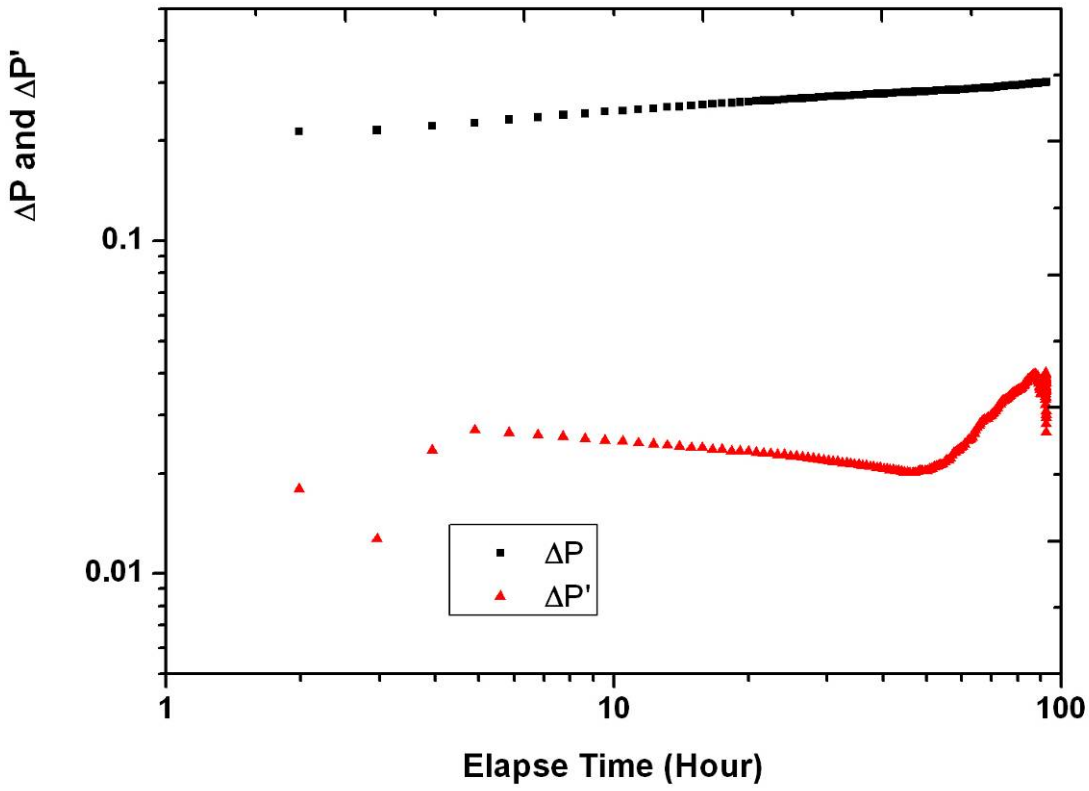

Figure 3.26 This is the log-log plot of well A for last BU. At late time the pressure derivative goes up.

The lesson learnt from this case was that the use of single phase theory to interpret the test is inappropriate. Although well test data had some ambiguities, if the impact of multiphase flow was not taken into account, especially at transition zone, which can affect the late time pressure response, the analysis result could lead to a completely wrong decision. In fact, in this well test log-log plot, the pressure derivative goes up at late time, purely due to the changes of total mobility in transition zone, and nothing to do with the reservoir outer boundary.

3.2.4.2 Well B-Oil Well Test

This reservoir is an anticline reservoir (**Figure 3.27**). The average buried depth of this reservoir is 1650 ft, and the oil viscosity is 120 cp. But the average permeability of the formation is 3 D, and the porosity is 0.27. Hence, although the oil property is very bad, the formation property is very good. Using conventional methods to produce, the single well productivity is very high. The key for field development is the evaluation of formation energy. So well testing was used (**Figure 3.28**). From the test data, the last DD and the last BU were selected for the analysis. The DD and BU plots show that at late time the pressure derivatives all go down (**Figure 3.29, Figure 3.30**), which was a sign of the pressure reaching aquifer, it means that the reservoir has higher energy.

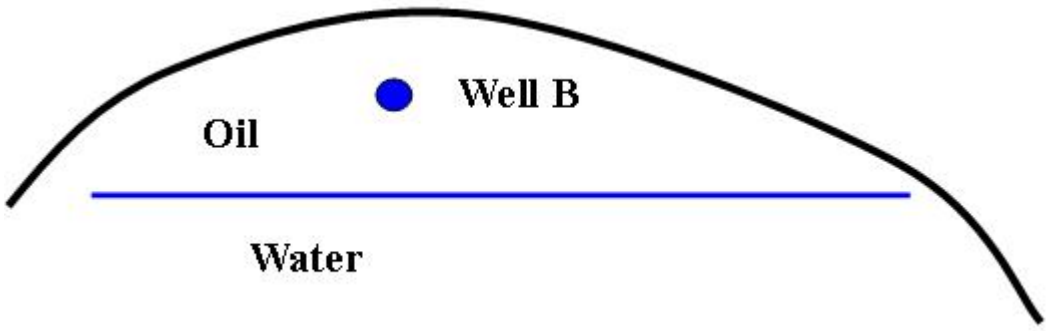

Figure 3.27 This is the plan view of Well B. This oil reservoir is an anticline reservoir.

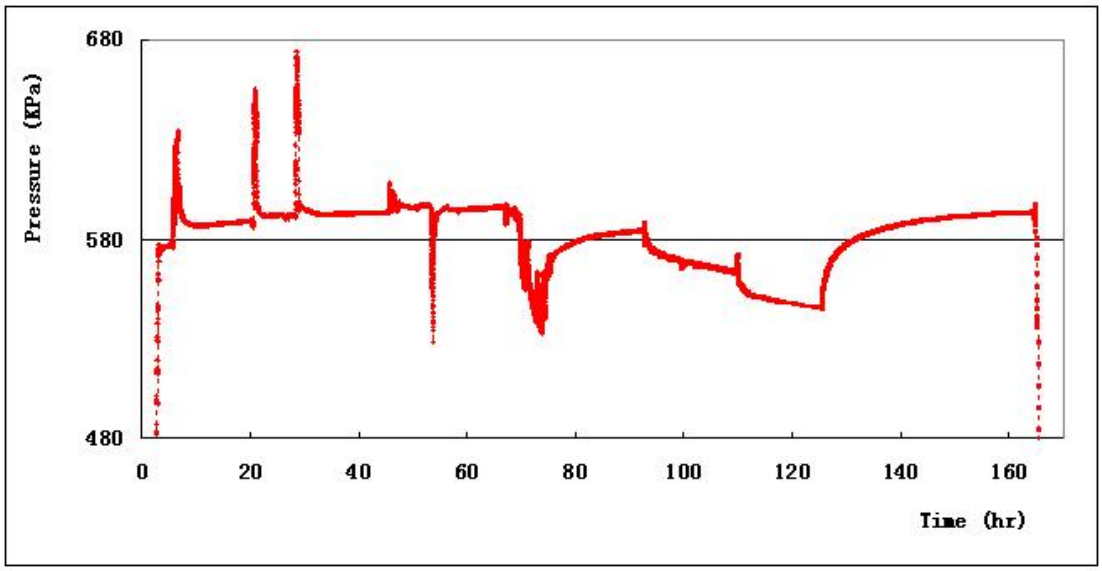

Figure 3.28 This figure is the test history of well B. The last DD and last BU are selected for analysis.

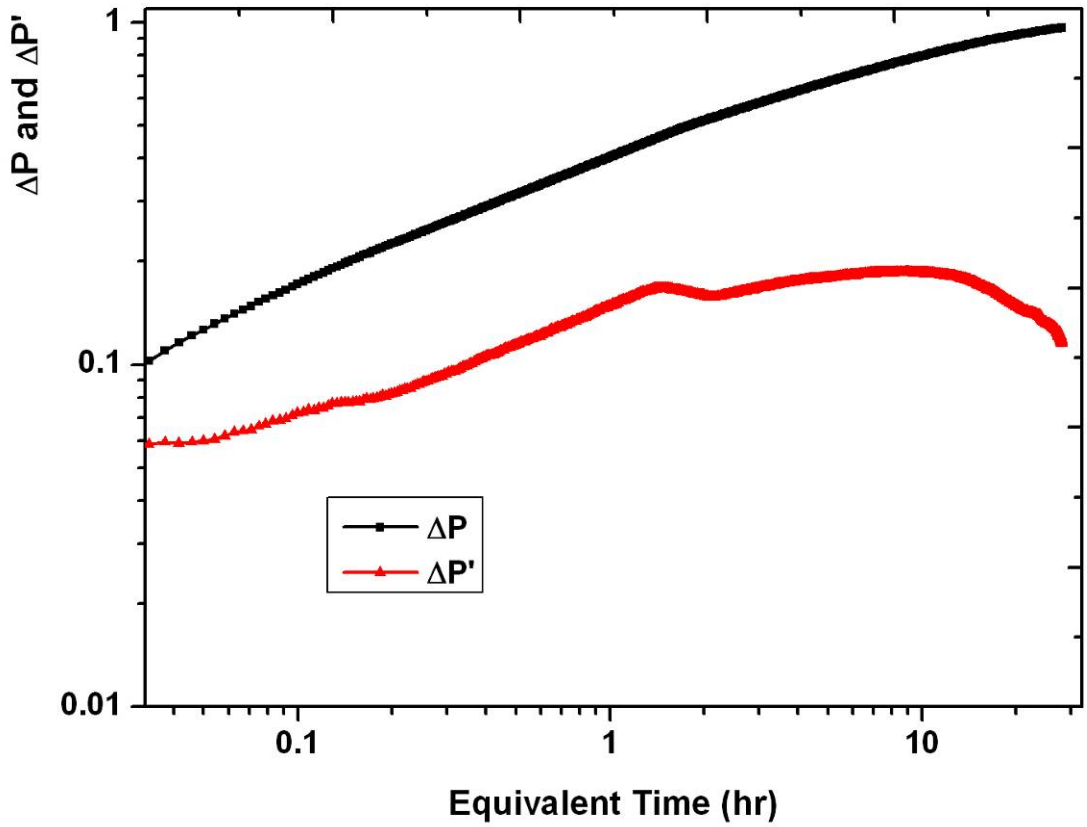

Figure 3.29 This is the log-log plot of well B for last DD. From this plot, the pressure derivative decreases at late time.

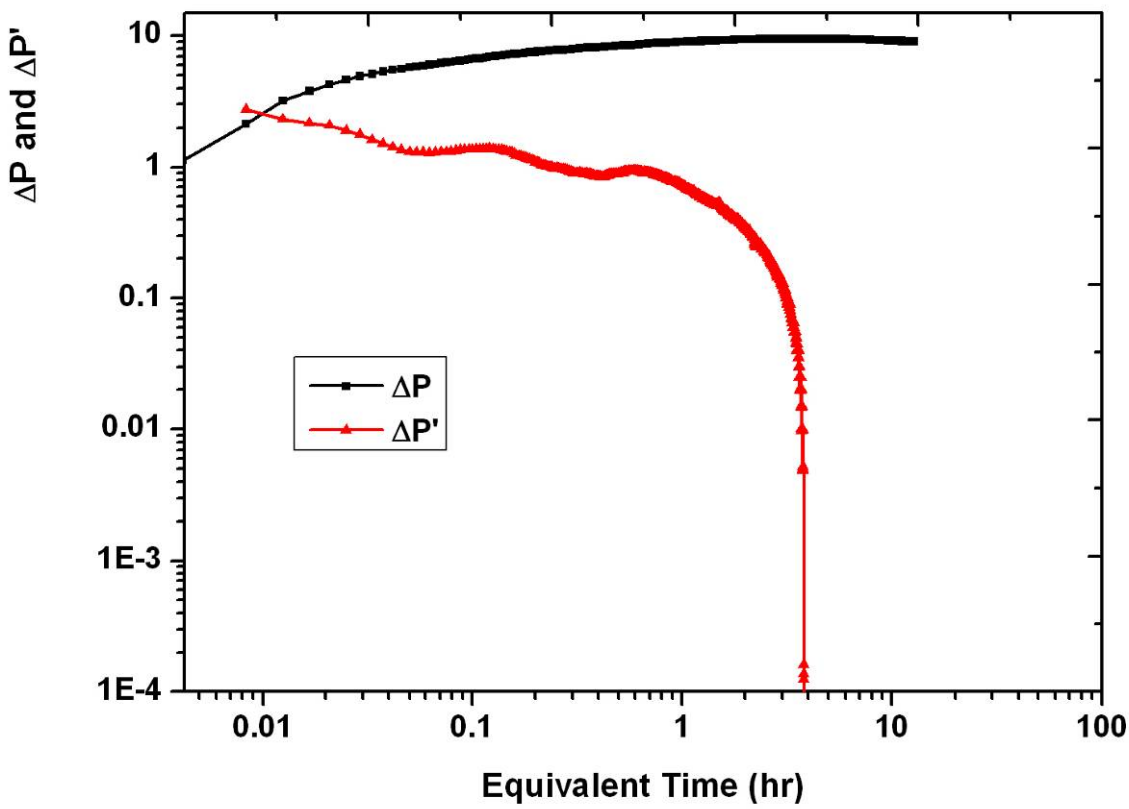

Figure 3.30 This figure shows the log-log plot of well B for last BU. On this plot, the pressure derivative also decreases quickly at late time.

According to the well testing result, at early development phase, the natural depletion mechanism development was advised. But after 6 months production, some wells in this reservoir could not continue production, including well B.

In fact, for this reservoir, if multiphase flow theory was used to interpret the well test, in the log-log plot of DD, the pressure derivative decreased, purely as a response to the change of the total mobility in the transition zone. Again, this is nothing to do with the outer boundary.

3.2.5 Summary

- Based on a theoretical development by Thompson, a new expression can be derived from Darcy's Law. According to this expression and to the numerical well test results, we reasonably interpret the pressure behavior of the transition zone in

oil-water and gas-water reservoirs. The results presented in this work are generally applicable to multiphase reservoirs, which have either an infinite-acting or a constant pressure outer boundary.

- Capillary pressure in the transition zone has an insignificant impact on pressure response.

- Two field examples were interpreted, based on this new understanding of pressure behavior in the transition zone. It seems to work well as an explanation of the situations of these two well tests.

3.3 Analysis of Transient Pressure Response for Two Phase Flow System after Water Breakthrough

3.3.1 General Remarks

It is well known that well test analysis involves the interpretation of BHP data to evaluate well and reservoir parameters like permeability, skin factor, average pressure, and well productivity, etc. These results are vital for reservoir management. Petroleum engineers can use these results to update simulation models or provide stimulations for individual wells.

Up to now, whether using transient well testing or stabilized well testing, the interpretation approach for well tests is used widely under single phase conditions. But in practice, single phase flow in the reservoir formation is rare. When oil fields enter middle- high water cut stage, conventional well testing approach is not applicable to multiphase flow well testing. Fortunately, many researchers have been focused on multiphase flow, and have found a number of methods to solve the multiphase flow problems.

For transient well testing, as described above in Chapter 1, there are three methods that may be used. The key concept for these approaches is the simplified black oil model,

making the non-linear system approximate to the linear system, and then using single phase well testing theory to interpret multiphase well testing data. But the influences of saturation gradient and pressure gradient are not considered for these approaches, and in fact, the fluid saturation is not homogeneous.

For stabilized well testing, many inflow performance relationships (IPR) for estimating the pressure/production behavior during multiphase flow have been published. These IPRs have been studied by Vogel [Vogel, J.V.,1968[32]]; Fetkovich [Fetkovich,M.J.,1973[6]]; Jones, Blount, and Jones and Glaze [Jones, L.G., Blount, E.M., and Glaze, O.H., 1976[33]]; Klins and Majcher [Klins, M.A. and Majcher, M.W., 1992[34]]; and Sukarno and Wisnogroho [Sukarno, P. and Wisnogroho, A., 1995[35]]; Umnuayponwiwat [Umnuayponwiwat, S., 2000[96]]; and Wiggins [Wiggins, M.L., 1994[36];1996[37]]; and Marhaendrajana [Marhaendrajana, T., 2003[46]]; and Zhong, Haiquan [Zhong, Haiquan, 2007[38]]. Using IPRs, reservoir engineers can evaluate operating conditions, determine the optimum production scheme, and design production equipment and artificial-lift systems.

Whether performing transient well testing or stabilized well testing, the basis of well testing analysis is that the curve of well testing is normal. But when mature fields with non-uniform saturation reached the middle-high water-cut stage, there is a big influence on bottom-hole pressure under multiphase flow condition. In this situation, two types of BHP data can be observed under different oil/water mobility ratio conditions (**Figure 3.31**). Under low mobility ratio, BHP data is normal, which can be interpreted by traditional multiphase flow well testing methods, but the error of analysis is large. But for high mobility ratios, the BHP curve may go up when the water-cut of oil well reaches a value. For this type of data, well testing approaches cannot be used for analysis.

For abnormal BHP data, many reservoir engineers think this phenomenon is due to changes in production rate, the change in skin factor near well bore or the interference

of multi-wells. (Economies, M.J., *et al*., 1985[39]; Leaver, J.D., *et al.*, 1988[40]; Onur,. M., *et al.*, 1991[41]; Grasman, T.J., *et al.*, 1990[42]; Britt, L.K., *et al.*, 1991[43]; Hallford, D.L., *et al.*, 1995[44]; Erwin,M.D., *et al.*, 2002[45]; Harper, T.R., *et al.*, 1985[47]; Bensadok, A., *et al*., 2004[91])

This chapter excludes the interferences of these reasons, and the objective of research focuses on multiphase flow and explains the phenomenon from the viewpoint of multiphase.

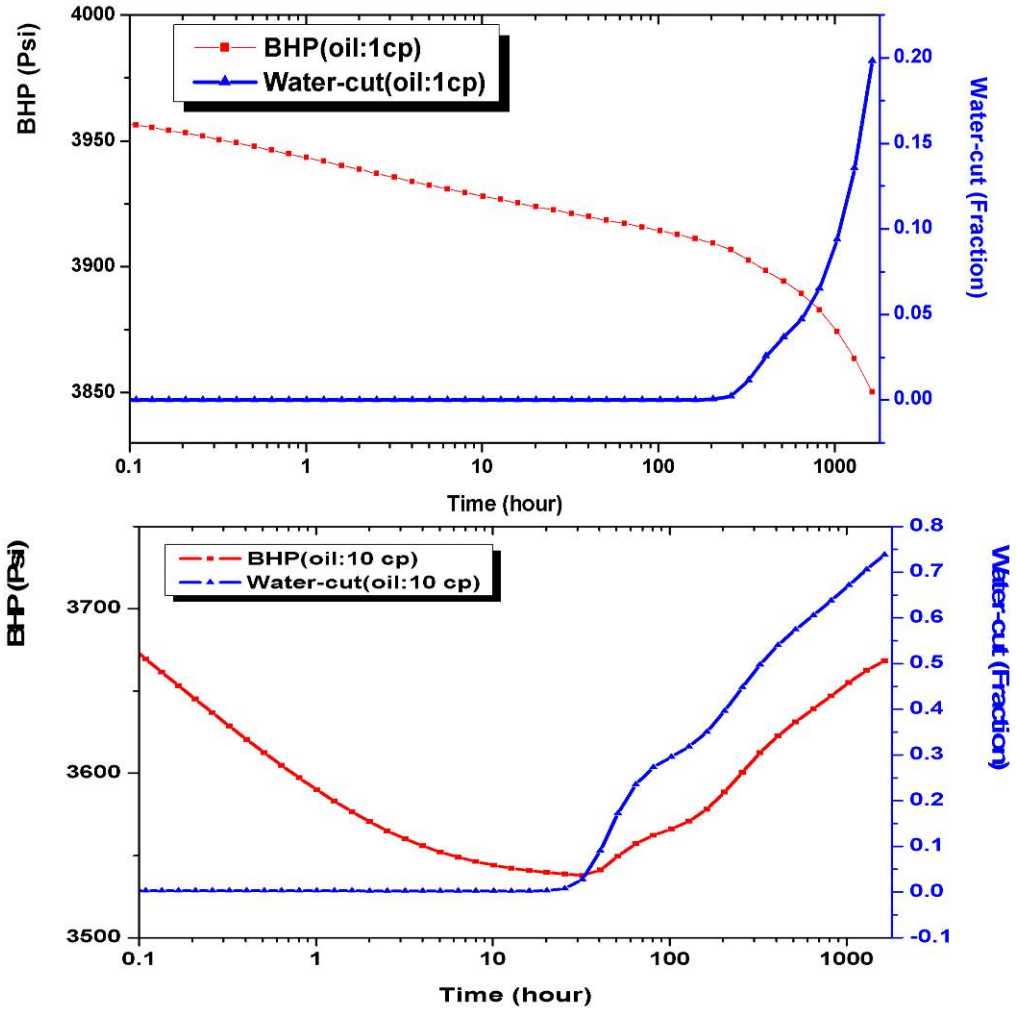

Figure 3.31 The curves of BHP and water-cut under multiphase flow conditions for different oil/water mobility ratio. For low mobility ratio (top figure), the BHP data is normal, but for high mobility ratio (lower figure), when water cut breaks through and reaches a critical point, the BHP may increase.

3.3.2 Numerical model

In order to study the problems of multiphase flow after water breakthrough for non-uniformly saturated reservoirs, a 3D model was built using the Eclipse simulator to examine the pressure response in a well located at the center of an anticline reservoir with closed system or constant pressure boundary system.

The simulation model is a homogeneous, anticline, and oil-water model. The absolute permeability of the model is 200md, which is equal in direction I, J, K respectively. The porosity is 0.25.

Grid description

In the constructed numerical model, the basic simulation grids consist of 100 in the radial direction, 1 in the theta direction, and with 1 layer (**Figure 3.32**). Because the bottom-hole pressure was sensitive to the size of grid, in order to avoid numerical dispersion, a very small grid was used in the near well-bore area, and the outer grid size increases gradually.

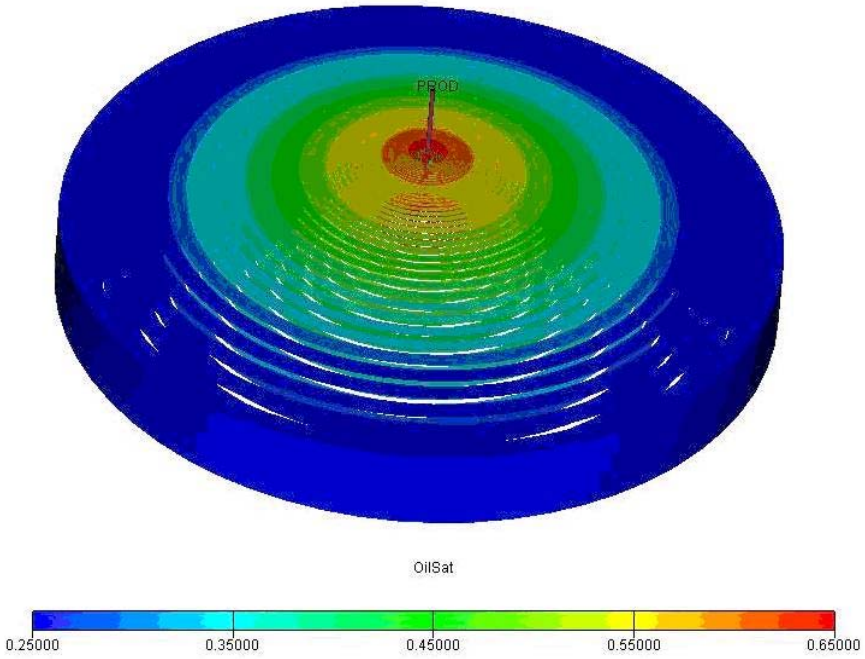

Figure 3.32 This figure shows a 3D model. The reservoir is radial anticline, and the water saturation is non-uniform in a horizontal direction.

Fluid and rock characterization

The reservoir is filled with two slightly compressible fluids: oil and water. Capillary pressure effect is assumed to be negligible. The viscosity of each fluid is assumed to be constant. Under reference pressure, the viscosity of water is 0.5cp, but the viscosity of oil is changed between 1cp and 20cp for different experiments. The basic oil/water relative permeability curve is shown in **Figure 3.33**.

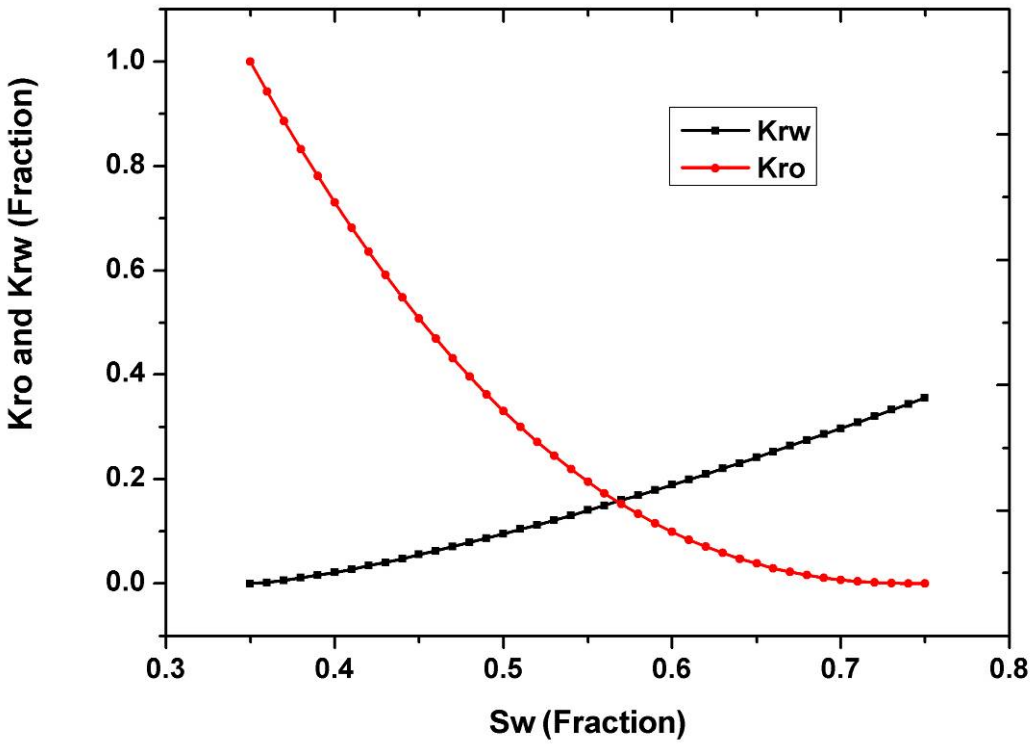

Figure 3.33 The oil/water relative permeability curve

3.3.3 Analysis of Normal Bottom Hole Pressure Data

As shown in **Figure 3.34**, long term data were generated by a numerical simulation model. This transient well test includes several DD and BU with water-cut from 0% to 80%.

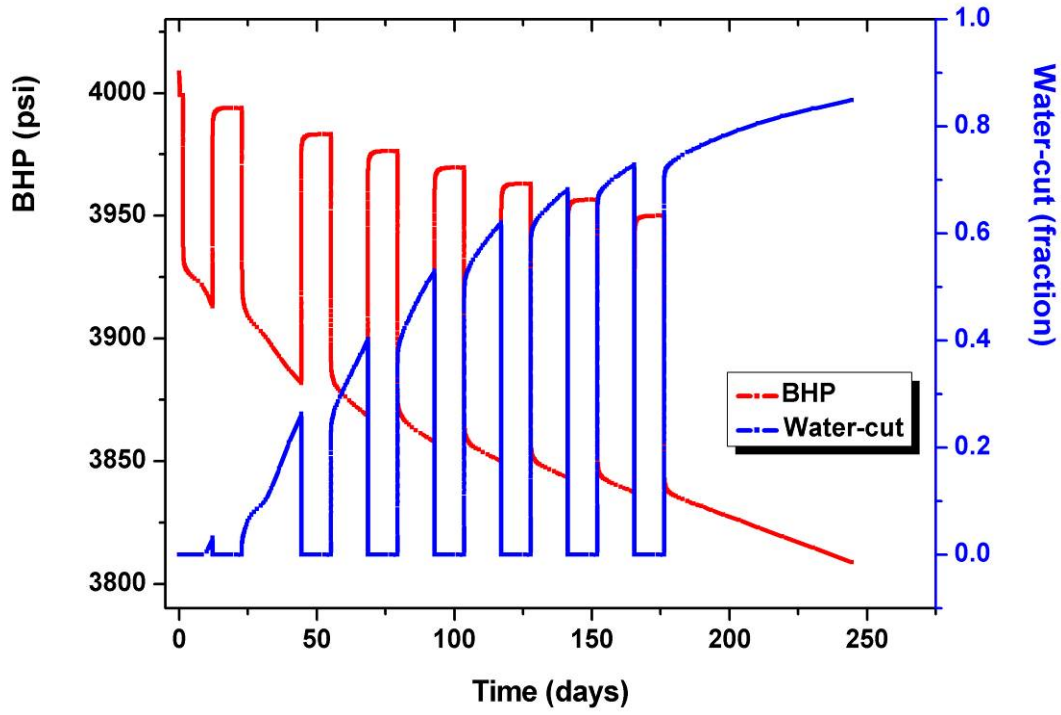

Figure 3.34 This figure shows a long term transient pressure curve and water-cut curve.

3.3.3.1 Traditional transient multiphase flow approach

According to the P-M approach, the phase permeability can be obtained under different water-cut conditions, which are shown in **Table 3.4**.

When water-cut is less than 30% or more than 80%, using single oil or single water to analyze multiphase flow well testing, calculation results may be accepted approximatively. But in this situation, radial flow can be determined accurately due to the change of fluid mobility. So it is difficult to obtain the slope of the straight line in semi-log plot. As shown in **Figure 3.35,** it is also very difficult to identify the radial flow from log-log plot under different water-cut conditions.

Hence, for mature fields, if saturation is non-uniform, when the reservoir reaches middle-high water-cut stage transient well testing is not applicable, even though using P-M approach to interpret the data, the error in interpreting the results is very large.

Table 3.4 Comparison of the interpretation results of P-M and model parameters

Average water-cut	**Input K** ($S_w = S_{wi}$)	**Ko**	**Kw**	**Ko**	**Kw**
%	md	md	md	Error (%)	Error (%)
0	200	201.7	0	0.85	100
10	200	186.2	20.6	6.9	89.7
30	200	169.4	72.5	15.3	63.75
40	200	146.9	97.9	26.55	51.05
50	200	92.4	107	53.8	46.5
60	200	75.9	113.9	62.05	43.05
70	200	56.9	132.9	71.55	33.55
80	200	42.1	168.2	78.95	15.9

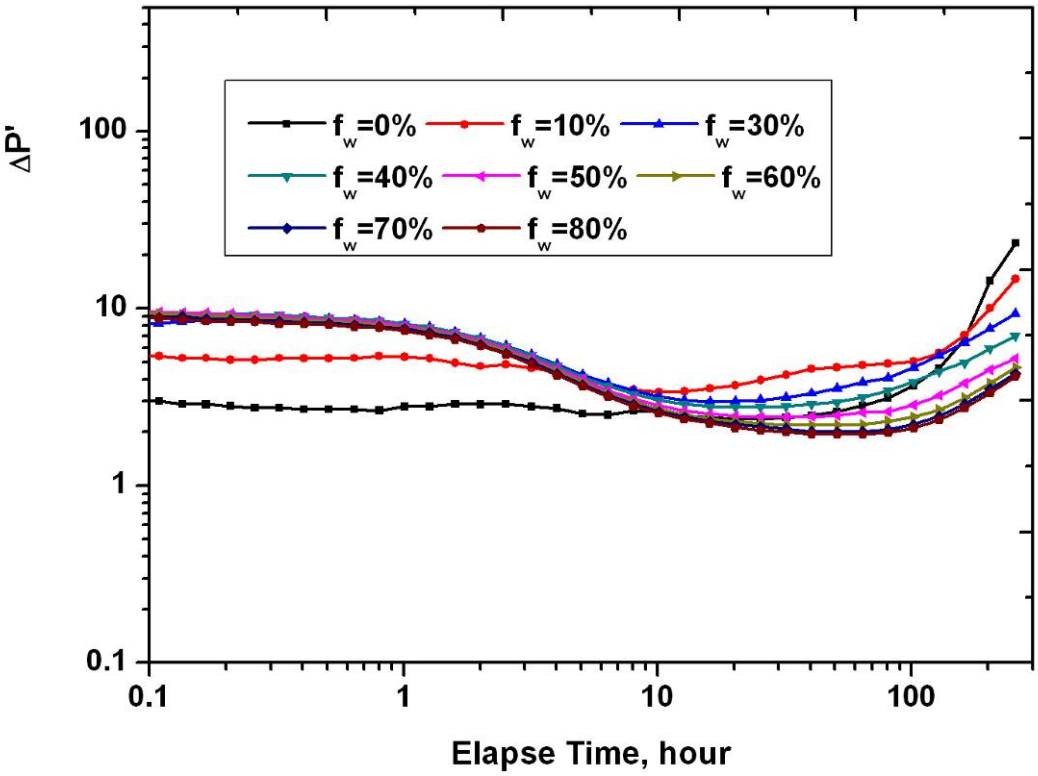

Figure 3.35 This figure shows the pressure derivatives for different water-cut conditions.

3.3.3.2 Stabilized well testing approach

For the oil-water system, two kinds of models were considered to apply to the stabilized well testing. One is the uniform saturation reservoir. The other is the non-uniform saturation reservoir. The main objective of the two models is to investigate the relationship between the wellbore flowing pressure and the flow rate under multiphase flow condition. According to the pseudo-steady state time, the flow rate was obtained. The beginning pseudo-steady state time is determined by using the following equation:

$$t_{pse} = \frac{\phi c_t r_e^{\,2}}{0.00088\left(k/\mu\right)_t} \tag{3.29}$$

Where: $\left(k/\mu\right)_t = \left(kk_{ro}/\mu_o\right) + \left(kk_{rw}/\mu_w\right)$

For the two models, setting the value of the wellbore flowing pressure as a fraction of reservoir pressure, the BHP between the reservoir pressure and 14.5 psi will be divided into several flowing pressures, for example: $(P_{wf})_1=0.95P_i$, $(P_{wf})_2=0.85P_i$, $(P_{wf})_2=0.75P_i$, … and $(P_{wf})_n=14.5$ psi.

In this work, the simulation results are compared with the calculation results by using the Sukarno approach and the Brown approach (**Appendix A**). The results are shown in **Figure 3.36, Figure 3.37, Figure 3.38** and **Figure 3.39.**

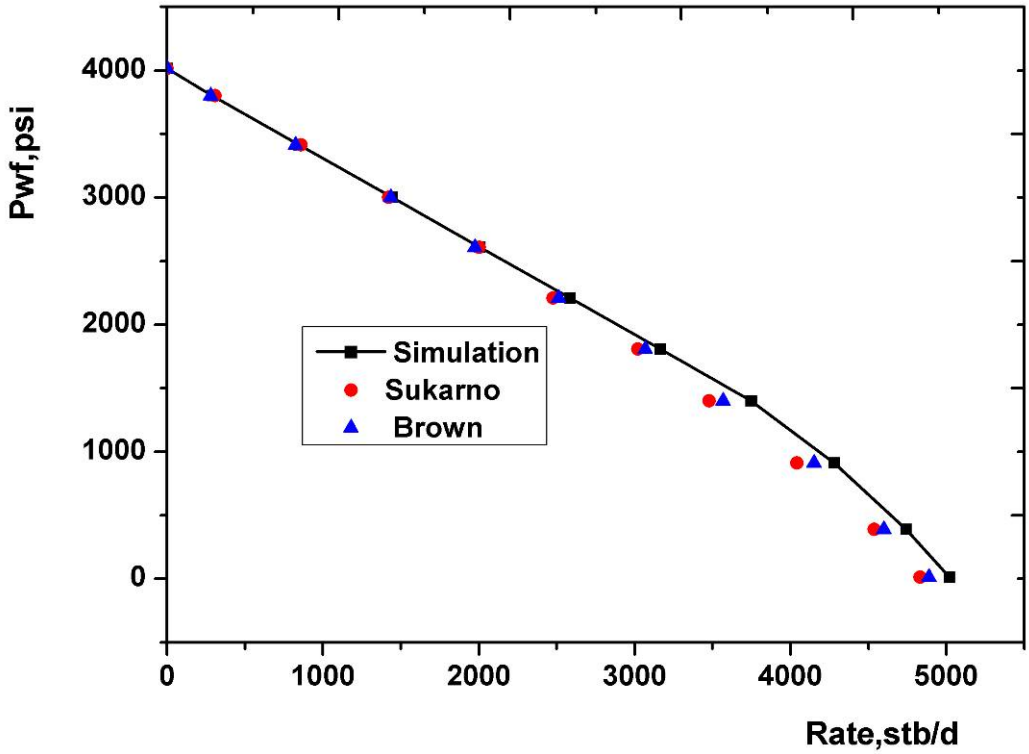

Figure 3.36 Oil IPR curves based on uniform saturation model under different methods

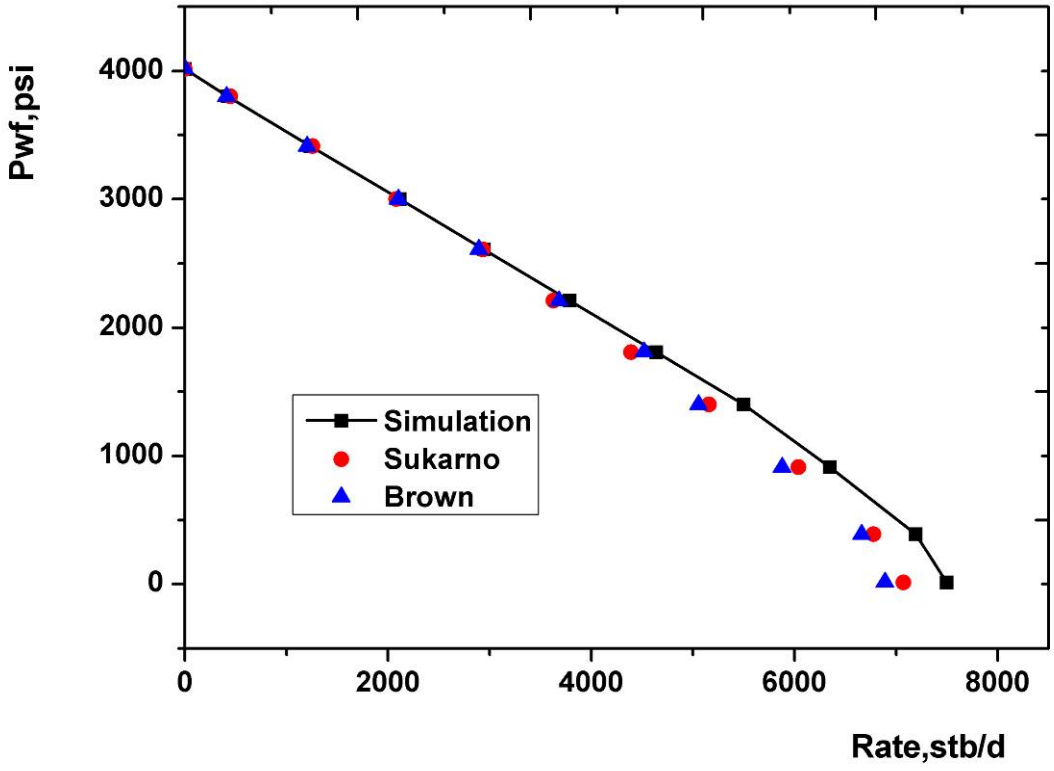

Figure 3.37 Water IPR curves based on uniform saturation model under different methods

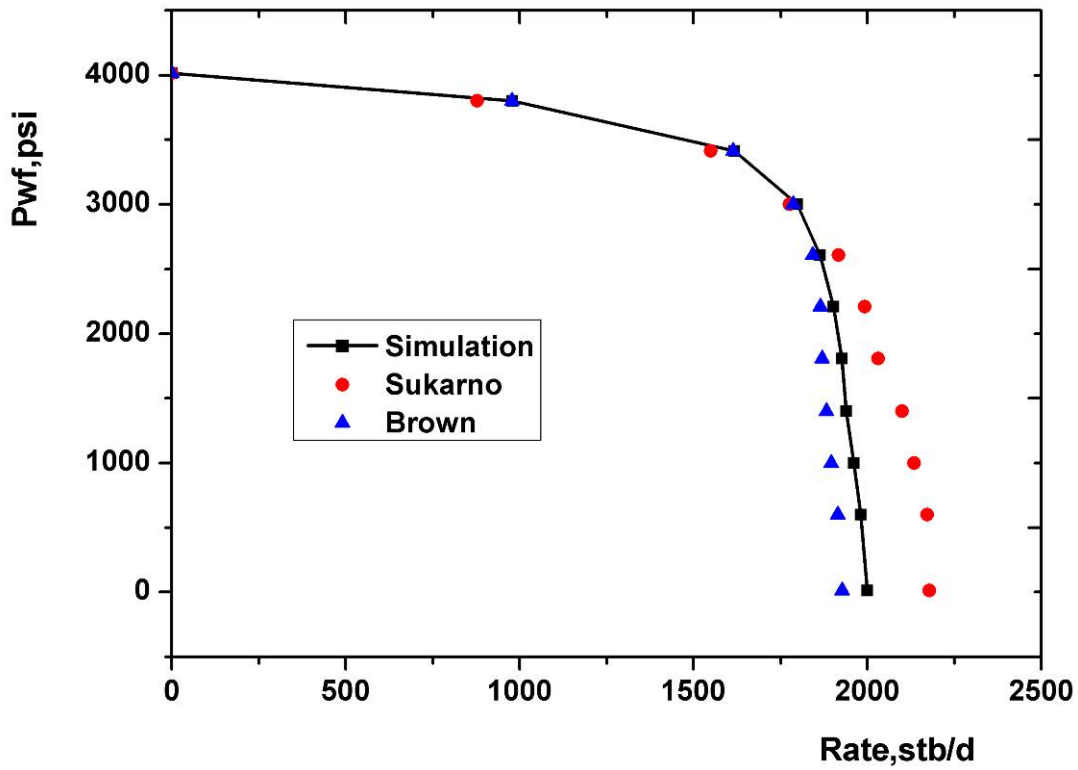

Figure 3.38 Oil IPR curves based on non-uniform saturation model under different methods

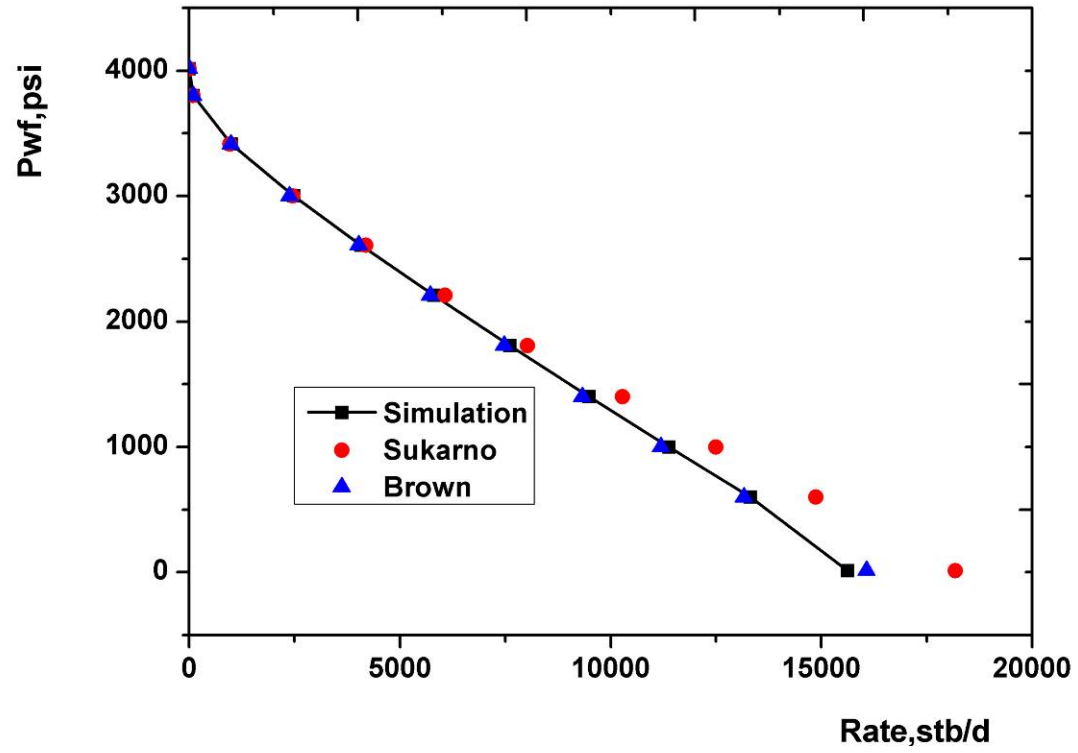

Figure 3.39 Water IPR curves based on non-uniform saturation model under different methods

Figure 3.36 and **Figure 3.37** show that stabilized well testing can be used to analyze the oil/water productivity index under uniform saturation reservoir conditions. However, the error increases with increasing drawdown pressure. But for non-uniform saturation reservoirs, **Figure 3.38** and **Figure 3.39** show that the calculation results cannot match the simulation results. So in real fields the efficacy of stabilized well testing of multiphase flow is not good.

3.3.3.3 Summary

Combining analysis of transient well testing and stabilized well testing for non-uniform saturation reservoirs and normal transient pressure data, there is no good method to solve multiphase flow problems.

3.3.4 Analysis of Abnormal Bottom Hole Pressure Data

As shown in **Figure 3.40**, abnormal BHP data were generated by the numerical simulation model. For this type of data, whether performing transient well testing or stabilized well testing, results cannot be analyzed.

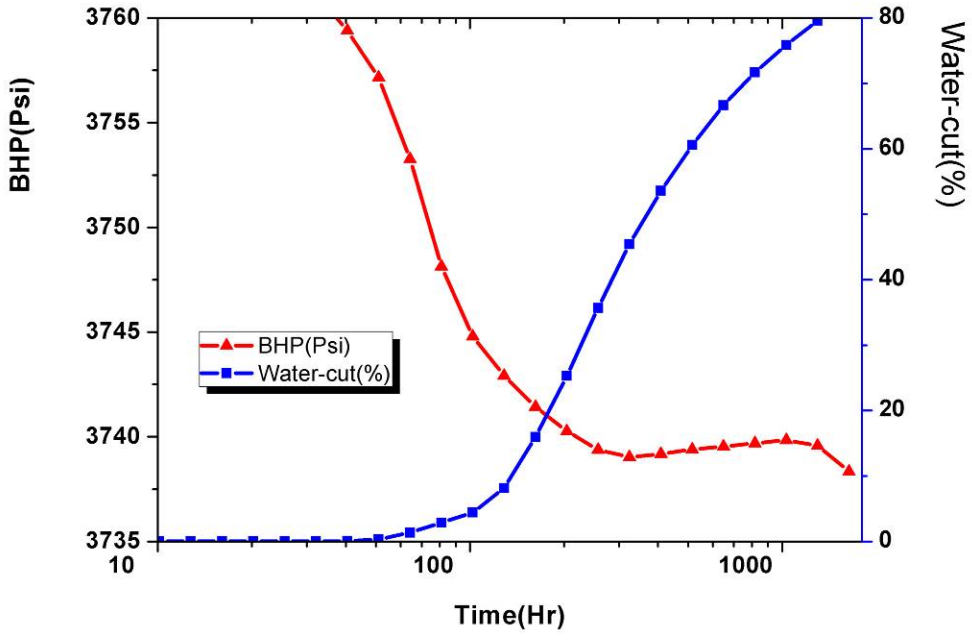

Figure 3.40 The curves of BHP and Water-cut under multiphase flow condition. When the water breaks through, the BHP decreases rapidly, once the water-cut reaches critical point, the BHP may increase.

3.3.4.1 Mathematical Model

As described above in section 3.2.2, considering **Equation 3.7**, **Equation 3.1** can be defined as:

$$q_t(r,t) = q_o(r,t) + q_w(r,t) = 2\pi r K h \lambda_t(r,t)\frac{\partial p}{\partial r} \tag{3.30}$$

Equation 3.30 applies to bounded or to infinite-acting reservoirs. If considering a bounded reservoir, **Equation 3.30** can be rearranged as:

$$\int_{r_w}^{r_e}\frac{\partial p}{\partial r}dr = \frac{1}{2\pi K h}\int_{r_w}^{r_e}\frac{q_t(r',t)}{r'\lambda_t(r',t)}dr', \tag{3.31}$$

Considering outer conditions, noting that

$$\lim_{r\to r_e} p(r_e,t) = p_e \tag{3.32}$$

From **Equation 3.32**, the following equation can be acquired:

$$P_e - P_{wf} = \frac{1}{2\pi K h}\int_{r_w}^{r_e}\frac{q_t(r',t)}{r'\lambda_t(r',t)}dr' \tag{3.33}$$

If the well is controlled by fixed production rates, the derivative of P_{wf} with respect to the time can be described as follows:

$$\frac{\partial P_{wf}}{\partial \ln(t)} = \frac{\partial P_e}{\partial \ln(t)} - \frac{1}{2\pi K h}\int_{r_w}^{r_e}\frac{1}{r'\lambda_t(r',t)}\frac{\partial q_t(r',t)}{\partial \ln(t)}dr' + \frac{1}{2\pi K h}\int_{r_w}^{r_e}\frac{q_t(r',t)}{r'\lambda^2{}_t(r',t)}\frac{\partial \lambda_t(r',t)}{\partial \ln(t)}dr' \tag{3.34}$$

Equation 3.34 is a general expression for the logarithm derivative of the wellbore pressure at any time. It applies to single or multiphase reservoir systems.

Further, **Equation 3.34** suggests that the pressure derivative observed at the wellbore is due to rate and total mobility changing as functions of time. But when the pressure reaches the boundary, and steady state flow or pseudo steady state flow occurs, the change of flow rate across the entire reservoir will approach an approximately constant level. **Figure 3.41** shows a plot of rate vs. radial location at different time points under

a constant rate of 500 RB/D. **Figure 3.42** shows a plot of rate vs. time at different radial locations. **Figure 3.43** shows a log-log plot $\partial q_t(r',t)/\partial \ln(t)$ vs. production time at various values of reservoir radius. There are some common characteristics in these figures, for example, the flow rate in the reservoir will approach the same constant flow rate in the late-time period. ($\partial q_t(r',t)/\partial \ln(t) \to 0$)

Hence, considering $\partial q_t(r',t)/\partial \ln(t) \to 0$, **Equation 3.34** can be simplified to obtain:

$$\frac{\partial P_{wf}}{\partial \ln(t)} = \frac{\partial P_e}{\partial \ln(t)} + \frac{1}{2\pi Kh}\int_{r_w}^{r_e} \frac{q_t(r',t)}{r'\lambda^2{}_t(r',t)} \frac{\partial \lambda_t(r',t)}{\partial \ln(t)} dr' \tag{3.35}$$

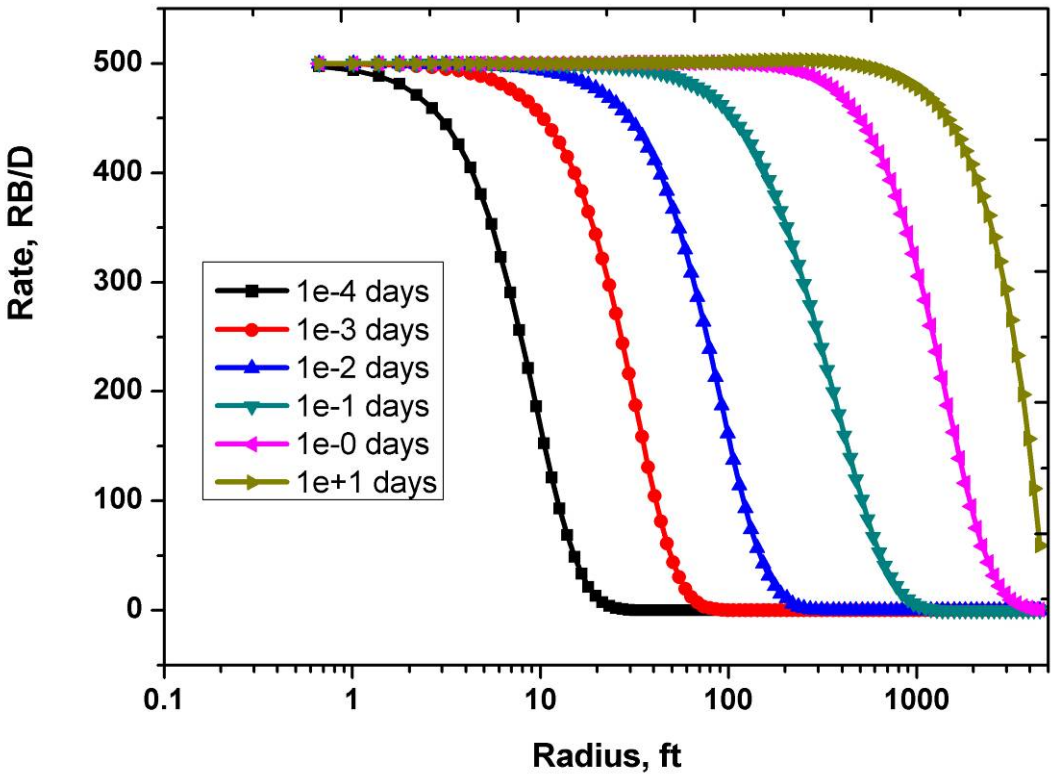

Figure 3.41 Rate vs. radius at various times

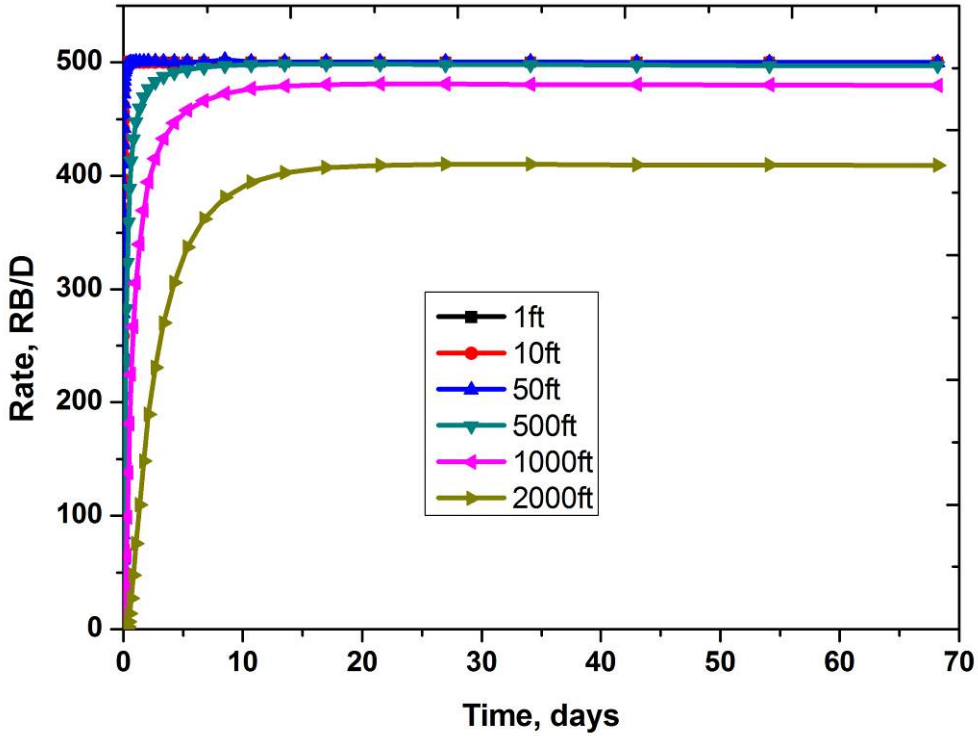

Figure 3.42 Rate vs. time at various radii

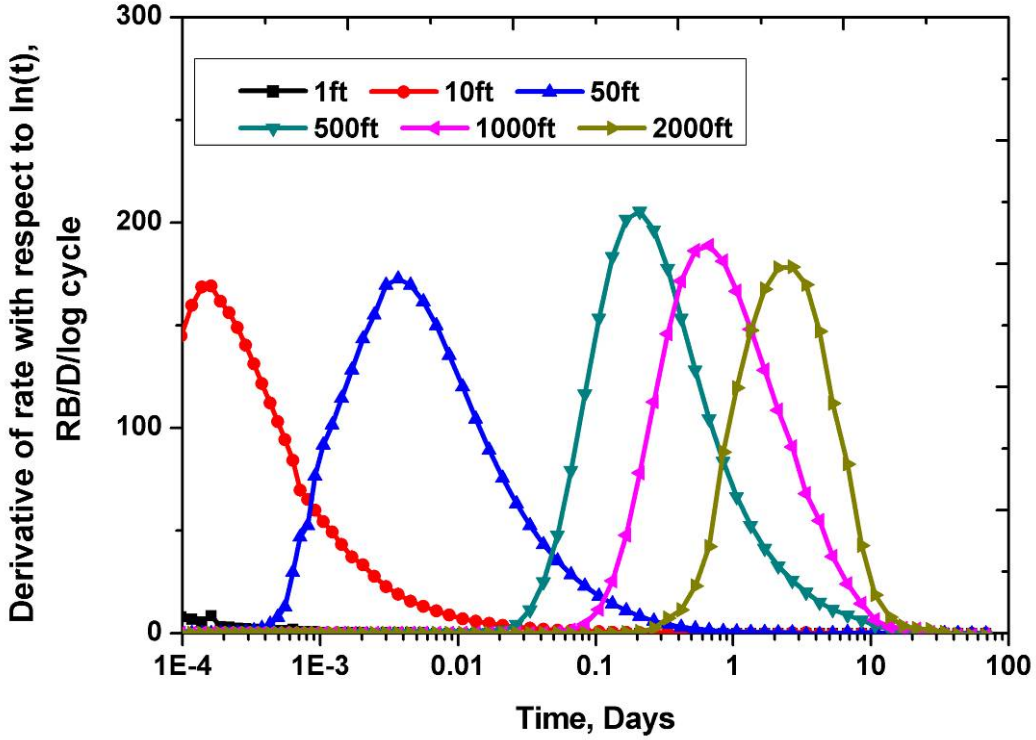

Figure 3.43 Derivative of rate vs. time at various radii

For two-phase black oil models, there are two kinds of outer boundary conditions. One is constant pressure boundary, the other is closed boundary. Description of different outer boundaries in detail as follows:

Constant pressure boundary

Because K_{ro} and K_{rw} are functions of water saturation,

Let

$$\frac{\partial \lambda_t(r',t)}{\partial S_w} = \frac{1}{\mu_o}\frac{\partial K_{ro}}{\partial S_w} + \frac{1}{\mu_w}\frac{\partial K_{rw}}{\partial S_w}. \tag{3.36}$$

The following description can be derived from **Equation 3.35**,

$$\frac{\partial P_{wf}}{\partial \ln(t)} = \frac{\partial P_e}{\partial \ln(t)} + \frac{1}{2\pi Kh}\int_{r_w}^{r_e} \frac{q_t(r',t)}{r'\lambda^2{}_t(r',t)}\frac{\partial S_w}{\partial \ln(t)}\left(\frac{1}{\mu_o}\frac{\partial K_{ro}}{\partial S_w} + \frac{1}{\mu_w}\frac{\partial K_{rw}}{\partial S_w}\right)dr' \tag{3.37}$$

Under constant pressure boundary conditions, the outer boundary pressure is fixed (i.e. $\frac{\partial P_e}{\partial t} = 0$),

Then **Equation 3.37** simplifies to:

$$\frac{\partial P_{wf}}{\partial \ln(t)} = \frac{1}{2\pi Kh}\int_{r_w}^{r_e} \frac{q_t(r',t)}{r'\lambda^2{}_t(r',t)}\frac{\partial S_w}{\partial \ln(t)}\left(\frac{1}{\mu_o}\frac{\partial K_{ro}}{\partial S_w} + \frac{1}{\mu_w}\frac{\partial K_{rw}}{\partial S_w}\right)dr' \tag{3.38}$$

The total mobility curve and the total mobility derivative can be calculated from the relative permeability curve. **Figure 3.44** is the relative permeability curve. **Figure 3.45** is the total mobility curve for set 1 relative permeability curve. **Figure 3.46** is the total mobility derivative curve for set 1 relative permeability curve. From **Figure 3.46**, if there exists a water saturation ($S_{w-\text{critical point}}$), which makes $\frac{\partial \lambda_t(r',t)}{\partial S_w} = \frac{1}{\mu_o}\frac{\partial K_{ro}}{\partial S_w} + \frac{1}{\mu_w}\frac{\partial K_{rw}}{\partial S_w} = 0$, the bottom-hole pressure P_{wf} has a local minimum value at $S_w = S_{w-\text{critical point}}$. That means the bottom-hole pressure increases when $S_w > S_{w-\text{critical point}}$.

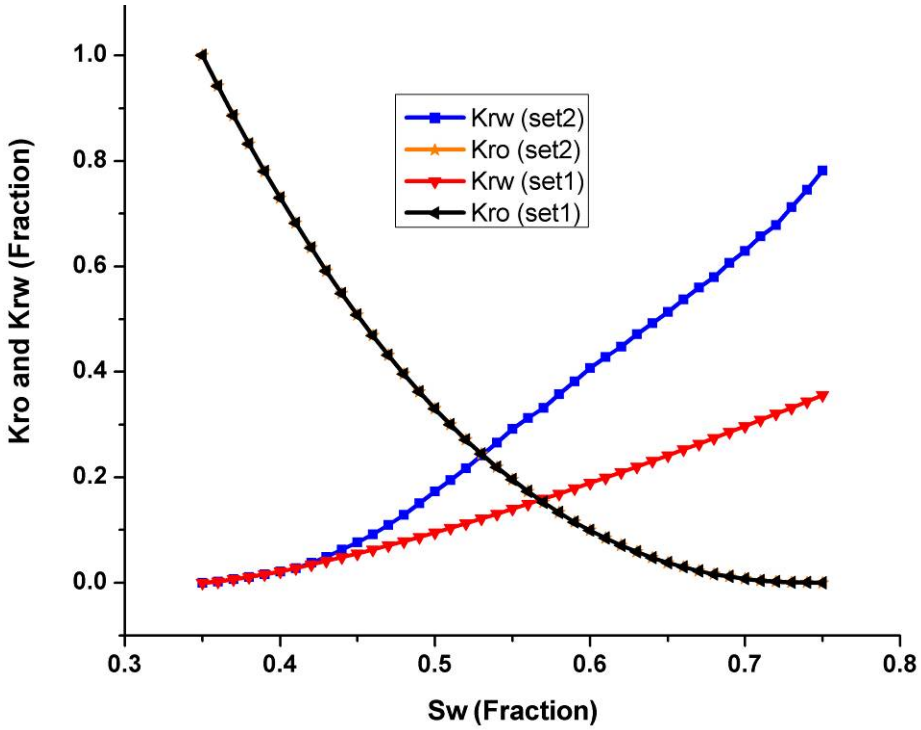

Figure 3.44 Two sets relative permeability data; Set1 is the base case. In set2, the oil relative permeability remains the same, but the water relative permeability has increased.

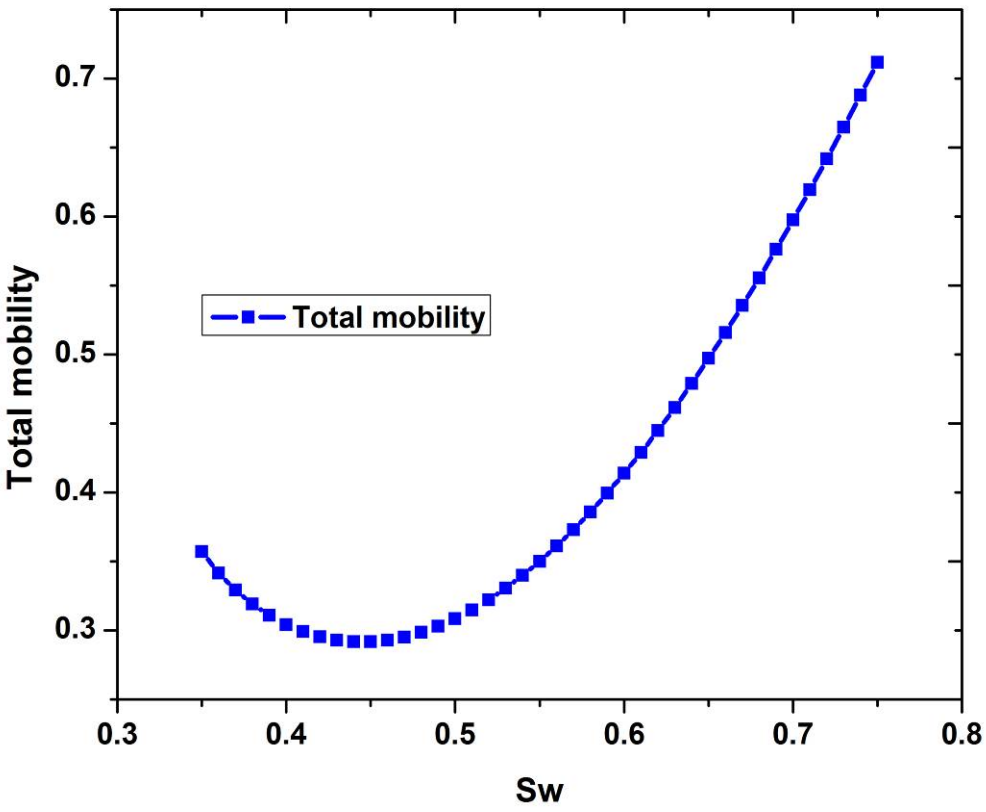

Figure 3.45 The total mobility curve for set 1 relative permeability curve

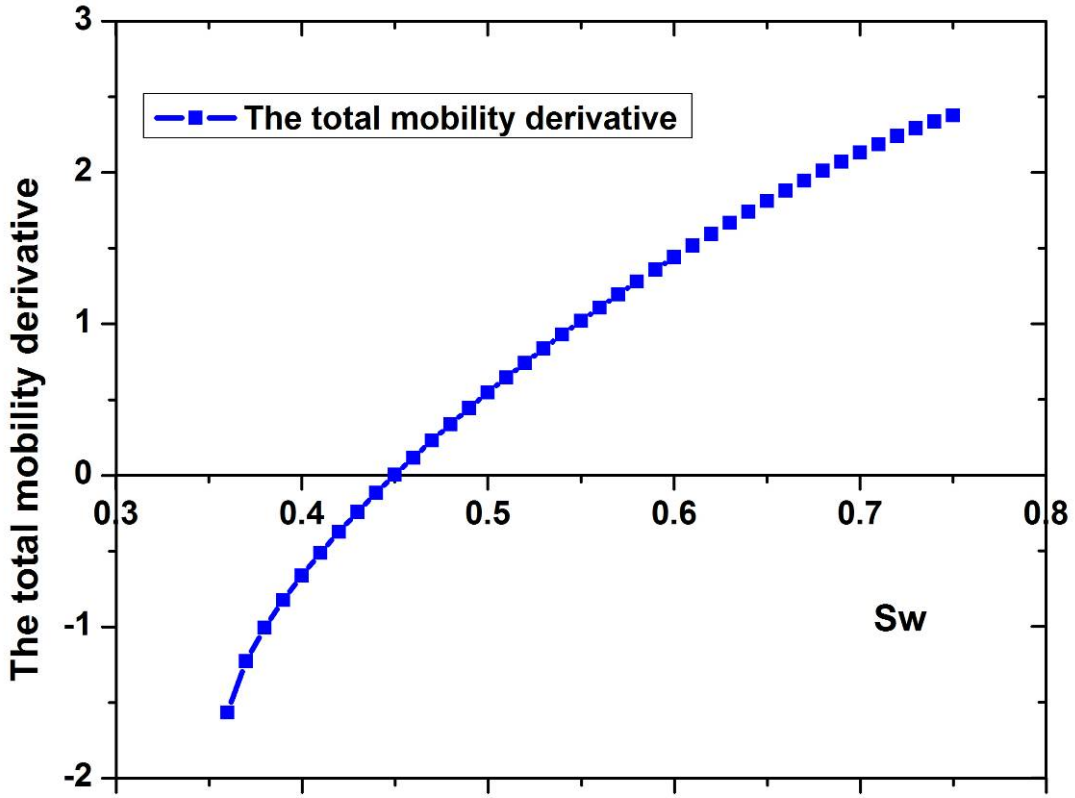

Figure 3.46 The total mobility derivative for set 1 relative permeability curve

Closed system conditions

For closed systems in late time, when semi-steady state flow occurs, and the change of pressure in reservoir approaches constant (i.e. $\frac{\partial P_e}{\partial \ln(t)} = C_3$ (C_3 = constant value)),

Equation 3.37 can be rearranged as:

$$\frac{\partial P_{wf}}{\partial \ln(t)} = C_3 + \frac{1}{2\pi Kh}\int_{r_w}^{r_e} \frac{q_t(r',t)}{r'\lambda^2{}_t(r',t)} \frac{\partial S_w}{\partial \ln(t)} \left(\frac{1}{\mu_o}\frac{\partial K_{ro}}{\partial S_w} + \frac{1}{\mu_w}\frac{\partial K_{rw}}{\partial S_w} \right) dr' \tag{3.39}$$

Where, $\frac{\partial P_e}{\partial \ln(t)} = C_3 < 0$, $\frac{\partial S_w}{\partial \ln(t)} > 0$

So, if there exists a water saturation between 0 and 1 ($0 < S_{wn} < 1$), controlling

$\frac{\partial \lambda_t(r',t)}{\partial S_w} = \frac{1}{\mu_o}\frac{\partial K_{ro}}{\partial S_w} + \frac{1}{\mu_w}\frac{\partial K_{rw}}{\partial S_w} > 0$ and keeping

$$\frac{1}{2\pi Kh}\int_{r_w}^{r_e}\frac{q_t(r',t)}{r'\lambda^2{}_t(r',t)}\frac{\partial S_w}{\partial \ln(t)}\left(\frac{1}{\mu_o}\frac{\partial K_{ro}}{\partial S_w}+\frac{1}{\mu_w}\frac{\partial K_{rw}}{\partial S_w}\right)dr' = -C_4 \quad (C_4 = \text{constant value})$$

Then $\dfrac{\partial P_{wf}}{\partial t} = 0$

The bottom-hole pressure P_{wf} has a local minimum value at $S_w = S_{w-\text{particular point}}$. That means the bottom-hole pressure increases when $S_w > S_{w-\text{particular point}}$.

Hence, the bottom-hole pressure is a complex nonlinear function with respect to time in multiphase flow system. The change of total mobility may lead to the partial minimum value of bottom-hole pressure. This phenomenon gives us useful information to adjust the fluid model in history matching. But on the other hand, it leads to the invalidation of traditional well testing methods.

3.3.4.2 Numerical experiments

In this section, a 3D model was built to simulate multiphase flow, and with this model, different kinds of transient data were generated under different conditions. At the same time, **Equation 3.35** was used to verify qualitatively the validity of the numerical solution.

Case study 1: Constant pressure boundary system

There are two sets of relative permeability data of oil-water, which are shown in **Figure 3.44**. The first set of relative permeability curve has been used, and the oil viscosity is 1cp, 2cp, 2.8cp, 4.4cp, 10cp, and 20cp respectively.

As shown in **Figure 3.47**, the BHP curve is normal under low oil viscosity, but with oil viscosity increasing, there were large variations in the BHP curves. When oil viscosity increased and water-cut reaches a particular value, the bottom-hole pressure may start to increase. Especially under high oil viscosity conditions, the BHP curve goes up further at lower water-cut percentage.

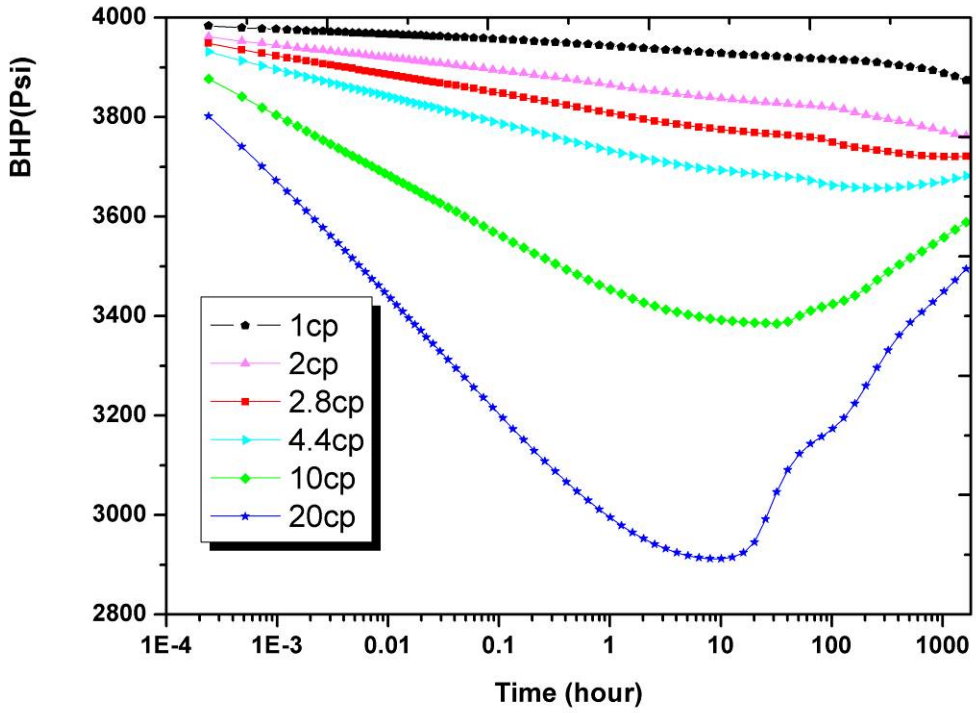

Figure 3.47 This figure shows the semi-log plots of the BHP under constant pressure boundary with different oil viscosities. It shows that with oil viscosity increasing, the BHP curve starts to go up, and the kick point of oil viscosity is 2.8 cp with set1 relative permeability curve.

Table 3.5 lists the detail of set 1 relative permeability data and corresponding water cut and $\frac{\partial \lambda_t(r',t)}{\partial S_w} = \frac{1}{\mu_o}\frac{\partial K_{ro}}{\partial S_w} + \frac{1}{\mu_w}\frac{\partial K_{rw}}{\partial S_w}$ when oil viscosity was 2.8 cp. From the theoretical description in the above section, the BHP curve has partial minimum value when $\frac{\partial \lambda_t(r',t)}{\partial S_w} = \frac{1}{\mu_o}\frac{\partial K_{ro}}{\partial S_w} + \frac{1}{\mu_w}\frac{\partial K_{rw}}{\partial S_w} = 0$, for which the corresponding water cut was about 0.38 from **Table 3.5**. As shown in **Figure 3.48**, the BHP began to increase when the water cut achieved 0.39. So, the above calculation result from theory derivation was consistent with the numerical simulation result.

Table 3.5 The result of relative permeability (set 1)

S_w	K_{rw}	K_{ro}	Water cut ($\mu_o = 2.8cp$, $\mu_w = 0.5cp$)	$\frac{\partial \lambda_t(r',t)}{\partial S_w} = \frac{1}{\mu_o}\frac{\partial K_{ro}}{\partial S_w} + \frac{1}{\mu_w}\frac{\partial K_{rw}}{\partial S_w}$
0.35	0	1	0	
0.36	0.0025	0.94209	0.014643	-1.56821
0.37	0.00634	0.88615	0.038522	-1.22986
0.38	0.01094	0.83218	0.068571	-1.0075
0.39	0.01611	0.78015	0.103653	-0.82421
0.4	0.02174	0.73004	0.142928	-0.66364
0.41	0.02778	0.68184	0.185773	-0.51343
0.42	0.03418	0.63552	0.231469	-0.37429
0.43	0.0409	0.59107	0.27928	-0.2435
0.44	0.04792	0.54846	0.328536	-0.11779
0.45	0.05521	0.50768	0.378495	0.001571
0.46	0.06275	0.4687	0.428484	0.115857
0.47	0.07054	0.4315	0.477934	0.229429
0.48	0.07855	0.39606	0.52621	0.336286
0.49	0.08678	0.36236	0.572854	0.442429
0.5	0.09522	0.33037	0.617451	0.5455
0.51	0.10385	0.30007	0.659642	0.643857
0.52	0.11266	0.27144	0.699181	0.7395
0.53	0.12166	0.24444	0.735951	0.835714
0.54	0.13083	0.21907	0.769816	0.927929
0.55	0.14017	0.19527	0.80079	1.018
0.56	0.14967	0.17304	0.828875	1.106071
0.57	0.15933	0.15234	0.854163	1.192714
0.58	0.16915	0.13314	0.876766	1.278286
0.59	0.1791	0.11542	0.896797	1.357143
0.6	0.18921	0.09914	0.91444	1.440571
0.61	0.19945	0.08426	0.929852	1.516571
0.62	0.20983	0.07076	0.943202	1.593857
0.63	0.22034	0.0586	0.954662	1.667714
0.64	0.23099	0.04773	0.964414	1.741786
0.65	0.24176	0.03813	0.972607	1.811143
0.66	0.25265	0.02975	0.979406	1.878714
0.67	0.26367	0.02254	0.984964	1.9465
0.68	0.27481	0.01645	0.989424	2.0105
0.69	0.28606	0.01144	0.992909	2.071071
0.7	0.29743	0.00745	0.995547	2.1315
0.71	0.3089	0.0044	0.997463	2.185071
0.72	0.32049	0.00223	0.998759	2.2405
0.73	0.33219	0.00086	0.999538	2.291071
0.74	0.344	0.00017	0.999912	2.337357
0.75	0.35591	0	1	2.375929

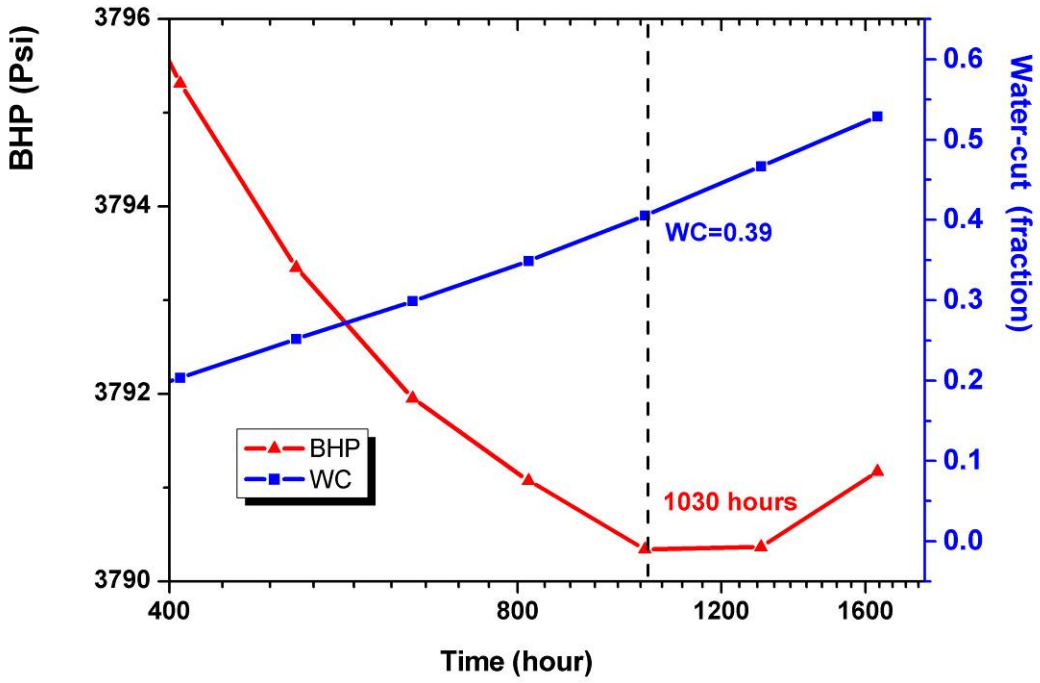

Figure 3.48 This figure shows the semi-log plots of BHP and water cut under a constant pressure boundary. It shows that the BHP curve starts to go up at 1030 hours, and at the same time point, the water cut is 39%.

Figure 3.49 shows the numerical simulation results of the average total mobility with oil viscosity at 2.8 cp. The average total mobility is given by

$$\overline{\lambda_t} = \frac{\sum_{1}^{n}\left(\overline{\lambda_t}\right)_n}{n} \tag{3.44}$$

Where, the subscript *n* represents grid cell.

For **Equation 3.35**, it is very difficult to calculate the value of the integral (i.e., $\int_{r_w}^{r_e} \frac{\partial \lambda_t(r',t)}{\partial \ln(t)} dr'$), according to numerical experience, so the average total mobility was approximate to replace the value of the integral. Hence, through the average total mobility curve to identify the kick point of the bottom-hole flowing pressure, but because this average total mobility is not an accurate analytical solution, the minimum

values of BHP and average total mobility were not same time point as shown in **Figure 3.49**.

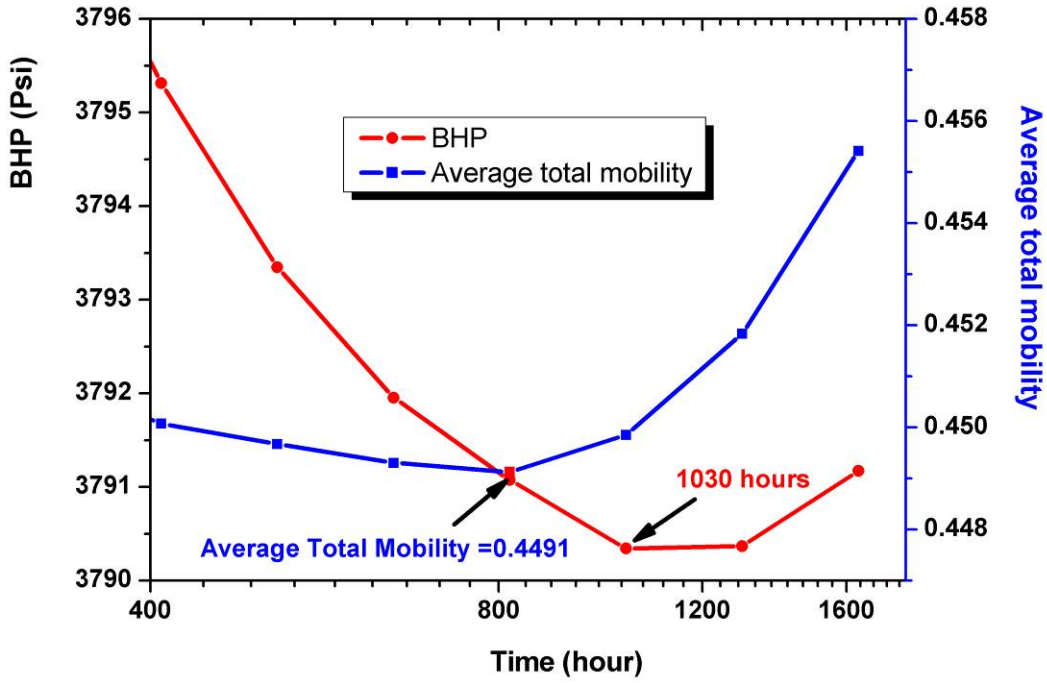

Figure 3.49 This figure shows the semi-log plots of BHP and average total mobility under constant pressure boundary. It shows that the BHP curve starts to go up from 1030 hours, and at same time point, the average total mobility is 0.4491.

Case study 2: Closed system

In this experiment, a closed system reservoir was considered. **Figure 3.50** shows the simulation results when the first set of relative permeability curves was chosen and the oil viscosity was 1 cp, 4 cp, 4.4 cp, 10 cp, and 20 cp respectively. Compared with case study 1, the different numerical solutions were obtained under different outer boundary conditions, which have been proven in the theory section. For example, if the oil viscosity is 4.4 cp, the BHP increases obviously when the outer boundary of reservoir is constant pressure boundary, but for closed systems, the BHP only increases a little, and does not dramatically increase..

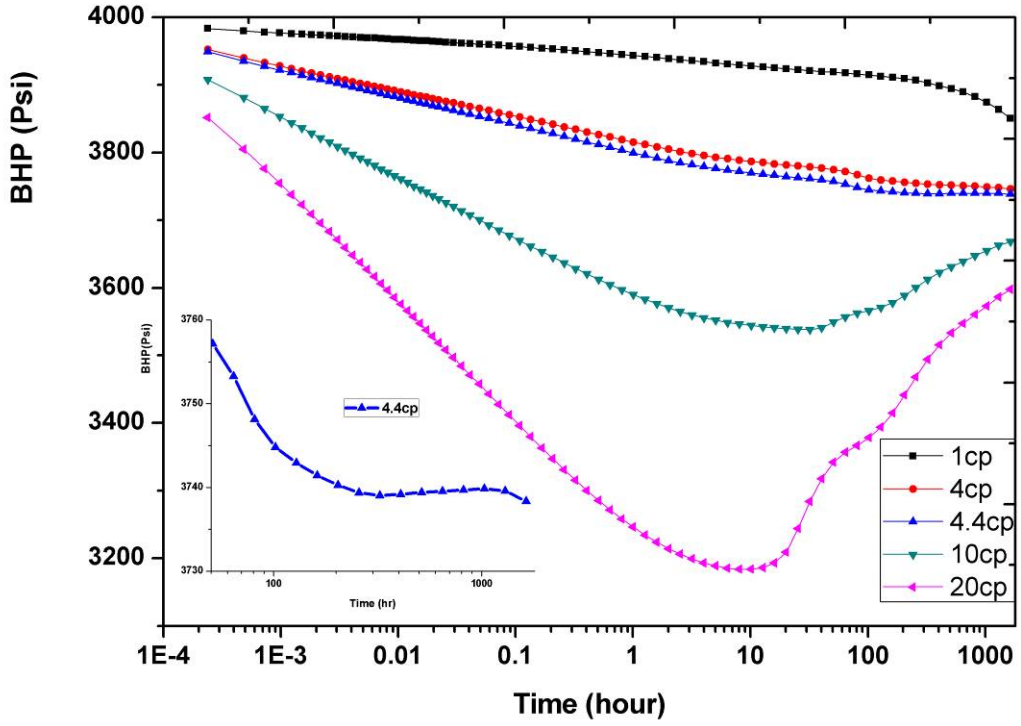

Figure 3.50 This figure shows the semi-log plots of BHP of a closed system. It shows that with oil viscosity increasing, the BHP curve starts to go up, and the "kick" point of oil viscosity is 4.4 cp with set1 relative permeability curve. (See the insert)

Figure 3.51 is the semi-plot of BHP. After 324.34 hours, the BHP curve starts to increase. It means that there is a zero point in the curve of the derivative of the bottom-hole pressure with respect to time.

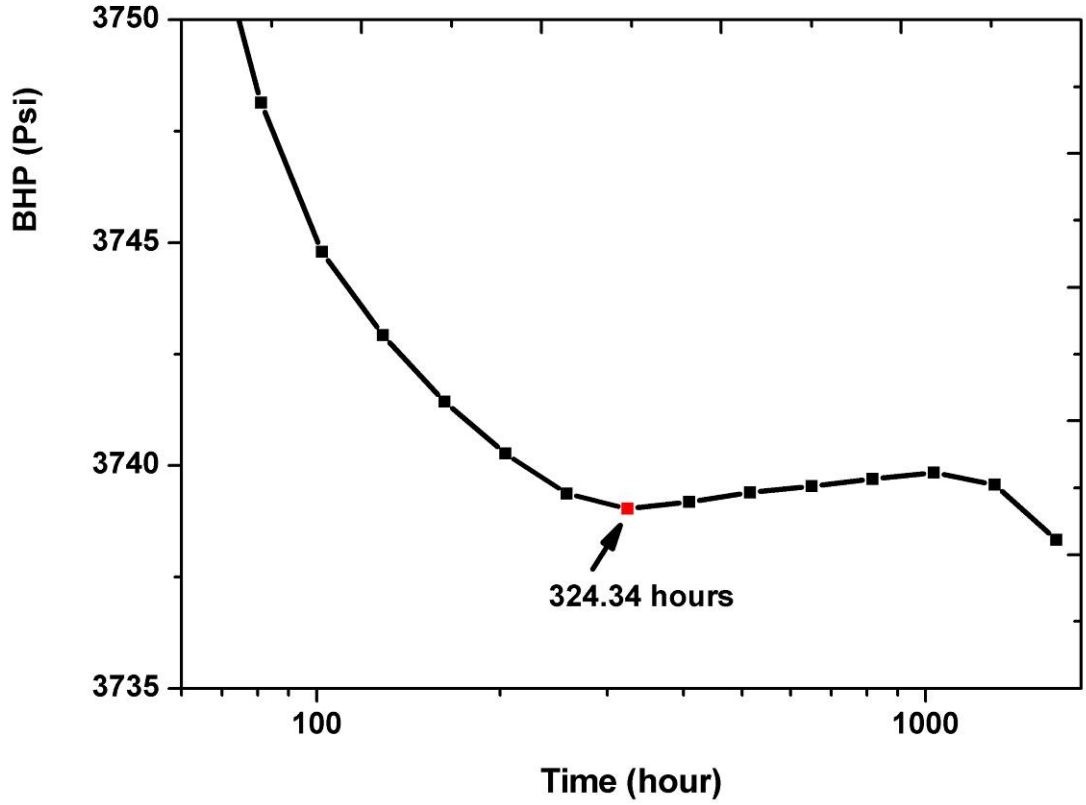

Figure 3.51 This figure shows the semi-log plot of BHP of a closed system with an oil viscosity of 4.4 cp. It shows that the BHP curve starts to go up at 324.34 hours.

As shown in **Figure 3.52,** there is a knee point at 128.59 hours, before this point, the average total effective mobility initially kept constant, then decreased, till at the lowest point, after 128.59 hours, the average total effective mobility started to increase.

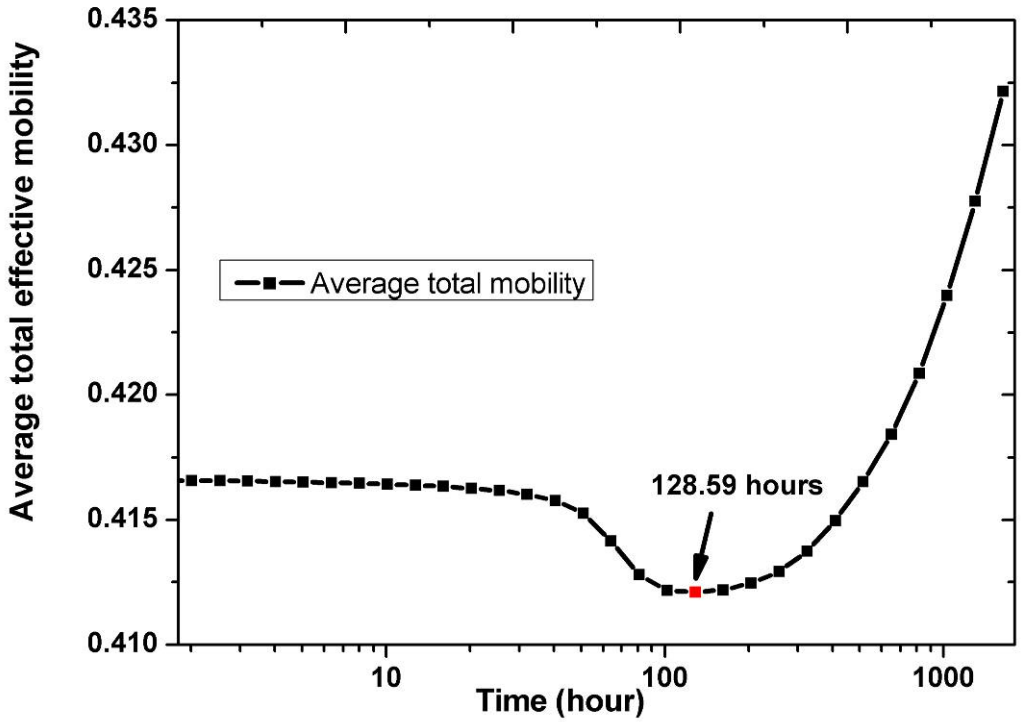

Figure 3.52 This figure shows the semi-log plot of the average total effective mobility of a closed system with oil viscosity of 4.4 cp. It shows that the point of 128.59 hours is the cutting point, the average total effective mobility keeps constant at first, then goes down, and after 128.59 hours, starts to go up.

Comparing **Figure 3.51** and **Figure 3.52**, the knee points of BHP and total mobility were not at the same time point. **Equation 3.39** and theory analysis in previous sections can be used to explain the reason for this phenomenon.

According to **Figure 3.50**, for the case, where the oil viscosity is 1cp and the BHP curve is normal, but using the second set of relative permeability curves, simulation results are shown in **Figure 3.53** and **Figure 3.54**. It can be seen that the BHP curve starts to increase at 408.75 hours, and there exists a lowest point in the average total effective mobility curve.

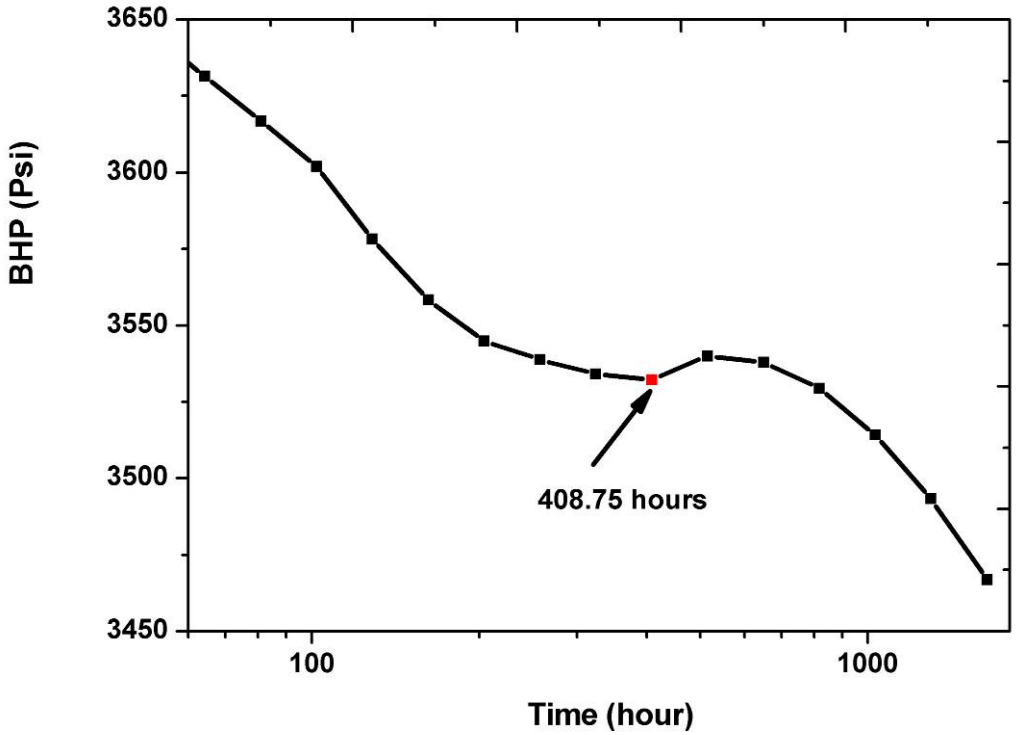

Figure 3.53 This figure shows the semi-log plot of BHP of a closed system with oil viscosity of 1 cp under set 2 relative permeability curve condition. It shows that the BHP curve starts to go up at 408.75 hours.

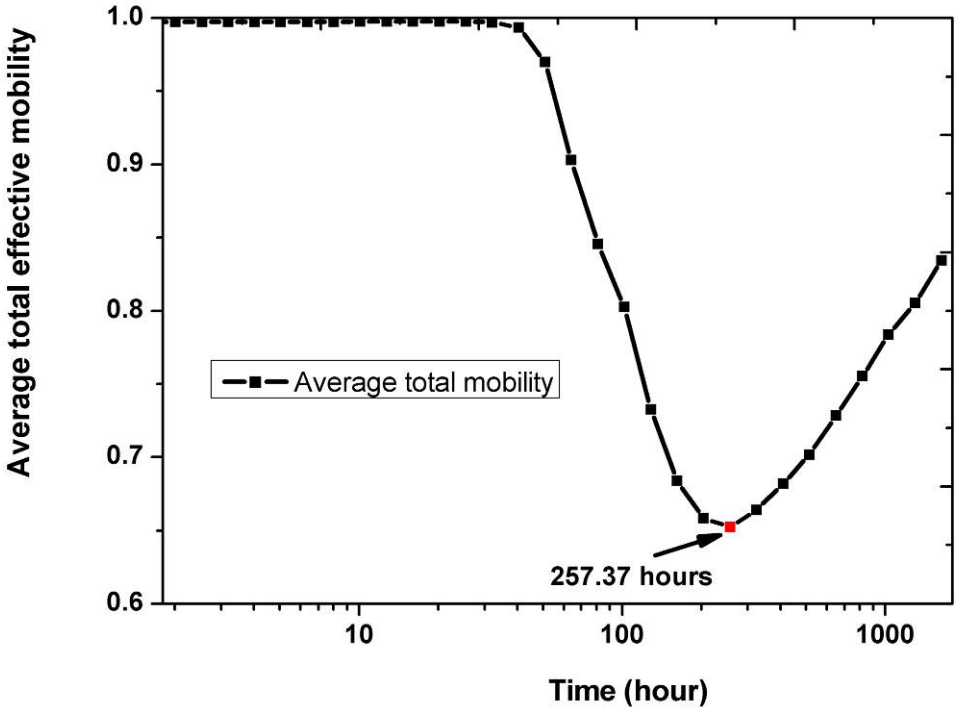

Figure 3.54 This figure shows the semi-log plot of the average total effective mobility of a closed system with oil viscosity of 1 cp under set 2 relative permeability curve conditions. It shows that the point of 257.37 hours is the cutting point, the average total effective mobility keeps constant firstly, then goes down, and after 257.37 hours, starts to go up.

If BHP is fixed, the total liquid rate can be generated under different oil viscosity conditions. **Figure 3.55** shows that with oil viscosity increasing, the total rate curve starts to go up, and the knee point of oil viscosity is 2 cp with set1 relative permeability curve.

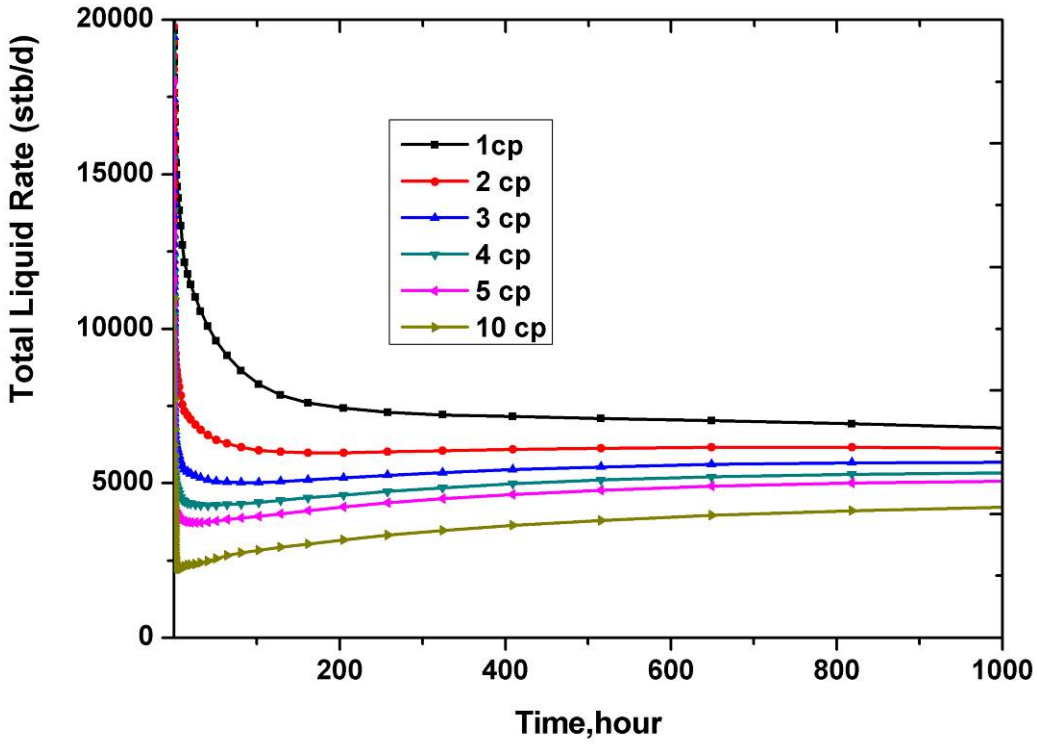

Figure 3.55 This figure shows the plot of total liquid rate of a closed system. It shows that with oil viscosity increasing, the total rate curve starts to go up, and the knee point of oil viscosity is 2 cp with set1 relative permeability curve.

According to the above analysis, under multiphase flow and steady state flow or pseudo steady state flow conditions, the derivative of bottom-hole pressure is a function of the integral of total mobility, which can be approximatively replaced with the average total effective mobility. Using **Equation 3.35**, the reason for BHP increasing may be reasonably interpreted.

3.3.4.3 Summary

According to the analysis of theory and simulation result, whether transient well testing or stabilized well testing, the irregular well test data in non-uniform saturation reservoir cannot be analyzed through traditional multiphase flow approach.

3.4 Chapter Conclusion

- Based on a theoretical development by Thompson, a new expression was derived from Darcy's Law. According to this expression and numerical well test results, we reasonably interpret the pressure behavior of transition zone in oil-water and gas-water reservoirs. The results presented in this work are generally applicable to multiphase reservoir, which are with either infinite-acting or a constant pressure outer boundary.
- Capillary pressure in the transition zone has no significant impact on pressure response.
- The derivative of bottom-hole pressure is a function of integral of total mobility under steady state flow or pseudo steady state flow conditions. According to numerical experience, this integral can be approximatively replaced with the average total effective mobility.
- It is normal for the BHP curve to go up under multiphase flow situations. The trend of the BHP curve is controlled by the total mobility. Comparing fluid property and relative permeability curve, oil viscosity is more sensitive to the trend of the BHP curve.
- For multiphase transient well testing, equations describing multiphase flow are highly nonlinear and do not result in simple analytical solutions, so traditional multiphase flow well testing approaches are only applicable to particular reservoirs, such as uniform saturation reservoirs, low water-cut or high water-cut reservoirs, etc.
- For non-uniform saturation reservoirs, after water breakthrough and water-cut of more than 30% or less than 80%, there are two kinds of BHP data, which cannot be analyzed by the transient well testing approach or the stabilized well testing approach.
- In the course of history matching, some irregular transient well testing data cannot be ignored. These data can be used to update the fluid model and improve history matching. This study is described in **chapter 5.**

Chapter 4
Analysis of Two Phase Flow Well Testing for Multi-layered Reservoirs

4.1 Background

Many reservoirs have been developed where the producing formation is composed of two or more layers of differing formation properties, such as permeability, porosity, and thickness. After a period of production, because a differential depletion should exist between the layers, the pressure behaviour between the layers can have a major effect on reservoir performance. Information on individual layer properties and the distribution of pressure and saturation of each layer under multiphase flow conditions can be useful in the mature field management.

Over the past few decades, the behaviour of transient pressure for layered systems has been studied in detail for two types of systems: (1) Layered commingled reservoirs, where fluid transfers from one layer to another only through the well bore (**Figure 4.1**). In this case, the vertical permeability across layer boundaries is zero. (2) Layered reservoirs with crossflow, where layers communicate at the contact planes throughout the reservoir (**Figure 4.2**).(Kato, E.T., *et al.,* 1991[57]; Jatmiko, W., *et al.,* 1996[59]; Almehaideb, R.A., *et al.,* 1996[60]; Al-Ajmi, N.M., *et al.,* 2003[63]; Verga, F.M., *et al.,* 2001[90]; Kuchuk, F.J., *et al.,* 1986 [84]; Sahni, A., *et al.,* 1996[97]; Hatzignatiou, D.G., *et al.,* 1993[98]; Britt, L.K., *et al.,* 1991[99]; Hatzignatiou, D.G., *et al.,* 1987

[100]; Onur, M., *et al.,* 1989[101];Lakovlev, S.V., *et al.,* 2000[102]; Larsen, L., *et al.,* 1981[115]; Agarwal, B., *et al.,* 1992[117]; Khalaf, A.A., *et al.,* 1993[120];)

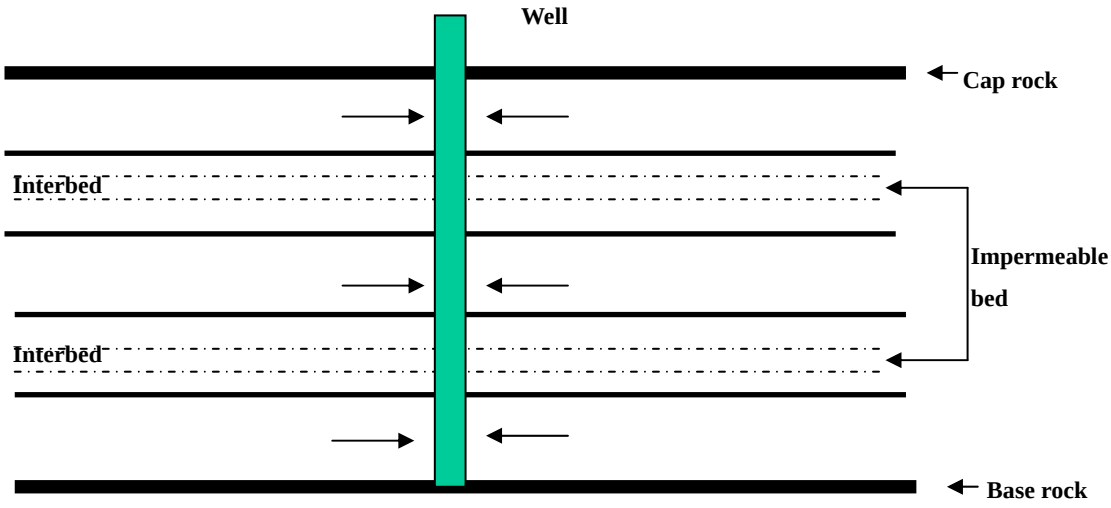

Figure 4.1 Cross-sectional view without crossflow

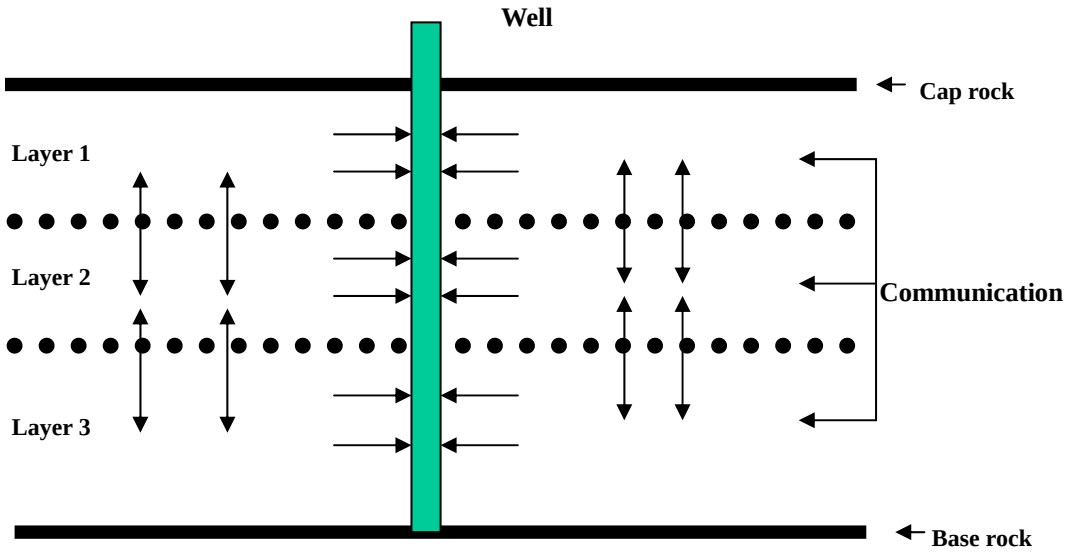

Figure 4.2 Cross-sectional view with crossflow

It is very important to determine the individual-layer permeability, skin factor and pressure. The information about individual-layers can help reservoir engineers to understand the reservoir performance. For example, the water-cut of the more permeable layer may be very high due to injection-water breakthrough.

For multi-layer reservoirs, if the pressure and the drainage radius of each layer is different, then the crossflow effect between layers through wellbore becomes very

severe. During the entire period of the well test, the wellbore crossflow may continue up to the end of the test. Hence, conventional drawdown and buildup tests of multi-layered reservoirs usually only reveal the behaviour of the total system. The performance of each layer cannot be obtained.

In the case of multi-layer interference, multi-rate multi-zone production logging and pressure transient testing can be used to monitor the individual-layer performance. This approach is the selective inflow performance (SIP) test. During testing, zonal isolation is not used. According to SIP, reservoir engineers can obtain the productivity index (P.I) of each layer and evaluate which layer has been flooded due to water coning, or had been depleted seriously due to lack of energy supplement. According to this information, the reservoir model can be updated and well productivity prediction and workover selection can be optimized in real time.

4.2 Review of multi-layer reservoirs well testing

The earliest study for the layered commingled reservoir was that of Lefkovits et al. in 1959[83]. He presented an analytical solution of the transient pressure of a well producing at a constant rate from a bounded, commingled, single phase model. They used a classical Horner method to determine the average formation flow capacity, but for the estimation of average reservoir pressure, this method is not satisfactory. According to the pressure buildup curve, the time to a pseudo-steady state is much longer for the layered commingled system than for the single layer system. Although Lefkovits et al. considered many assumptions, such as each layer being homogeneous and isotropic, and being filled during one phase with constant compressibility, viscosity, and uniform initial pressure, their study provided a basis of well testing interpretation for layered commingled systems.

In the 1970's, Cobb [Cobb, W.M., *et al.*, 1972[52]] examined the pressure behavior of a two layer reservoir with equal layer thickness. The results show that conventional analysis methods, such as the Muskat approach, Miller-Dyes-Hutchinson approach, and Horner approach, can also be applied to two-layer commingled systems.

Earlougher [Earlougher, R.C., *et al.,* 1974[53]] gave some characteristics of pressure buildup behavior in commingled systems. The semi-log plots of buildup show that the different properties of each layer cause different pressure transient responses. Raghavan [Raghavan, R., *et al.,* 1974[54]] presented the extended conventional methods of analyzing pressure buildup for two layer commingled systems, in which the unequal thickness was considered.

In the 1980's, Kucuk [Kucuk, F., *et al.,* 1986[81]] introduced the logarithmic convolution method and the nonlinear least-squared method to obtain individual layer permeability and skin factor for commingled systems. They applied these methods to a field case and its results were compared to those from conventional analysis. Ehlig-Economides [Ehlig-Economides, C.A., *et al.,* 1987[82]] developed a complete analytical solution for the N layered system to analyze the flow-rate transient data of each layer, and its results can be used to determine the layer permeability and skin factor and the effective vertical interlayer communication. Raghavan [Raghavan, R., *et al.,* 1989[80]] reviewed the same techniques in layered reservoirs. He pointed out *that "transient wellbore pressure data from a multilayer reservoir with certain combinations of layer parameters may not yield average values of the flow capacity, skin factor, and reservoir pressure for the whole system.*" Yeh [Yeh, N., *et al.,* 1989[55]] studied the pressure behavior from a restricted-entry well in a commingled reservoir. In this study, the new type curves are used to estimate the total flow capacity and the total skin factor. Park [Park, H., *et al.,* 1989[56]] studied the effects of reservoir parameters (such as permeability, vertical permeability, skin factor, well bore storage and boundary conditions, etc.) for the well bore response (such as bottom hole pressure and individual layer rate) in a multilayered system and made some discoveries. In addition, two new methods to determining the layer parameters were described.

In the 1990's, Aly [Aly, A., *et al.,* 1994[58] [118]] provided a new well test method and derived the analytical solution to the multilayered commingled model with unequal initial pressure. Furthermore, several synthetic cases were verified by new well test procedures. As with the above description, all studies for multilayer reservoirs were

based on analytical solutions. Before 1996, Jatmiko [Jatmiko, W., *et al.,* 1994[116]] had first introduced pseudo-pressure to the dissolved gas reservoir with layered commingled system and had studied the pressure behavior of multilayer reservoir under multiphase flow conditions.

However, because of the limitations of the equations governing multiphase flow, analysis of multiphase flow well testing in layered commingled systems cannot be solved. In particular, many mature fields have entered the late development period, and the interference of multi-layers is very serious. How to evaluating the degree of crossflow through wellbore is a big challenge for the reservoir engineer. Fortunately, in the 21st century, with developments in computers and in test techniques, numerical well testing and the multilayer transient test (MLT) have been developed to asses the performance of the individual layer. Jackson [Jackson, R.R., *et al.,* 2000[62]] described the MLT procedure and analysis method of selective inflow performance (SIP). According to these results, through numerical well testing analysis, each layer performance can be understood. Weiland [Weiland, J., *et al.,* 2008[65]] and Eissa [Eissa, M., *et al.,* 2008[66]] applied MLT and SIP to practical cases and carried out dynamic management for mature fields, respectively.

4. 3 Analysis of Transient Well Test in Layered Reservoir without Crossflow

As shown in **Figure 4.2**, such transient pressure analysis is similar to the homogenous reservoir. Consequently, in this chapter, this system is not the research emphasis. The main objective focuses on the layered commingled reservoir. As with the description at section 4.2, although pressure transient testing has been used in layered commingled reservoir analysis for many years, few studies under multiphase flow conditions were made.

Under multiphase flow conditions, analytic solutions cannot be obtained from conventional well test analysis. The transient behaviour of commingled systems under multiphase flow conditions may be very different from single-layer system or layered reservoirs with crossflow. So in this work, numerical well testing approach is applied

in such systems. According to numerical well testing results, some rules and type curves of well testing in layered commingled systems have been derived.

4.3.1 Two layered commingled model

Grid and fluid description

In the constructed numerical model, a bounded multi-layered commingled model was built. The grid for this model consists of 100 cells in the radial-direction, 1 in the theta-direction, with 2 layers in anticline model. (**Figure 4.3**)

The interlayer properties were different for this model. The fluid properties in the lateral and vertical directions have been taken into account. Under reference pressure, the viscosity of oil and water is 1cp and 0.5cp. The total compressibility is 1.8×10^{-6} 1/psi, and the radius of the wellbore is 0.3ft. The wellbore storage and skin factor were not considered.

Relative permeability modelling

Figure 4.4 is the Oil/water Relative Permeability Curve.

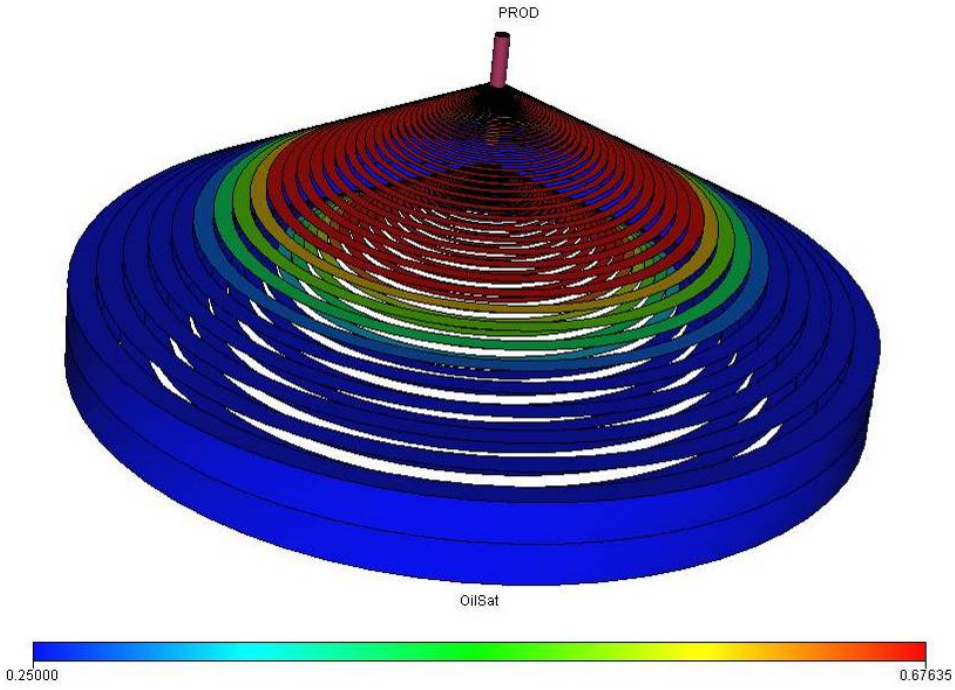

Figure 4.3 Layered commingled model

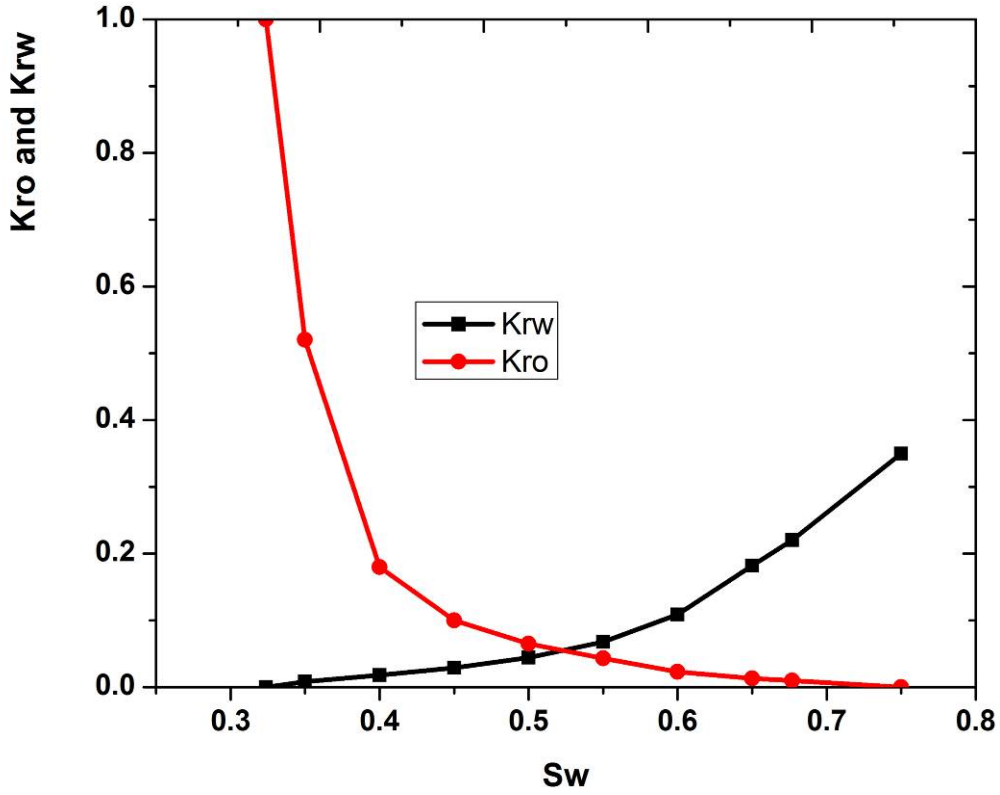

Figure 4.4 The Oil/water Relative Permeability Curve

Design of cases

In order to study the characteristics of pressure buildup analysis in layered commingled systems, taking into consideration the influence of initial pressure, permeability, porosity, formation thickness and radius of each zone, some cases are designated as follows. (**Table 4.1**). All these cases are fully perforated.

4.3.2 Influence of interlayer permeability

In order to understand the influence of buildup behavior under different interlayer permeability conditions , some cases have been designated to keep the permeability sum of two layers constant (K1+K2=300md), only changing the ratio of permeability （K1/K2=2/1, 5/1, 14/1）and initial pressure of each zone.

According to the results of these two types, one case shows that the more permeable layer has low pressure, and the other case shows that the more permeable layer is high pressure. **Figure 4.5** and **Figure 4.6** show different shapes of semi-log plot under different conditions. This is step shaped for the more permeable zone with low

pressure, but for the more permeable zone with high pressure, the shape of the plot is a hump. Comparing the two cases, the permeability ratio affects the amplitude of the step-shaped and hump-shaped plots and the shift time of the straight line for the semi-log plot.

Table 4.1 The design plans of different conditions

Parameters	Case	Production Pattern	Zone No.	Characteristics				
				Perm.（md）	Poro.	H (ft)	Radius (ft)	Initial P
Permeability	Case1	Commingled Production	1	**200**	0.3	30	1960	High
			2	**100**	0.3	30	1960	Low
	Case1-1	Commingled Production	1	**200**	0.3	30	1960	Low
			2	**100**	0.3	30	1960	High
	Case2	Commingled Production	1	**250**	0.3	30	1960	High
			2	**50**	0.3	30	1960	Low
	Case2-1	Commingled Production	1	**250**	0.3	30	1960	Low
			2	**50**	0.3	30	1960	High
	Case3	Commingled Production	1	**280**	0.3	30	1960	High
			2	**20**	0.3	30	1960	Low
	Case3-1	Commingled Production	1	**280**	0.3	30	1960	High
			2	**20**	0.3	30	1960	Low
Porosity	Case4	Commingled Production	1	100	**0.4**	30	1960	High
			2	100	**0.2**	30	1960	Low
	Case4-1	Commingled Production	1	100	**0.4**	30	1960	Low
			2	100	**0.2**	30	1960	High
	Case5	Commingled Production	1	100	**0.48**	30	1960	High
			2	100	**0.12**	30	1960	Low
	Case5-1	Commingled Production	1	100	**0.48**	30	1960	Low
			2	100	**0.12**	30	1960	High
	Case6	Commingled Production	1	100	**0.54**	30	1960	High
			2	100	**0.06**	30	1960	Low
	Case6-1	Commingled Production	1	100	**0.54**	30	1960	High
			2	100	**0.06**	30	1960	Low

Table 4.1 The design plans of different conditions (continued 1)

Parameters	Case	Production Pattern	Zone No.	Characteristics				
				Perm.（md）	Poro.	H (ft)	Radius (ft)	Initial P
Thickness	Case7	Commingled Production	1	100	0.3	**40**	1960	High
			2	100	0.3	**20**	1960	Low
	Case7-1	Commingled Production	1	100	0.3	**40**	1960	Low
			2	100	0.3	**20**	1960	High
	Case8	Commingled Production	1	100	0.3	**48**	1960	High
			2	100	0.3	**12**	1960	Low
	Case8-1	Commingled Production	1	100	0.3	**48**	1960	Low
			2	100	0.3	**12**	1960	High
	Case9	Commingled Production	1	100	0.3	**54**	1960	High
			2	100	0.3	**6**	1960	Low
	Case9-1	Commingled Production	1	100	0.3	**54**	1960	High
			2	100	0.3	**6**	1960	Low
Radius	Case10	Commingled Production	1	100	0.3	30	**1007**	High
			2	10	0.5	120	**1007**	Low
	Case10-1	Commingled Production	1	100	0.3	30	**382**	High
			2	10	0.5	120	**3003**	Low
	Case11	Commingled Production	1	100	0.3	30	**1007**	Low
			2	10	0.5	120	**1007**	High
	Case11-1	Commingled Production	1	100	0.3	30	**382**	Low
			2	10	0.5	120	**3003**	High
Initial pressure	Case12	Commingled Production	1	100	0.3	30	1007	**Very Low**
			2	10	0.5	120	1007	**Normal**
	Case12-1	Commingled Production	1	100	0.3	30	382	**Very Low**
			2	10	0.5	120	3003	**Normal**

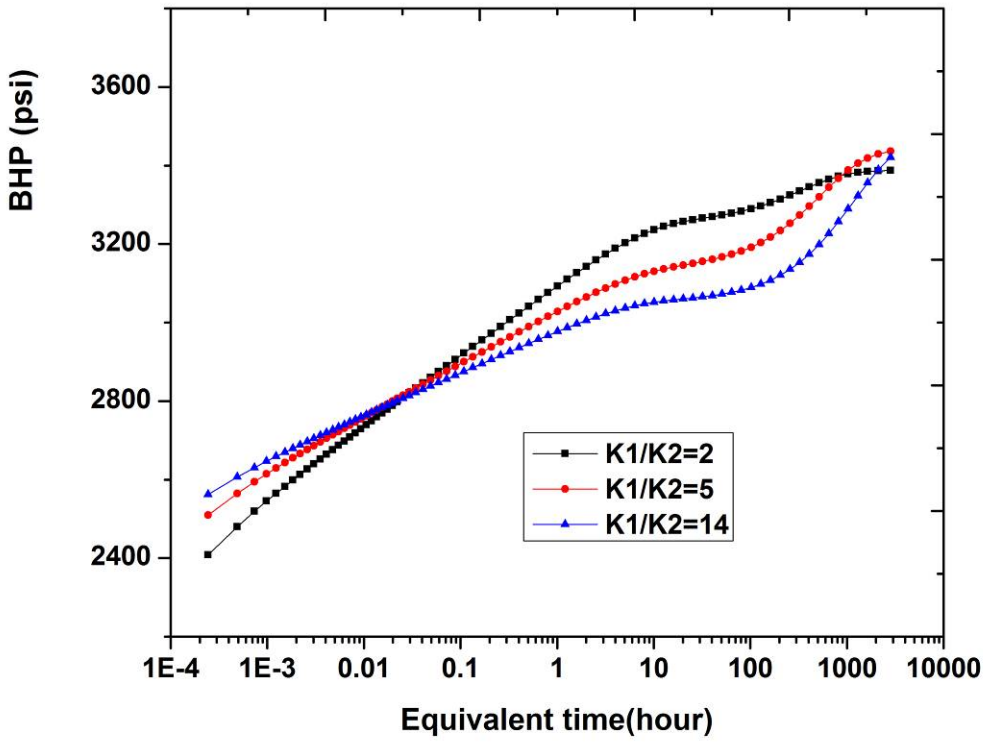

Figure 4.5 The semi-log plot under different permeability ratios for the more permeable zone with low pressure

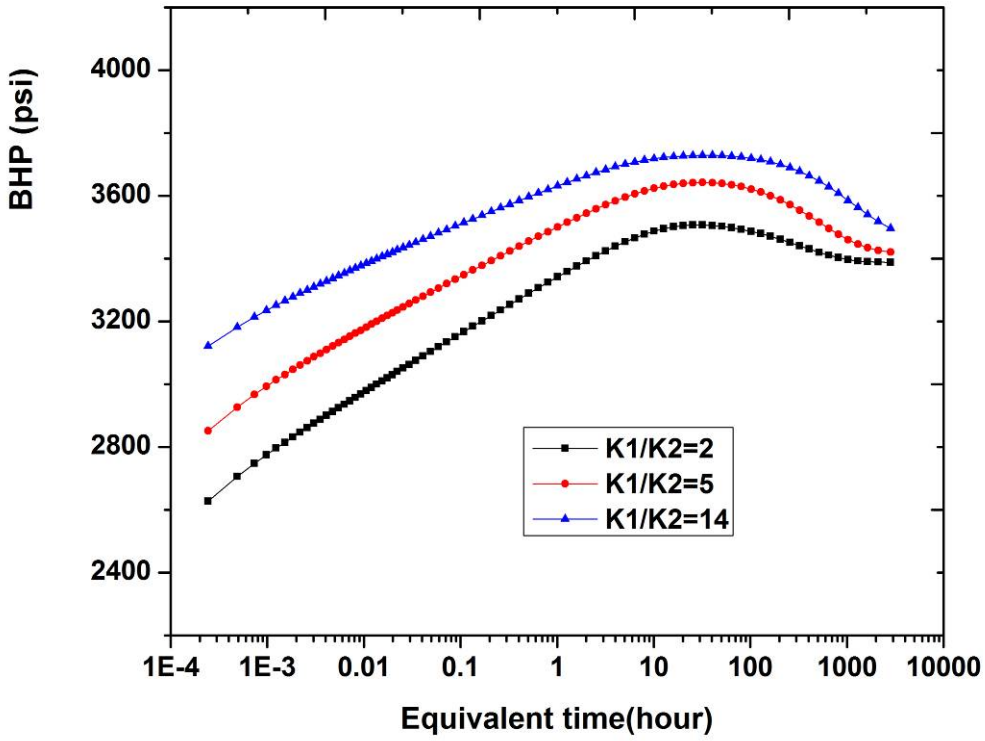

Figure 4.6 The semi-log plot under different permeability ratios for the more permeable zone with high pressure

It is noteworthy from the semi-log plot that there is a straight line before the curve starts to shift. If the wellbore storage and the skin factor effect are not considered, then the knee point of the straight line indicates that the system pressure has reached the boundary of the more depleted zone, in which pressure propagates quickly. Hence, if the pressure did not reach the boundary of any zone during the buildup test, the semi-log plot is always a straight line. Now the reservoir produces as if it were composed of one bounded layer and one infinite layer. After some time, the less permeable layer also feels its boundary. From then on, the reservoir behaves as a fully bounded reservoir.

For example, **Figure 4.7** shows that the shift point of the straight line is 10.11hr, but from the flow profile of the more permeable zone with low pressure (**Figure 4.8**), the early portion of the downhole flow rate plot, the crossflow rate from the less permeable zone to the more permeable zone is very high, but after the pressure reaches the boundary of the more depleted zone, the crossflow rate decreases quickly to zero and then to stabilization. The knee point of the flow profile is 10.11 hour. If using investigation equations to calculate radius ($R_{inv} = 0.033\sqrt{\frac{kt}{\phi\mu c_t}}$), the conduction time of pressure in 1960ft is about 10.13hour; very close to 10.11. This result confirms that once pressure reaches the boundary of the more depleted zone, in which pressure propagates quickly, the straight line of semi-log plot starts to shift.

According to the shift point of the straight line, the radius of the more depleted zone can be obtained, in which the drainage boundary is first detected at the well.

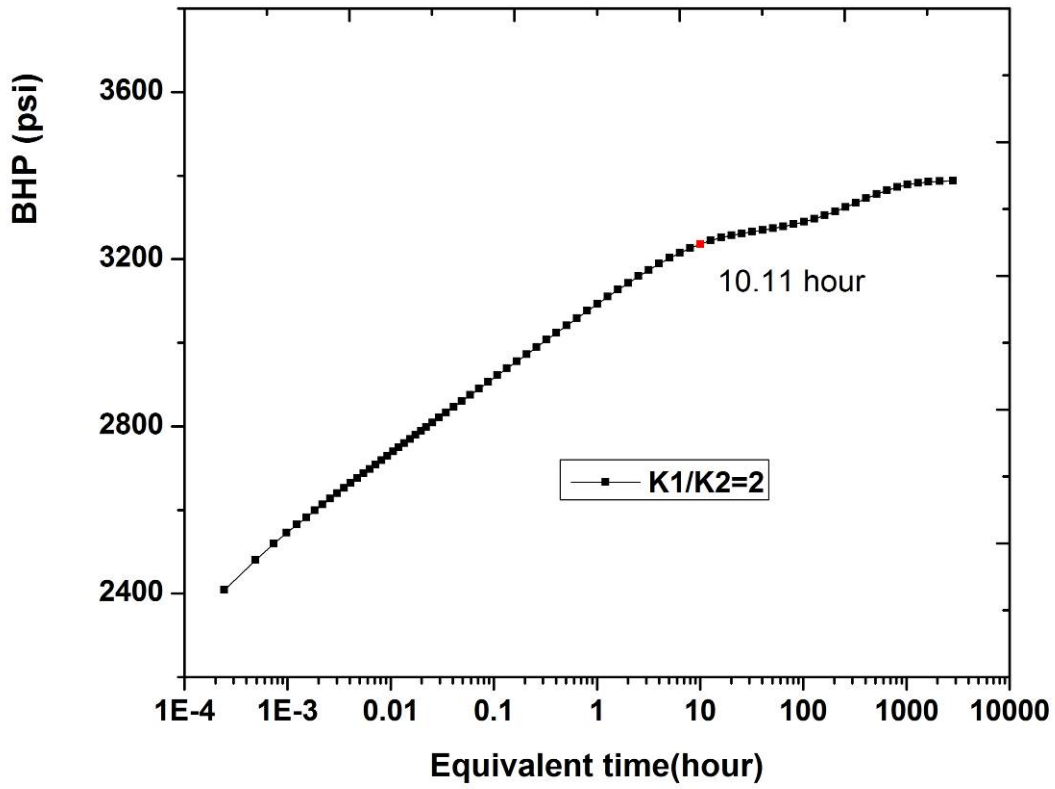

Figure 4.7 The semi-log plot for the more permeable zone with low pressure (K1/K2=2)

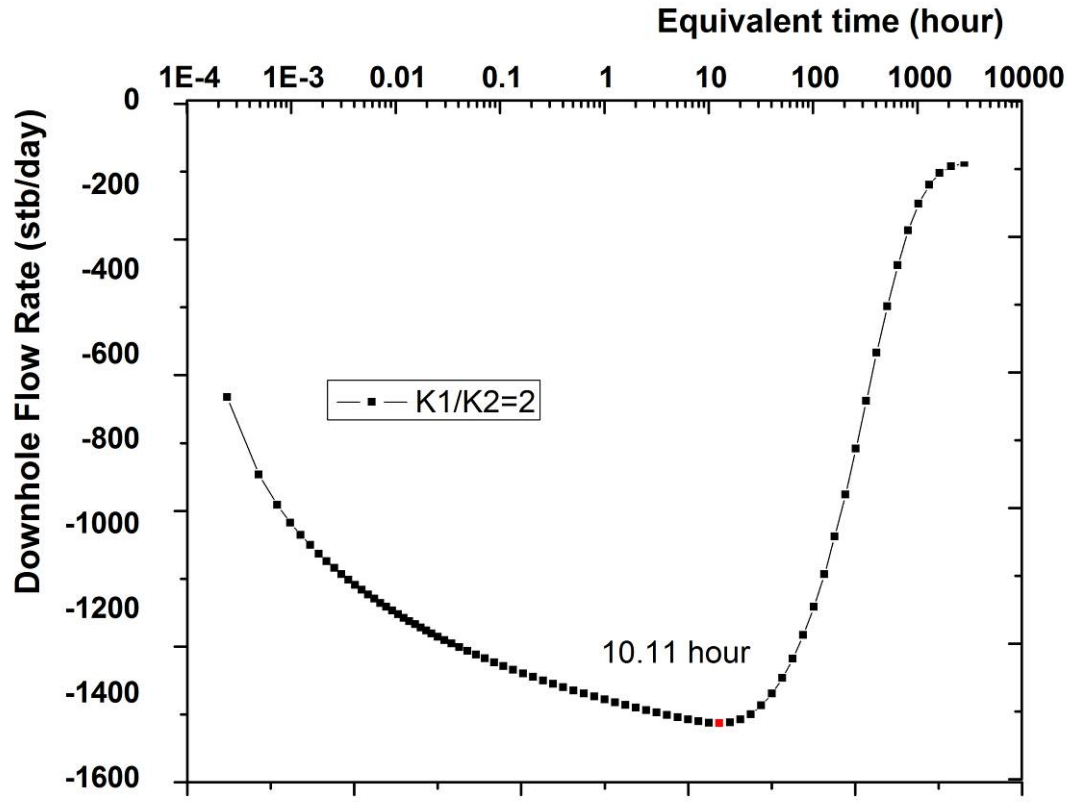

Figure 4.8 The flow profile for the more permeable zone with low pressure (K1/K2=2)

4.3.3 Influence of interlayer porosity

Like permeability design plans, some cases have been designed, which keep the porosity sum of two layers constant (φ1+φ2=0.6), only changing the ratio of porosity （φ1/φ2=2/1，4/1, 9/1）and the initial pressure of each zone.

According to the diffusivity coefficient equation, $\eta = \frac{K}{\Phi \mu C_t}$, there is a similarity in behavior between porosity and permeability, so that the influence of porosity is similar to the influence of permeability, but the result is adverse. **Figure 4.9** and **Figure 4.10** show that there is hump shape for the higher porosity zone with low pressure, but for the higher porosity zone with high pressure, the shape of semi-log plot is step shaped.

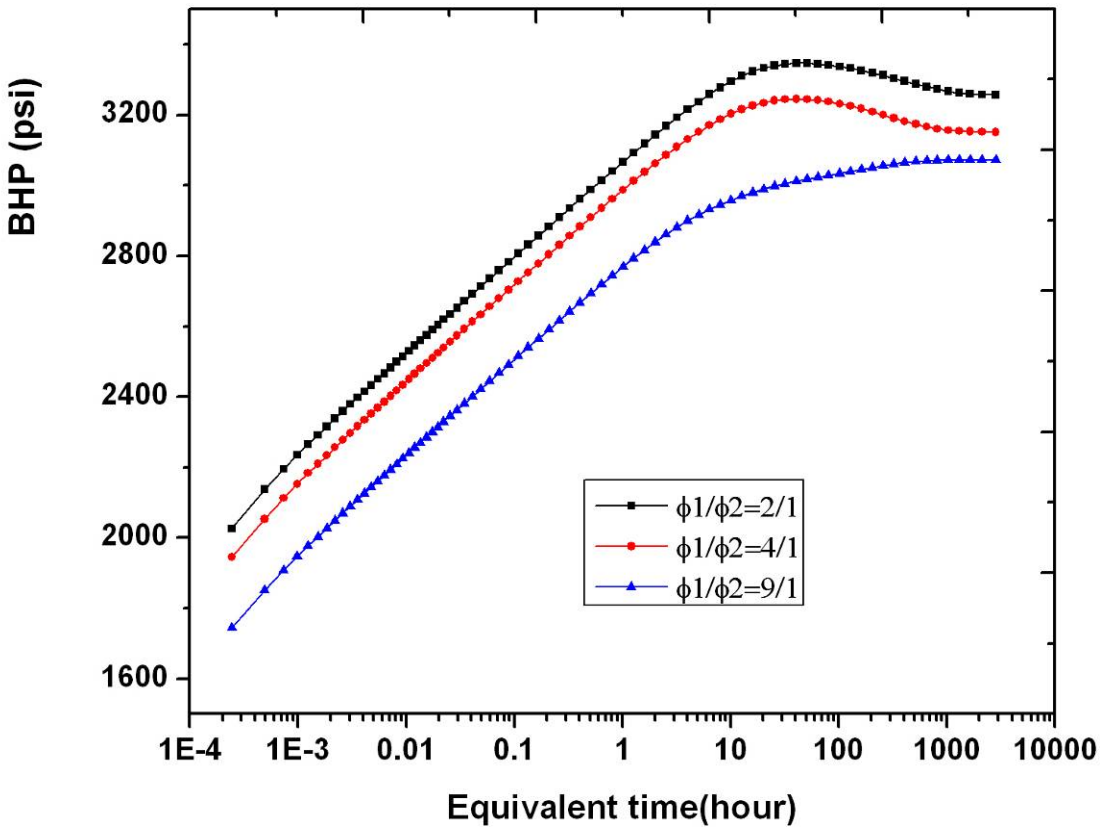

Figure 4.9 The semi-log plot under different porosity ratios for the higher porosity zone with low pressure

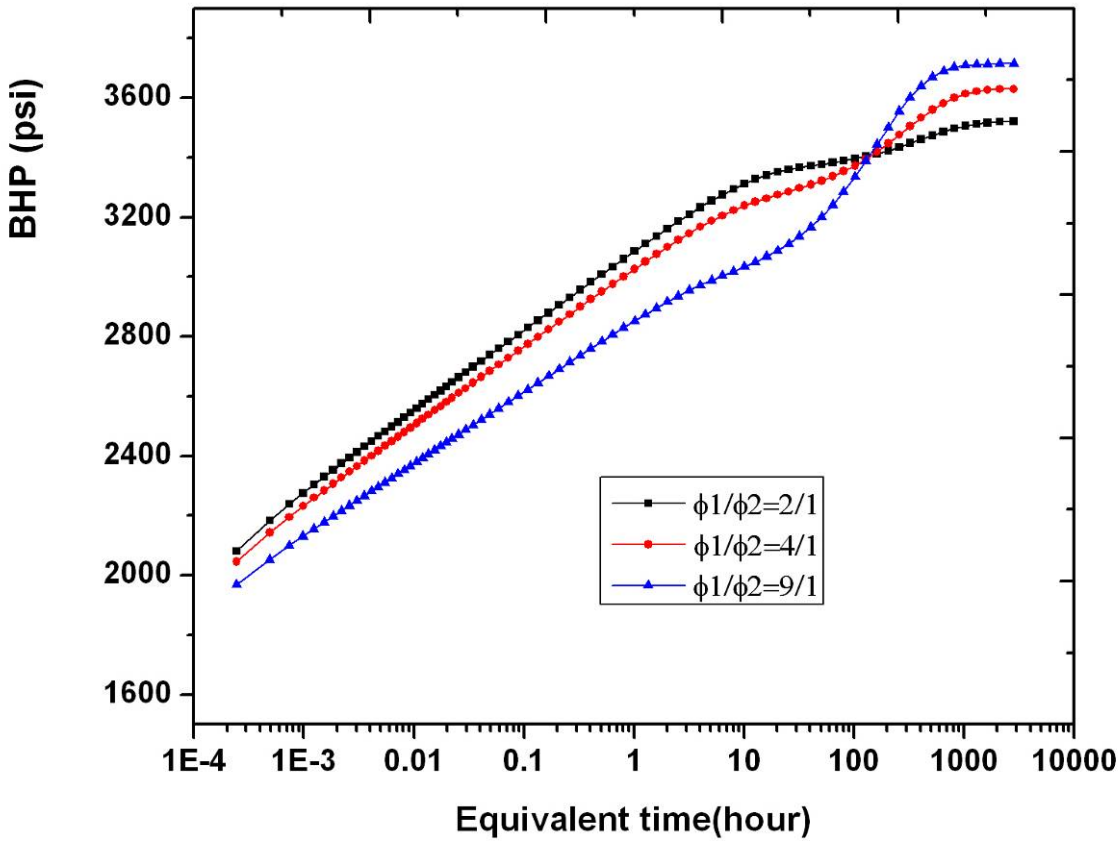

Figure 4.10 The semi-log plot under different porosity ratios for the higher porosity zone with high pressure

4.3.4 Influence of interlayer thickness

Like permeability design plans, some cases have been designed, which keep the thickness sum of two layers constant (H1+H2=60ft), only changing the ratio of thickness（H1/H2=2/1，4/1, 9/1）and initial pressure of each zone.

According to the results, whether the thick zone has a high-pressure or a low-pressure, there is small influence on the shape of the semi-log plot under different thickness conditions. (**Figure 4.11**, **Figure 4.12**)

Figure 4.13 shows that the change of pressure is merely 0.2 psi at late time. Hence, the influence of the interlayer thickness in multi-layered system can be ignored.

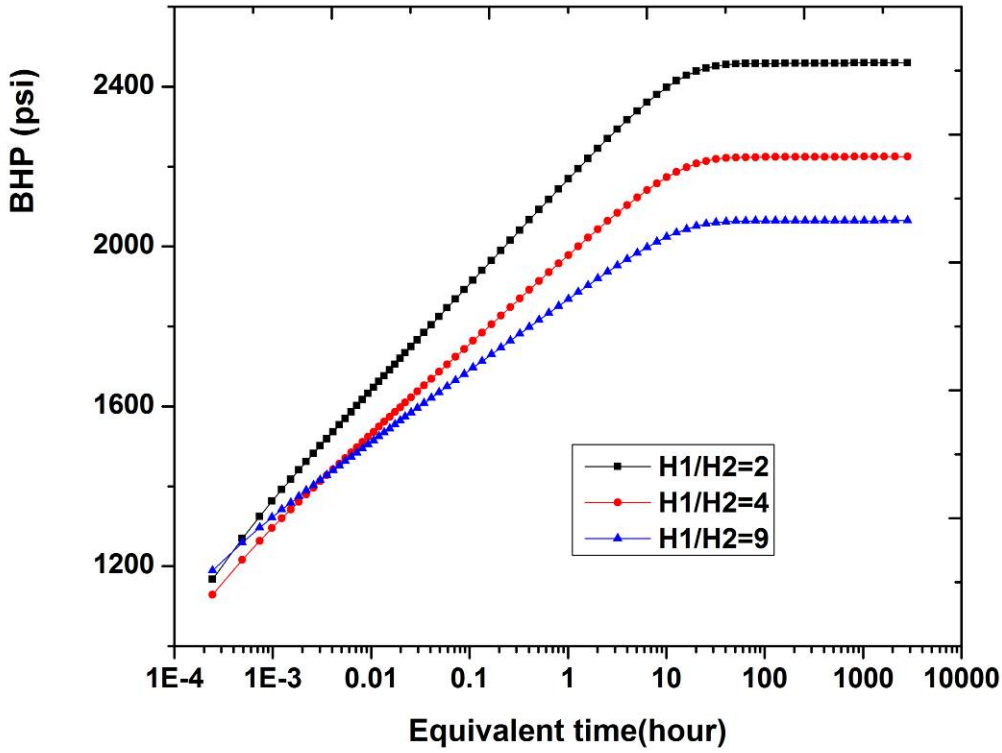

Figure 4.11 The semi-log plot under different thickness ratios for a thick zone with low pressure

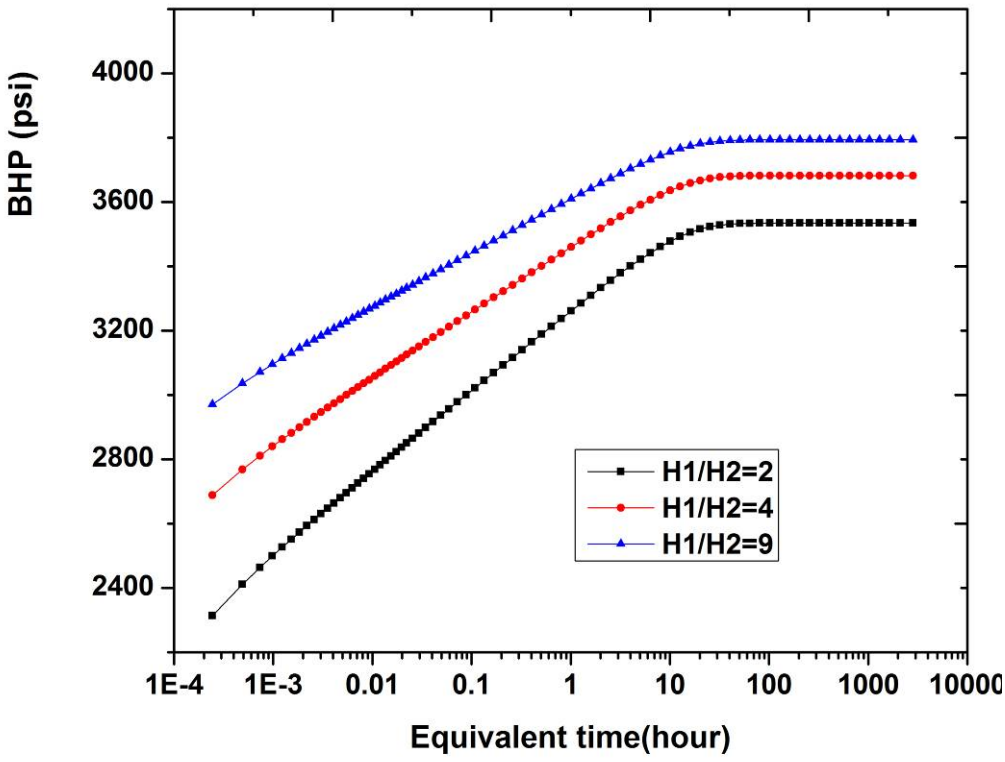

Figure 4.12 The semi-log plot under a different thickness ratio for a thick zone with high pressure

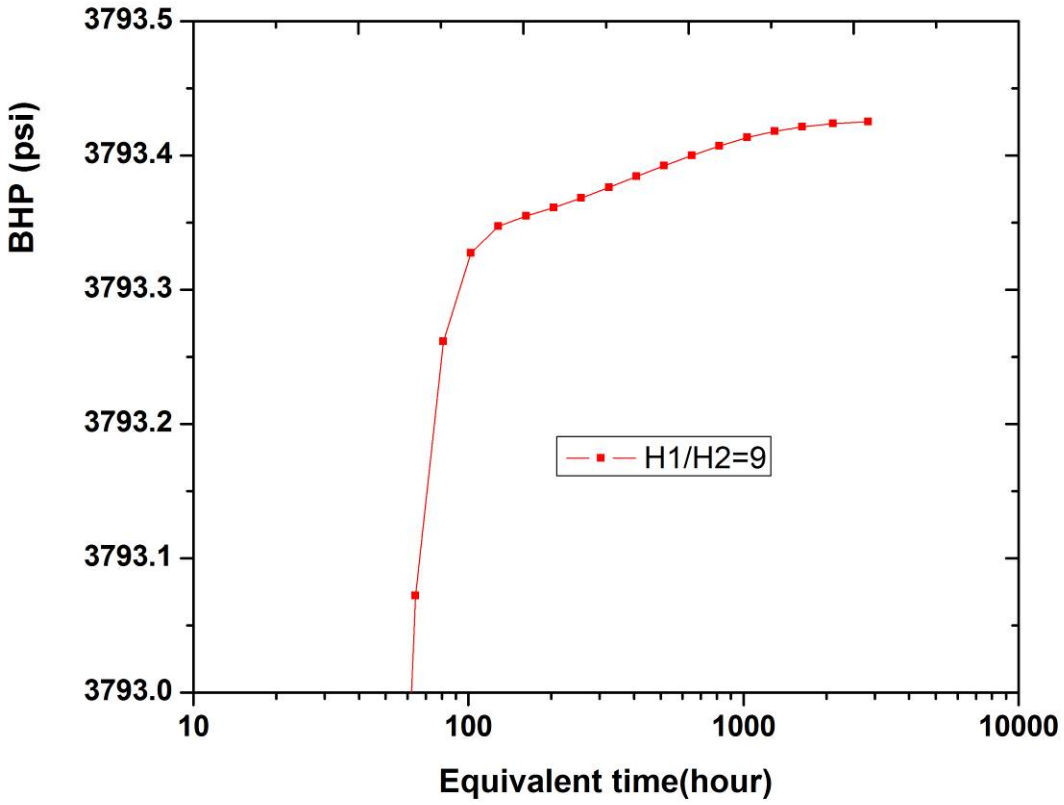

Figure 4.13 The semi-log plot under H1/H2=9 for a thick zone with high pressure

4.3.5 Influence of reservoir radius

For layered commingled systems, the radius of each zone is different, and this situation is ubiquitous in the field. It is therefore useful to study the shape of buildup tests under different layer radius conditions.

Like permeability design plans, some cases have been designed, which only change the ratio of layer radius（R1/R2=1/1，1/8） (**Figure 4.14**) and initial pressure of each zone. Under different layer radius conditions, the propagation speed of pressure is different, according to the term, $K/\phi\mu CR_e^2$, Depending on whether the more permeable zone is a high-pressure or low-pressure zone, the calculation result of $K/\phi\mu CR_e^2$ is bigger, so the more permeable zone is the more depleted zone, in which the propagation speed of pressure is higher than in the less permeable zone.

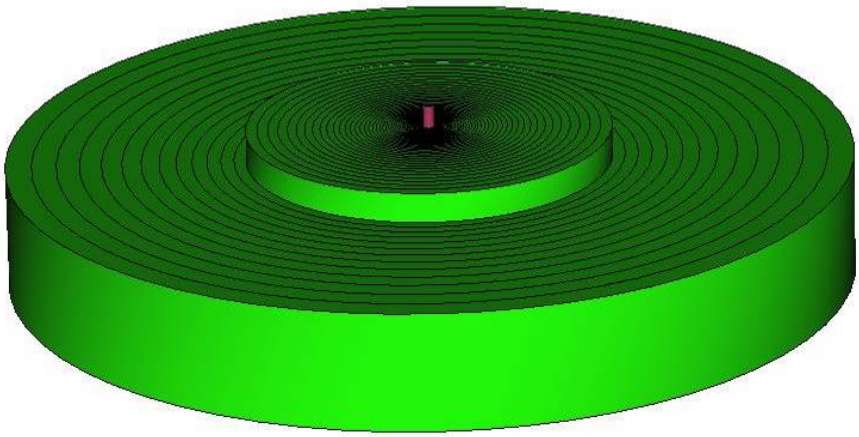

Figure 4.14 Layered commingled model for different layer radius ration (R1/R2=1/8)

4.3.5.1 The more permeable zone with high pressure

Comparing case 10 and case 10-1, **Figure 4.15** and **Figure 4.16** show some rules. When the pressure reaches the drainage boundary of any zone, the straight line of semi-log plot starts to shift and a hump shape occurs. But for a different reservoir radius, the shape of semi-log plot is different. Before the pressure builds up to a steady state, the shape of the semi-log plot can be divided to a front transition period and a back transition period (**Figure 4.17**). The front transition period stands for the zone in which the pressure propagation is quick. The back transition period stands for the zone in which the pressure propagation is slow.

Figure 4.17 and **Figure 4.18** show the tendency of the semi-log plot, which indicates the pressure behavior of a high-pressure zone. After the pressure reaches the drainage boundary of a high-pressure zone, the crossflow rate from high-pressure zone to low-pressure zone will decrease quickly till it reaches zero. At the same time, the pressure of a high-pressure zone will go down step-by-step, till it flattens out, and a hump starts to form. This phase belongs to the front transition period and reveals the characteristic of any zone in which the pressure propagation is quick.

Once the crossflow rate decreases to zero, the pressure of a zone does not reach its boundary. When the pressure propagation is slow the boundary of the zone has more energy, so the fluid of this zone starts to back flow into another zone, and the total

pressure goes up. When the pressure reaches the boundary of this zone, the curve of pressure will be flattened till it reaches a steady state. This phase belongs to the back transition period and indicates the characteristic of a zone in which the pressure propagation is slow.

From the log-log plot (**Figure 4.19**), the pressure derivative can be divided two phases. In the middle of the log-log plot, the pressure derivative is negative. The first phase indicates the characteristic of a zone in which the pressure propagation is quick. The second phase indicates the characteristic of a zone in which the pressure propagation is slow.

If the radius of zones is the same**, Figure 4.15** shows that the back transition period does not occur at the end of the curve. The reason is that the elastic energy of a zone pressure propagating slowly is low. In the course of crossflow from a high-pressure zone to a low-pressure zone, the boundary pressure of zone pressure propagating slowly is less than the pressure of a high-pressure zone, and hence the back flow does not appear. (**Figure 4.20**)

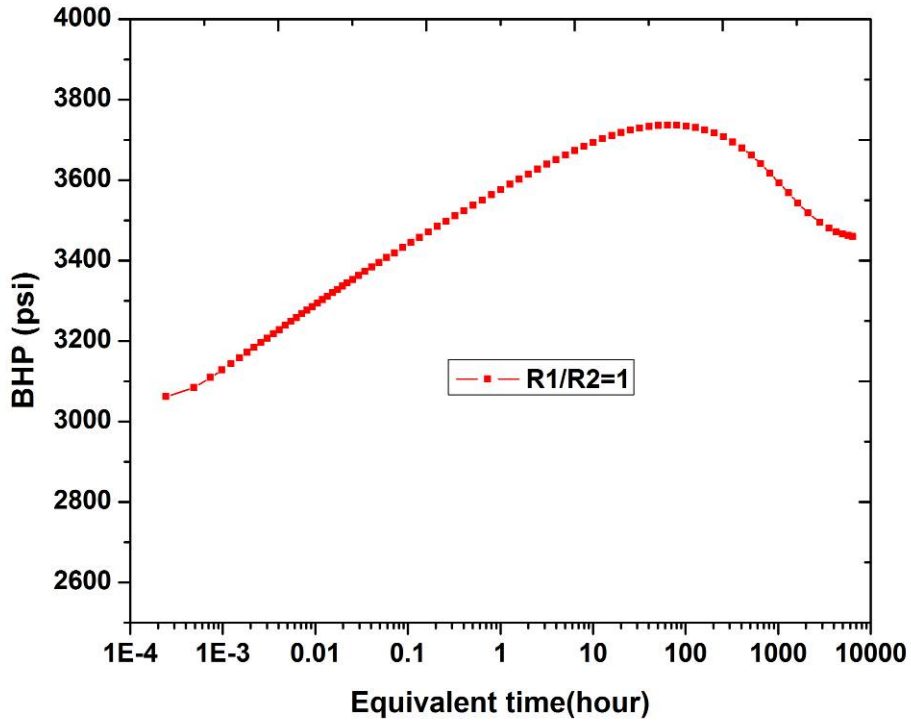

Figure 4.15 The semi-log plot under R1/R2=1 for the more permeable zone with high pressure

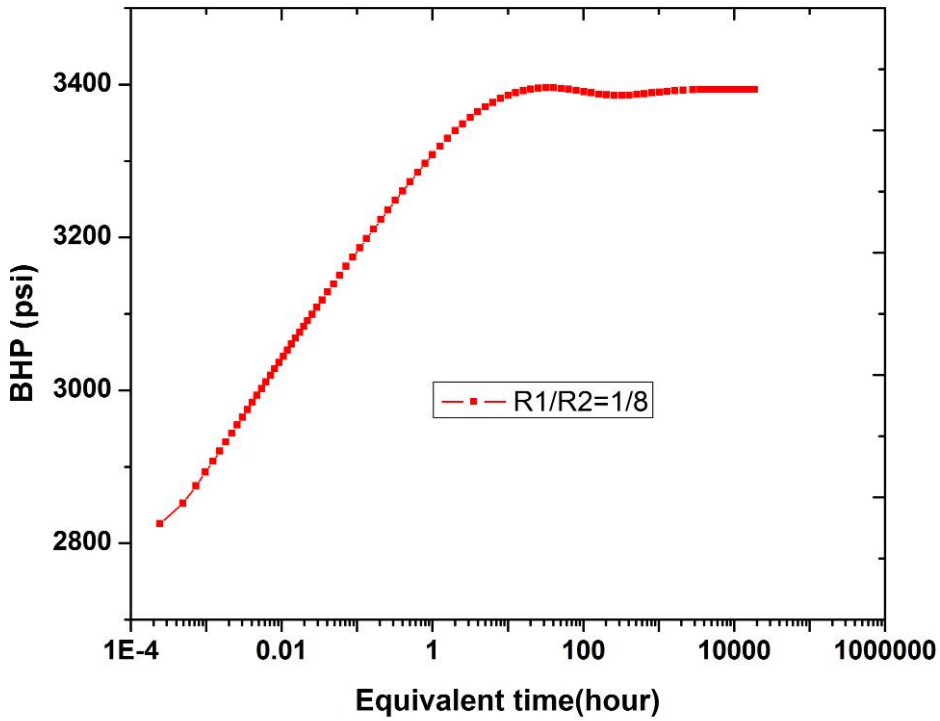

Figure 4.16 The semi-log plot under R1/R2=1/8 for the more permeable zone with high pressure

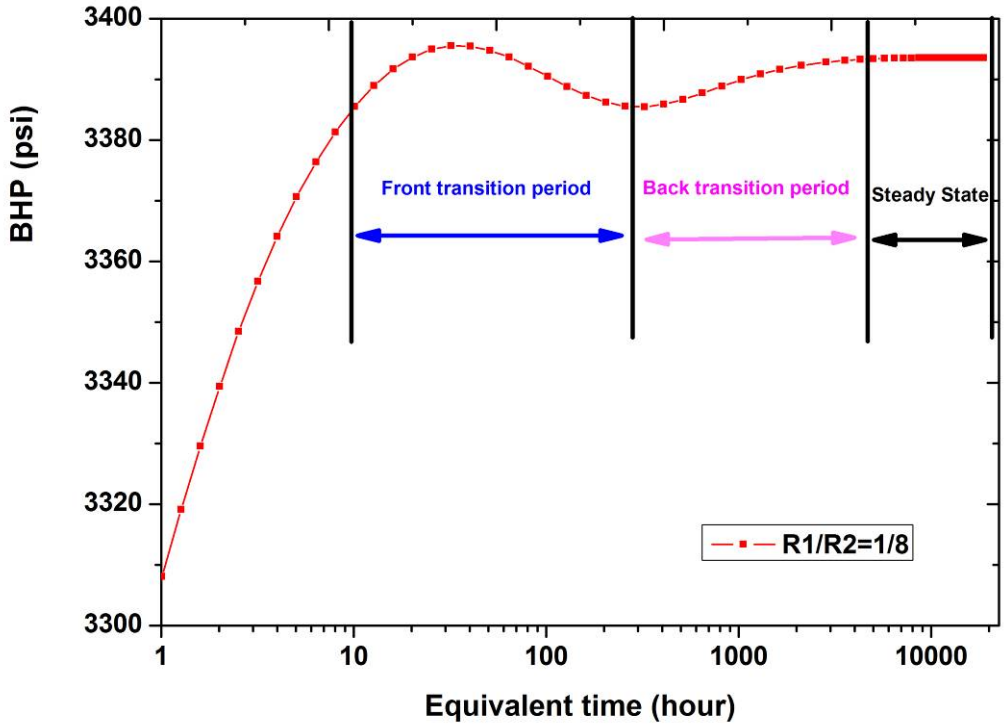

Figure 4.17 The semi-log plot under R1/R2=1/8 for the more permeable zone with high pressure (zoom in)

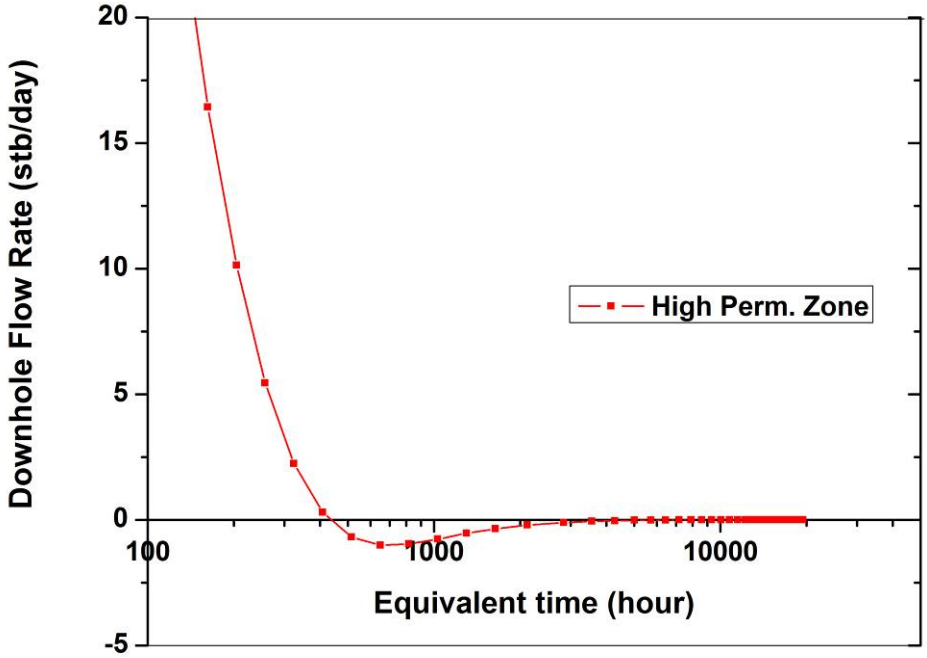

Figure 4.18 The flow profile under R1/R2=1/8 for the more permeable zone with high pressure

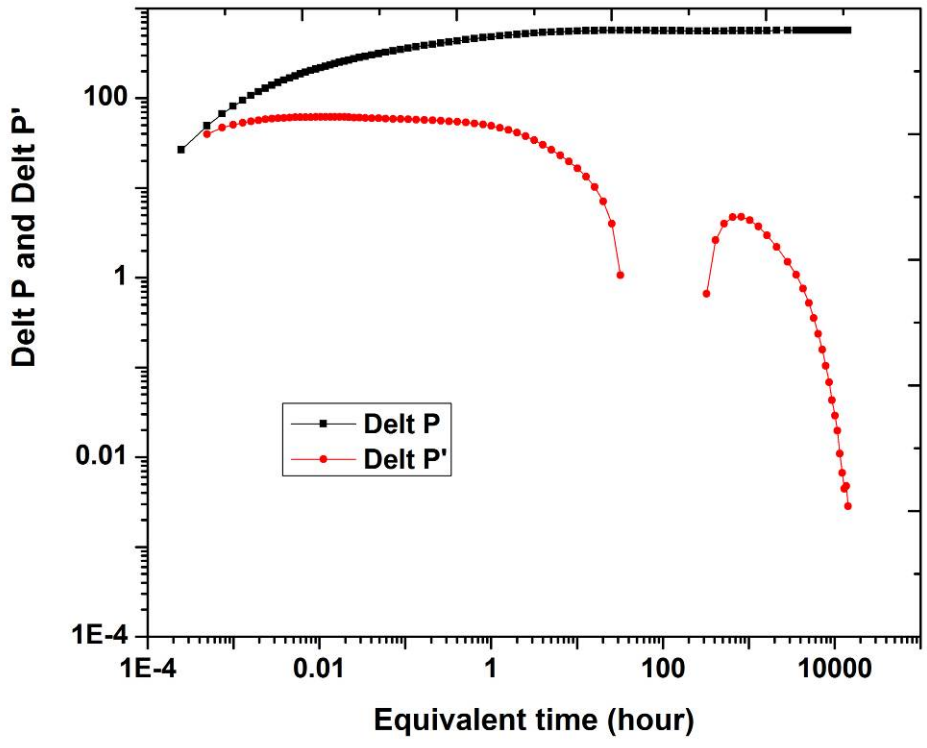

Figure 4.19 The log-log plot under R1/R2=1/8 for the more permeable zone with high pressure

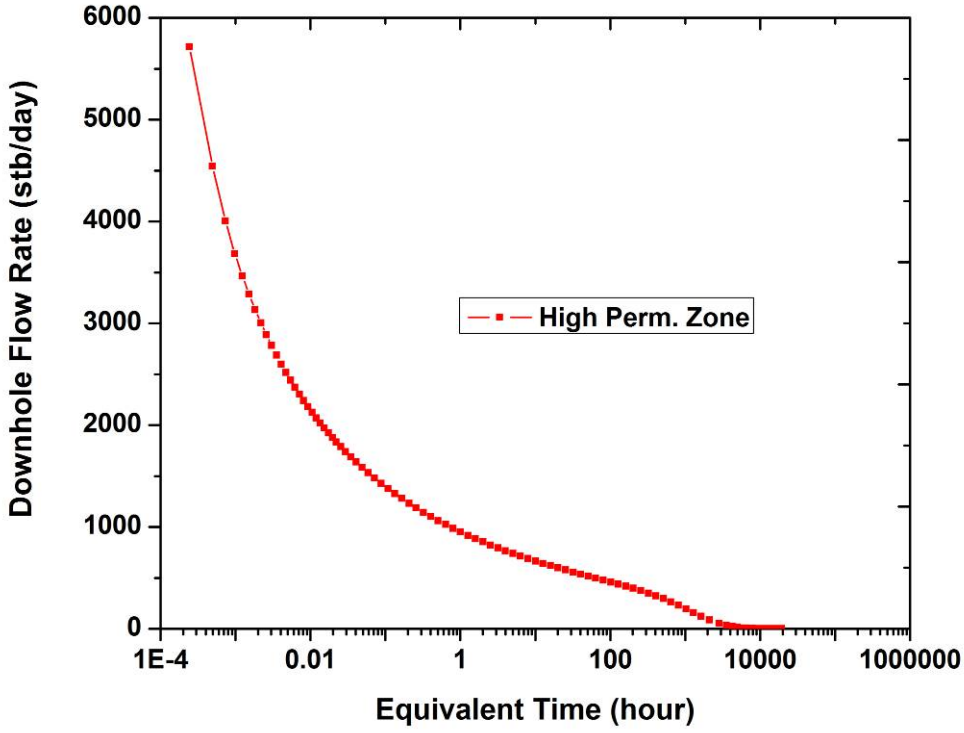

Figure 4.20 The flow profile under R1/R2=1 for the more permeable zone with high pressure

4.3.5.2 The more permeable zone with low pressure

In contrast to case 11 and case 11-1, **Figure 4.21** and **Figure 4.22** show some rules of a high permeability zone belonging to low pressure under different layer radius conditions. Although the high permeability zone is a low-pressure zone, the pressure propagation of this zone is quick. Before pressure reaches the boundary, fluid crosses flow from the less permeable zone with high pressure to the more permeable zone with low pressure. After pressure reaches the boundary, the crossflow rate decreases step by step, the pressure curve will flatten out, and this flat curve indicates the characteristic of the zone, in which the pressure propagation is quick. The length of the flat curve is determined by the elastic energy of the zone pressure propagating quickly.

From then on, the fluid continues to cross flow from the less permeable zone to the more permeable zone because the zone for the pressure propagating slowly has high

elastic energy, so the curve goes on up, till the pressure reaches the boundary of this zone, then the curve starts to flatten and to steady. The transition period of this curve is step shaped.

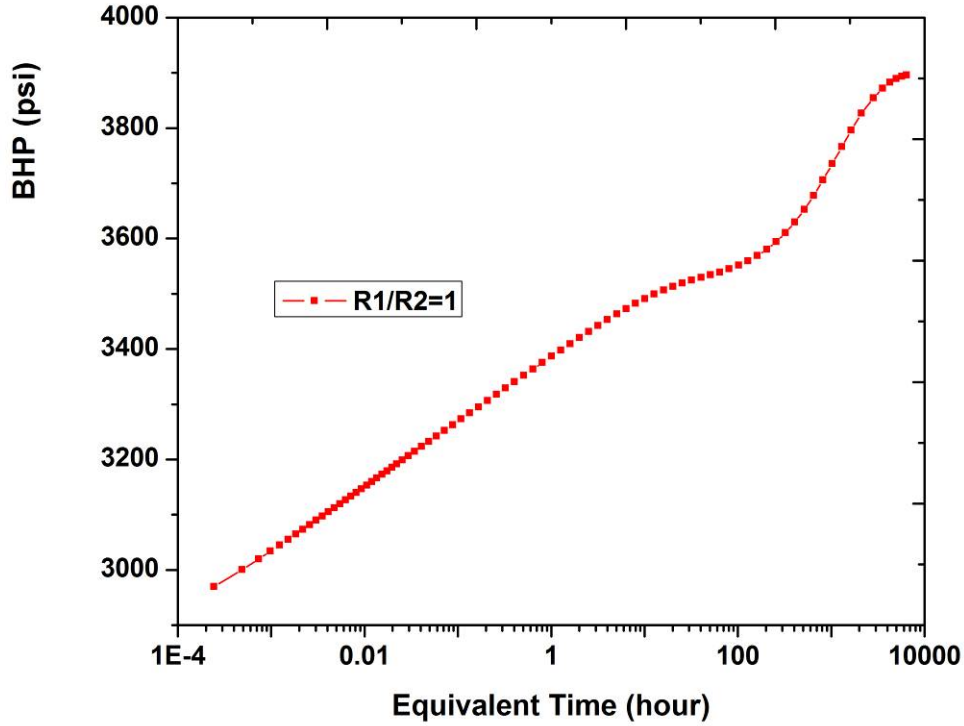

Figure 4.21 The semi-log plot under R1/R2=1 for the more permeable zone with low pressure

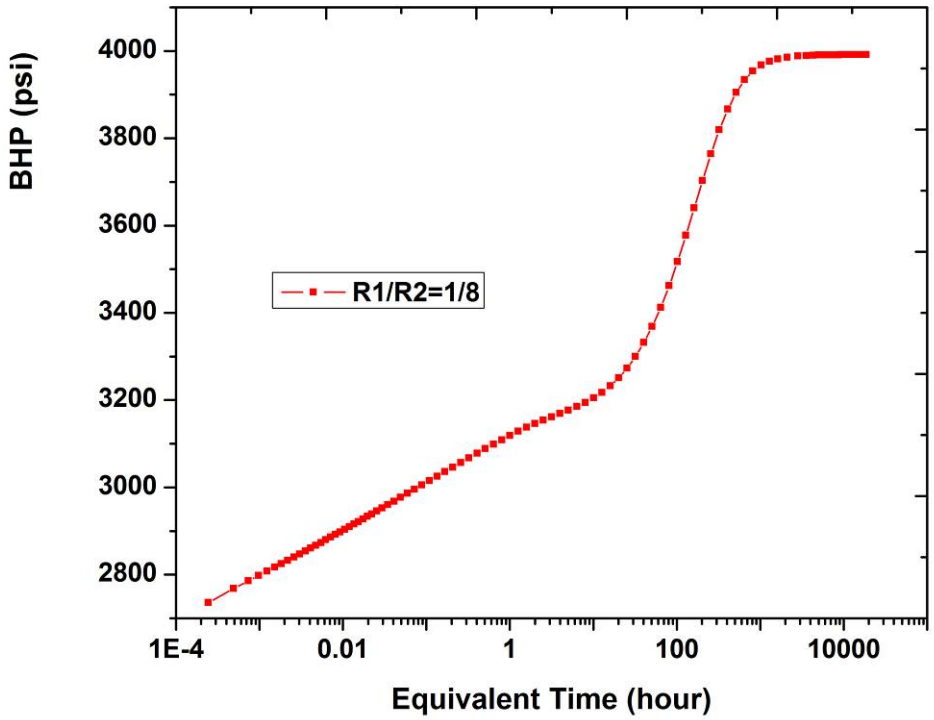

Figure 4.22 The semi-log plot under R1/R2=8 for the more permeable zone with low pressure

4.3.6 Influence of initial pressure

At late development period for the mature field, because of the heterogeneity of layered commingled reservoirs, the layer pressure between zones depletes very seriously. The pressure of these zones may equal to or be less than bottom-hole pressure. Under this situation, if these zones are perforated, there is no production. But the question is whether these zones affect the buildup curve of multi-layered commingled reservoirs. Two cases have been designed under different reservoir radius conditions.

Figure 4.23 shows that there is a large variation when comparing all the figures above. When the pressure reaches the drainage boundary, the straight lines of the semi-log plot go up directly and the step shape and hump shape does not occur. According to this result, reservoir engineers can determine from transient well testing that the pressure of some production zones is very low, and that these layers may not contribute to the total production rate.

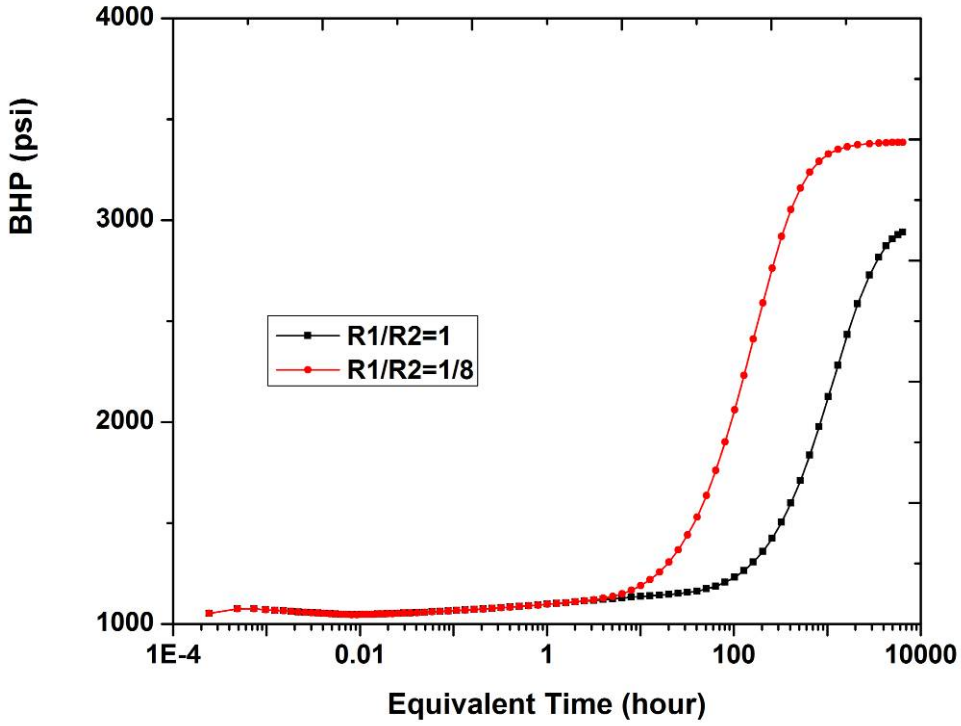

Figure 4.23 The semi-log plot under different reservoir radius for a high permeability zone with lowest pressure

4.4 Analysis of Selective Inflow Performance test (SIP Approach)

The response of pressure of multi-layered reservoirs is different to single layered reservoirs. If using conventional well testing methods to analyse and obtain the average formation parameters of multi-layered commingled systems, no sense can be made of the results. The goal of multi-layered reservoirs is how to obtain individual-layer properties and productivities. Currently, the multi-layer transient test (MLT) with production logging (PL) tool can be used to monitor individual-layer performance. Using a production-logging gauge, the flow rate and the bottom hole flowing pressure of an individual-layer can be measured. According to this data, the selective inflow performance (SIP) curve can be plotted. From the SIP figure, the productivity index (P.I) and initial pressure of the each layer can be obtained. Using individual-layer transient well test data and individual-layer rate, the parameters of the individual-layer can be calculated. (**Figure 4.24**)

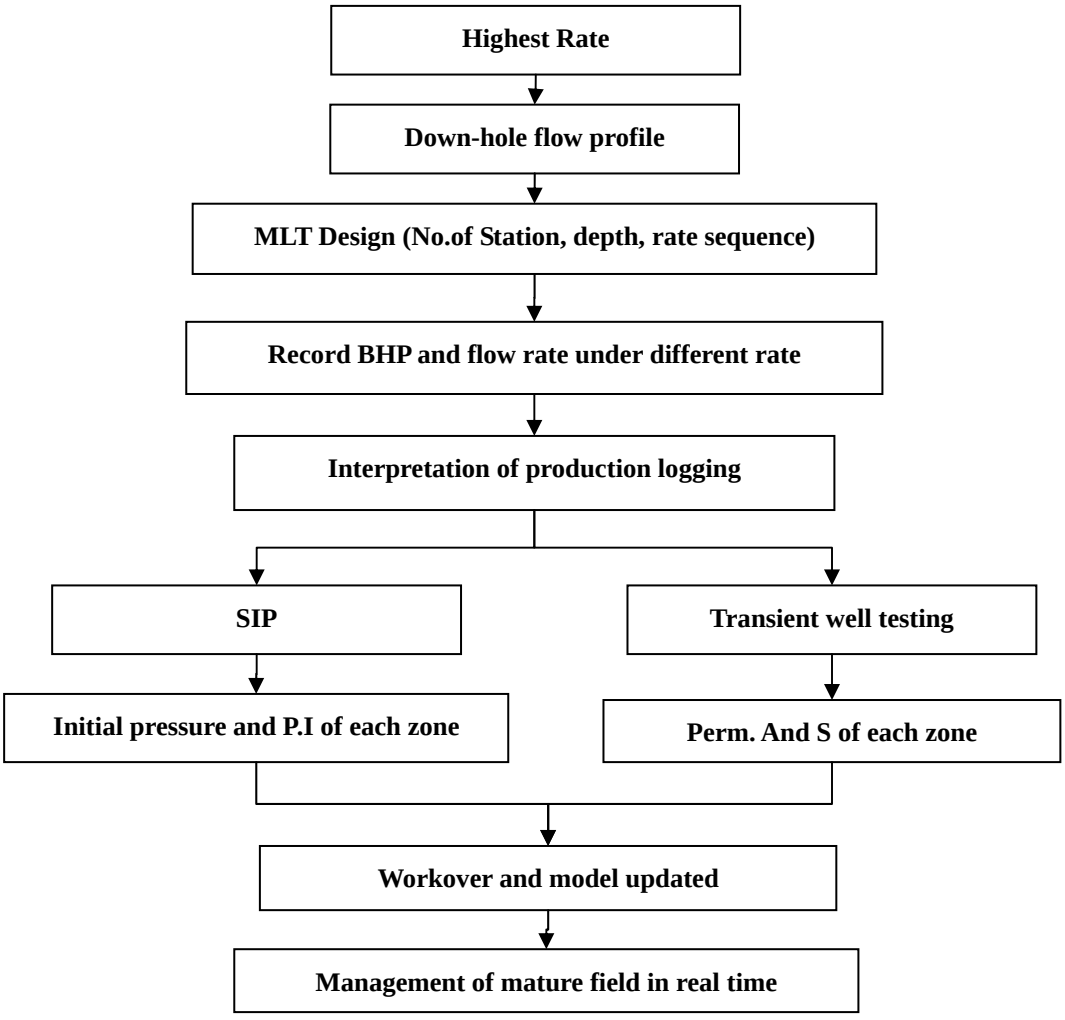

Figure 4.24 Illustrates the workflow of MLT approach

4.4.1 Numerical model

This case is a real field example, where the field had entered the high water-cut stage. The reservoir is a multi-layered commingled system. Using the numerical well test method to study multi-phase well testing in layered commingled reservoirs, the procedure for study is as follows (**Figure 4.25**):

Step 1: history matching in full model. In this case, the field dynamic production data and single well data need to match accurately.

Step 2: before numerical well testing, because the simulation model has more than 500000 grid cells, a rather large number, a window is cut from the full model. There are three types of the boundary of the window. One is the flux boundary, which is controlled by fluid flow. A second is the pressure boundary, whose behaviour can be extracted from existing simulation result files. The third is the no-flow boundary, in which the window is a closed system. In this case, the flow pressure boundary was selected as the boundary of the window.

Step 3: for the window, because a numerical well test simulation needs to avoid numerical dispersion, the time step and the cells near the well bore require local refinement. Only by this can the accuracy degree of numerical solution be ensured. (**Figure 4.26**)

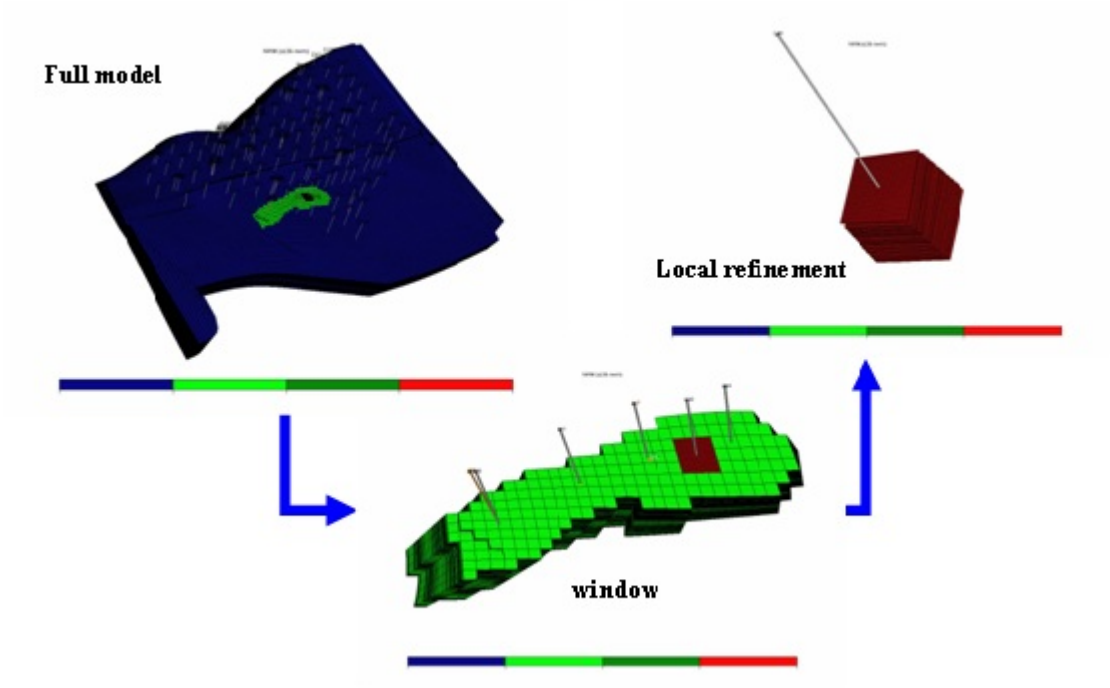

Figure 4.25 Illustrates the workflow of numerical well test

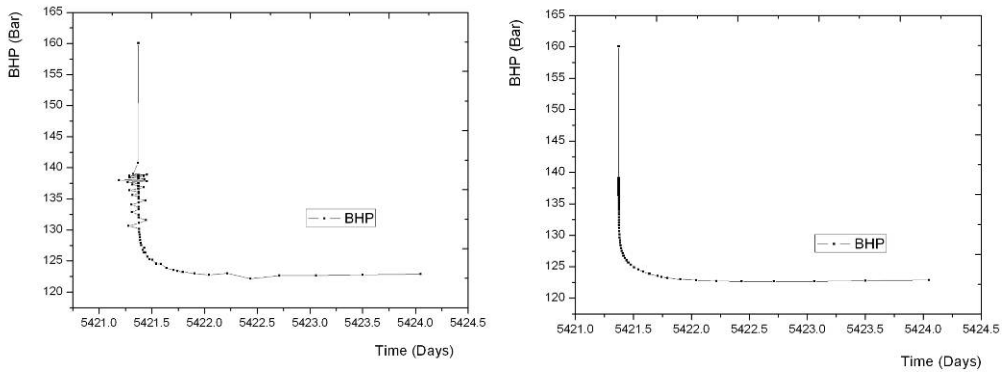

Without LGR（numerical dispersion） with LGR

Figure 4.26 The bottom-hole pressure curve

4.4.2 Selective inflow performance (SIP)

In order to understand the degree of interference of a layered commingled system, well C30 was selected to study. This well has a total of 14 layers (**Figure 4.27**). For this study, three layers have been chosen (**Table 4.2**).

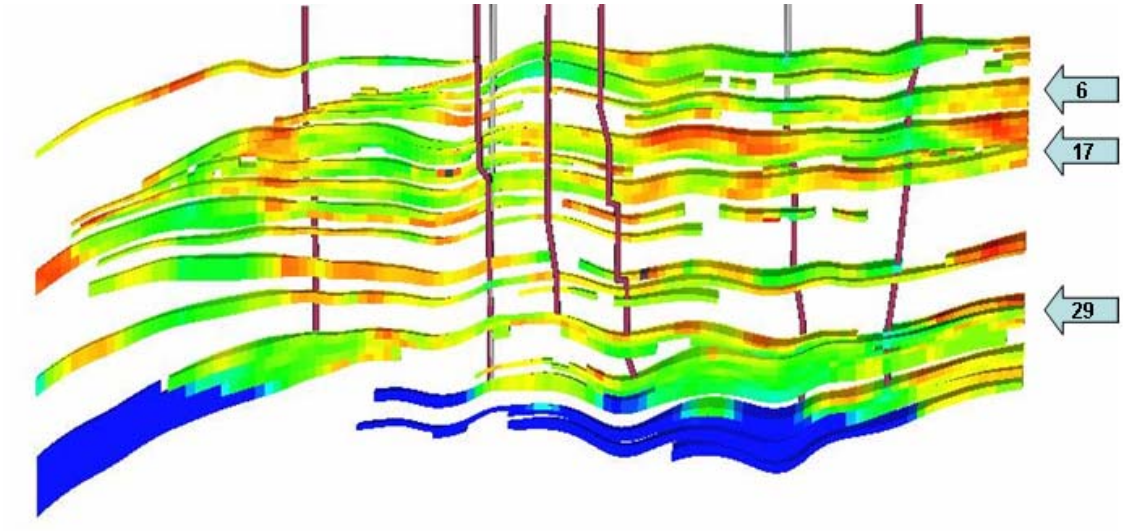

Figure 4.27 Section profile of layered commingled reservoirs

Table 4.2 Some parameters of well C30

Zone No.	Pressure (Bar)	Permeability (md)			Porosity
		X	Y	Z	
6	166.97	6221.8	6220	20.877	0.31452
17	157.54	1735.7	1719	3.3937	0.27948
29	152.72	6537.7	6319.4	19.6	0.34717

As described above, using a multi-rate multi-zone (MRMZ) test to confirm and provide valuable data for an evaluation of the layer contribution to the total production, a step-rate production test was designed. Under different production rates, after the pressure and the flow rate has stabilized, the flow rate, pressure and water-cut of each layer can be measured by a production logging gauge.

Figure 4.28 shows the sequence of MRMZ test, at first the well shut in about 3.37days, then the well was opened and changed rate from 360m^3/day, up to 720 m^3/day, and then 1200 m^3/day, and produced 3.4days for each flow rate period. Finally the well shut in about 6.7days.

Has the flow rate stabilized? The criterion is that pressure reaches the boundary of the reservoir. According to BHP data **(Figure 4.29**), making the log-log plot of the last DD and the last BU, **Figure 4.30** and **Figure 4.31** show that the pressure derivatives of DD and BU both go down. This indicates that the pressure had reached the constant pressure boundary during test period.

According to the simulation results, the downhole flowing rate curve and pressure curve of each layer can be obtained (**Figure 4.32, Figure 4.33, Figure 4.34,** and **Figure 4.35**).

Using the flow rate and pressure of each layer (**Table 4.3**), the downhole flow rate profile and IPR of each layer can be plotted (**Figure 4.36**, **Figure 4.37**). From the SIP curve, the initial pressure and productivity index (PI) can be obtained (**Table 4.4**).

Figure 4.37 shows that the IPR curve of layer 29 intersects the IPR curve of the other two layers. It indicates that the initial pressure of layer 29 is very low. Under shut in or low flow rate conditions for the well, there is cross flow from interval 6 and 17 to interval 29, but after enhancing drawdown pressure, **Figure 4.36** shows that when the flow rate increases, cross flow will be avoided. This shows that more layers can be contributed under a reasonable production sequence.

From this SIP curve, the division of production strata is illogical, because there is a large variation in difference of the interlayer pressure, so the production cannot be

stabilized due to crossflow effect. From **Table 4.4**, the PI of each layer has a large variation. Layer 29 is best, layer 6 takes second place, and layer 17 is worst. This result is in accordance with the properties of each layer. Although the PI of layer 29 is highest, the initial pressure is lowest. It means that the energy depletion of this layer is very serious, so this layer needs to add energy by the injection of water.

Table 4.3 Down-hole flow rate and pressure of each zone

Rate	Zone 6			Zone 17			Zone 29			BHP,Bar		
（m^3/day）	Oil	Water	Liquid	Oil	Water	Liquid	Oil	Water	Liquid	6	17	29
0	14.6	111.6	126.2	0.74	0	0.74	-15.1	-112.34	-127.44	152.6	156.7	162.6
360	29.8	229.2	259	16.4	0	16.4	7.3	77.5	84.8	137.2	141.3	147.2
760	41.2	323.1	364.3	27.9	0	27.9	18.2	309.6	327.8	125.1	129.3	135.2
1200	57.1	438.2	495.3	42.98	0	42.98	30.3	631.4	661.7	110.1	114.3	120.2

Table 4.4 Initial pressure and P.I of each zone

	Zone 6	Zone 17	Zone 29
Initial pressure（Pi）（Bar)	167.5	157	154
P.I（m^3/d/Bar)	8.68	1.00	18.61

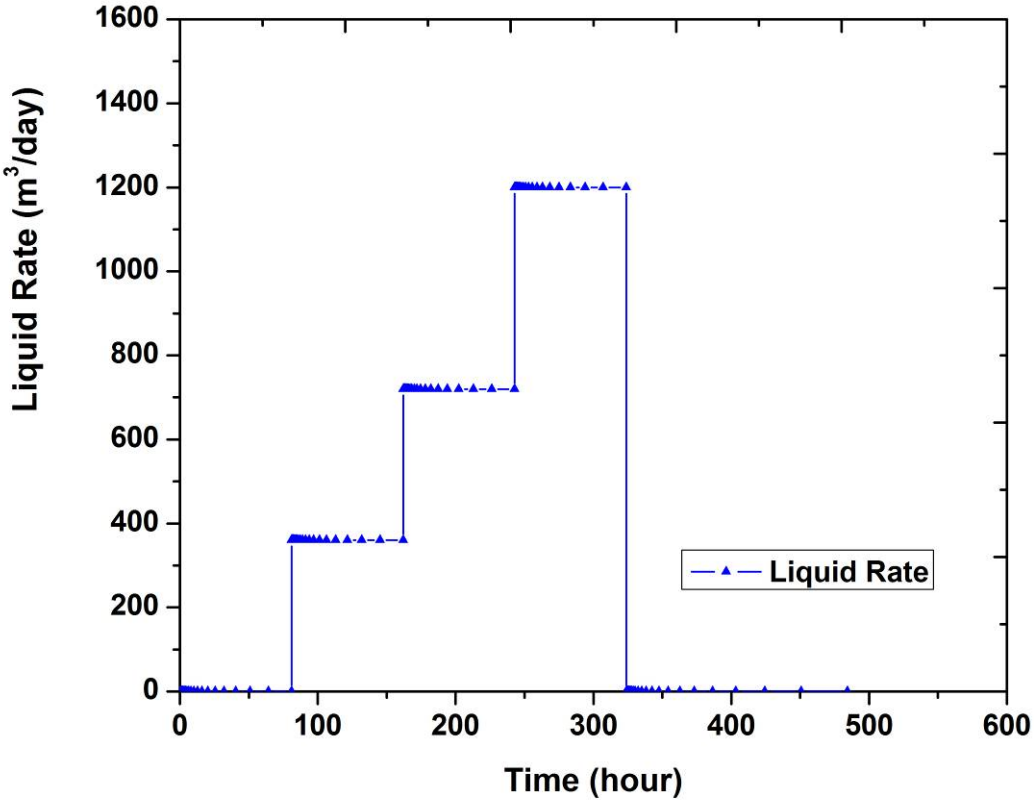

Figure 4.28 Liquid rate curve of MRMZ test

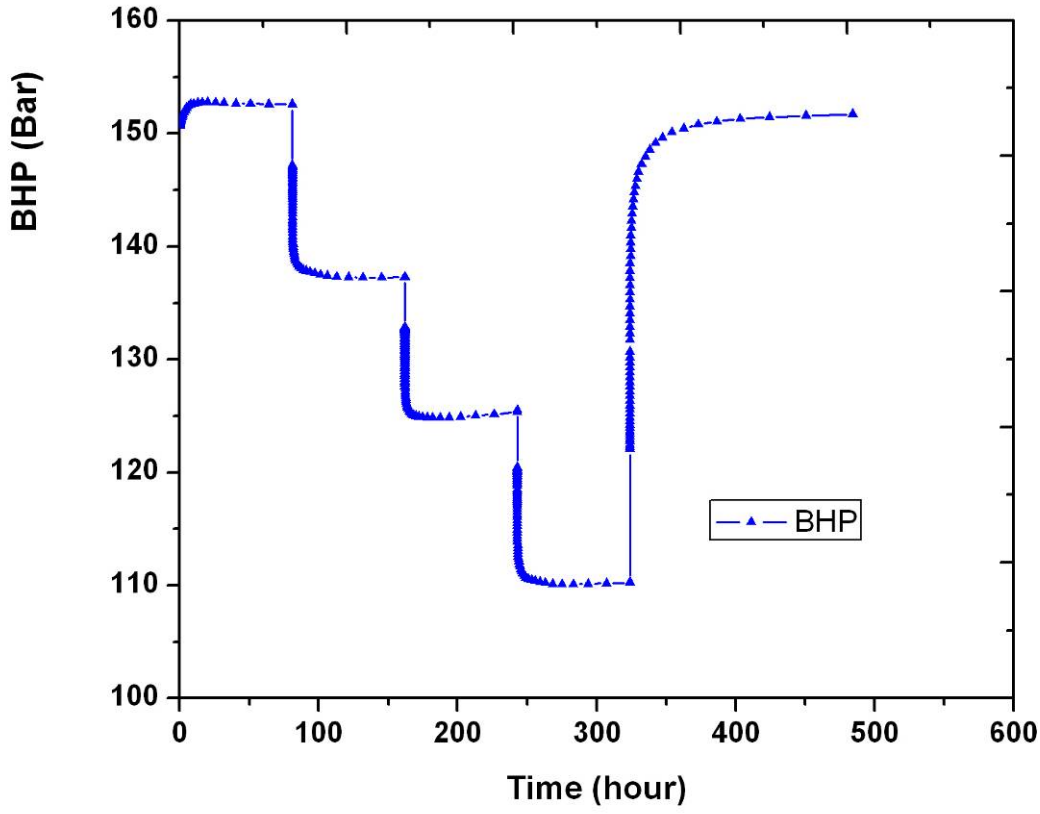

Figure 4.29 BHP curve of MRMZ test

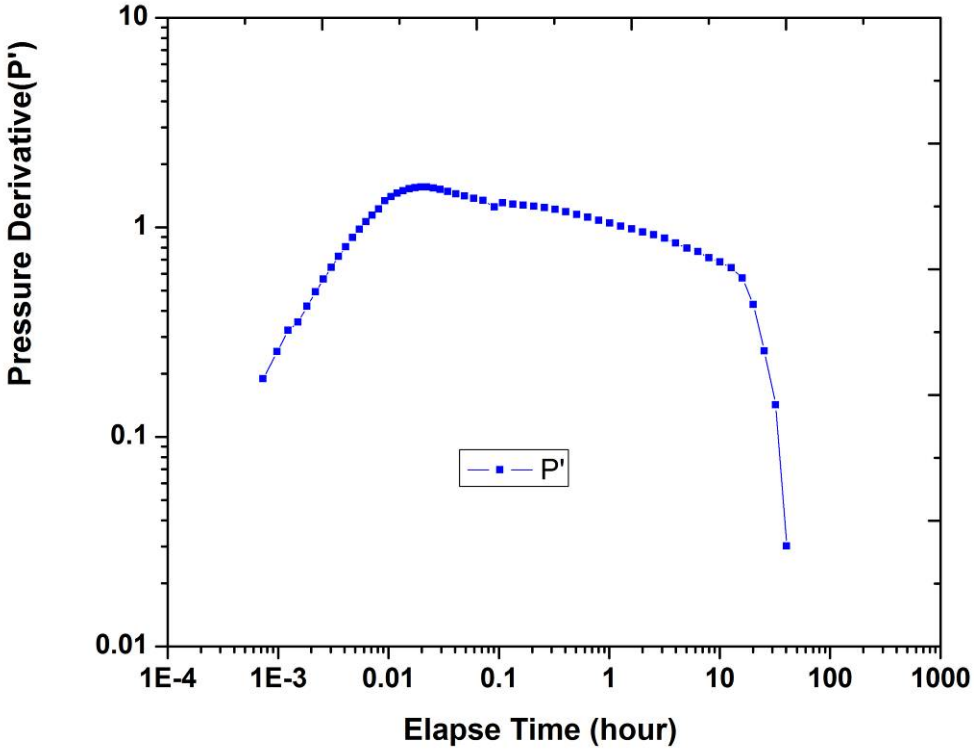

Figure 4.30 The log-log plot of last DD

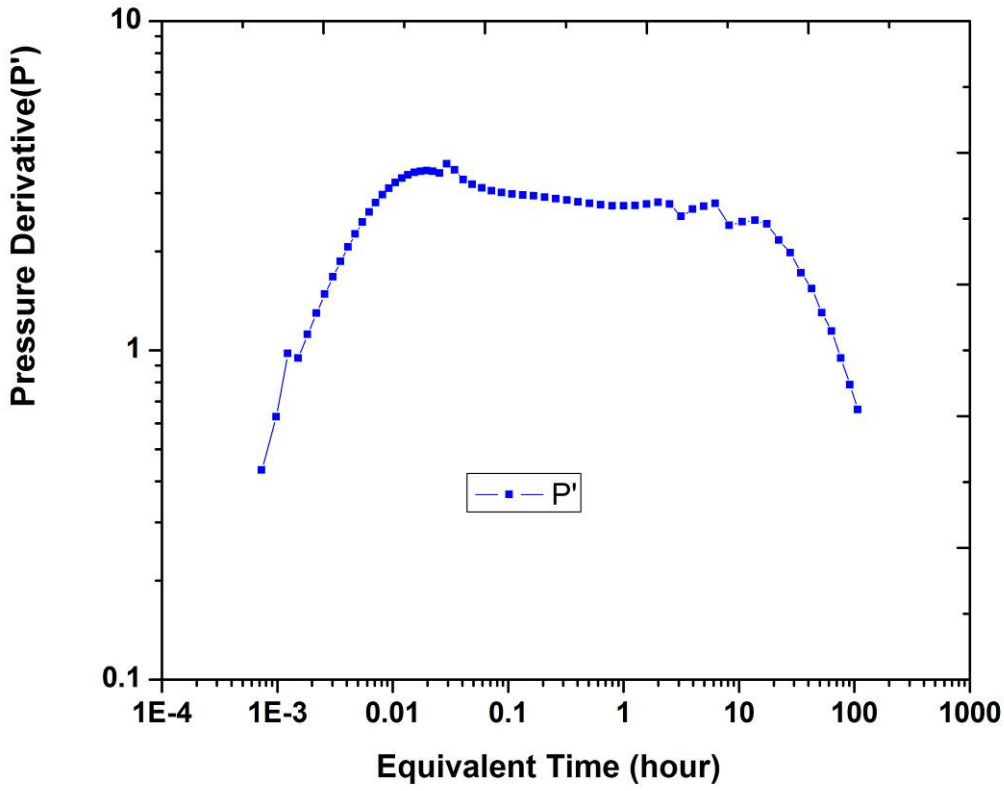

Figure 4.31 The log-log plot of last BU

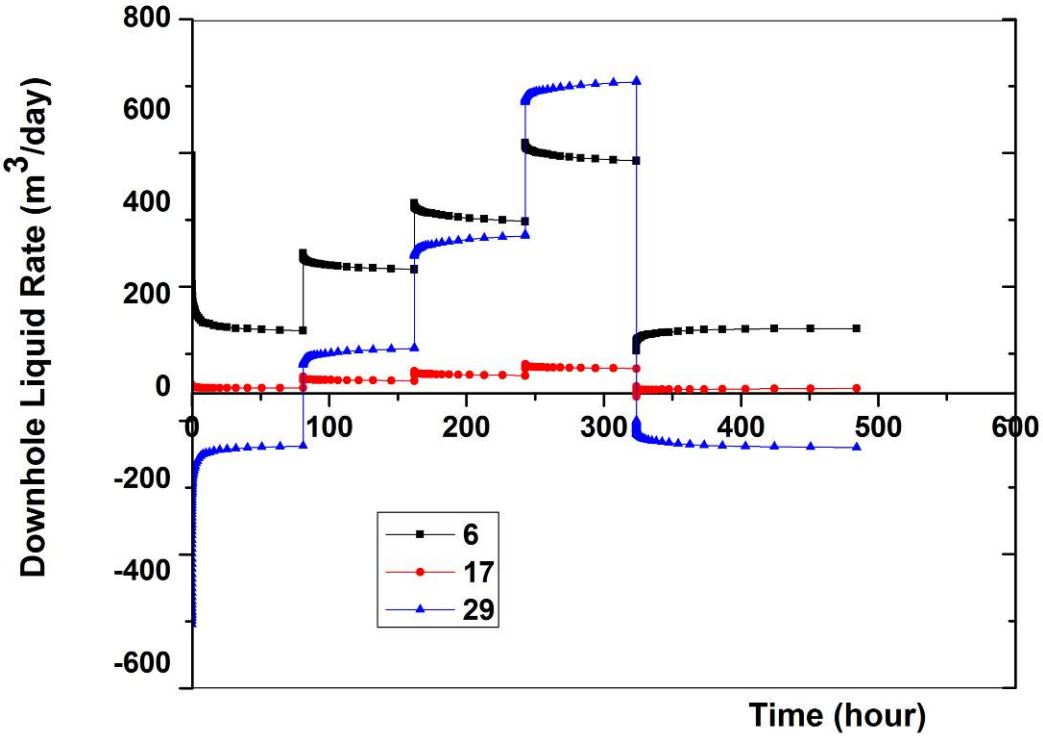

Figure 4.32 The downhole liquid rate of each zone

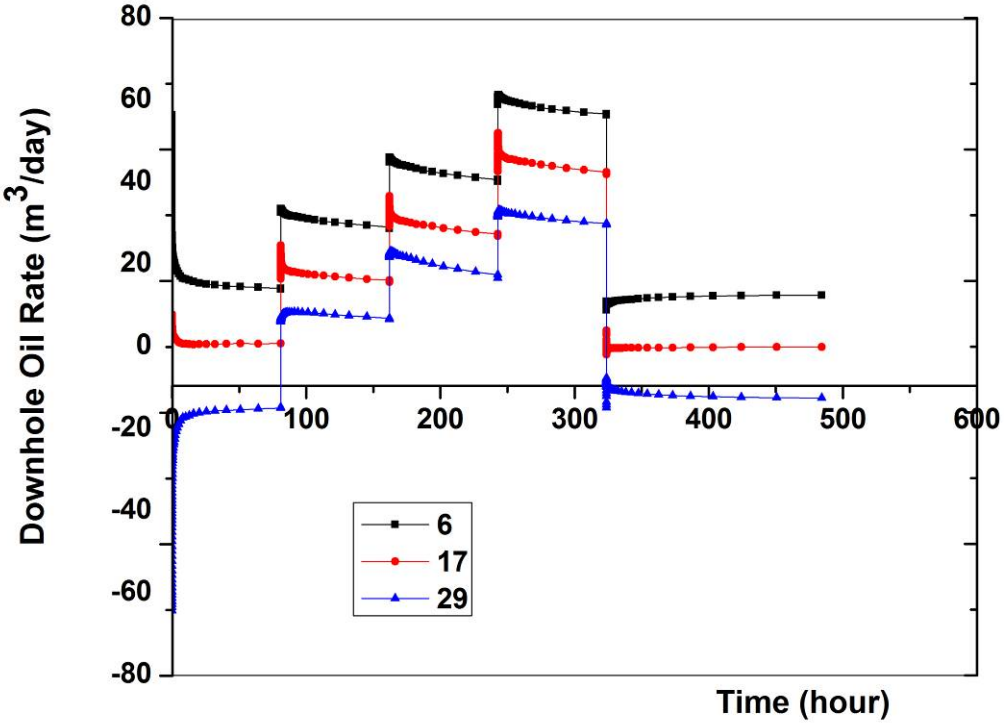

Figure 4.33 The downhole oil rate of each zone

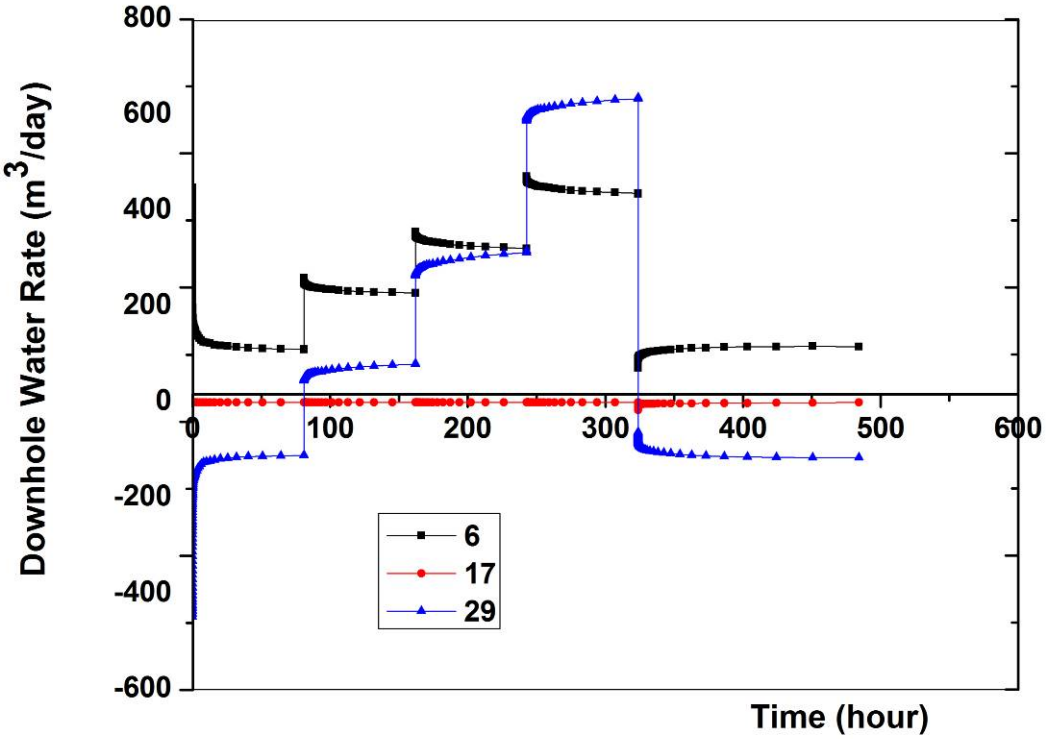

Figure 4.34 The downhole water rate of each zone

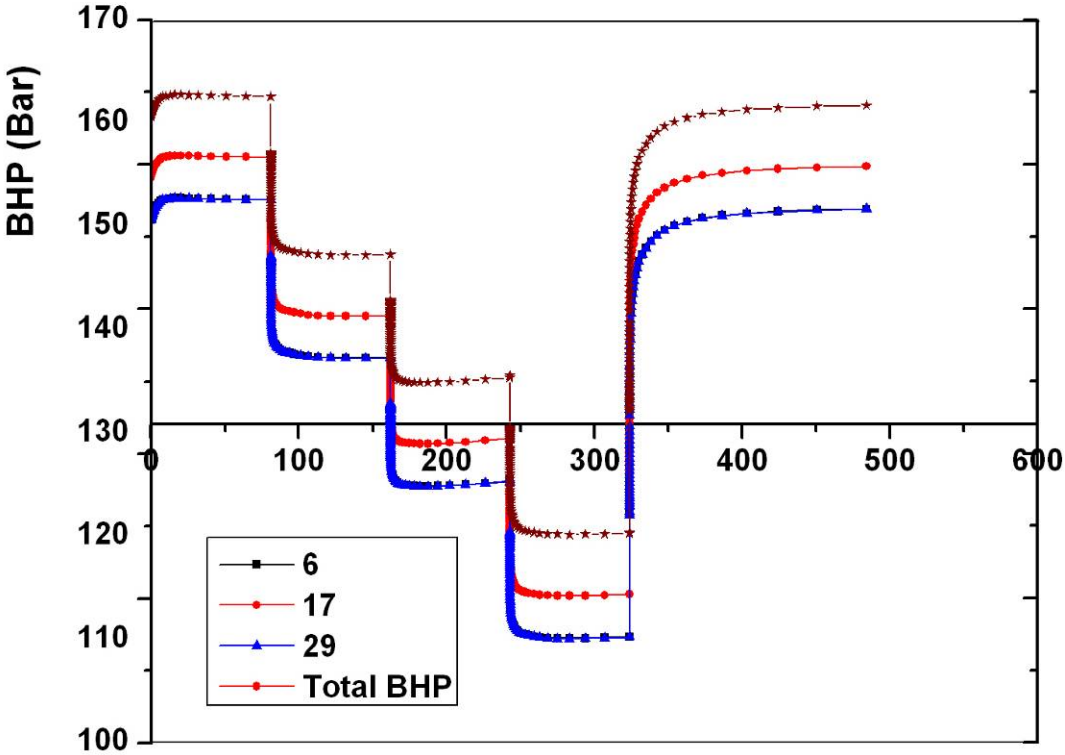

Figure 4.35 The BHP of each zone

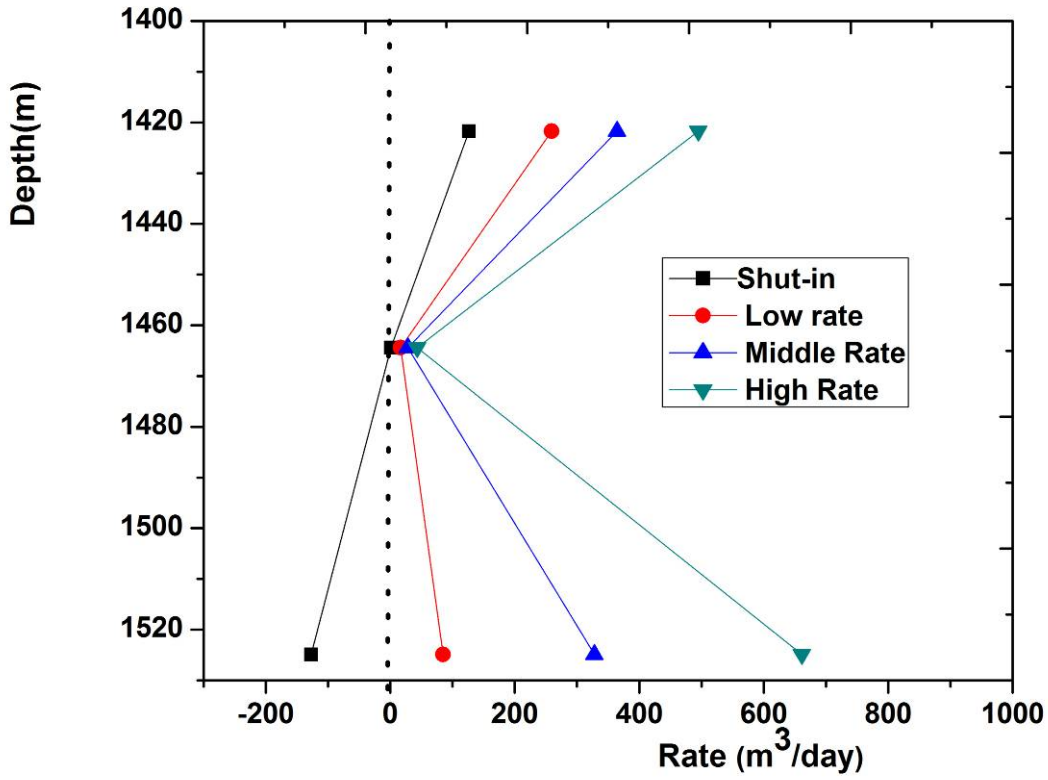

Figure 4.36 The downhole flow profile of each zone

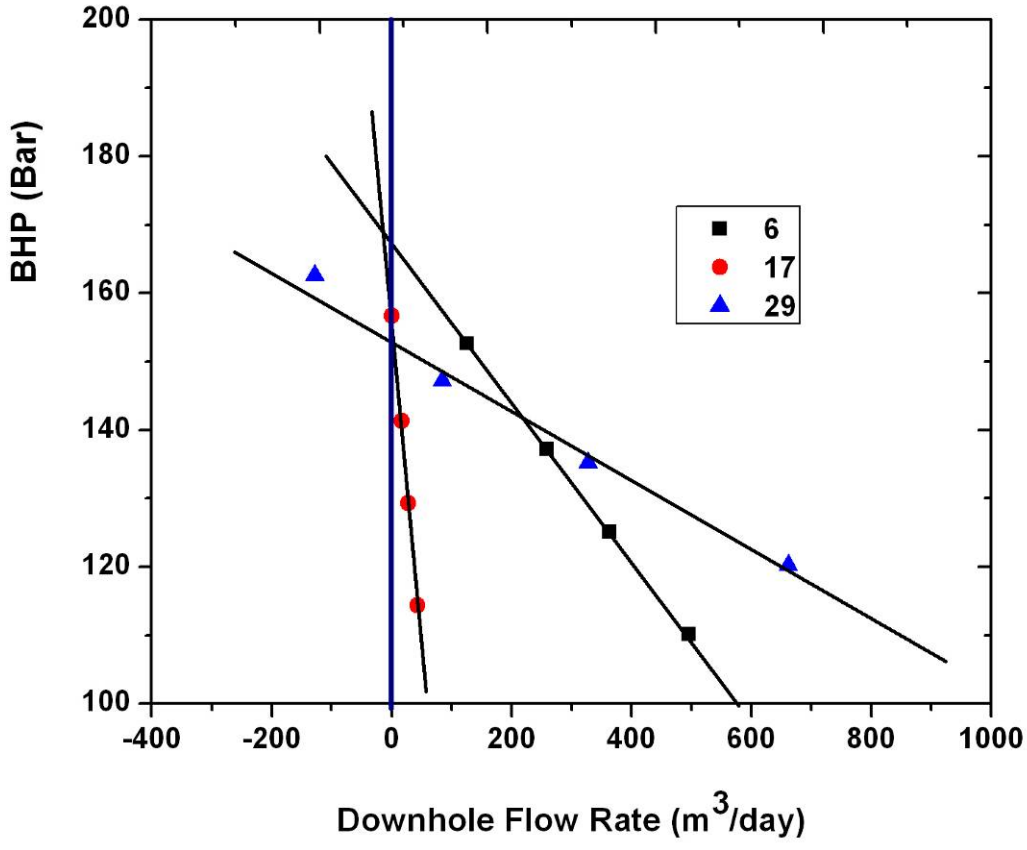

Figure 4.37 The SIP curve of each zone

4.4.3 Interpretation of well test for each zone

According to the production logging test, the downhole flow rate of each layer can be obtained. Combining this with the bottom-hole flowing pressure of each layer, the effective permeability and skin factor of each zone can be explained by conventional a multi-phase well test.

For example, aiming at layer 17, choosing the last DD to interpret and draw log-log plot (**Figure 4.38**), from this plot, the radial flow was diagnosed. Then determining the straight line from semi-log plot (**Figure 4.39**), the slope of radial flow can be obtained. Finally the P-M method was selected to calculate the phase permeability and skin factor of each zone. (**Table 4.5**)

In S.I metric units, **Equation 1.10** and **Equation 1.12** are rearranged as:

$$k_l = \frac{2.121\times10^{-3} q_l B_l \mu_l}{mh} \tag{4.1}$$

$$S = 1.151\left\{\frac{\Delta P_{1hour}}{m} - \log\left(\frac{\lambda_t}{\phi c_t r_w^2}\right) - 0.9077\right\} \tag{4.2}$$

Where: k-Phase permeability， μm^2 (1 μm^2 =1013.25md);

q- Flow rate，m^3/d;

B-volume factor，m^3/m^3

μ - Viscosity，mPa.s;

h- Thickness，m;

l - Stand for oil or water；

m- Slope of straight line for semi-log plot；

ϕ -porosity；

c_t -total compressibility，1/MPa;

r_w -well radius，m;

λ_t -total mobility, μm^2 /mPa.s;

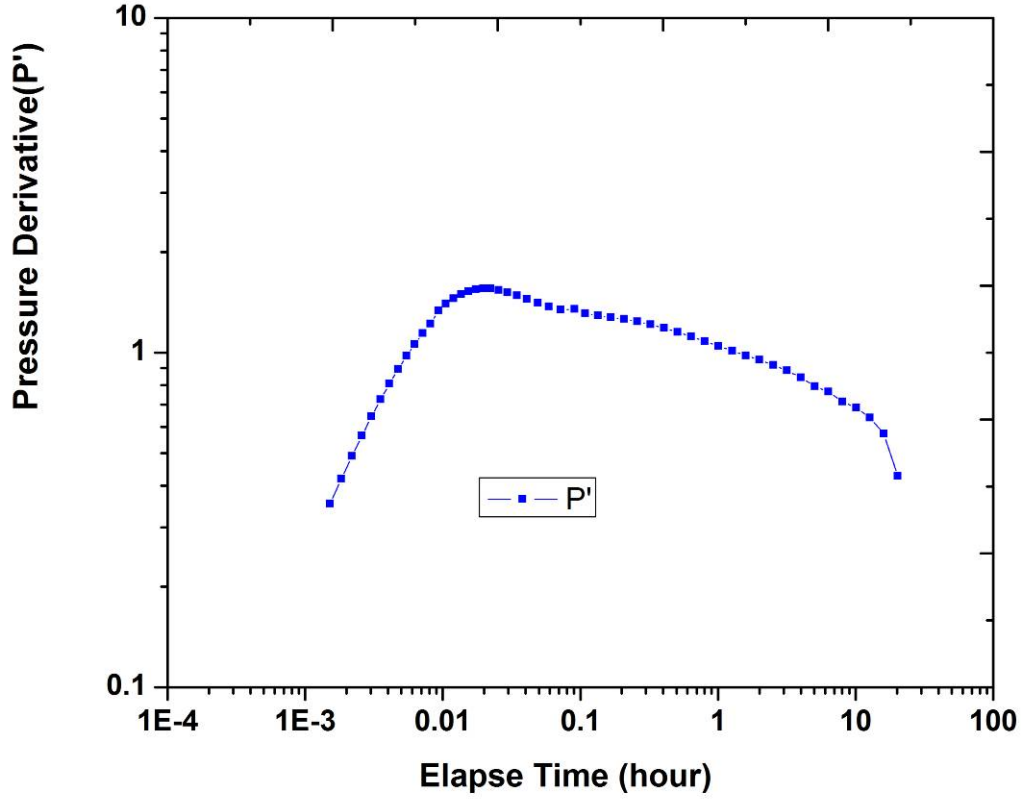

Figure 4.38 The log-log plot of DD for layer 17

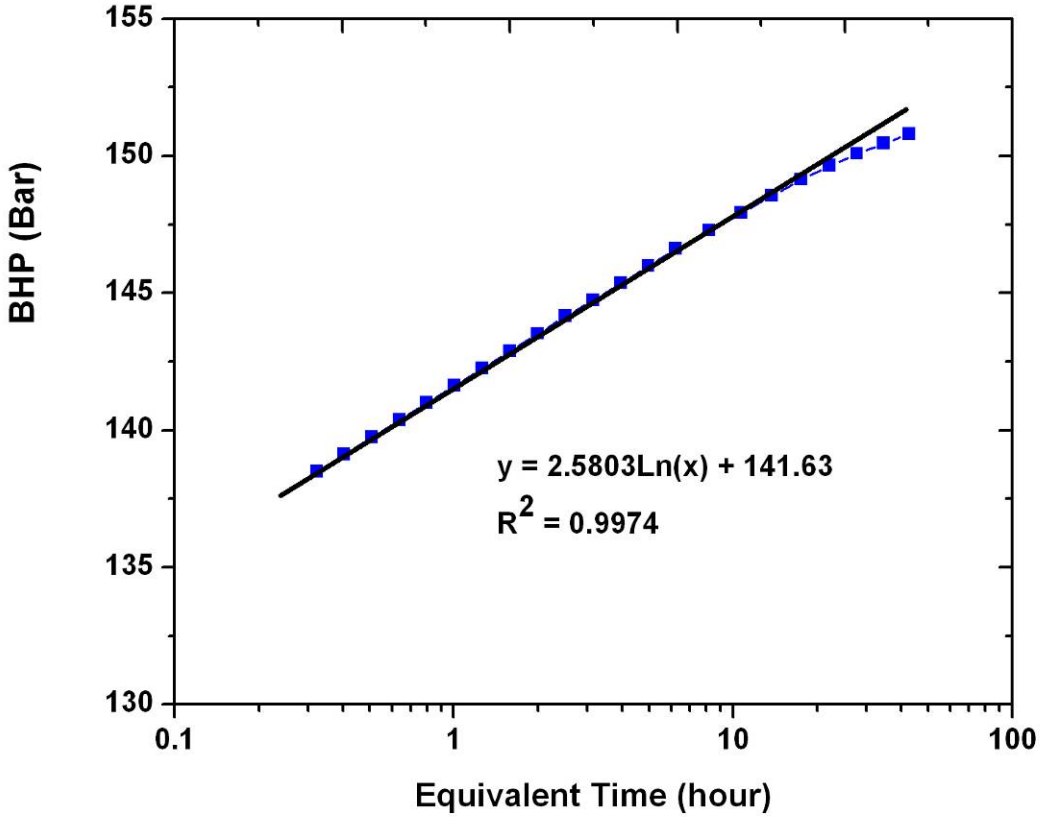

Figure 4.39 The semi-log plot of DD for layer 17

Table 4.5 The result of the well test for each zone

Zone No.	Thickness（m）	Porosity	Rate（m^3/d）		Oil phase Permeability (md）	Water phase permeability （md）	Skin factor
			Oil	Water			
6	5.16	0.31	57.1	438.2	4674.47	358.57	-0.49
17	7.60	0.28	43.0	0.0	2392.08	0.00	-1.83
29	5.55	0.35	30.3	631.4	2308.18	480.68	-1.9

Using the results of transient well testing analysis and SIP analysis, the reservoir model can be updated in real time, and the workover of each layer can be optimized.

4.5 Chapter Conclusion

- According to theoretical models for multi-layered commingled reservoirs, the shapes of the buildup curve vary greatly under different conditions. Permeability, porosity and radius of each zone are very sensitive, but the thickness of each zone is insensitive.

- In fact, for multi-layered commingled reservoirs, using transient well test data to calculate the average properties of reservoir is not practical. Currently, multi-rate multi-zone production logging and transient testing can be used to calculate the properties of each zone and evaluate the layer contribution to the total production.

- For multi-layered commingled reservoirs, under low flow rate, cross flow is very severe. Hence, for these reservoirs, the production rate for more perforated layers is low or even negative due to crossflow, but if selecting a reasonable production type, the crossflow effect can be avoided.

Chapter 5
New Approach for Multiphase Flow Numerical Well Testing

5.1 Introduction

According to the previous analysis from theory to simulation validation, in non-uniformly saturated reservoirs or layered commingled reservoirs, due to the limitation of multiphase flow governing equations, the multiphase flow problem cannot be solved analytically. But numerical models have flexibility in terms of handling spatial variations of reservoir properties and multiphase effects. In recent years, there has been an increase in the use of reservoir simulation or numerical well testing as a tool for reservoir management, which can be used to integrate seismic data, geological data, production data, logging data etc. into the interpretation of well tests (such as transient well test, PDG, mini-DST etc.). Furthermore, under multiphase flow conditions, there is only the history matching approach available to update the reservoir model and then the use of a calibrated model to evaluate future development performance for the mature field.

History matching of reservoir performance is difficult due to the large uncertainties associated with properties in the reservoir models. Moreover, there is a big difference

between the history matching of production data and the history matching of transient test data. In general, the rate history is used as input information and the reservoir properties changed until the measured and calculated pressures or production data (such as average reservoir pressure, bottom-hole flowing pressure, liquid rate, water-cut, accumulation rate, etc.) are visually matched on a Cartesian plot. But for transient test data or PDG data, during history matching, this data may seldom be used to match, due to the noise and large volume of data. Even though it was used to match, the fitting curve takes place only on a Cartesian plot. It is well known that pressure derivative analysis has been used in well testing many years, and this has the advantage of displaying different flow regimes for easy identification and definition. Hence, from the logarithmic scale for the time axis, dynamic information of reservoir can be made known. However, if data were matched on Cartesian plots, such information would be lost.

The numerical well testing approach applied in the petroleum industry can be used to improve history matching of simulation models by incorporating a large amount of performance data (for example, pressures - transient pressure data, PDG data, cumulative oil, water-cut and GOR -both field and individual wells, in addition to having some data on which wells are in communication and possibly some production logs). But the link between reservoir simulation and well testing is a challenge for reservoir engineers. This chapter firstly reviews the previous workflow on the history matching of numerical models to observed well test data. Later, a new multiphase flow numerical well testing workflow is developed. It is suitable for the matching of PDG data with multiphase flow effects.

5.2 Previous workflow

Existing commercial simulation software packages, including well testing and near wellbore modeling, can be used to carry out the model to dynamic update. But previous works focus on single phase heterogenous reservoir. The numerical well

testing method was composed of five steps. (Bischoff, R., *et al*., 2005[113]; Sahni, A., *et al*., 2007[110]; Al-Mohannadi, N., et al., 2007[23])

Step1: Analytical Analysis

According to the analytical method, transient pressure can be interpreted by the traditional well testing analysis approach to obtain reservoir or well parameters, such as skin factor, effective permeability, wellbore storage, distances to boundaries, fracture length, and so on. These results can be used to update the reservoir model properties as initial values and reduce the uncertainty of the model in the course of late numerical well testing analysis. Some results, such as well parameters (skin factor, wellbore storage, etc.) will not change, whereas the values of formation properties (effective permeability, distances to boundary, etc.) will change during numerical well testing analysis. In particular at this stage, the important investigation radius of influence for well test will be provided, and this result is useful to determine the area of adjusting model properties.

Step 2: Local Grid and Time-stepping Refinement

The accuracy of the numerical solution depends on the grid generation. According to step1, used to obtain the influence area, in this area, the grid size and time step need to be optimized. Through using a refinement technique, the pressure gradients of bottom hole flowing pressure and near well bore pressure are controlled to be very small so as to avoid numerical dispersion. At the same time, the cells near a fault can be coupled to the boundary. (Gunasekera, D., *et al*., 1997[104]; Mlacnik, K.J., *et al*., 2001[105],2003[71]; Al-Thawad, F.M., *et al*., 2007[109];)

Step 3: History Match

According to the first step, the results of analytical analysis should be used as the

initial values during history match. Through modifying the parameters of the area of influence for the well test, the simulated results from the model and measured pressure and pressure derivative on a log-log plot can be matched well, until the modified model with local grid refinement are put back into the full field model.

Step 4: Upscaling of the Local Grid Refinement (LGR)

When the area with LGR returns to the full field model, the reservoir properties need to be upscaled to the original model and used to replace the modified area in the simulator. (Pickup, G.E.*, et al*., 1994[16],1996[17]; Meddaugh, W.S., *et al*., 2006[112]; Zhang, P.G., *et al*., 2008[77])

Step 5: Validating the full field model

Through matching all available production history of all wells in the reservoir, including the tested wells, the full field model can be verified and used to predict the reservoir performance of the future.

The procedure of numerical well testing is based on single phase flow, and it can be carried out by existing commercial numerical well testing software. But under multiphase flow conditions, using PDG data to calibrate reservoir model is a challenge for reservoir engineer. This chapter introduces new procedure and is carried out by Eclipse software.

5.3 New multiphase flow numerical well testing workflow

Currently, numerical solution is the only method available to study multiphase flow. Through history matching of transient data or PDG data, the reservoir model can be updated continually. The procedure of study is as follows (**Figure 5.1**):

Step 1: History Matching in Full Model

In order to obtain a relatively precise full field model, the original reserve in place, the accumulation production rate, and the average reservoir pressure need to match accurately. This step does not consider the history matching of transient data or PDG data, so the matching is a little coarse.

Step 2: Processing and Analysis of Transient Data or PDG Data

Through data denoising and data reduction, the drawdown test and the build-up test can be identified, and then by calculating the pressure derivative for different drawdown or build-up, according to the pressure derivative, the wellbore storage, boundary conditions, and investigation radius can be identified. The observed pressure derivative can be matched by the calculated results of the model in the fifth step. The investigation radius can be used to determine the area of influence for the well test, and this area is a basis for numerical well testing.

Step 3: Definition of the Volume of Interest (VOI) Model

According to the investigation radius, the volume of interest (VOI) is cut from the full model. There are three types of boundary for VOI model. One is the flux boundary, which is controlled by fluid flow, and it means that the fluid near the boundary of VOI model is exchanging with the full model during simulation. The second is the flow pressure boundary, which is controlled by pressure, and it means that the energy near the boundary of VOI model is exchanging with the full model during simulation. The third is the no-flow boundary, it means that there is no exchange of energy and fluid between the boundary of VOI model and full model, and VOI model is closed system.

Step 4: Local Grid and Time-stepping Refinement for VOI Model

In order to avoid numerical dispersion, the time and the local grid of near well bore must be refined. Only by doing this, the accuracy degree of the numerical solution can be ensured.

Step 5: Adjusting of Properties of the Geological Model and Fluid Model (History Matching)

Through adjusting of the properties of the VOI model (such as geology parameters, fluid parameters, the relative permeability data, etc) to match the well testing data (transient pressure or transient rate), in this way, considering the boundary effect of VOI, in order to improve simulation speed, only the VOI model is run, until a satisfactory match is achieved between the simulated results from the VOI model and measured pressure and pressure derivative on a log-log. In this way, under multiphase flow conditions, the adjusting of the fluid model and relative permeability model is very important. If there is a demand, individual fluid properties and relative permeability curve for VOI model may be provided respectively.

Step 6: Validation of the VOI Model

In order to validate the VOI model, the time-stepping is upscaled to the original time scale, using the production history data of all wells in the VOI model to finish history match on a Cartesian plot. During this step, the full field model is run and further modifications of the properties of the VOI model are made, until consistent results are achieved. After completing this step, the VOI model will be put back the full field model.

Step 7: Selecting another VOI model, where some wells have well testing data, repeat step 2 to step 6.

Step 8: Validation of Full Field Model

After all confirmed VOI models were obtained from history matching of transient data in Cartesian plots and in log-log plots through numerical well testing approach, these confirmed VOI models return to full model, then all available production history of all wells in the full field model are used to validate the full field model, and this updated full model can be used to forecast future performance.

This new multiphase flow numerical well testing procedure will be developed in detail on later sections through the simple reservoir model, and this model comes from Eclipse software.

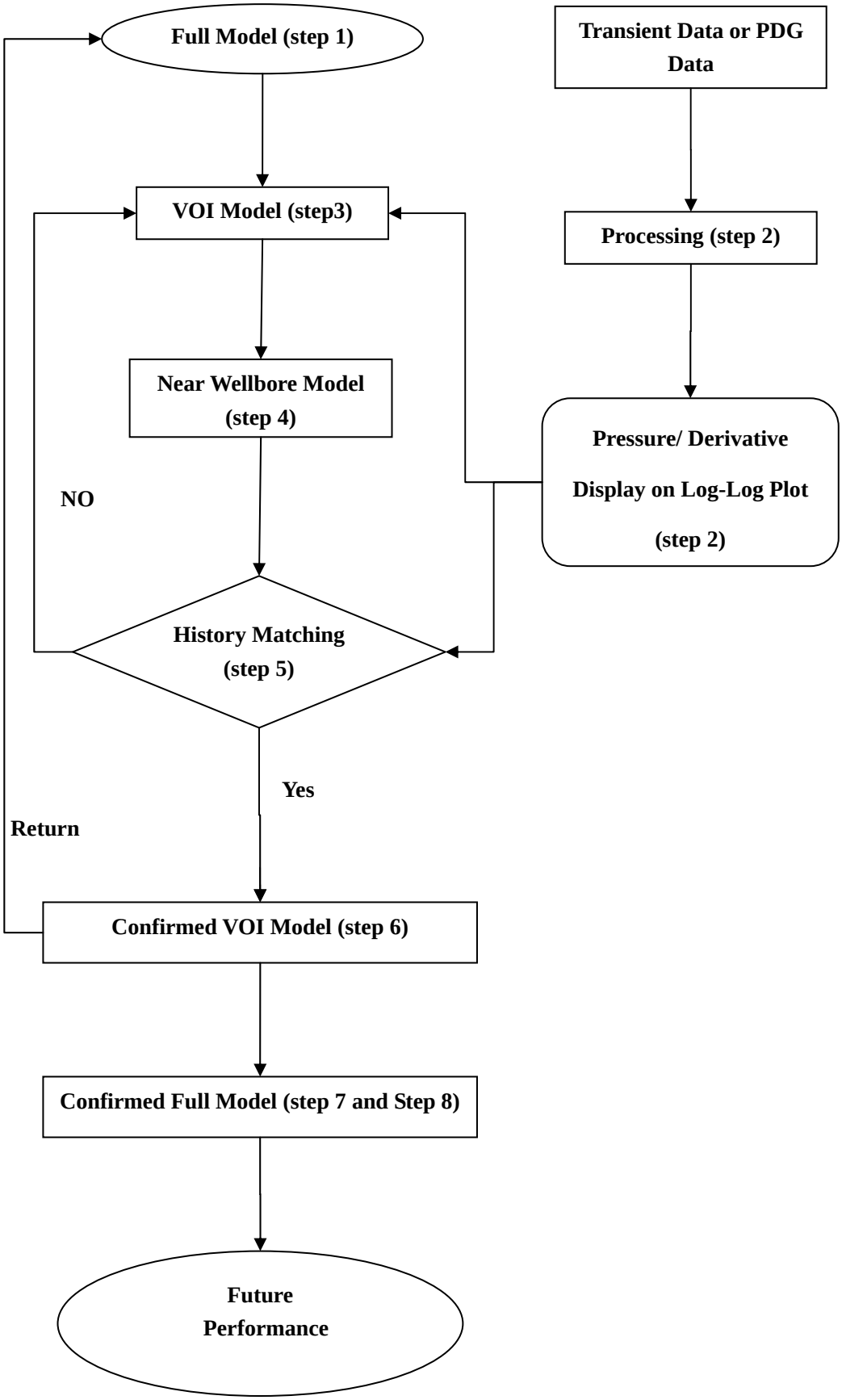

Figure 5.1 New Numerical Well Testing Workflow

5.3.1 History Matching of Full Field Model

Numerical reservoir simulation provides a powerful tool for analyzing the production history of a reservoir and for predicting future performance in mature field management. Experience has shown that an accurate reservoir description is essential to the success of any numerical simulation study and to the development of an effective reservoir plan.

Although the reservoir simulation can take us forward with the best current view of the reservoir, if major features of the reservoir model (e.g. the stock tank oil initially in place, STOIIP) are uncertain, then the forward predictions may be very inaccurate. So for the mature field, the STOIIP will be firstly matched, because this is the reserve basis of any reservoir development and reservoir simulation. In this course, some sensitive parameters (such as formation thickness, porosity, net/gross ratio, etc.) need to be adjusted to match the reservoir reserve. The reserves of individual zones must also coincide with actual value, and the relative error must be as small as possible.

For reservoir pressure, according to the material balance method, using all actual history production data, the measured static pressures for different development periods can be matched until the calculation results from the full field model are acceptable.

Only after finishing the matching of the reserves and the pressure of the reservoir from the macro scale, the reservoir model can be balanced for injection/production and be calibrated further through the numerical well testing approach.

5.3.2 Transient Data or PDG Data Processing and Analysis

This simple reservoir model comes from Eclipse software and is a schematic model, which includes 7 wells (one injection well, four vertical oil wells, two horizontal oil wells). The object of the study is a horizontal well, because this well has PDG test data (**Figure 5.2**). As noted previously in chapter 1, PDG data has extremely high volume,

and it cannot be directly analyzed and be used to match.

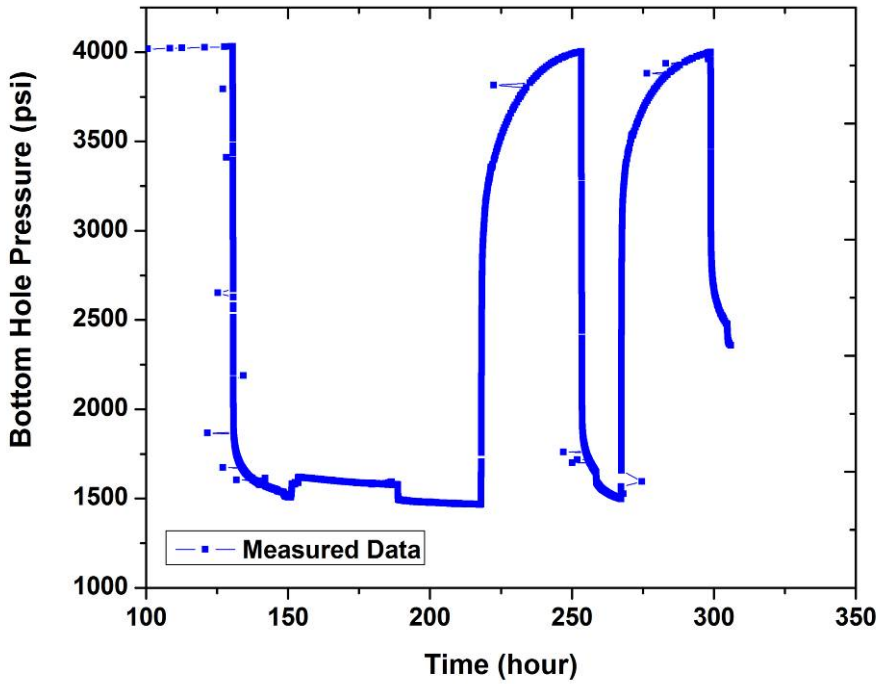

Figure 5.2 The original PDG data

Using the Wavelet method (ToolBox software, developed by the PRIME Group of Institute of Petroleum Engineering of Heriot-Watt University) to process the PDG data, the volume of Data was reduced, and some drawdown tests and buildup tests were identified. (**Figure 5.3**)

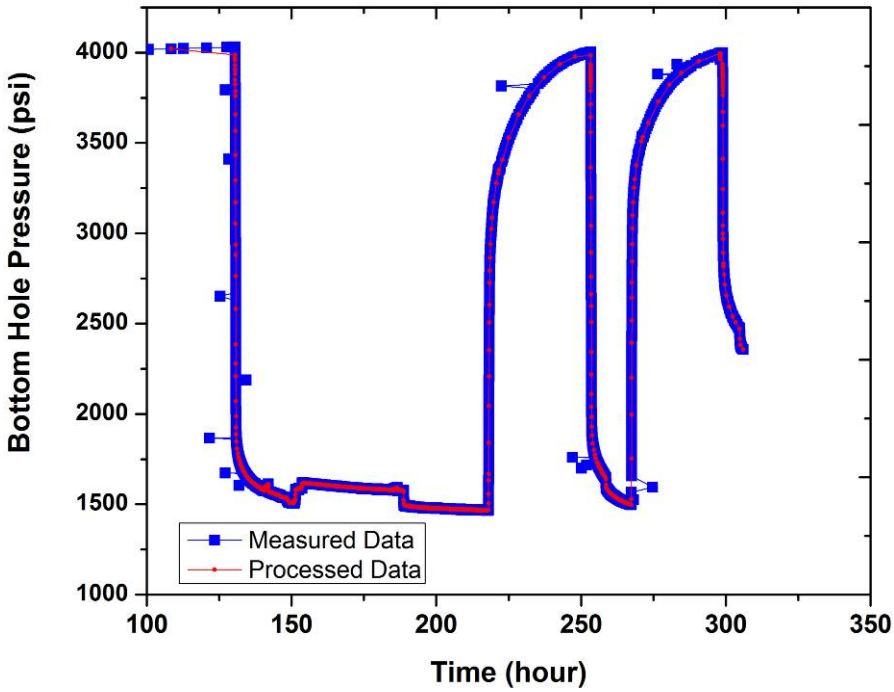

Figure 5.3 Comparison of the original PDG data and the processed data

From processed PDG data, one well test (longest time) was selected to analyze and plot the measured pressure and pressure derivative on a log-log scale (**Figure 5.4**). Then using the investigation radius equation, the radius of influence for the well test can be obtained.

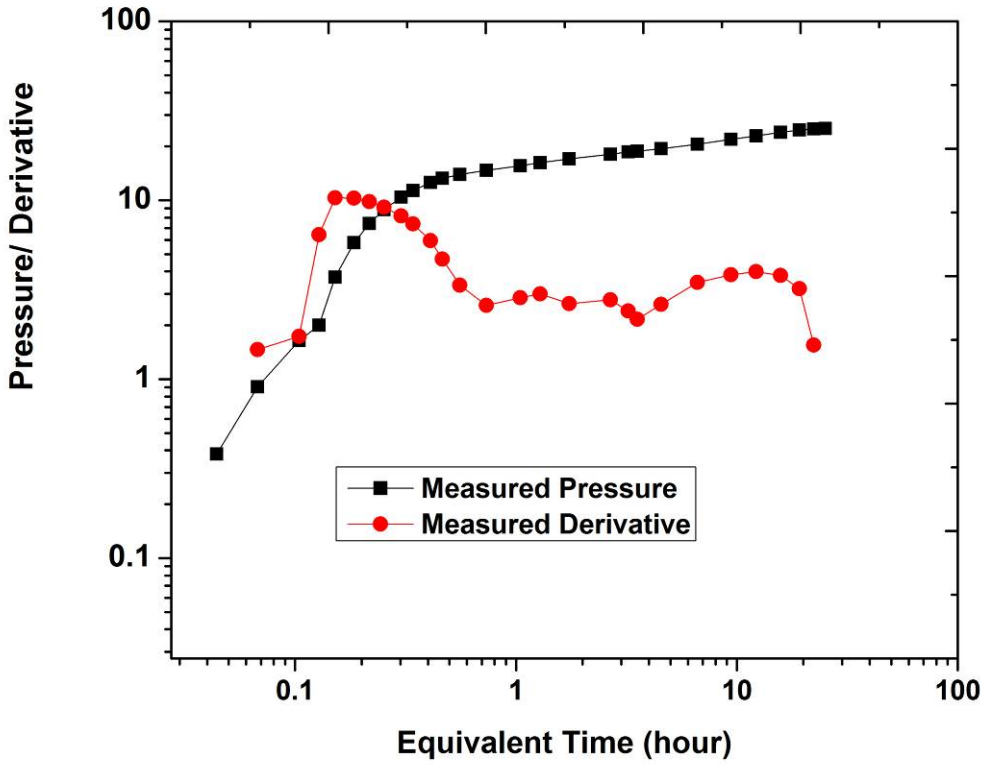

Figure 5.4 The log-log plot of the measured data

5.3.3 Definition of VOI Model

In many mature fields, well test steps are short and the radius of investigation is small, so in order to use well test data to improve history matching, it is not required to run the full field model. Existing commercial simulation software can cut a block or a window or VOI model from the full field model and be used to study numerical well testing problems on a small model or window. But it is difficult to define the size of the block, and the criterion is the investigation radius. From the analysis of processed PDG data, the boundary of influence for the well test can be made known (**Figure 5.5**).

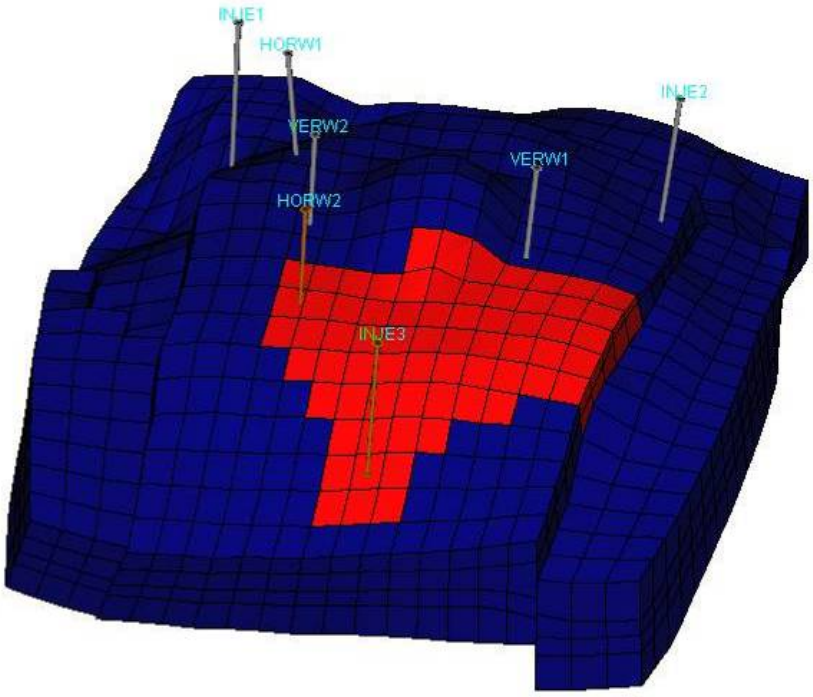

Figure 5.5 A block or a window cut from the full field model

For the boundary conditions of the VOI model, the software provided three types to choose. One is the flux boundary; the second is the flow pressure boundary; the third is the no-flow boundary. Because well test data is dynamical data, it has to be transferred between the VOI grid and the full model grid. So in general, the first or second boundary condition was selected. When the VOI model is activated at some point in time, its grids will be updated from the full field model, and then after deactivating the VOI model, the full field model will be overlapped from the VOI model.

5.3.4 Local Grid and Time-stepping Refinement for VOI Model

The VOI model allows use of the local grid refinement technique and the local time-stepping technique during a simulation run. The VOI grid can be refined using a Cartesian or unstructured grid, if there are some faults or an irregular boundary, the Perpendicular-Bisectional grid will be selected. (**Figure 5.6**)

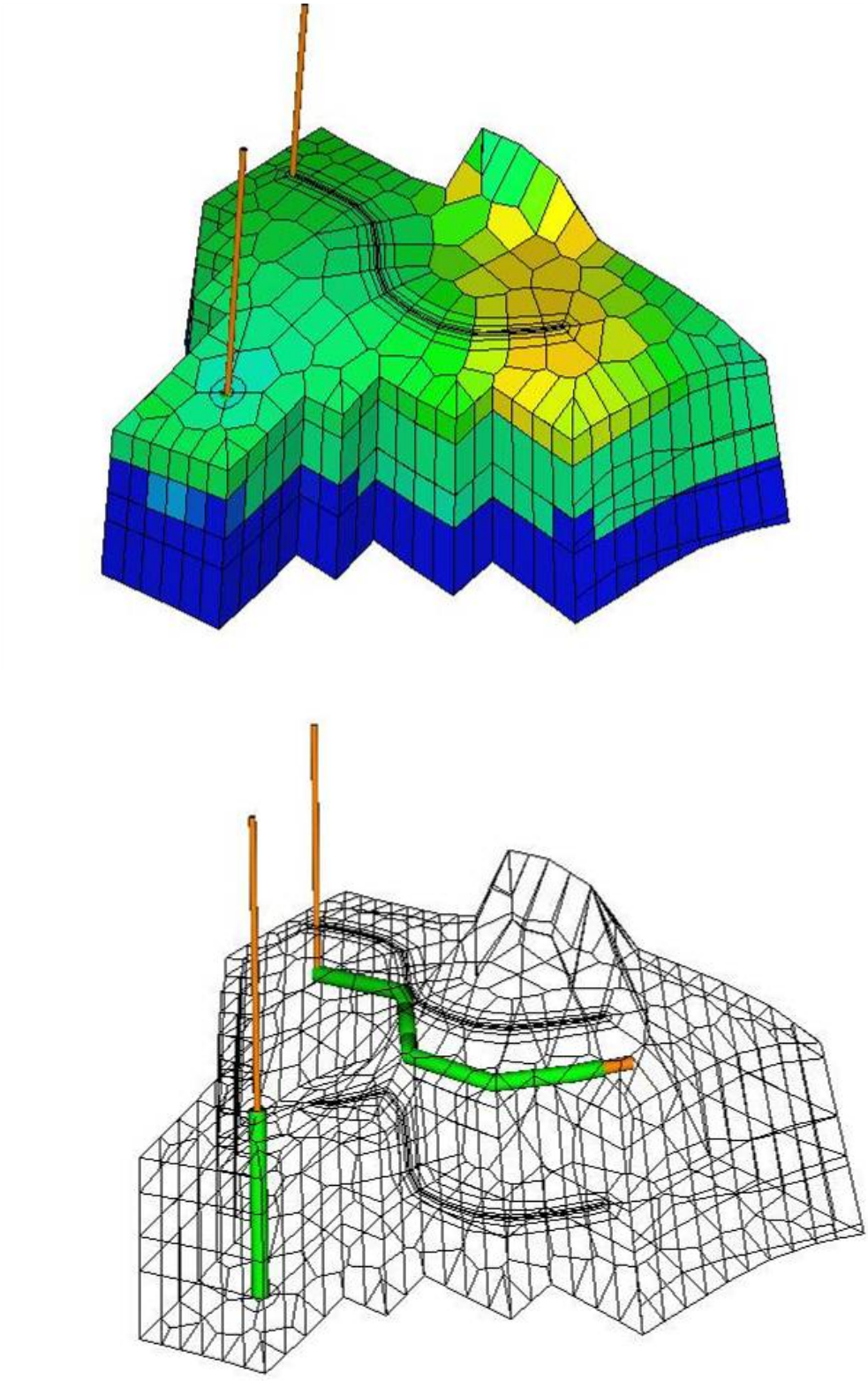

Figure 5.6 The local grid refinement of VOI model

Because this well is a horizontal well and the direction is irregular, the grid cells near the well bore need to be further refined. (**Figure 5.7**)

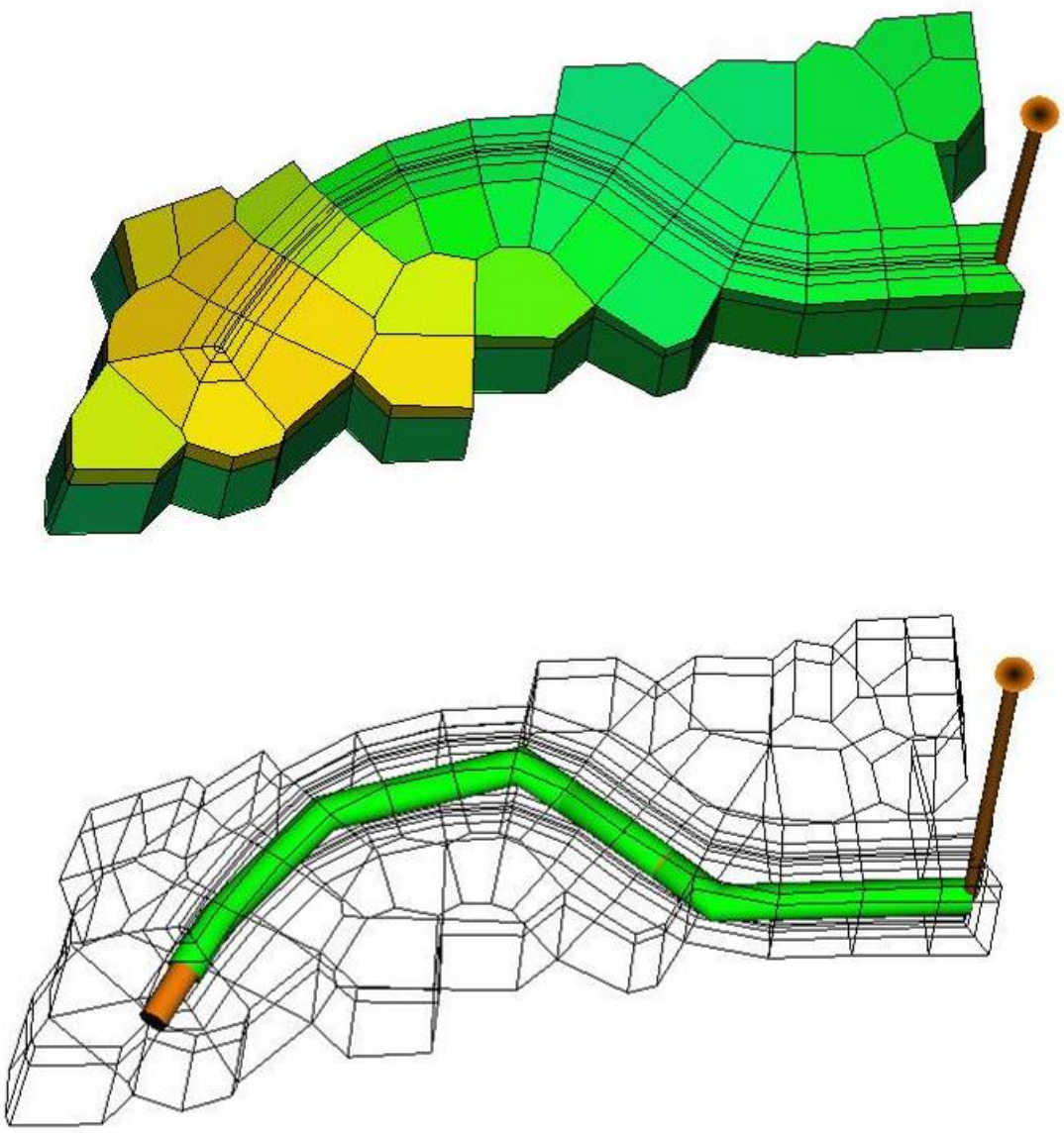

Figure 5.7 The local grid refinement of near well bore model

After finishing the LGR of the VOI model and the near wellbore model, the numerical instabilities can be overcome, and the pressure gradient and saturation gradient of the near well bore area can be controlled at the small scale. But if the time steps at the beginning of the simulation are not refined, the convergence problems are also likely to occur, so the local time-stepping for each VOI model is very important.

5.3.5 Adjusting of Properties Geological Model and Fluid Model

To match the well test data, two methods were used to adjust the property distribution in the VOI model. One is to modify the permeability distribution, which can be adjusted in three directions. The second is to define another fluid model in the VOI model, which includes the PVT data and the relative permeability curve. Comparing with the full field model, this step is very important under multiphase flow conditions. Because the multiphase effect has a big influence on bottom hole flowing pressure, the accuracy of history matching can be improved through modifying the PVT properties of the VOI model or defining another effective permeability curve in the VOI model,. If required, each well in the influence area can be provided with an effective permeability curve respectively. As a result, the latter method is more important in a mature field.

Through adjusting the properties of the VOI model by the above two methods, and only running the VOI model, the results after history matching to the well test data will be obtained in the Cartesian plot and the log-log plot. (**Figure 5.8, Figure 5.9**)

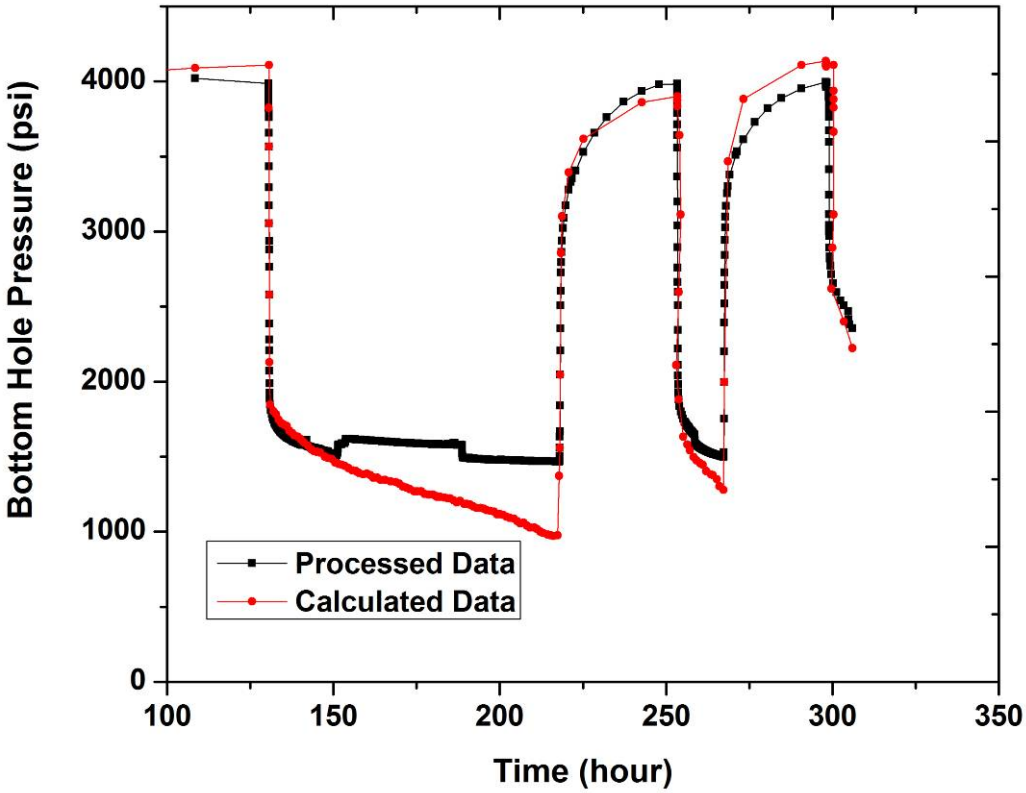

Figure 5.8 History matching of PDG data in a Cartesian plot

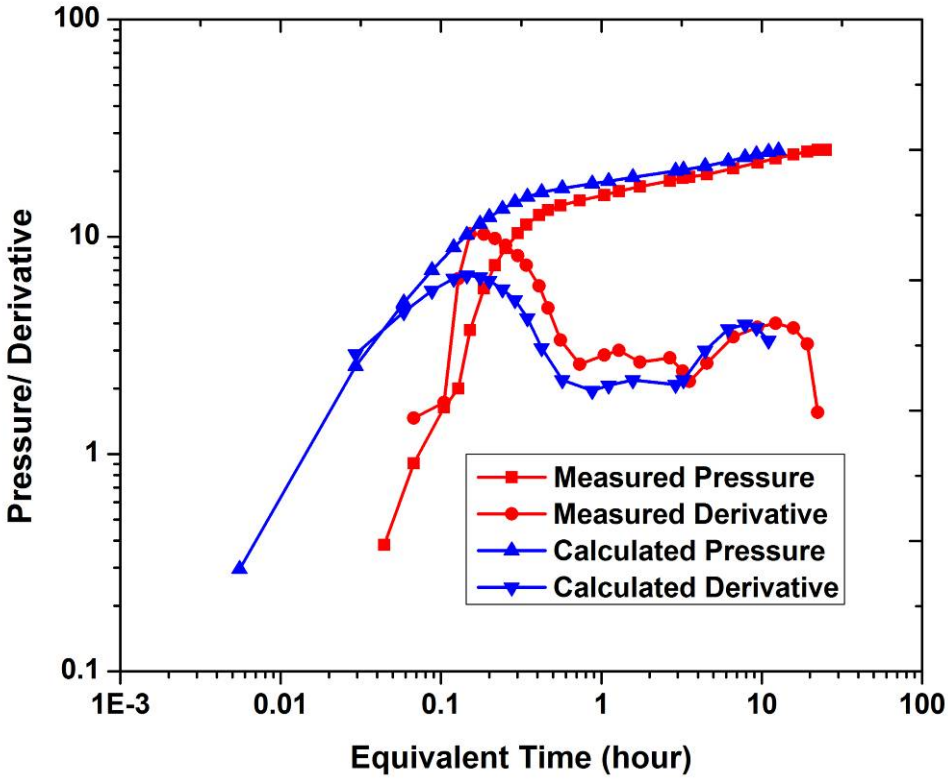

Figure 5.9 History matching of buildup (the last of PDG) pressure in a log-log plot

5.3.6 Validation of VOI Model

After finishing the history matching of well test data, the VOI model needs to be validated. In this step, running the full field model, through further modifying the properties of the VOI model, upscaling the time-stepping refinement to the original time steps, all production data of all the wells in VOI model, including the test wells, can be matched. If the results of matching are acceptable, the VOI model may be put back into the full field model.

5.3.7 Validation of Full Model

After the VOI model has been returned to the full field model, another VOI model can be defined, repeating the previous procedure. When all VOI models are put back into the full field model, the full field model is run, matching all available production history of all wells in the reservoir, until satisfactory results are obtained. This precise updated model is the foundation of reservoir performance prediction and corresponding adjustments and development plans.

5.4 Chapter Conclusion

The conventional numerical well testing procedure, which can be carried out in commercial well testing software, are appropriate for problems of complicated geology under single phase flow conditions. But the multiphase flow effect cannot be interpreted using this approach. During the development of a new improved method, several conclusions were obtained, as follows:

- The windowing and local grid refinement and local time-stepping techniques can be carried out through existing commercial reservoir simulation software. This can improve the CPU time and the accuracy of history matching.

- Under multiphase flow conditions, numerical solutions can be used to model field bottom-hole flowing pressure. Numerical models can consider the capillary pressure effect, the gravity effect, effective permeability, complex geology, etc.

- The new numerical well testing workflow presents a practical process for using well test data or PDG data to update the reservoir model. In this case, through matching the well test data in the Cartesian plot and the log-log plot, the VOI model or the window can be calibrated. Especially under multiphase flow conditions, the modification of the fluid model and effective permeability model is very important, due to the high influence of the multiphase effect for bottom hole flowing pressure.

- The new multiphase flow numerical well testing procedure can provide a systematic, practicable and integrated approach to improve the quality of reservoir description through combining all the available data (such as geology data, geophysics data, well test data, PDG data, dynamical data, production history, etc.). According to this new workflow process, the ultimate objective of a well test – dynamic monitoring, continuous model calibration and real time reservoir management can be achieved. (**Figure 5.10**)

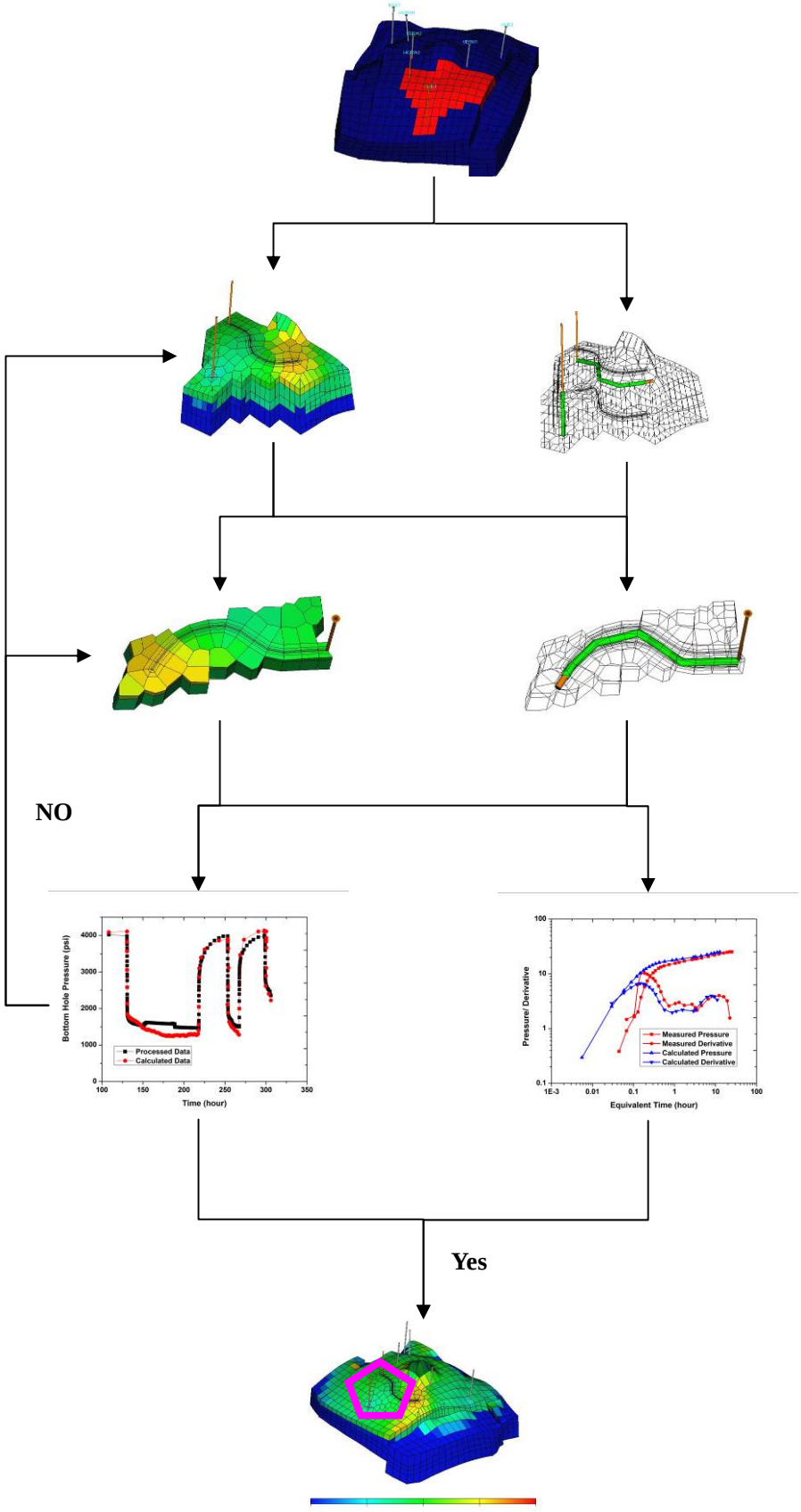

Figure 5.10 Illustration of the workflow of the numerical well test approach

Chapter 6
Field Application

6.1 Introduction

Evaluating mature fields is significantly more challenging than studying with synthetic models. Although the aim of reservoir engineering is to predict performance from real reservoirs, it is very difficult to reduce the uncertainty of a real model and to update it in real time. Hence two real field cases have been chosen to test the applicability of a new numerical well testing approach to mature field models.

This chapter brings together the developments of chapters 2-5 to carry out reservoir model calibrating in real time through multiphase flow well test data or PDG data. The first example is a layered commingled reservoir, which has been developed over ten years through water injection. In order to further improve the recovery factor, an adjustment plan will be conducted. But the basis for the plan is the detailed evaluation of production situations, such as water cut (both field and individual wells), recovery factor and the distribution of remaining reserves (both field and each layer), and these understandings depend on a precise reservoir model. This example will represent in detail the procedure for updating the reservoir model, using the available data through history matching. For this particular process the challenge is to how to use transient pressure or PDG data as inputs for reservoir simulation, in order to improve the quality of the reservoir model.

The second example is a special mature field. The geological properties are good, with 1~2D of permeability and 33% of mean porosity. But the oil property is relatively poor, with 1.5~150cp of viscosity, in a horizontal direction, and the fluid has serious heterogeneity. In this situation, there is a major influence on bottom hole flowing pressure due to this heterogeneity, and yields abnormal bottom-hole pressures. It is also a challenge to how to use this abnormal well test data to improve the accuracy of history matching.

This chapter provides two successful cases through new multiphase flow numerical well testing to update the reservoir model and fulfill dynamic management in mature fields.

6.2 Example 1

6.2.1 Field Overview

This field is operated and owned by CNOOC, located in the Bohai bay basin in the North-East of China. The field is an anticline structural reservoir, and its area is 11.15 km2. The geological reserves (STOIIP) are $118.24\times10^{6}m^{3}$.

The depth of the reservoir is 1175~ 1605 m. The field consists of three main producing reservoir units, named units A, B and C, which are further subdivided into 14 layers due to the distribution of a number of interbedded mudstones, which indicates that there is serious heterogeneity in both vertical and horizontal directions. The geological report quotes sand porosities of between 28%-35% (average value about 31%), with permeabilities of 100-10000 mD (average value about 2000mD). These figures indicate that the formation is of good quality. The oil property is relatively poor, with 23.5~452cp of viscosity.

This field commenced production through a"reverse nine spot pattern" water injection in 1993. Up to 2008, the field has produced more than $18.27\times10^{6}m^{3}$, and the field water cut has reached 69.8%. Because of the influence of interlayer heterogeneity, the

crossflow effect between layers through wellbore has become very severe. In this situation, the development condition has started to worsen, the production rate decreased quickly, while the water cut increased rapidly. In order to control and maintain production rates, some infill wells will be drilled. Before fulfilling these infill wells, a detailed evaluation of the production situation (such as the distribution of remaining oil, the interference degree of between-layers, etc.) must be understood. But such information relies on a precise reservoir model, which requires dynamical data to update it.

6.2.2 Reservoir Model and Data description

Presently, there are two ways to set up a reservoir model: the deterministic model or the stochastic model. A deterministic model is where parameters of known control points (mainly well point) are used to predict the sole correct reservoir parameters of the unknown zones. This method is suitable for simple reservoir structures. However, for a complex reservoir with the incomplete information, it is difficult to obtain the deterministic and correct reservoir parameters under any scale. In fact, this method has rarely been used to build up a reservoir model. As a result, people widely use the stochastic approach to carry out reservoir models.

As regards the special geological conditions of this oil field, software for stochastic reservoir modelling was selected. During the process of modelling, according to the sediment environment of the sandstone, sedimentary facies were simplified to sand and mud. With reference to stochastic function theory, and based on present geological knowledge, logging data, well information, and seismic data, the stochastic modelling method was adapted to generate a selective and equiprobable reservoir model. Through the processes of comparison and selection for each model, the best stochastic model will be upscaled and developed into a reservoir model.

In the upscaling process, according to the actual geological conditions of this region, (such as the shape of reservoir, the direction of faults, the thickness of each layer, well

spacing density, etc.) the model grid was designed as 75×117×56 with cell size about 50 m. There are 37 sandstone layers and 19 mudstone layers (**Figure 6.1**). The total numbers of grid nodes are 491400. The distribution of properties (such as porosities, permeabilities, thickness, etc.) is heterogeneous.

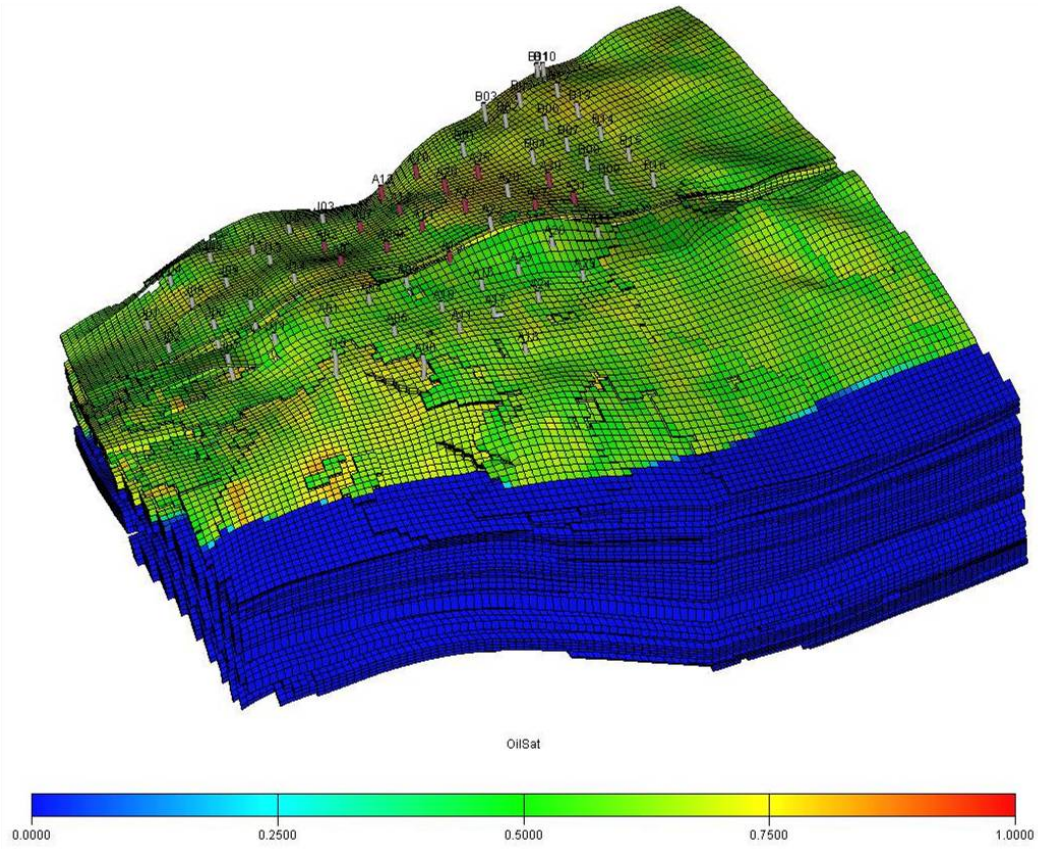

Figure 6.1 The construction of 3D Model

6.2.3 PDG processing

For this mature field, there are three new infill wells (well E30、well E31、well E32). Near these new infill wells, the well B18 has PDG data, as shown in **Figure 6.2**, **Figure 6.3** and **Figure 6.4**. This data contains six days of PDG pressure data and records 160000 points. The interval between two points is 3 seconds. In order to evaluate the production situation of these new infill wells, the PDG data was used to update the reservoir model through the new multiphase flow numerical well testing procedure. In order to conveniently interpret and apply the results, the original data was processed from 160000 points to 10000 points by the wavelet transform approach (ToolBox software, developed by the PRIME Group of Institute of Petroleum Engineering of Heriot-Watt University).

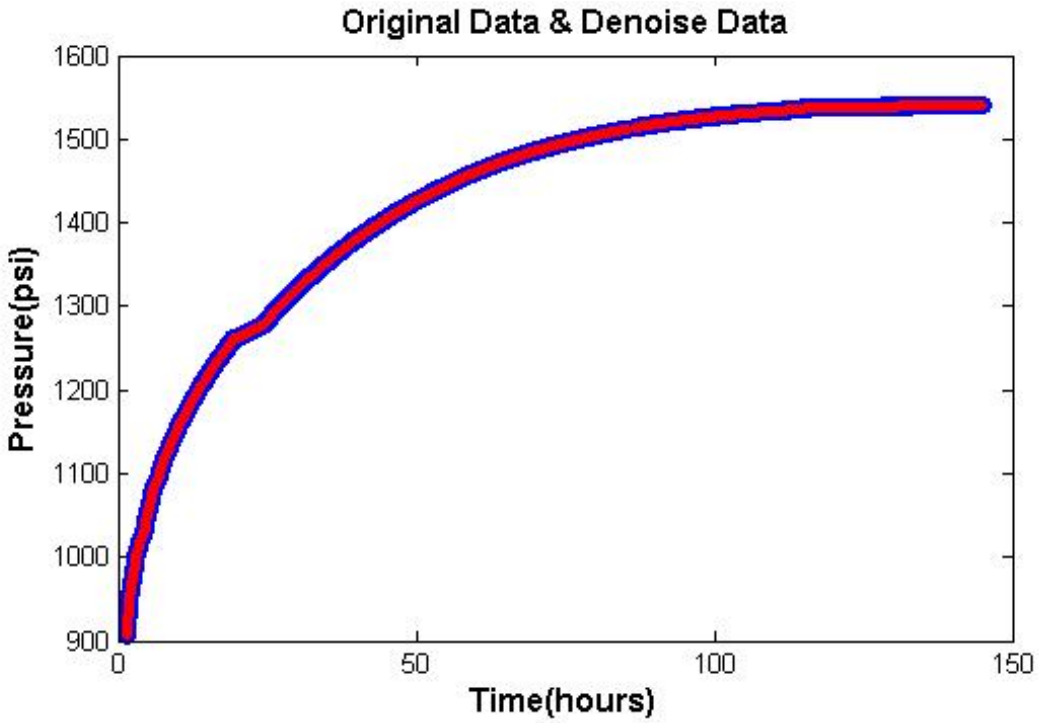

Figure 6.2 Original well testing data for well B18

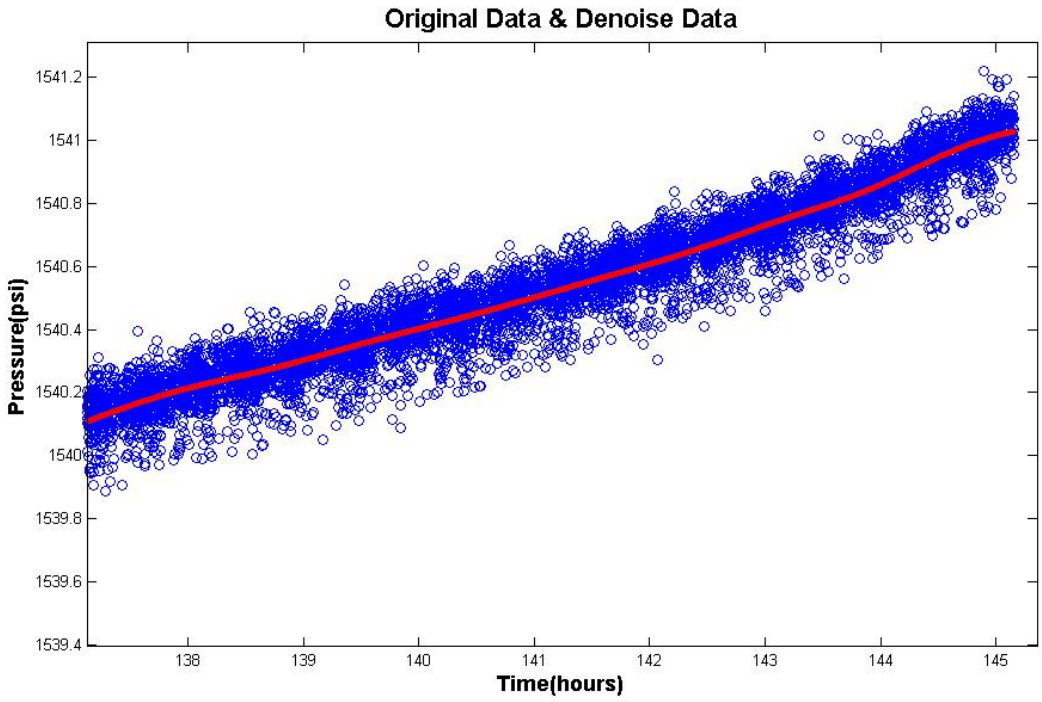

Figure 6.3 Zoom-in of original well testing data in late time for well B18

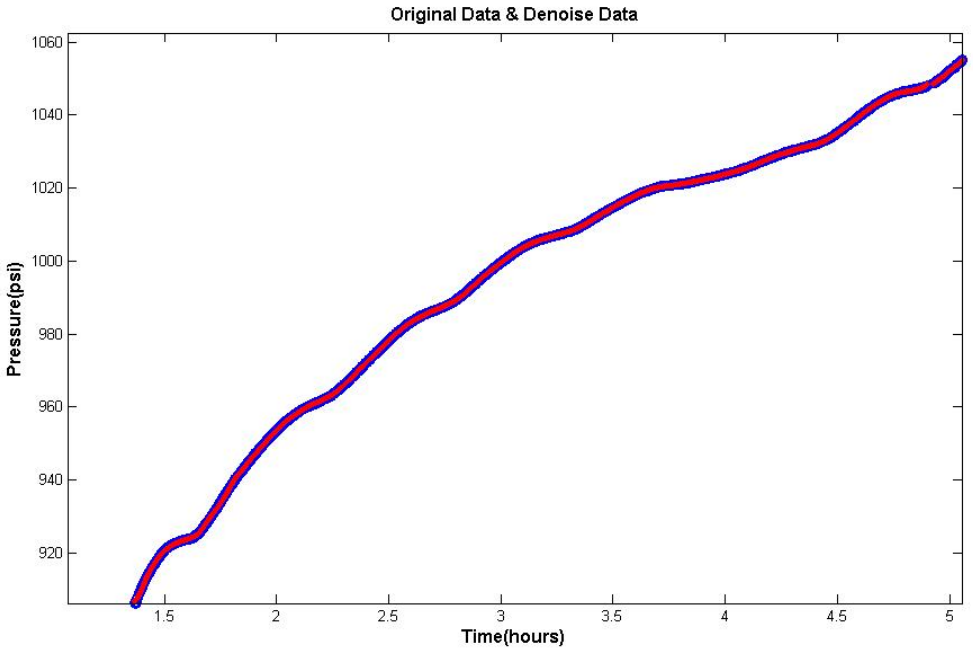

Figure 6.4 Zoom-in of original well testing data in early time for well B18

According to the processed well testing data, the log-log plot can be obtained. **Figure 6.5** shows that the pressure derivative has a concave down in early time due to the interlayer cross flow. In middle time, the pressure derivative starts to go up due to the variation of the total mobility, and in late time, the pressure derivative goes down quickly due to the pressure reaching a constant pressure boundary or closed system.

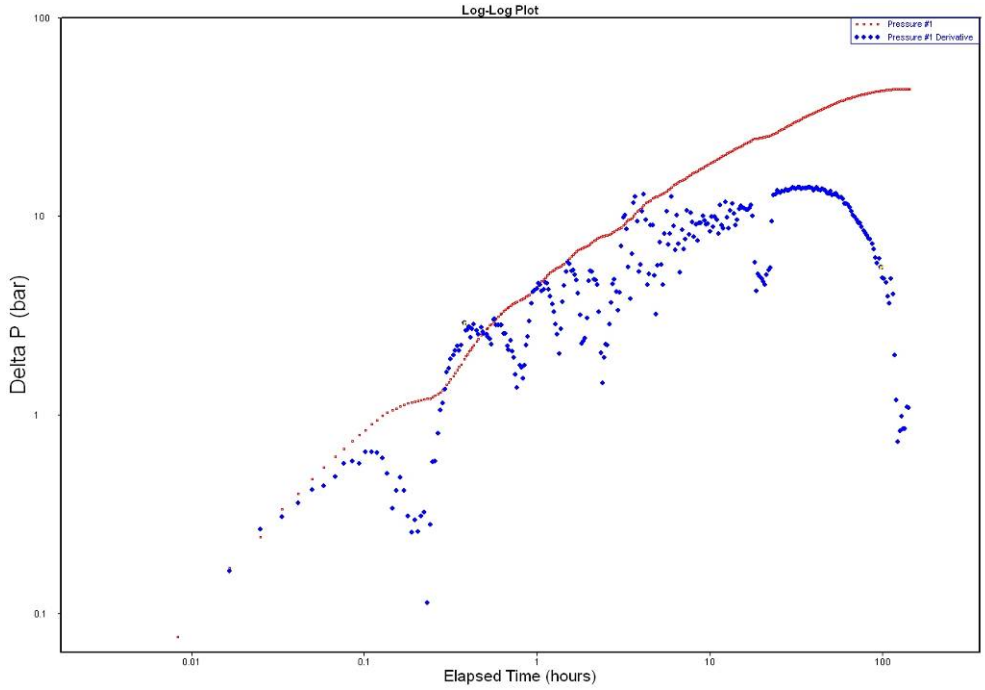

Figure 6.5 The log-log plot of BU for well B18

At the same time, according to the equation of investigation radius ($R_{inv} = 0.033\sqrt{\frac{kt}{\phi\mu c_t}}$), the influence area for the well test can be obtained. This parameter is the foundation for numerical well testing.

6.2.4 History matching

Before the numerical well testing process is carried out, the reservoir model needs to match the production history of the full field and the reserves of each layer. Only by completing this step can the material balance be ensured from macro scale. The matching error is as small as possible.

Figure 6.6, Figure 6.7 and Figure 6.8 are the history matching results for field production. **Table 6.1** is the history matching results for each layer reserve.

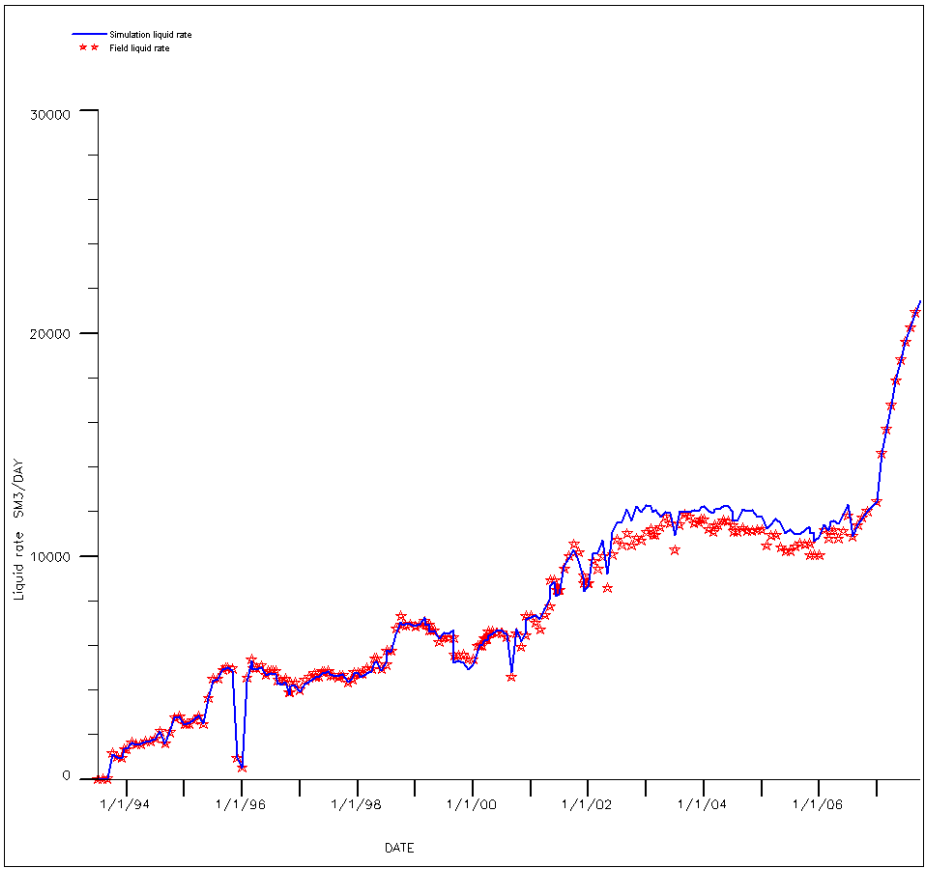

Figure 6.6 Total liquid rate curve of full field

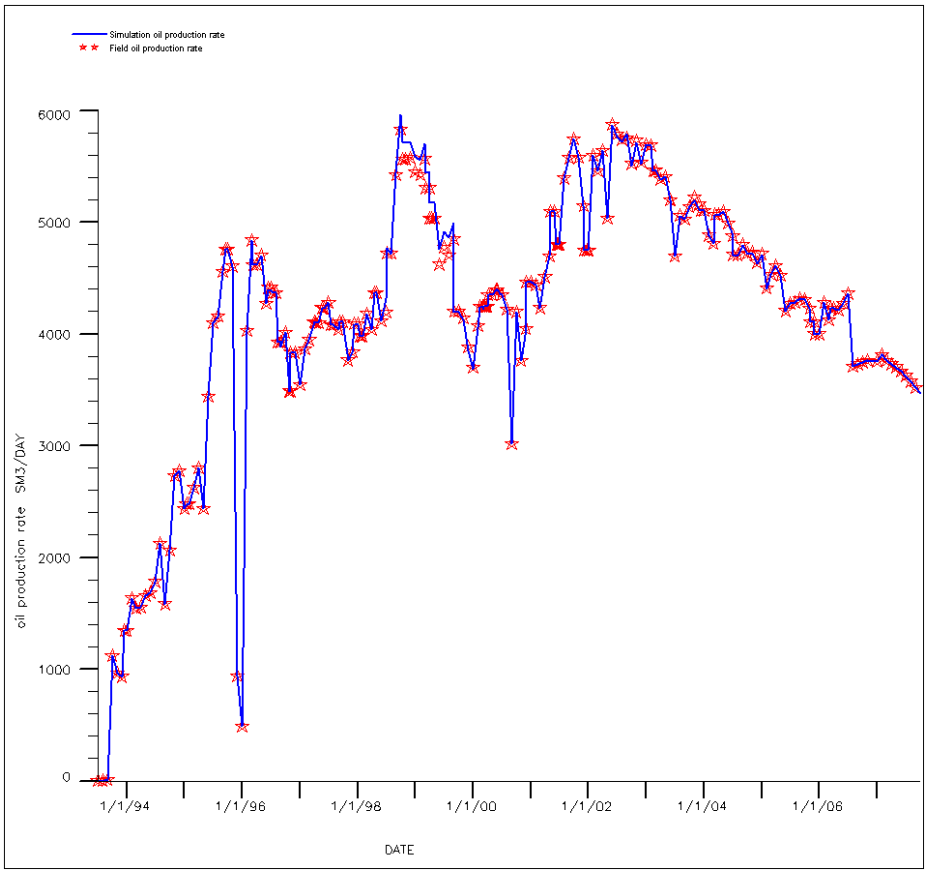

Figure 6.7 Total oil rate curve of full field

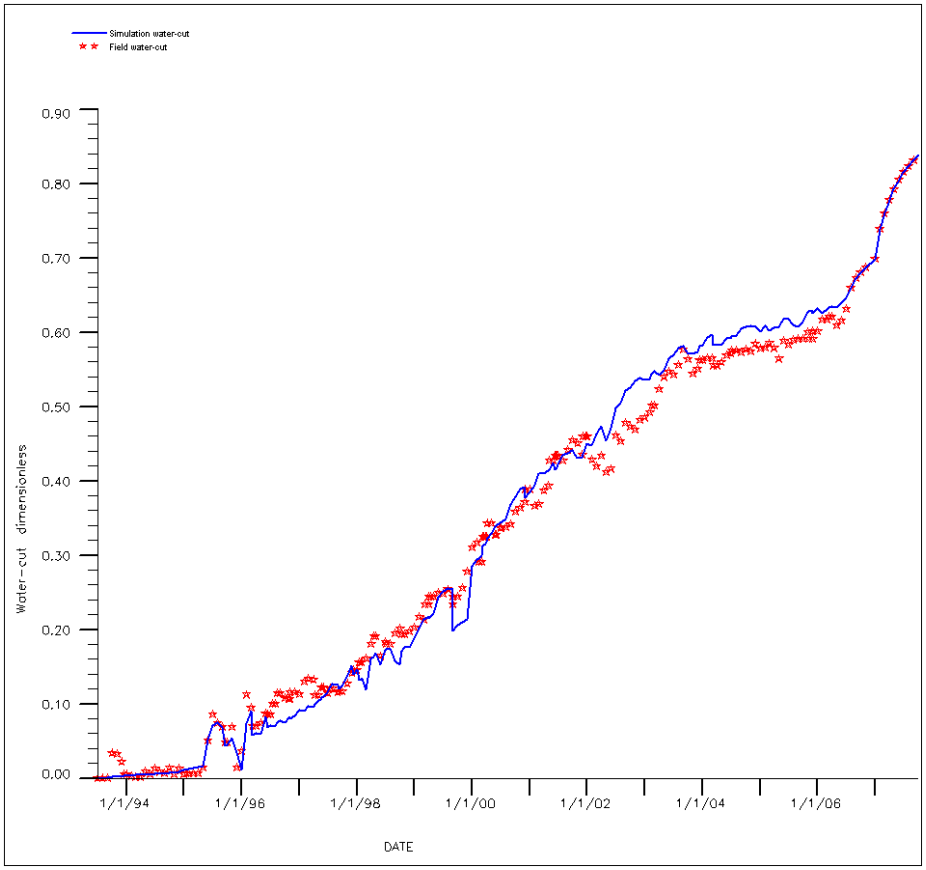

Figure 6.8 Total water cut curve of full field

Table 6.1 The matching results for each layer reserve

Unit	Zone No.	STOIIP (10^4m^3)	Calculated value (10^4m^3)	Absolute Error (10^4m^3)	Relative Error (%)
A	1	894.31	889.24	-5.07	0.57
	2	579.13	589.4	10.27	1.77
	3	1386.93	1398.57	11.64	0.84
	subtotal	2860.37	2877.21	16.84	0.59
B	4	2292.47	2328.35	35.88	1.57
	5	960.58	961.35	0.77	0.08
	6	1558.2	1557.24	-0.96	0.06
	7	1460.98	1398.74	-62.24	4.26
	8	160.38	175.04	14.66	9.14
	subtotal	6432.61	6420.72	-11.89	0.18
C	9	527.5	530.61	3.11	0.59
	10	398.2	403.99	5.79	1.45
	11	1026.28	1026.42	0.14	0.01
	12	345.08	351.09	6.01	1.74
	13	180.85	180.69	-0.16	0.09
	14	33.1	34.05	0.95	2.87
	subtotal	2511.01	2526.85	15.84	0.63
Total		**11824**	**11824.78**	**0.78**	**0.01**

6.2.5 Numerical Well Testing

According to the new multiphase flow numerical well testing procedure in chapter 5, the numerical well testing workflow is as follows (**Figure 6.9**):

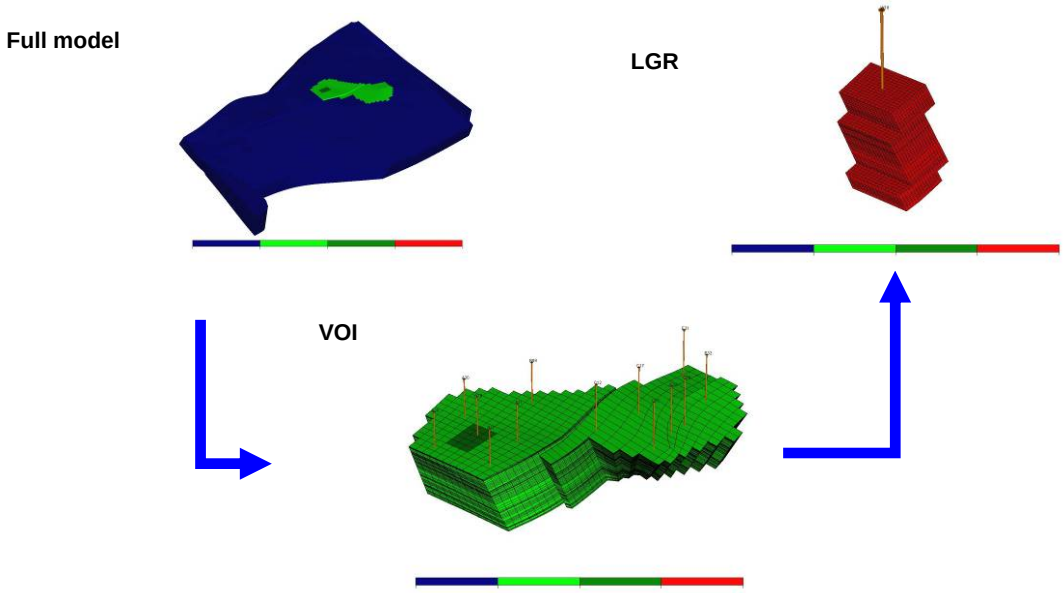

Figure 6.9 Illustrations the workflow of numerical well testing approach

As shown in **Figure 6.9**, the VOI model was cut from the full model, which includes thirteen wells (A26、A27、A30、A31、B09、B18、C12、C13、C17、C18、E30、E31、E32). Well C17 is an injection well; well E30, well E31 and well E32 are infill wells in the late development phase. In order to match the well testing data of well B18, near well bore grid cells are refined. At the same time, the timestepping technique will be used.

The well testing data of well B18 can be matched in the Cartesian plot and pressure derivative in the log-log plot through adjusting the properties of the VOI model. **Figure 6.10** and **Figure 6.11** are history matching results. During the matching process, besides modifying the geological properties of the VOI model, the fluid model can also be independently defined in the VOI model, which includes PVT data and relative permeability data. If only adjusting the properties of geological model, the effect of history matching is not good, but further calibrating the properties of fluid, the history matching of well test data can readily achieve good results.

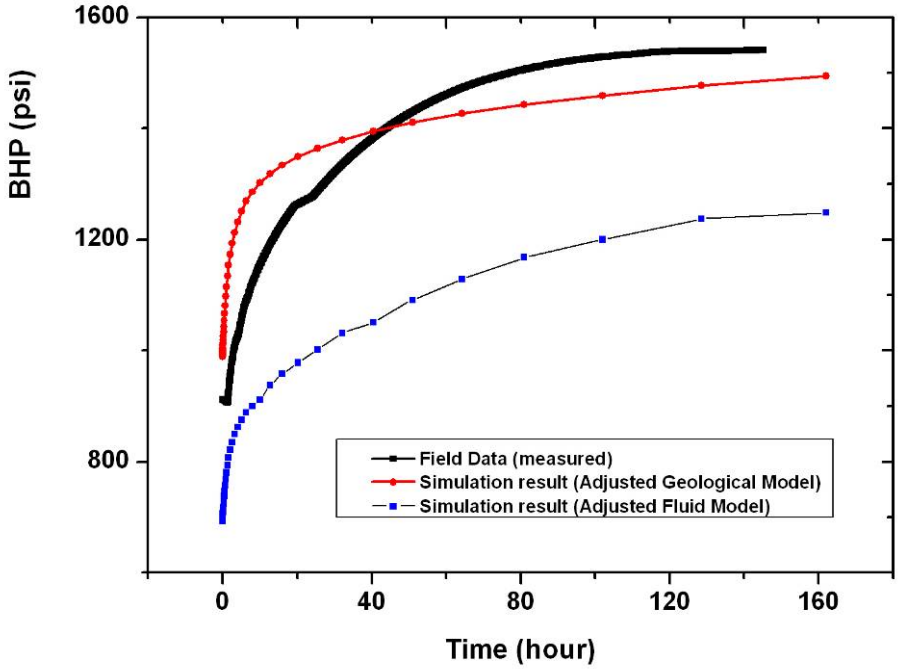

Figure 6.10 The BHP matching curve of well B18

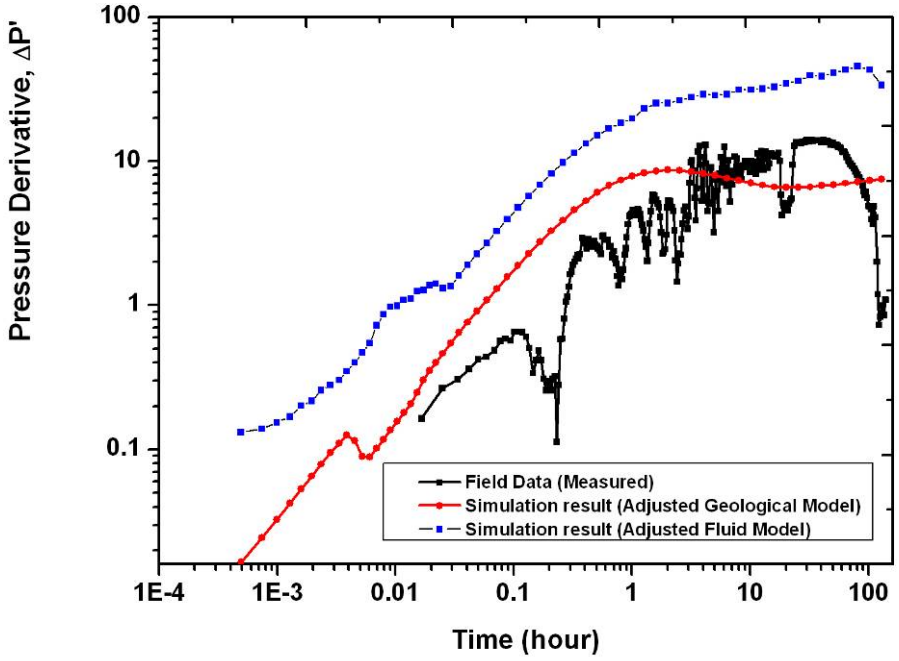

Figure 6.11 The pressure derivative matching curve of well B18

After finishing the history matching of the well test, the VOI model needs to be verified. In this step, by running the full field model, and further adjusting the properties of the VOI model (such as geological parameters, PVT data, relative permeability curve, etc), all history production data of all wells in the VOI model are matched. The results are as follows (**Figure 6.12—Figure 6.27**). Through the history matching of transient data by the numerical well testing approach and validation by the history matching of

production data of all wells in VOI model, the confirmed VOI model can be returned to the full model, and the full model will be updated in real time and used to forecast future performance.

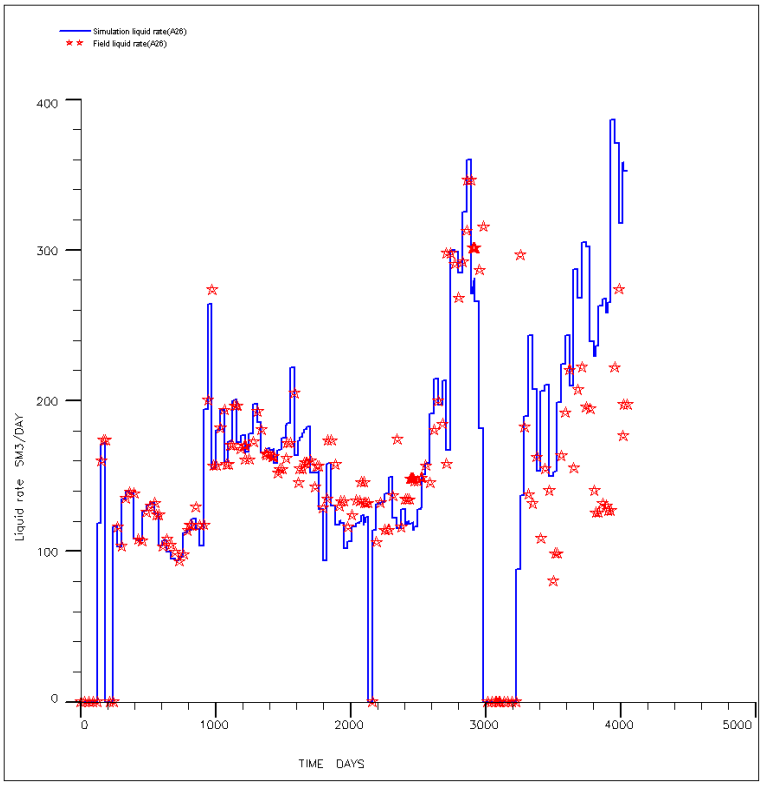

Figure 6.12 Total liquid rate curve of well A26

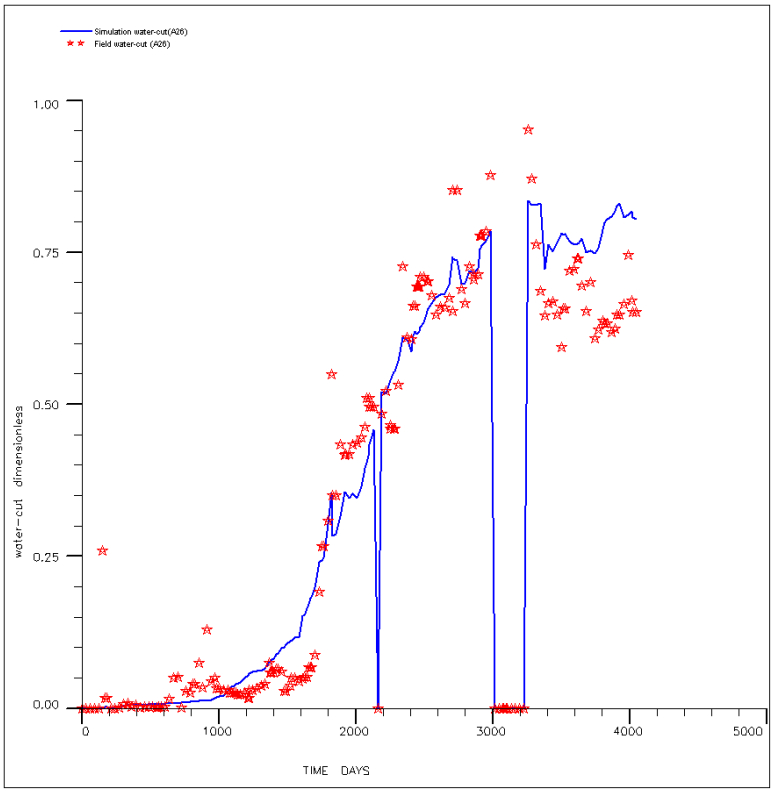

Figure 6.13 Water-cut curve of well A26

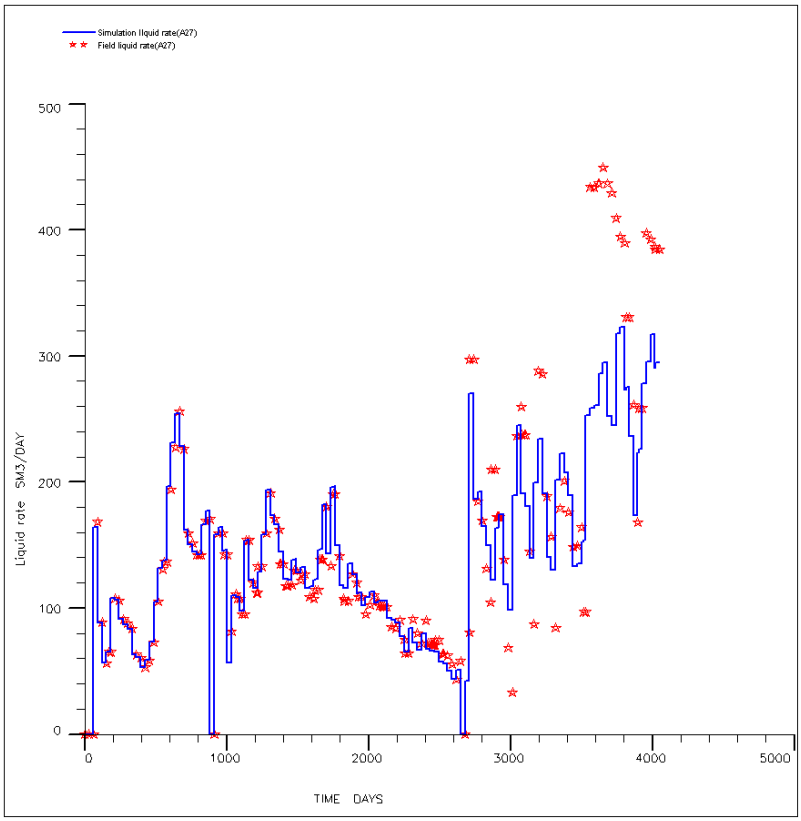

Figure 6.14 Total liquid rate curve of well A27

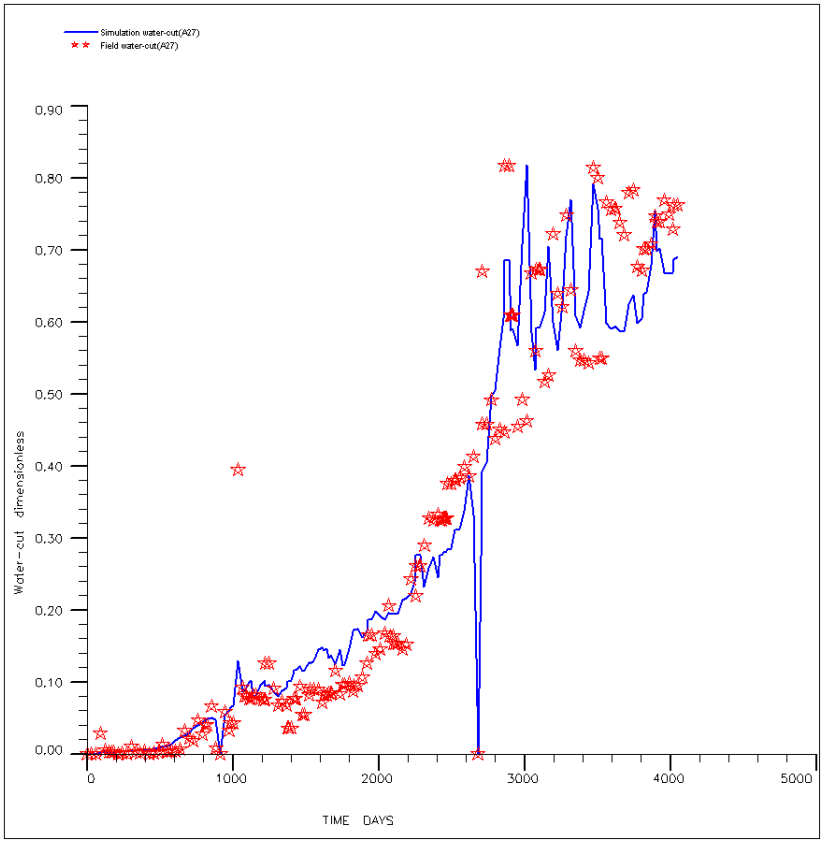

Figure 6.15 Water-cut curve of well A27

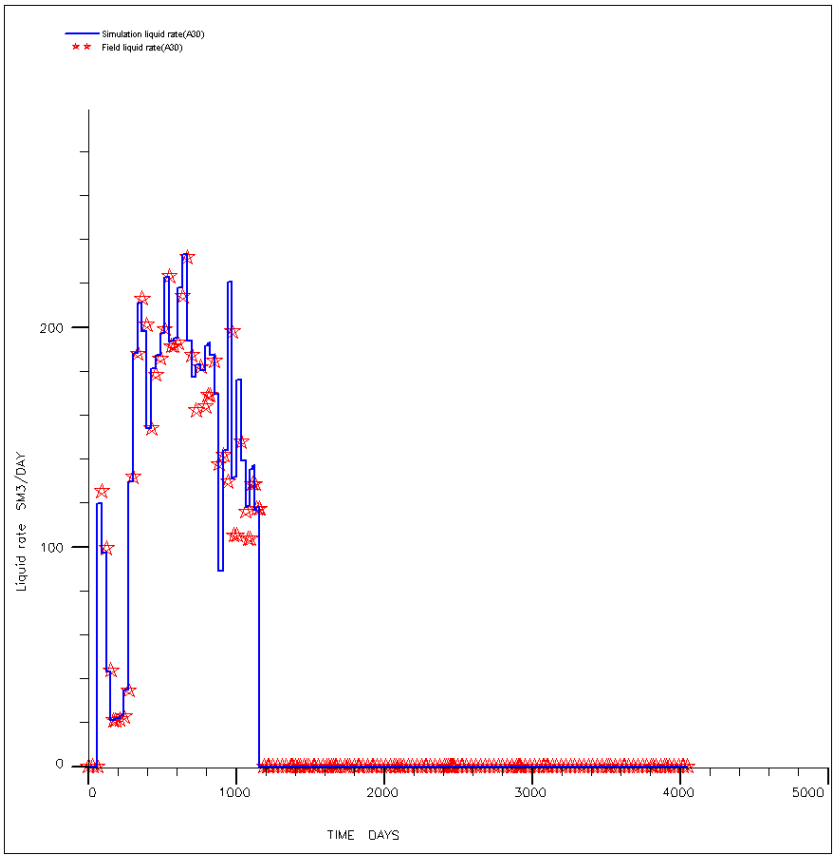

Figure 6.16 Total liquid rate curve of well A30

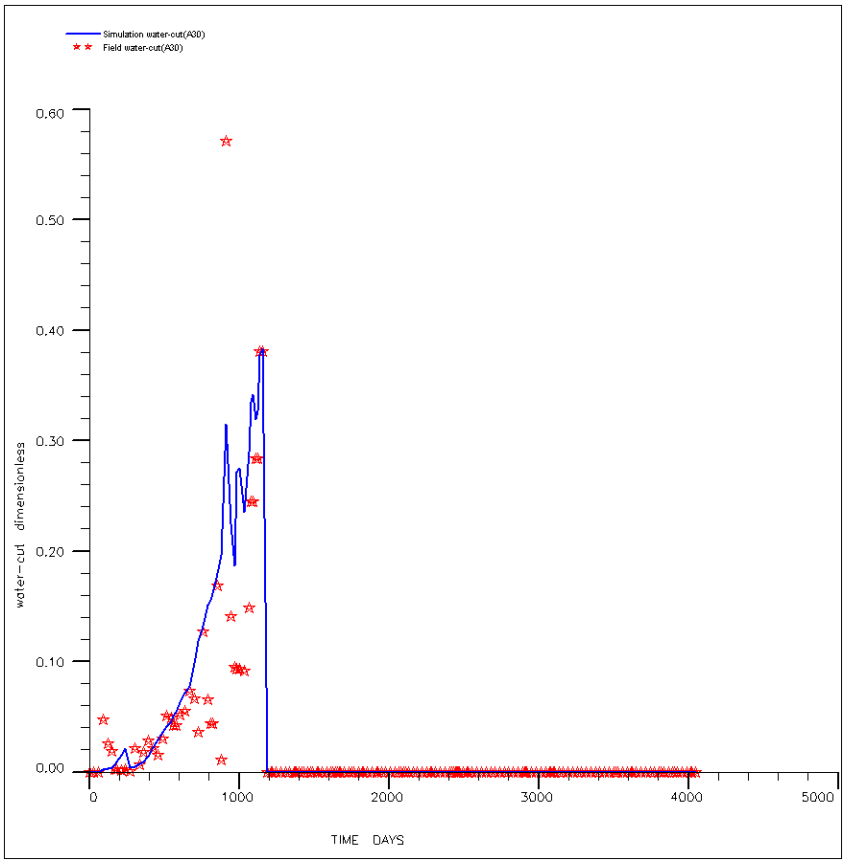

Figure 6.17 Water-cut curve of well A30

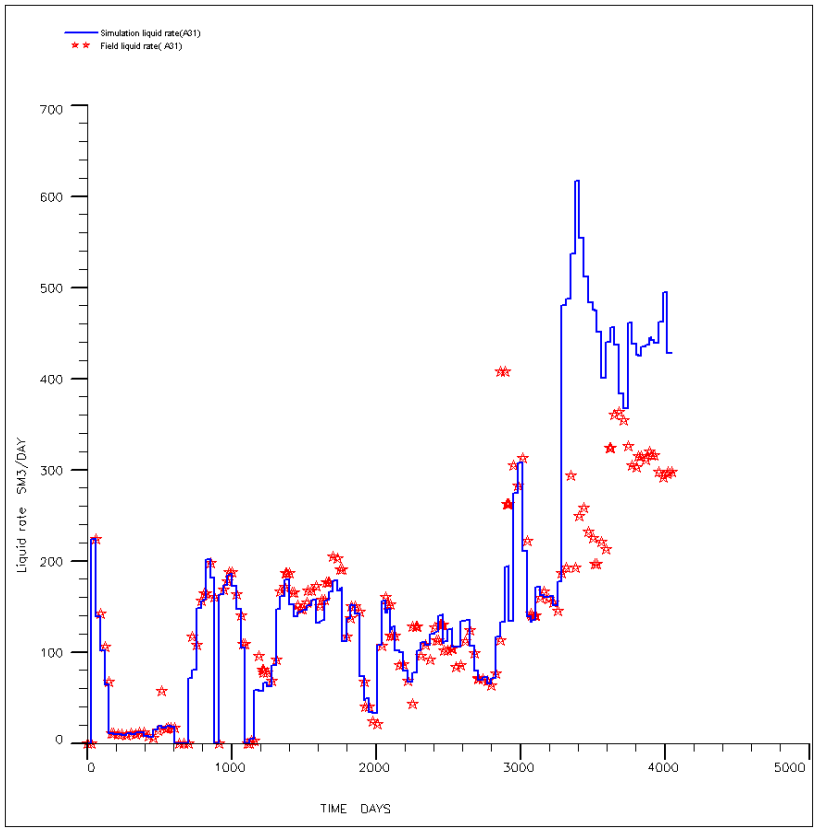

Figure 6.18 Total liquid rate curve of well A31

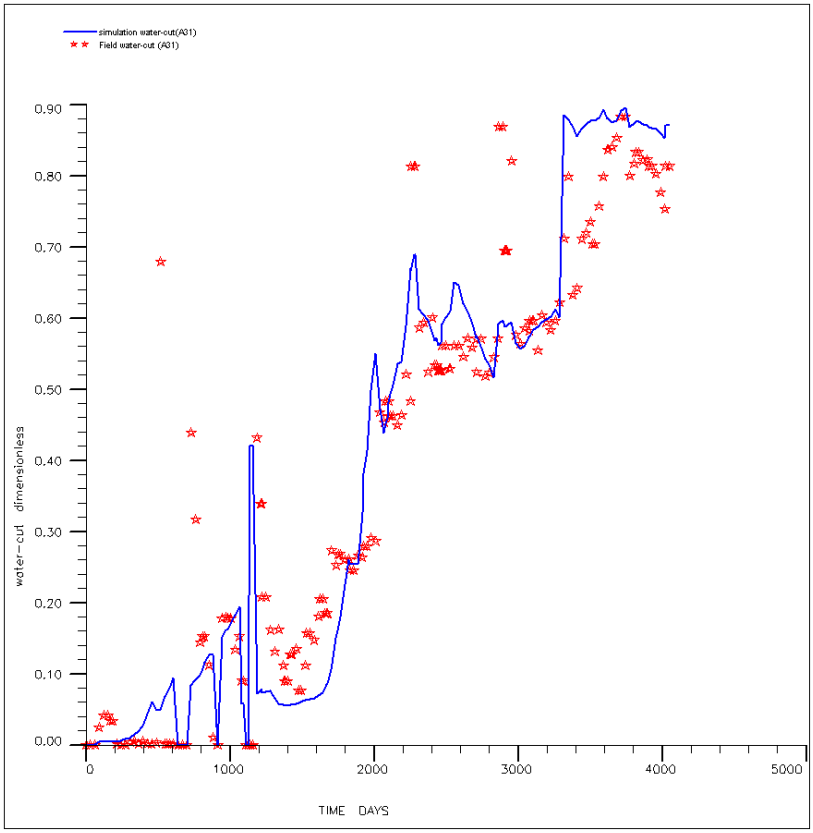

Figure 6.19 Water-cut curve of well A31

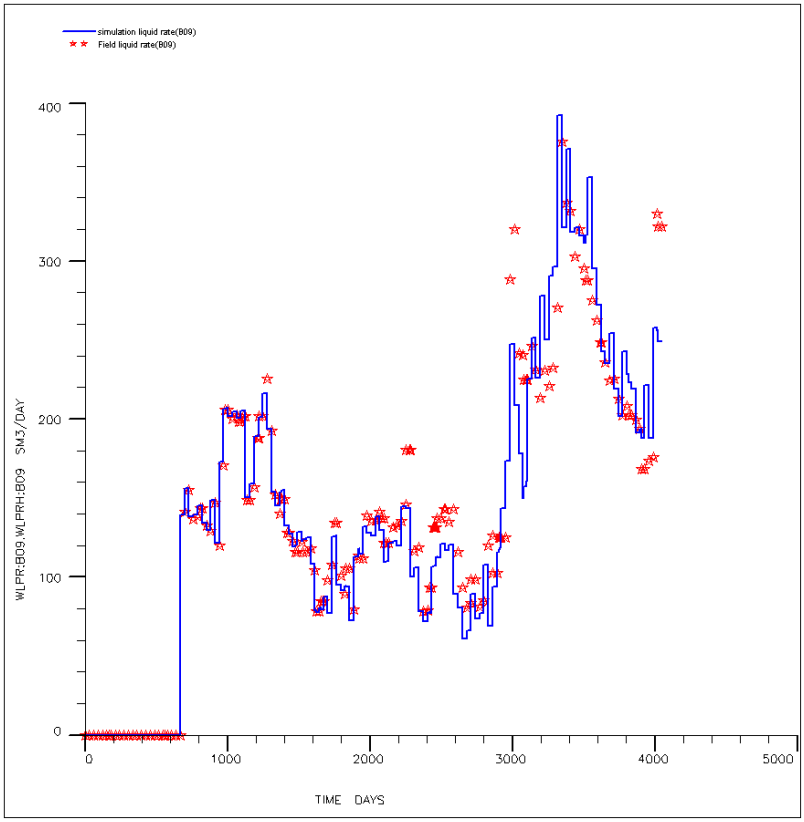

Figure 6.20 Total liquid rate curve of well B09

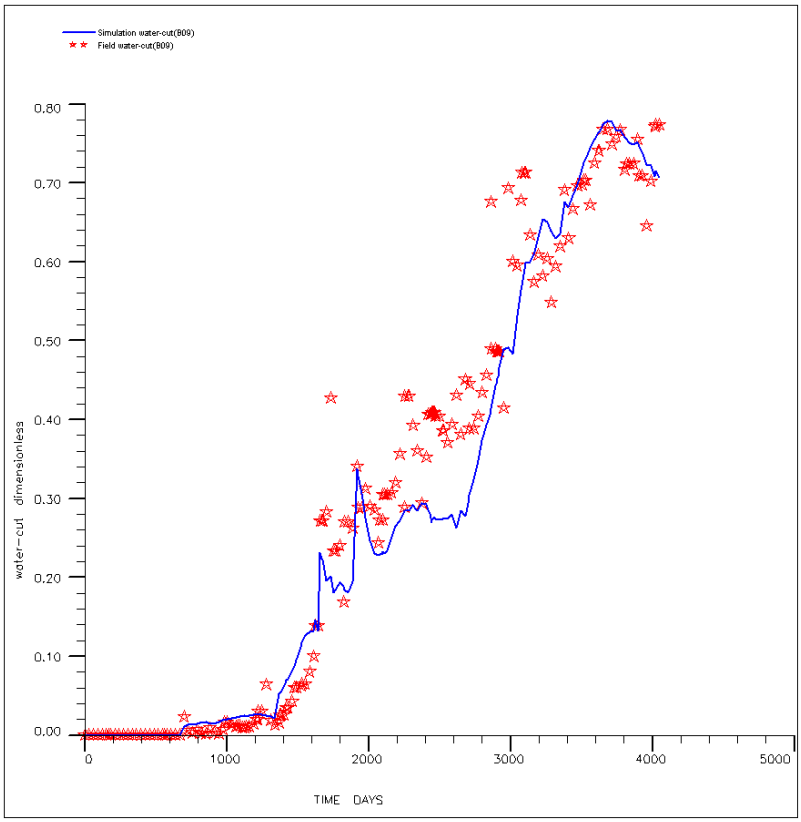

Figure 6.21 Water-cut curve of well B09

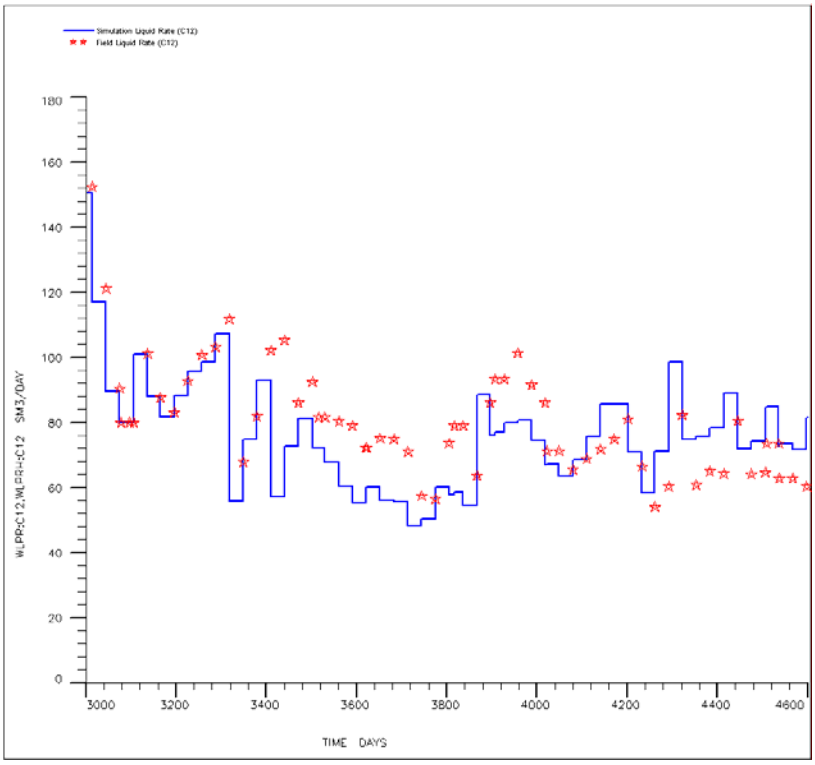

Figure 6.22 Total liquid rate curve of well C12

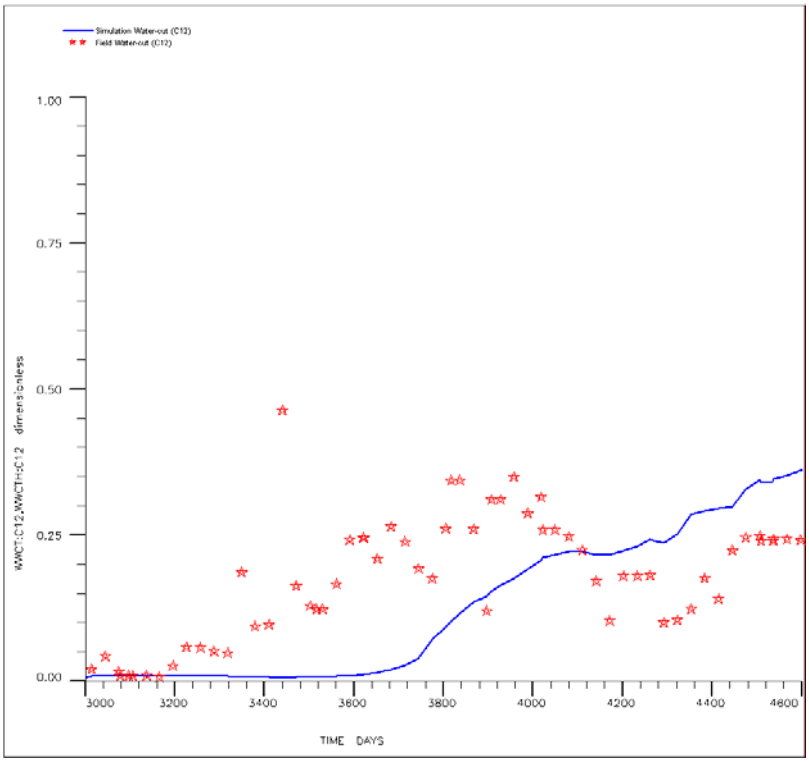

Figure 6.23 Water-cut curve of well C12

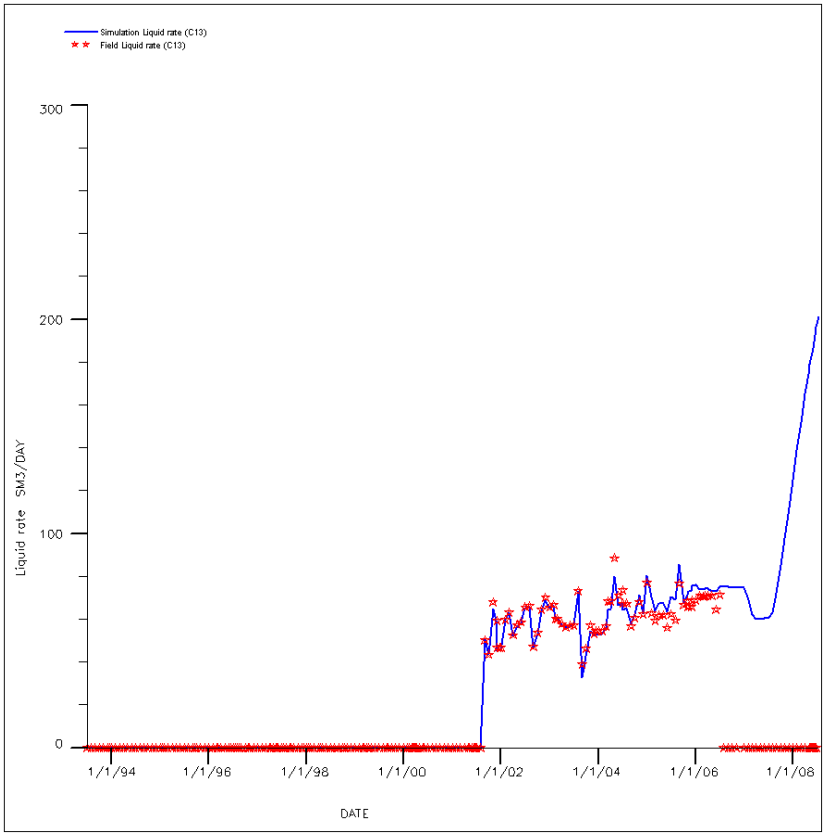

Figure 6.24 Total liquid rate curve of well C13

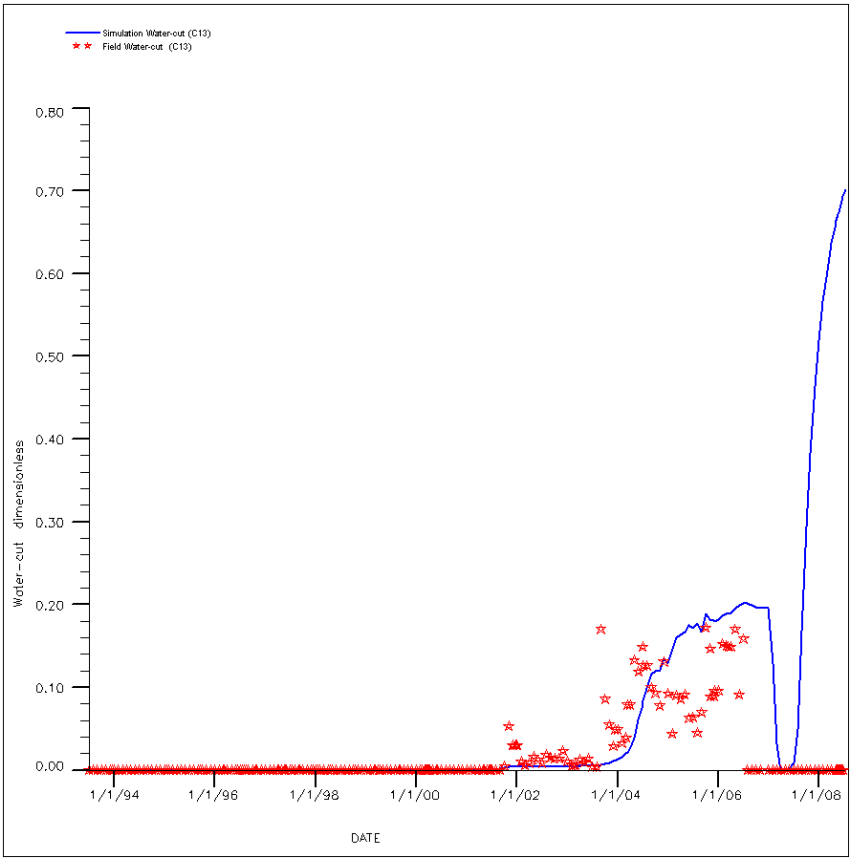

Figure 6.25 Water-cut curve of well C13

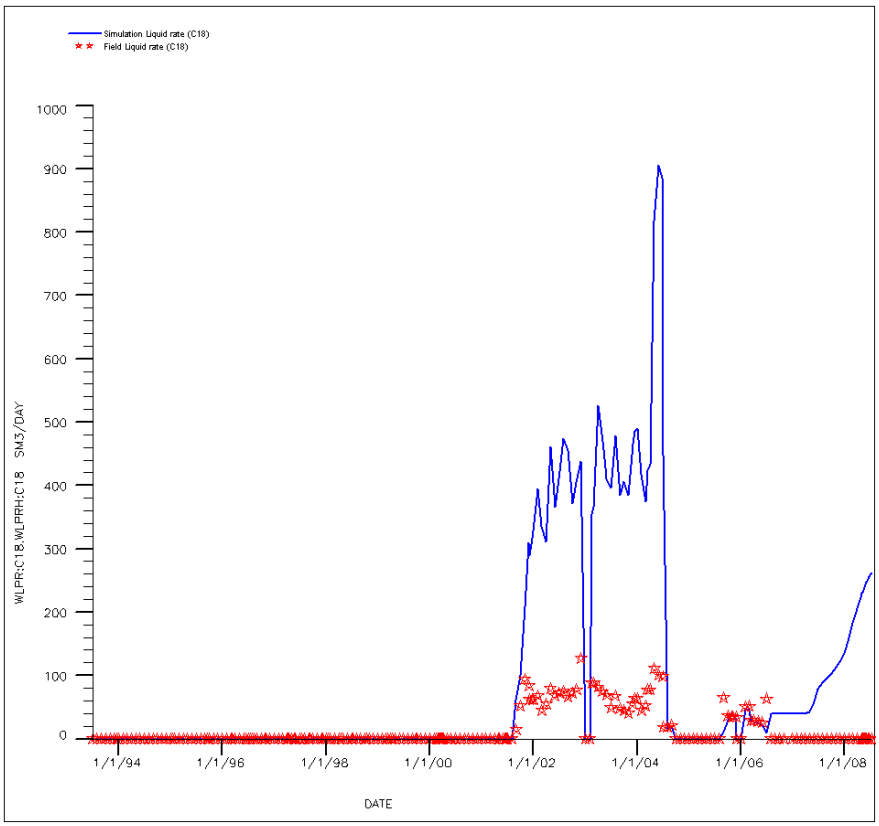

Figure 6.26 Total liquid rate curve of well C18

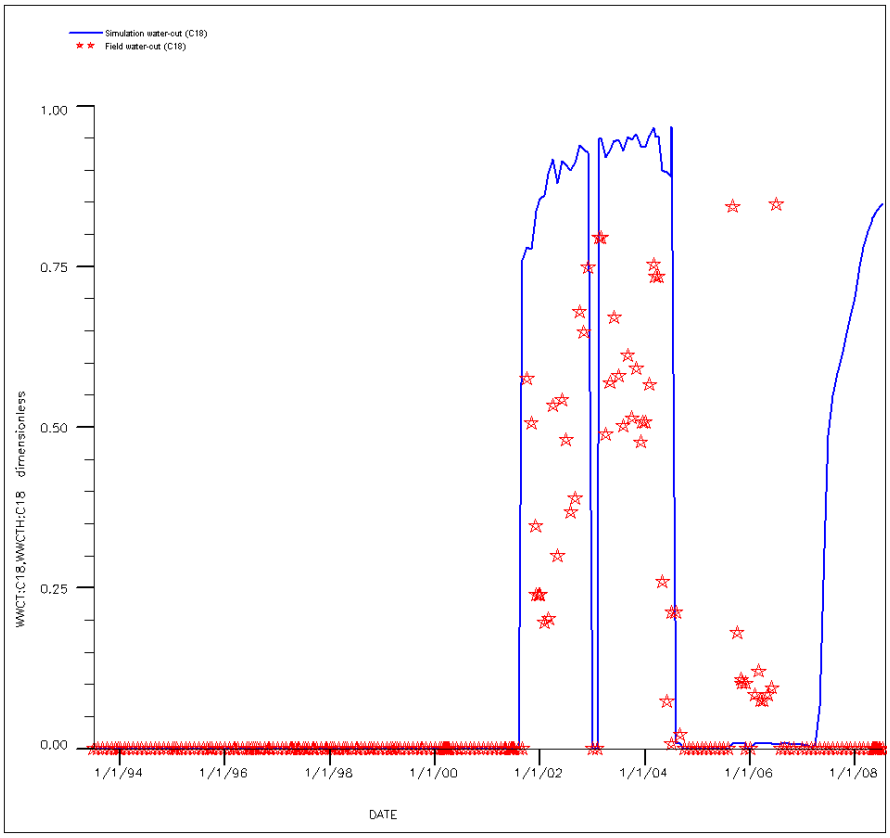

Figure 6.27 Water-cut curve of well C18

6.2.6 Performance Forecast

According to the new updated full model, the distribution of oil saturation and remaining oil near the infill wells (E30, E31 and E32) is shown in **Figure 6.28 and Figure 6.29**.This is the foundation for the location of the infill well.

In order to evaluate the production situation of the area near the infill wells, the VOI model (which includes E30, E31 and E32, and one injection well of C17) is cut from the full field model (**Figure 6.30, Figure 6.31**). Through numerical well testing analysis, the interlayer interference and the relation of injection versus production is shown.

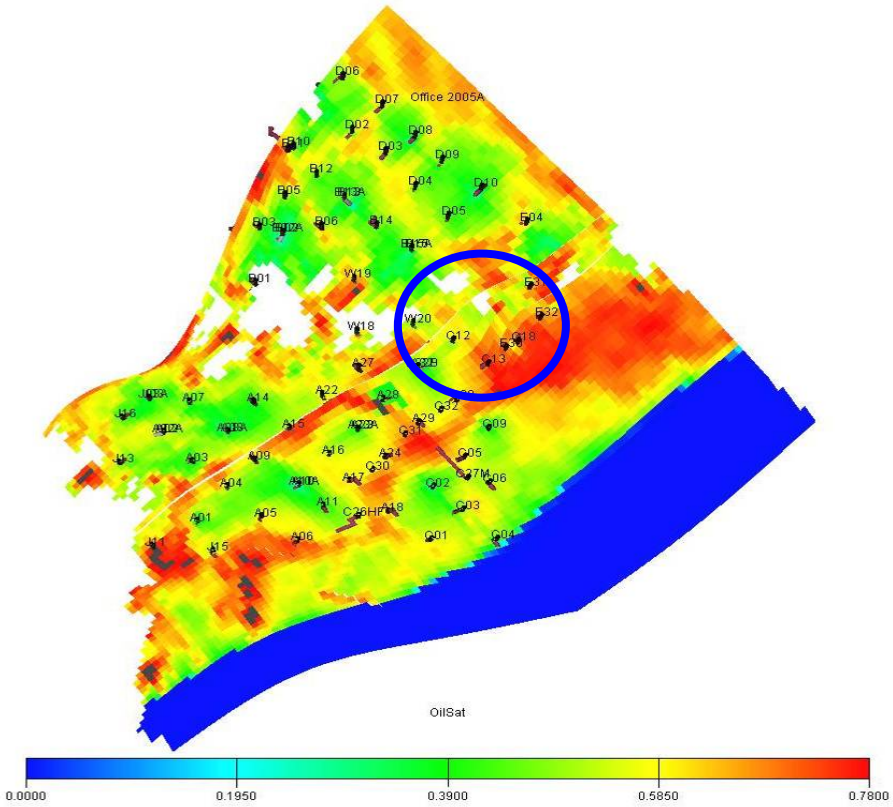

Figure 6.28 The distribution of oil saturation of the area near infill wells

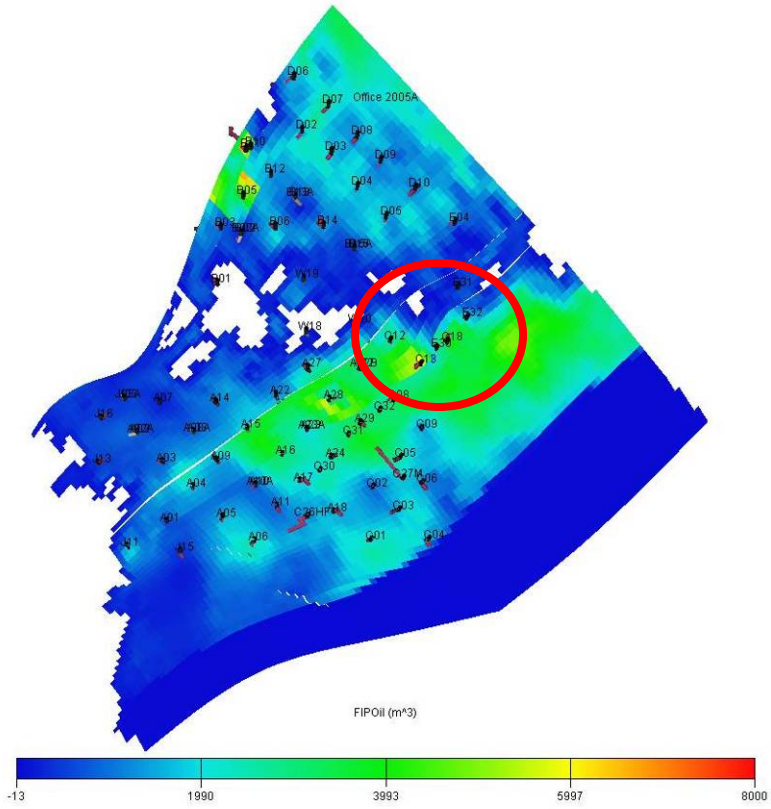

Figure 6.29 The distribution of the remaining oil of the area near infill wells

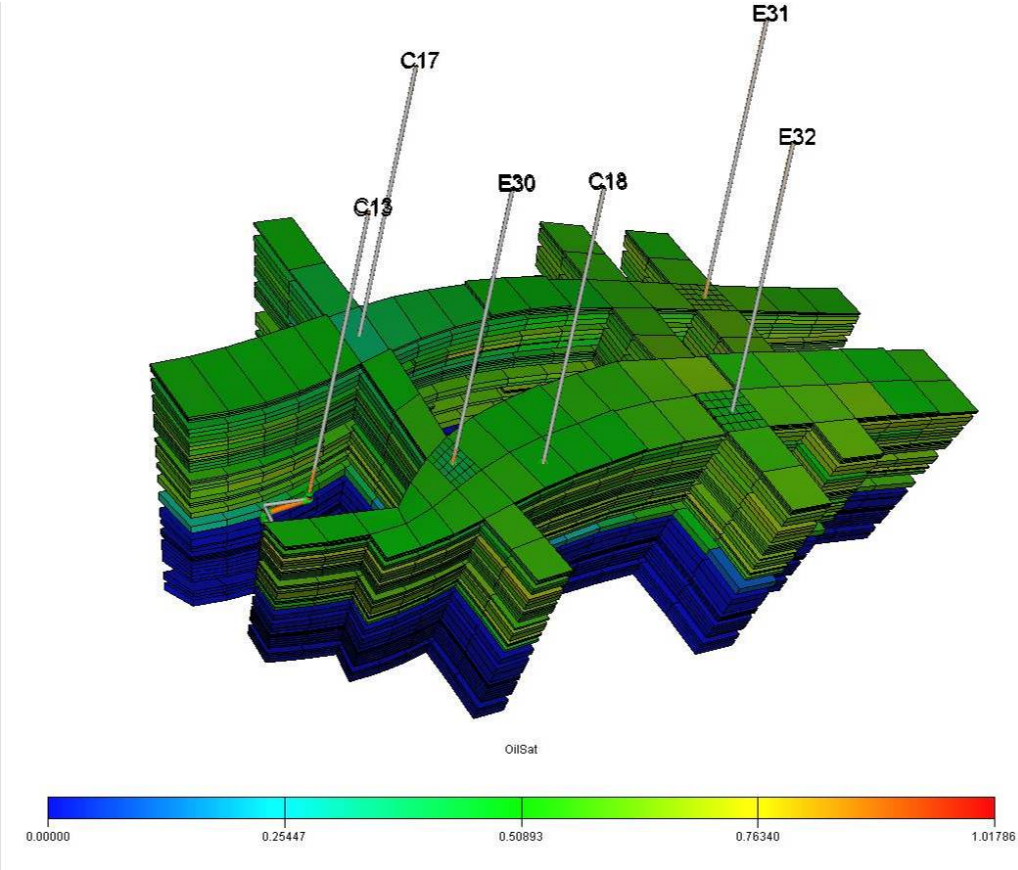

Figure 6.30 Fence diagram of injection versus production (VOI model)

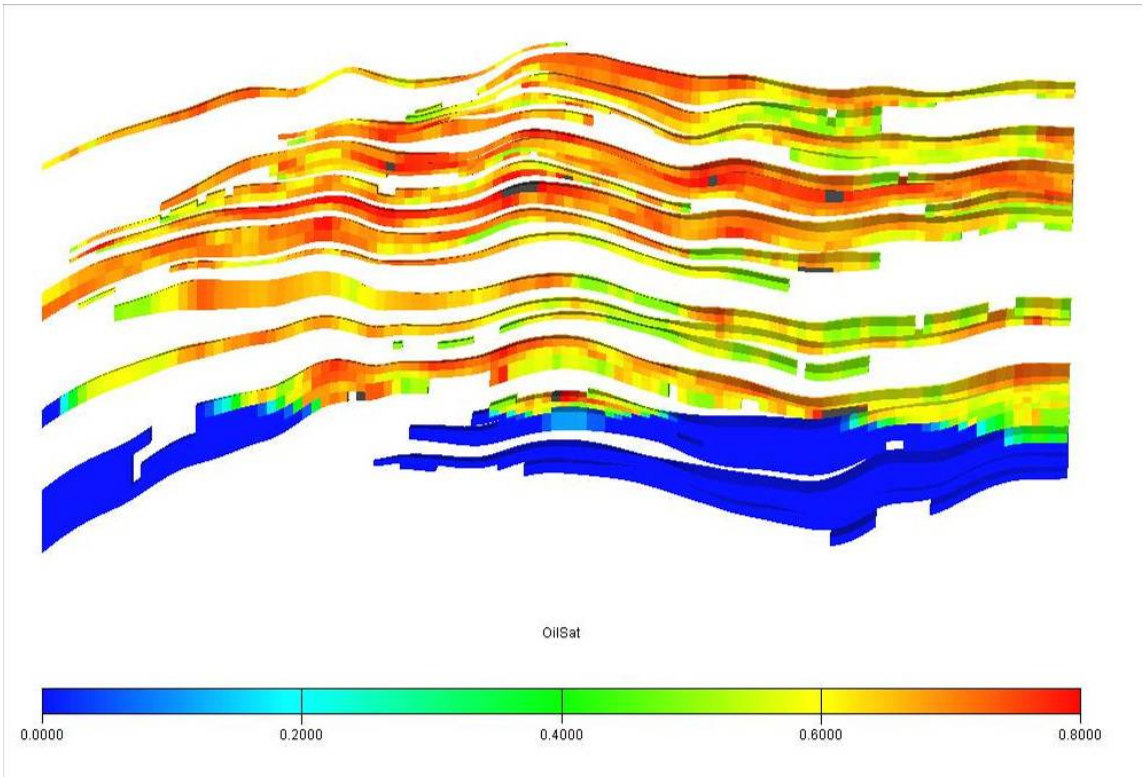

Figure 6.31 Section profile of layered commingled reservoirs

6.2.6.1 Performance of infill wells

Because this reservoir is a multi-layer reservoir, before drilling new infill wells (Well E30, well E31 and well E32), the performance of each zone needs to be understood. In general, if the pressure and the drainage radius of each layer in commingled layered reservoirs are different, the crossflow problem between layers becomes very severe. During the whole period of the well test, wellbore crossflow may continue until the end of the test. Hence, conventional drawdown and buildup tests of multi-layered reservoirs usually reveal the behaviour of the total system. The performance of each layer cannot be obtained. Using multi-rate multi-zone (MRMZ) test to confirm and provide valuable data for the evaluation of the layer contribution to total production, step-rate production testing was designed. Under different production rates, after pressure and flow rate has stabilized, the flow rate, pressure and water-cut of each layer can be measured by a production logging gauge. According to this data, a selective inflow performance (SIP) curve can be plotted. From the SIP curve, the productivity index (P.I) and initial pressure of each layer can be obtained.

The numbers of perforated layers in well E30, well E31 and well E32 are 15, 11, and 13 respectively. The simulation results are as shown in **Tables 6.2 to Table 6.7**.

From **Table 6.2** and **Table 6.5,** when the well E30 was at shut-in or low production rate condition, there are eight layers with crossflow, including zone 3, zone 11, zone 12, zone 14, zone 23, zone 26, zone 27 and zone 29. When the production rate increases and reaches 300m^3/d, however, there are five layers with crossflow, including zone 3, zone 23, zone 26, zone 27 and zone 29. If the production rate reaches 900m^3/d, there are only two layers with crossflow, including zone 23 and zone 29. **Table 6.5** shows that the initial pressure and productivity indexes of layers with crossflow are very low. In particular, the depletions of zone 23 and zone 29 are very severe. According to the above analysis results, this well has many layers that make no contribution to productivity, so the separation zone commingled production is not correct.

From **Table 6.3** and **Table 6.6,** when the well E31 was at shut-in or low production rate condition, there are six layers with crossflow, include zone 5, zone 11, zone 12, zone 14, zone 26, and zone 27. When the production rate increases and reaches 300m^3/d, however, there are two layers with crossflow, including zone 26 and zone 27. If the production rate reaches 900m^3/d, there are no layers with crossflow. **Table 6.6** shows that the initial pressures of zone 26 and zone 27 are very low. But the productivity index per meter of zone 26 is high, and it means that this zone needs to supply energy. The productivity index per meter of zone 11 is very low due to adverse properties, where the absolute permeability is just 157md.

From **Table 6.4** and **table 6.7**, when the well E32 was at shut-in or low production rate condition, there are six layers with crossflow, include zone 3, zone 5, zone 11, zone 12, zone 26 and zone 27. When the production rate increases and reaches 300m^3/d, there are no layers with crossflow. **Table 6.7** shows that the initial pressures of zone 3, zone 5, zone 26 and zone 27 are very low. The productivity index per meter of zone 27 is high,

but the logging of this well reveals that zone 27 is a high permeability formation. The reason for the low initial pressure for this layer is that there is no response in the course of waterflood development. For zone 3, the initial pressure and productivity indexes of layers are very low due to adverse properties, where the absolute permeability is just 313md.

Figure 6.32, Figure 6.33 and **Figure 6.34** are the downhole flow profile of each zone under different production rates. These downhole flow profiles show that the interlayer interferences are very severe under shut-in or low production rate conditions, but if drawdown pressure is increased, interlayer interference can be avoided step by step.

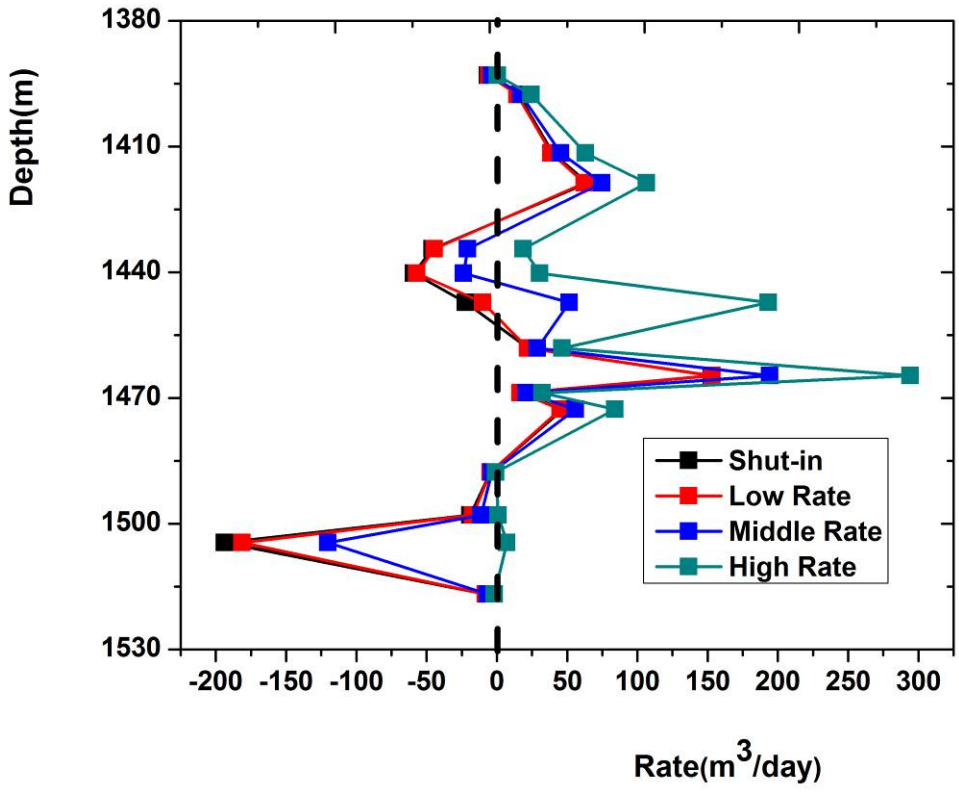

Figure 6.32 The downhole flow profile of well E30

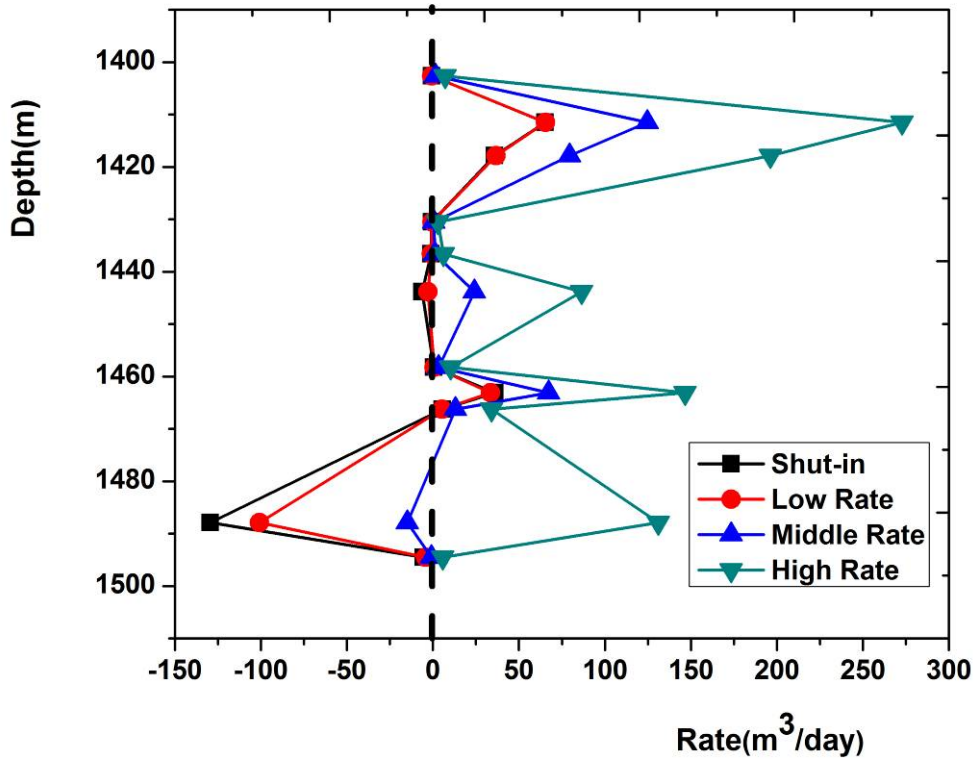

Figure 6.33 The downhole flow profile of well E31

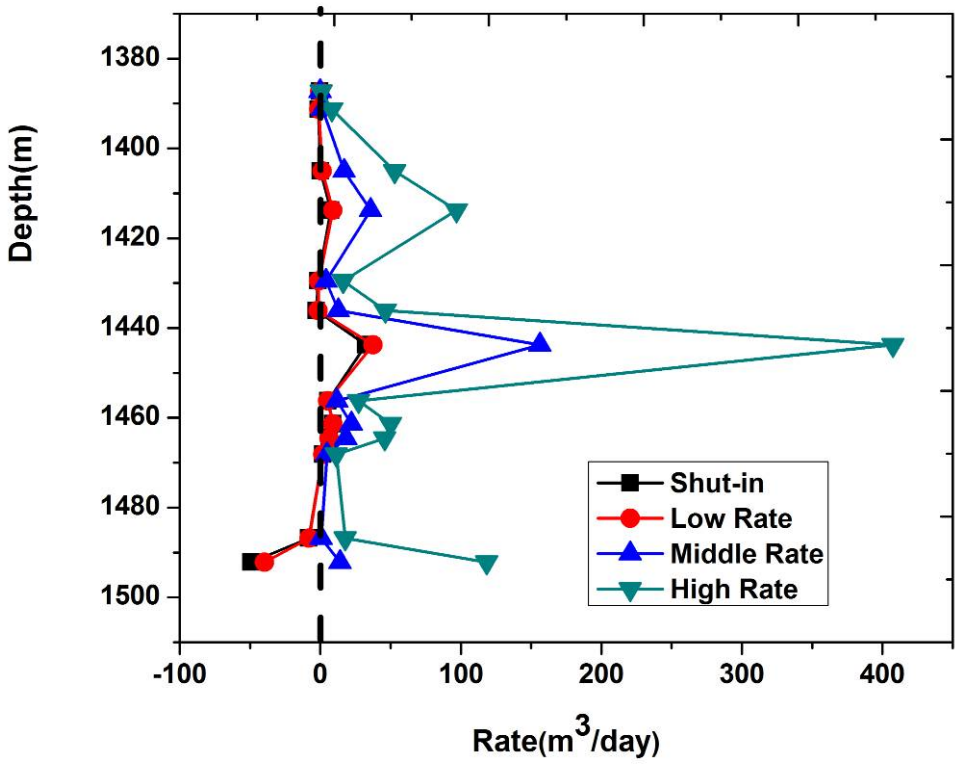

Figure 6.34 The downhole flow profile of well E32

Table 6.2 The downhole flow rate of each zone of well E30

Rate（m^3/day）	Zone 3			Zone 5			Zone 8			Zone 9			Zone 11		
	Oil	Water	Liquid	Oil	Water	Liquid	Oil	Water	Liquid	Oil	Water	Liquid	Oil	Water	Liquid
0	-0.44	-6.14	-6.58	1.03	14.40	15.43	2.76	37.12	39.88	4.43	60.10	64.53	-3.07	-42.76	-45.82
25	-0.37	-5.31	-5.68	0.98	13.47	14.45	2.63	36.07	38.70	4.27	58.18	62.45	-2.87	-41.52	-44.39
300	-0.23	-3.30	-3.52	1.25	16.01	17.26	3.17	42.39	45.56	5.30	69.60	74.91	-1.33	-19.42	-20.75
900	0.05	0.53	0.58	2.06	22.46	24.52	4.72	58.32	63.04	8.28	98.23	106.50	3.72	15.24	18.96

Table 6.2 The downhole flow rate of each zone of well E30（continued 1）

Rate（m^3/day）	Zone 12			Zone 14			Zone 17			Zone 19			Zone 20		
	Oil	Water	Liquid	Oil	Water	Liquid	Oil	Water	Liquid	Oil	Water	Liquid	Oil	Water	Liquid
0	-3.95	-55.10	-59.05	-1.48	-20.63	-22.11	2.30	19.98	22.28	5.63	147.01	152.64	2.38	14.92	17.30
25	-3.68	-53.14	-56.82	-0.64	-9.26	-9.90	2.23	19.70	21.93	5.39	147.86	153.25	2.22	14.50	16.72
300	-1.51	-22.03	-23.55	2.87	48.73	51.60	2.94	26.00	28.95	6.81	187.35	194.16	2.78	18.26	21.05
900	7.31	23.35	30.66	10.53	182.69	193.22	4.94	41.61	46.55	10.97	283.14	294.11	4.44	27.76	32.20

Table 6.2 The downhole flow rate of each zone of well E30（continued 2）

Rate（m^3/day）	Zone 21			Zone 23			Zone 26			Zone 27			Zone 29		
	Oil	Water	Liquid	Oil	Water	Liquid	Oil	Water	Liquid	Oil	Water	Liquid	Oil	Water	Liquid
0	5.51	41.38	46.88	-0.32	-4.41	-4.73	-1.28	-17.82	-19.10	-12.97	-180.71	-193.68	-0.53	-7.35	-7.88
25	5.11	40.10	45.22	-0.30	-4.39	-4.69	-1.10	-15.92	-17.02	-11.74	-169.53	-181.27	-0.51	-7.43	-7.95
300	6.33	49.69	56.02	-0.23	-3.40	-3.64	-0.73	-10.57	-11.30	-7.73	-112.56	-120.29	-0.41	-6.04	-6.45
900	9.96	74.08	84.04	-0.05	-0.65	-0.70	0.08	0.84	0.91	0.54	6.62	7.16	-0.13	-1.62	-1.75

Table 6.3 The downhole flow rate of each zone of well E31

Rate（m^3/day）	Zone 5			Zone 8			Zone 9			Zone 11			Zone 12		
	Oil	Water	Liquid	Oil	Water	Liquid	Oil	Water	Liquid	Oil	Water	Liquid	Oil	Water	Liquid
0	-0.26	-0.49	-0.75	16.71	48.69	65.40	24.30	11.62	35.93	-0.20	-0.37	-0.57	-0.36	-0.69	-1.05
32	-0.22	-0.36	-0.58	18.06	47.40	65.46	26.39	10.41	36.80	-0.17	-0.28	-0.45	-0.31	-0.51	-0.81
300	1.36	0.21	1.58	40.94	83.78	124.72	61.20	18.24	79.44	0.40	0.10	0.50	0.96	0.20	1.16
900	6.98	0.24	7.22	110.11	162.78	272.89	161.79	34.52	196.31	2.72	0.23	2.95	5.64	0.42	6.05

Table 6.3 The downhole flow rate of each zone of well E31（continued 1）

Rate（m^3/day）	Zone 14			Zone 17			Zone 19			Zone 20			Zone 26			Zone 27		
	Oil	Water	Liquid	Oil	Water	Liquid	Oil	Water	Liquid	Oil	Water	Liquid	Oil	Water	Liquid	Oil	Water	Liquid
0	-2.13	-4.07	-6.20	0.54	0.00	0.54	4.72	31.37	36.09	2.92	2.53	5.45	-44.38	-84.98	-129.36	-1.88	-3.59	-5.47
32	-1.08	-1.79	-2.87	0.81	0.00	0.81	5.10	28.48	33.58	3.13	2.19	5.31	-38.02	-62.90	-100.92	-1.64	-2.71	-4.34
300	9.66	14.49	24.15	3.43	0.00	3.43	14.61	52.79	67.40	8.99	4.20	13.20	-6.64	-8.16	-14.79	-0.35	-0.43	-0.78
900	41.67	44.81	86.48	10.15	0.20	10.35	44.43	102.16	146.59	26.48	7.73	34.21	102.86	28.29	131.15	4.25	1.54	5.79

Table 6.4 The downhole flow rate of each zone of well E32

Rate（m^3/day）	Zone 3			Zone 5			Zone 8			Zone 9		
	Oil	Water	Liquid	Oil	Water	Liquid	Oil	Water	Liquid	Oil	Water	Liquid
0	-0.19	-0.12	-0.31	-0.82	-0.50	-1.31	0.27	0.00	0.27	7.40	0.00	7.40
19	-0.19	-0.13	-0.32	-0.59	-0.41	-1.01	1.32	0.00	1.32	8.86	0.00	8.86
300	0.01	0.00	0.01	1.50	0.21	1.70	17.03	0.00	17.03	35.38	0.57	35.95
900	0.63	0.08	0.71	7.92	0.33	8.25	52.54	0.49	53.02	92.07	4.98	97.05

Table 6.4 The downhole flow rate of each zone of well E32（continued 1）

Rate（m^3/day）	Zone 11			Zone 12			Zone 14			Zone 17		
	Oil	Water	Liquid	Oil	Water	Liquid	Oil	Water	Liquid	Oil	Water	Liquid
0	-0.89	-0.54	-1.43	-1.67	-1.02	-2.69	18.24	14.12	32.36	5.56	0.00	5.56
19	-0.57	-0.40	-0.97	-0.88	-0.61	-1.49	18.45	18.99	37.44	5.35	0.00	5.35
300	3.86	0.32	4.18	12.23	0.64	12.86	74.64	81.78	156.43	11.93	0.00	11.93
900	15.95	0.30	16.25	45.86	0.42	46.28	213.28	194.19	407.47	27.32	0.06	27.37

Table 6.4 The downhole flow rate of each zone of well E32（continued 2）

Rate（m^3/day）	Zone 19			Zone 20			Zone 21			Zone 26			Zone 27		
	Oil	Water	Liquid	Oil	Water	Liquid	Oil	Water	Liquid	Oil	Water	Liquid	Oil	Water	Liquid
0	1.13	7.93	9.06	4.55	1.88	6.43	1.93	0.00	1.93	-5.02	-3.07	-8.09	-30.51	-18.67	-49.18
19	1.09	7.82	8.91	4.41	1.92	6.33	1.86	0.00	1.86	-4.59	-3.19	-7.77	-23.32	-16.20	-39.53
300	2.82	19.37	22.19	12.76	5.40	18.16	4.72	0.00	4.72	0.50	0.27	0.77	9.74	4.34	14.07
900	7.11	42.95	50.05	32.65	13.15	45.80	11.47	0.02	11.49	15.84	1.90	17.74	105.04	13.48	118.52

Table 6.5 The initial pressure and the PI of each zone of E30

	3	**5**	**8**	**9**	**11**	**12**	**14**	**17**	**19**	**20**	**21**	**23**	**26**	**27**	**29**
Initial pressure（Pi）（Bar)	141	208	219	214.00	164	167.00	182.00	210.00	214.00	215.00	217.00	146.00	150.00	153.00	148.00
P.I（m^3/d/Bar)	0.23	0.30	0.76	1.37	1.89	2.93	7.03	0.79	4.63	0.49	1.22	0.13	0.66	6.59	0.20
Thickness, m	1.73	2.73	7.07	7.07	5.86	5.86	7.97	3.56	4.30	3.90	3.90	2.53	4.75	8.36	2.38
P.I of per meter（m^3/d/m/Bar)	0.135	0.109	0.107	0.194	0.323	0.500	0.882	0.223	1.076	0.125	0.312	0.052	0.138	0.788	0.084

Table 6.6 The initial pressure and the PI of each zone of E31

	5	**8**	**9**	**11**	**12**	**14**	**17**	**19**	**20**	**26**	**27**
Initial pressure（Pi）（Bar)	180	225	218.00	177	180.00	190.00	203.00	220.00	220.00	144.00	145.50
P.I（m^3/d/Bar)	0.07	1.83	1.42	0.03	0.06	0.82	0.09	0.98	2.30	2.30	0.10
Thickness, m	1.72	6.48	6.48	5.95	5.95	8.12	2.35	3.01	3.45	7.17	6.29
P.I of per meter（m^3/d/m/Bar)	0.041	0.283	0.219	0.005	0.011	0.101	0.037	0.324	0.667	0.321	0.016

Table 6.7 The initial pressure and the PI of each zone of E32

	3	**5**	**8**	**9**	**11**	**12**	**14**	**17**	**19**	**20**	**21**	**26**	**27**
Initial pressure（Pi）（Bar)	140	145	161	179.00	160	161.00	174.00	184.00	183.50	180.00	180.50	145.00	151.00
P.I（m^3/d/Bar)	0.01	0.13	0.70	1.19	0.23	0.65	4.98	0.29	0.54	0.52	0.13	0.34	2.23
Thickness, m	2.17	2.51	8.71	8.71	6.45	6.45	8.58	2.56	2.84	3.64	3.64	6.17	4.56
P.I of per meter（m^3/d/m/Bar)	0.006	0.051	0.080	0.137	0.036	0.101	0.581	0.113	0.192	0.144	0.035	0.056	0.488

6.2.6.2 Performance of injection well

Similarly, in order to evaluate the effect of water injection, the well C17 was selected as the key well to study. Firstly, using a multi-rate multi-zone (MRMZ) test to provide and confirm valuable data for evaluation of layer contribution to the total injection rate, a step-rate injection test was designed. **Figure 6.35** shows that the injection procedure is 0 m^3/day, 350 m^3/day, 1050 m^3/day, 1750 m^3/day, and 0 m^3/day. Currently, the well C17 includes nine perforated intervals (zone 5, zone 8, zone 9, zone 14, zone 17, zone 19, zone 20, zone 21, and zone 26), and the simulation results are shown in **Table 6.8 to Table 6.9**.

From **Table 6.8**, when the well C17 is in shut-in or low injection rate condition, there are four layers with crossflow, including zone 5, zone 8, zone 9 and zone 21. When the production rate increases, there are no layers with crossflow.

Using the downhole injection rate and the pressure of each zone (**Figure 6.36**), the SIP curve can be obtained. **Figure 6.37** and **Table 6.9** show that there is a large variation in the injectivity index. The injectivity index of Zone 26 is 0, zone 21 is low. But zone 14 and zone 20 are very high, which may cause a serious cusping event. Hence, the injection profile for these zones needs to be adjusted.

According to the previous study, the relationships of injection-production for well C17, well E30, well E31 and well E32 can be obtained. The results are shown in **Table 6.10 to Table 6.12**. These Tables show that some production zones did not show water flooding development. There are six layers, three layers, and four layers for well E30, well E31 and well E32 respectively. The productivity indexes of these zones are very low due to the formation pressure decreasing quickly.

For well E30, the PIs of zone 14 and zone 19 are very high, but for the corresponding injection zone, the injectivity indexes are very high. These relationships reveal that some measures need to be taken to avoid serious early water breakthrough.

Table 6.8 The downhole injection rate of each zone of well C17

Injection Rate (m^3/day)	Zone 5	Zone 8	Zone 9	Zone 14	Zone 17	Zone 19	Zone 20	Zone 21	Zone 26
	Water	Water	Water	Water	Water	Water	Water	Water	Water
0	-14.78	-239.06	-25.71	213.00	5.31	15.37	46.08	-0.36	0.14
350	-6.75	-95.16	-10.43	240.03	12.43	51.05	157.63	1.07	0.14
1050	11.27	175.20	16.96	339.13	31.72	115.53	357.01	3.01	0.16
1750	29.83	435.77	42.77	454.99	51.64	179.05	550.95	4.81	0.18

Table 6.9 The initial pressure and the PI of each zone of C17

	Zone 5	Zone 8	Zone 9	Zone 14	Zone 17	Zone 19	Zone 20	Zone 21	Zone 26
Initial pressure（Pi）（Bar)	219	220	220	197.00	215	216.00	215.00	218.00	147.00
Injectivity index (P.I)（m^3/d/Bar)	2.16	3.32	3.32	11.73	2.25	7.94	24.48	0.25	0.00
Thickness, m	2.64	7.58	7.58	6.94	2.61	3.20	3.68	3.68	7.06
P.I of per meter（m^3/d/m/Bar)	0.819	0.438	0.438	1.690	0.861	2.480	6.652	0.068	0.000

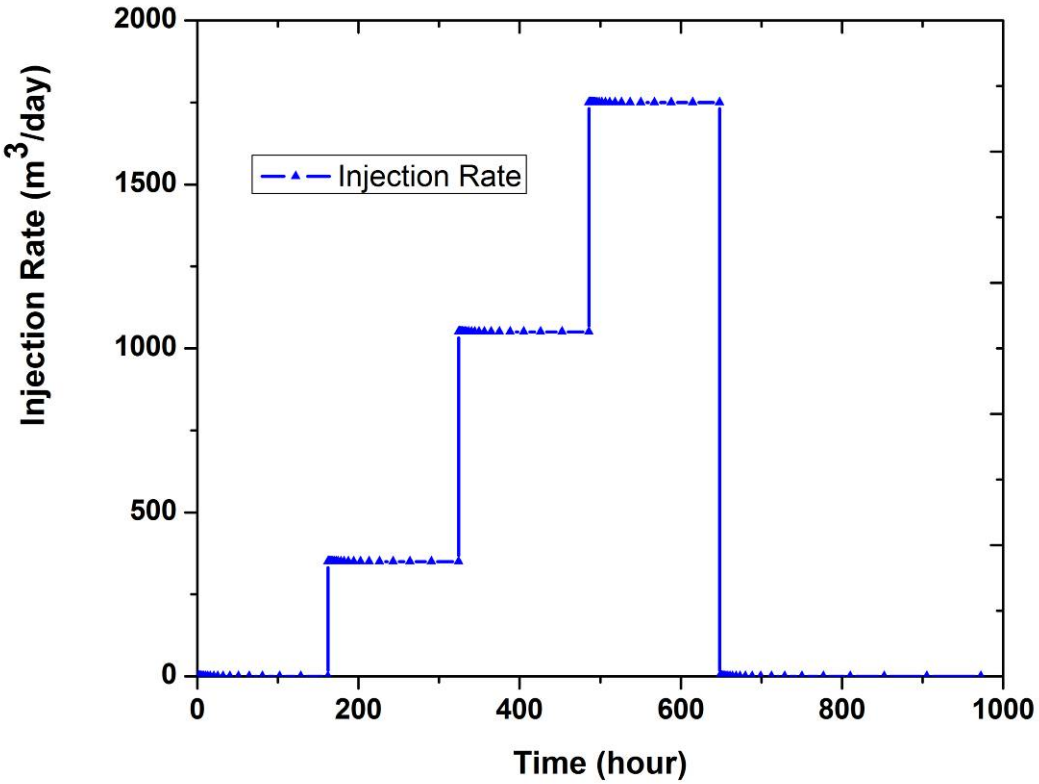

Figure 6.35 Water injection curve of MRMZ test of well C17

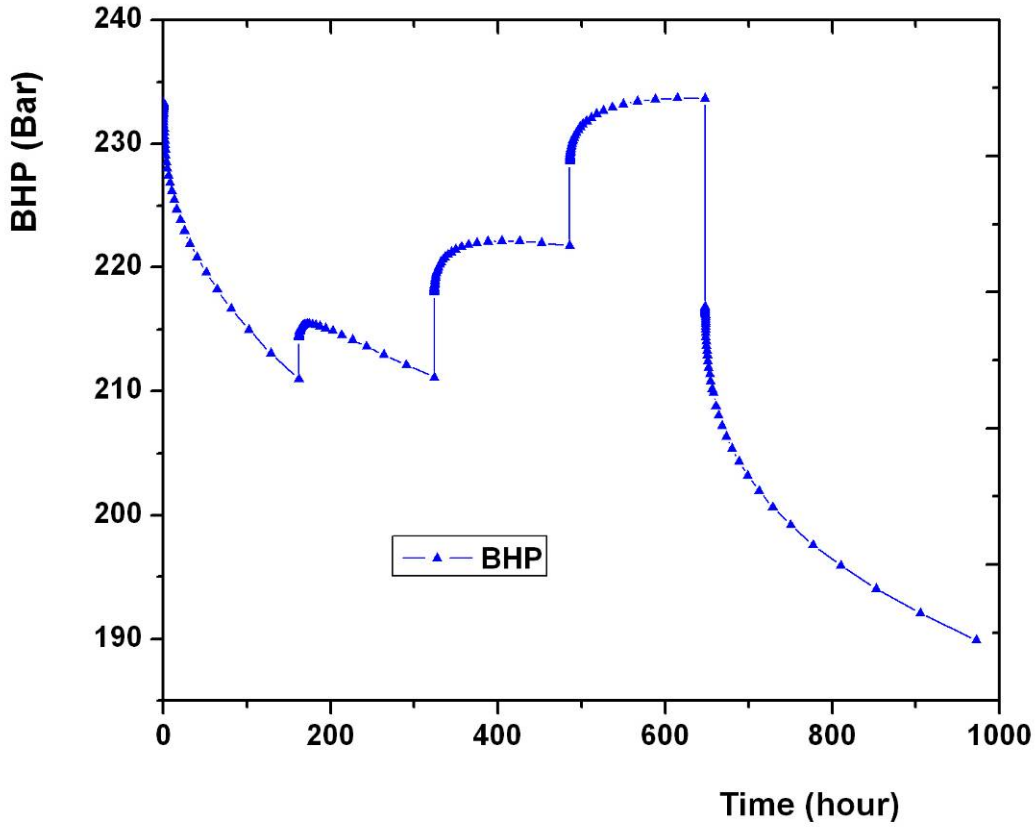

Figure 6.36 The BHP curve of MRMZ test of well C17

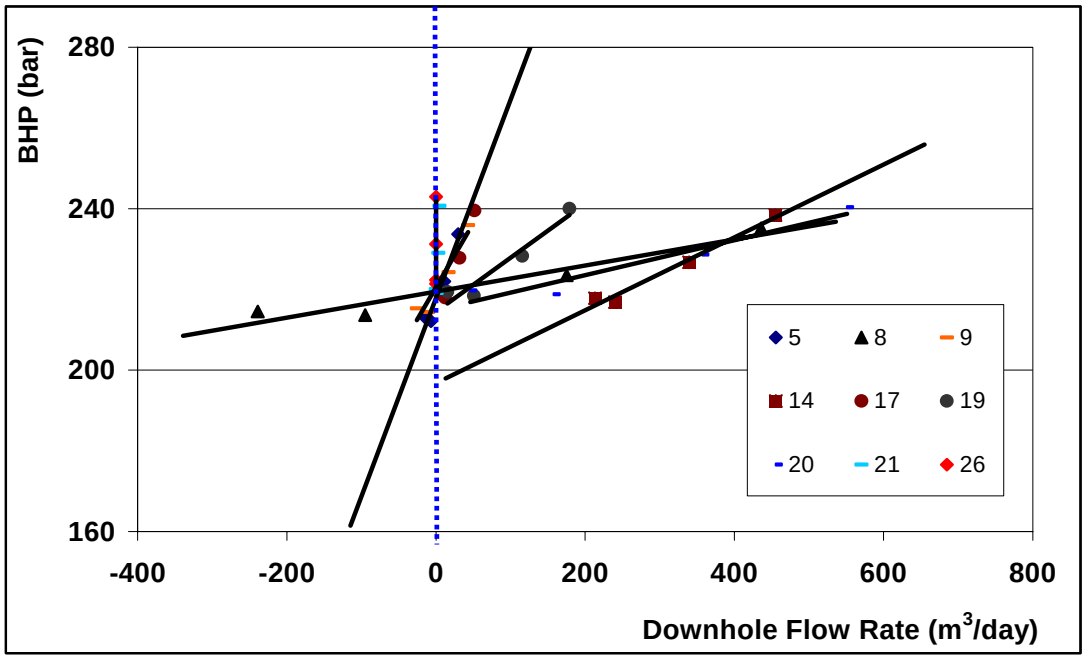

Figure 6.37 The SIP curve of each zone of well C17

For well E31, zone 14, zone 19, zone 20 and zone 26 are major formations. As a result the relationships between injection-production of zone 14, zone 19 and zone 20 are very good. But the relationship of injection-production of zone 26 is poor, so this zone has no energy supplement. As the next step the corresponding injection zone needs to have its injection rate adjusted to increase the energy of the corresponding production zone.

For well E32, zone 14 and zone 27 are major formations, both of which are high permeability. The relationship of injection-production of zone 14 is very good, which is needed to avoid a cusping event. But the relationship of injection-production of zone 27 is poor, so as a next step the corresponding injection zone needs to be re-perforated to keep the injection and production fluid balance.

Table 6.10 The relationship of injection-production of well C17 and well E30

Zone No.	Injection well					Production well				
	C17					E30				
	Thickness (m)	Porosity (fraction)	Injection pressure (Bar)	PI (m^3/d/Bar)	P.I per meter (m^3/d/m/Bar)	Thickness (m)	Porosity (fraction)	Initial pressure (Bar)	PI (m^3/d/Bar)	P.I per meter (m^3/d/m/Bar)
3						1.73	0.25	141.0	0.23	0.14
5	2.64	0.28	219.0	2.16	0.82	2.73	0.26	208.0	0.30	0.11
8	7.58	0.32	220.0	3.32	0.44	7.07	0.29	219.0	0.76	0.11
9	7.58	0.29	220.0	3.32	0.44	7.07	0.29	214.0	1.37	0.19
11						5.86	0.26	164.0	1.89	0.32
12						5.86	0.30	167.0	2.93	0.50
14	6.94	0.26	197.0	11.73	1.69	7.97	0.29	182.0	7.03	0.88
17	2.61	0.26	215.0	2.25	0.86	3.56	0.27	210.0	0.79	0.22
19	3.20	0.28	216.0	7.94	2.48	4.30	0.28	214.0	4.63	1.08
20	3.68	0.29	215.0	24.48	6.65	3.90	0.26	215.0	0.49	0.12
21	3.68	0.25	218.0	0.25	0.07	3.90	0.28	217.0	1.22	0.31
23						2.53	0.31	146.0	0.13	0.05
26	7.06	0.31	147.0	0.00	0.00	4.75	0.31	150.0	0.66	0.14
27						8.36	0.35	153.0	6.59	0.79
29						2.38	0.25	148.0	0.20	0.08

Table 6.11 The relationship of injection-production of well C17 and well E31

Zone No.	Injection well					Production well				
	C17					E31				
	Thickness (m)	Porosity (fraction)	Injection pressure (Bar)	PI (m^3/d/Bar)	P.I per meter (m^3/d/m/Bar)	Thickness (m)	Porosity (fraction)	Initial pressure (Bar)	PI (m^3/d/Bar)	P.I per meter (m^3/d/m/Bar)
3										
5	2.64	0.28	219	2.16	0.82	1.72	0.26	180	0.07	0.04
8	7.58	0.32	220	3.32	0.44	6.48	0.31	225	1.83	0.28
9	7.58	0.29	220	3.32	0.44	6.48	0.3	218	1.42	0.22
11						5.95	0.28	177	0.03	0.01
12						5.95	0.26	180	0.06	0.01
14	6.94	0.26	197	11.73	1.69	8.12	0.29	190	0.82	0.1
17	2.61	0.26	215	2.25	0.86	2.35	0.27	203	0.09	0.04
19	3.2	0.28	216	7.94	2.48	3.01	0.28	220	0.98	0.32
20	3.68	0.29	215	24.48	6.65	3.45	0.27	220	2.3	0.67
21	3.68	0.25	218	0.25	0.07					
23										
26	7.06	0.31	147	0	0	7.17	0.35	144	2.3	0.32
27						6.29	0.32	145.5	0.1	0.02
29										

Table 6.12 The relationship of injection-production of well C17 and well E32

Zone No.	Injection well					Production well				
	C17					E32				
	Thickness (m)	Porosity (fraction)	Injection pressure (Bar)	PI (m^3/d/Bar)	P.I per meter (m^3/d/m/Bar)	Thickness (m)	Porosity (fraction)	Initial pressure (Bar)	PI (m^3/d/Bar)	P.I per meter (m^3/d/m/Bar)
9	7.58	0.29	220	3.32	0.44	8.71	0.31	179	1.19	0.14
11						6.45	0.22	160	0.23	0.04
12						6.45	0.29	161	0.65	0.1
14	6.94	0.26	197	11.73	1.69	8.58	0.31	174	4.98	0.58
17	2.61	0.26	215	2.25	0.86	2.56	0.28	184	0.29	0.11
19	3.2	0.28	216	7.94	2.48	2.84	0.28	183.5	0.54	0.19
20	3.68	0.29	215	24.48	6.65	3.64	0.27	180	0.52	0.14
21	3.68	0.25	218	0.25	0.07	3.64	0.3	180.5	0.13	0.03
23										
26	7.06	0.31	147	0	0	6.17	0.32	145	0.34	0.06
27						4.56	0.35	151	2.23	0.49
29										

According to the above analysis, for a mature field, using the history matching of well testing data to update the full field model through a numerical well testing approach, the updated model is closer to the real reservoir model, and this model can be used to predict future performance, such as the injection-production ratio, the interlayer interference, the distribution of remaining oil, etc.

6.3 Example 2

6.3.1 Field Overview

This field is a structural-lithological oil reservoir concerned with stratigraphic overlap and pinch-out (**Figure 6.38**). It was discovered in 1992, and commenced production in 1998. It has a quoted geological reserve of $1055.2\times10^4 m^3$ and a recoverable reserve of $276.4\times10^4 m^3$. The reservoir quality is good, with 1~2 D of permeability and 33% of mean porosity. Oil viscosity is between 1 cp and 120 cp. At the up-structure location the oil viscosity is low, but at the down-structure location the oil viscosity is high due to the oxidation action of water. Hence, the spatial distribution of fluid has big heterogeneity.

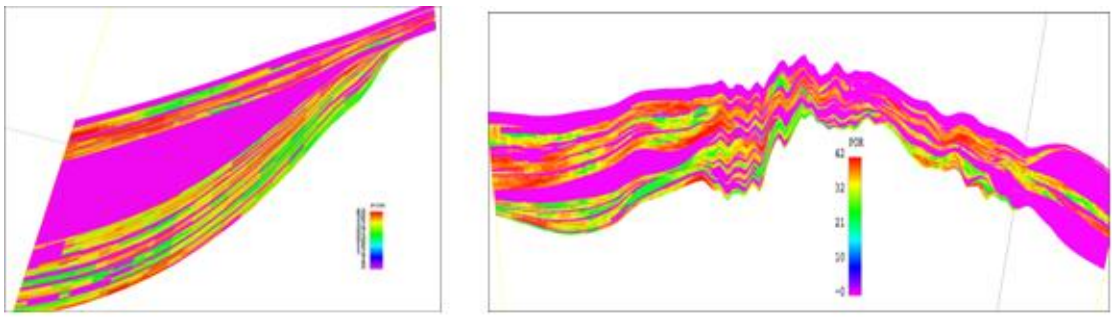

Figure 6.38 These figures are porosity profiles; on the left is the South-North section, and on the right is the East-West section.

Up to 2008, the field produced more than $126.4\times10^4 m^3$, and the field water cut reached 82.9%. In order to control the water cut and maintain the production rate, an adjustment plan was developed. Some infill wells were drilled, and in the down structure, several infill wells were located (**Figure 6.39**). Before these wells commenced production, some drill stem tests (DST) were adopted to evaluate the productivity index. These tests have as a feature that the BHP curve of each drawdown

goes up (**Figure 6.40**). Because these test wells have already reached high water-cut during the test process, due to low location, according to the description in chapter 3, this abnormal phenomenon was controlled by the multiphase flow effect. This type of BHP data is invalid for traditional well test analysis.

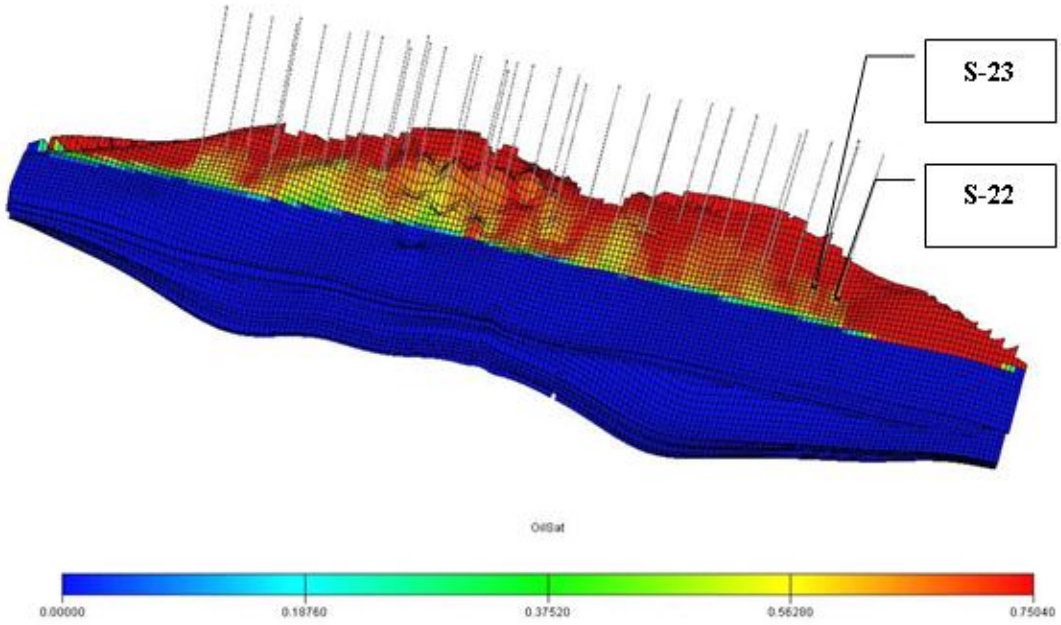

Figure 6.39 This figure is the oil saturation distribution of S field. There are two wells near oil-water contact.

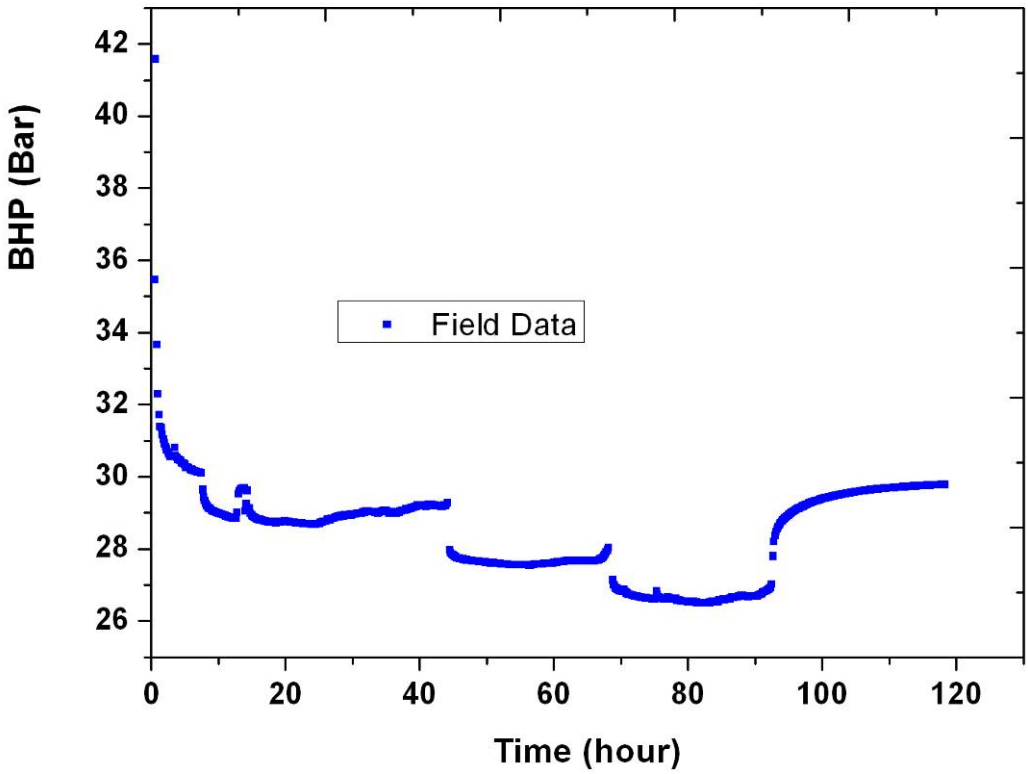

Figure 6.40 This figure is the transient well testing curve of S-22. At the end of each DD test, the BHP curve goes up.

Although traditional multiphase well testing does not work for these data, it contains a lot of reservoir information, and so it cannot be abandoned. According to chapter 5, through using the multiphase flow numerical well testing procedure, it can be used to identify the fluid model and improve history matching.

History matching in numerical simulations is a process of adjusting the simulator input in such a way as to achieve a better fit to the actual reservoir performance. Hence, the changes to the simulation model should most closely reflect changes in knowledge of the geology and fluid. Especially, in course of matching, the transient well test data, as dynamic test data, is a reflection of the real reservoir geology and fluid, even though these data are abnormal.

6.3.2 Numerical well testing

In order to illustrate the use procedure for abnormal transient pressure, as shown in **Figure 6.39**, two wells (S-22 and S-23) were selected on the down-dip side and near oil-water contact, and well S-22 has transient well test data. **Figure 6.40** shows that the BHP curve increased at the end of each DD test.

In order to match well test data and update the reservoir model, a numerical well testing technique was used (**Figure 6.41**).

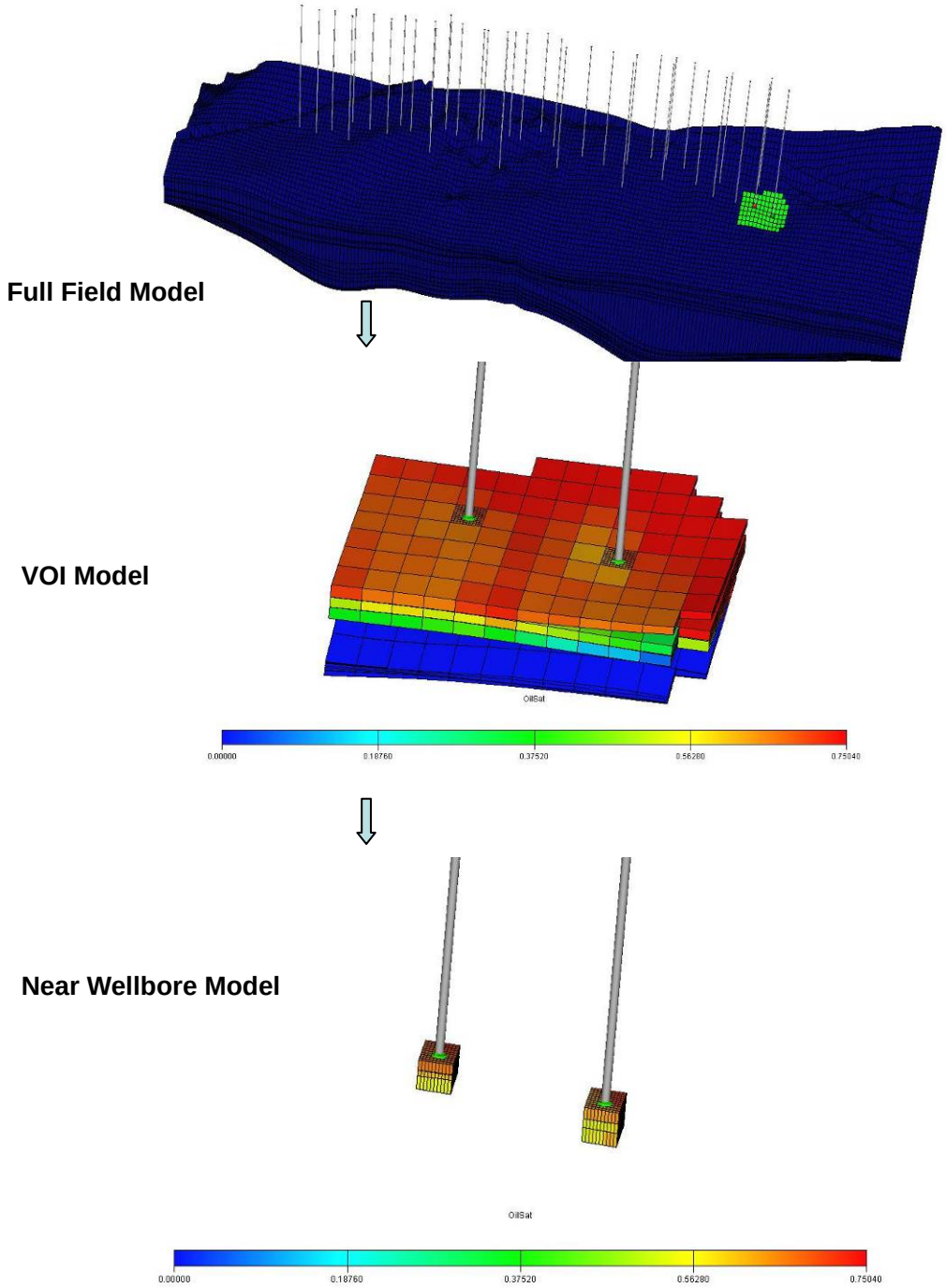

Figure 6.41 This figure is the NWM flow chart. The VOI model was cut from the full field model, selecting a single well to LGR and time-stepping, and through adjusting the properties of the fluid model and the geological model to match the transient well testing data.

Before matching the transient data of S-22, two cases were designed. In one case the oxidation action of fluid in the down-structure location was not considered, and reservoir engineers simply adjusted the geological parameters to match well

performance. In the other case, there were different fluid data (including PVT data and relative permeability curves) at the up-structure location and the down-structure location. Here author defined new PVT data and the relative permeability curves in the VOI model, as shown in **Figure 6.42** and **Figure 6.43**, the properties of the PVT data (comparing with oil viscosity and oil volume factor, the effect of varying Bo had little effect.) and the relative permeability data in the down-structure location were adjusted to match the transient test data.

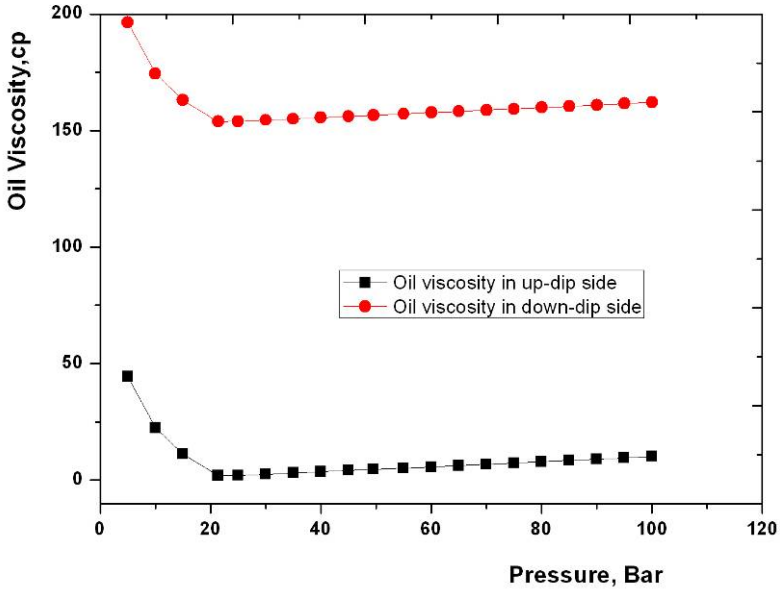

Figure 6.42 This figure shows the difference in oil viscosity between the up-structure location and the down-structure location.

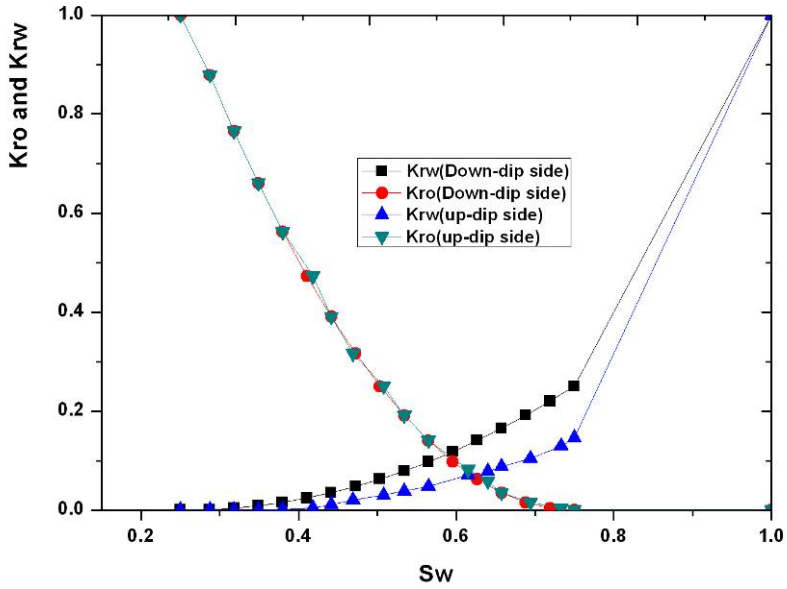

Figure 6.43 This figure shows the difference between the relative permeability curves in the up-structure and the down-structure locations.

Simulation results of the matching appear in **Figure 6.44**, **Figure 6.45** and **Figure 6.46**. If reservoir engineers only adjusted the geological model parameters to match well test data, the DD curve of the simulation was not close to observed data and the effect of matching was not good. But with regards to matching the curve for a single well, matching results can be accepted.

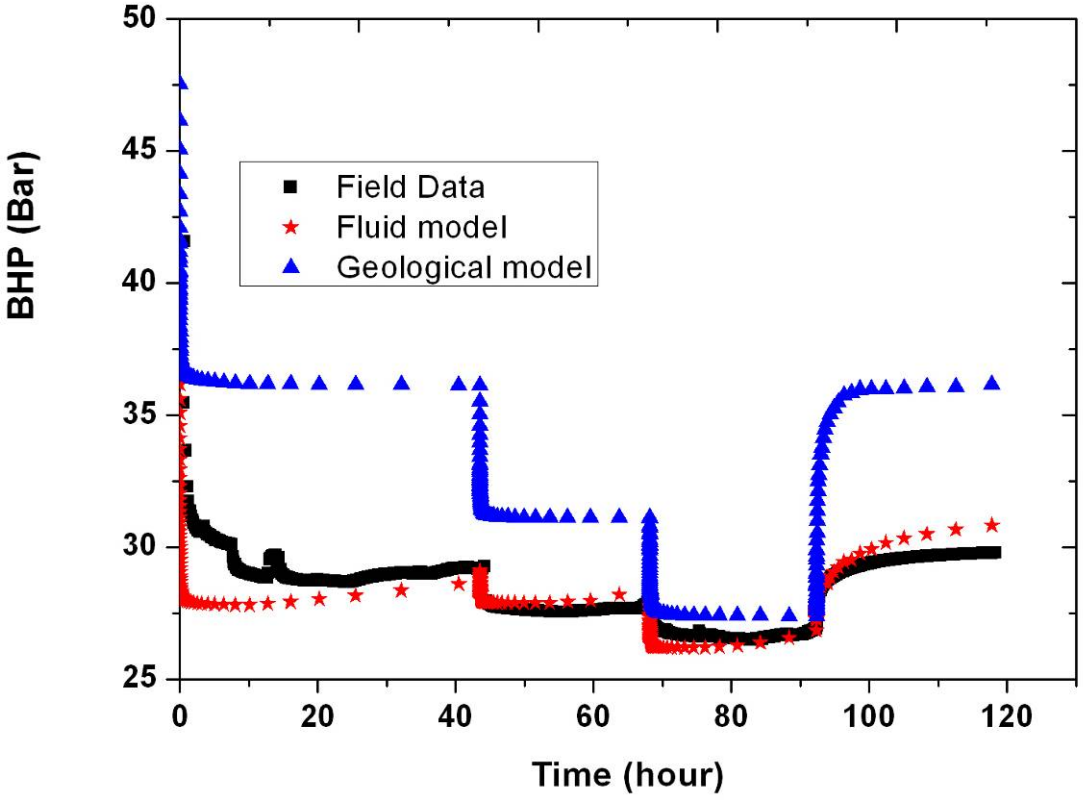

Figure 6.44 This figure shows the matching results of transient well test data. If only the parameters of the geological model were adjusted, then the observed transient data cannot be matched well. In particular the DD curve of the simulation did not follow the trend of increasing. If the fluid model was changed, then the observed data was matched very well.

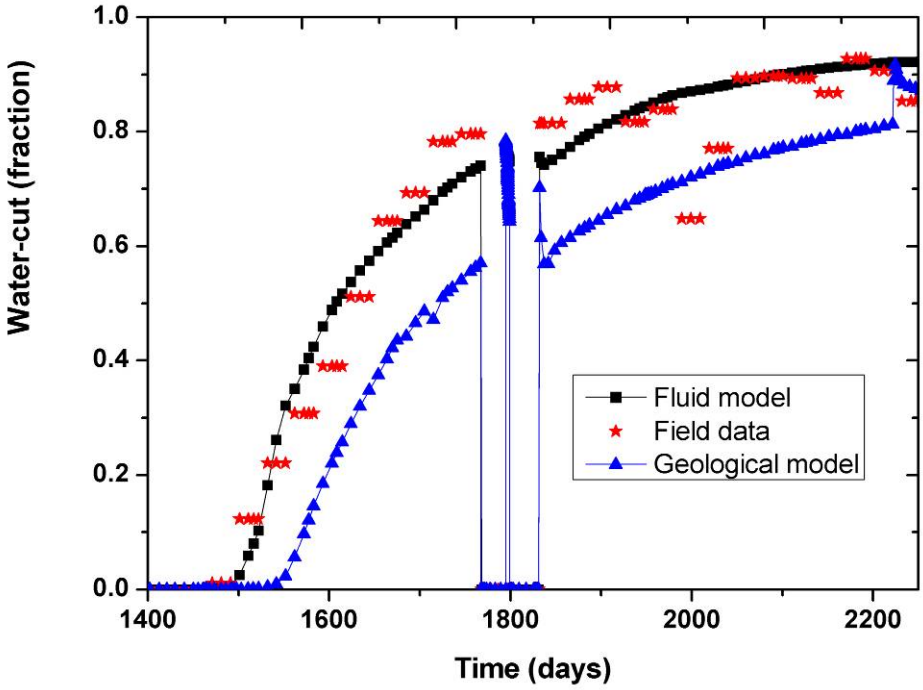

Figure 6.45 This figure is the comparison of water-cut under different matching conditions for well S-22. Through adjusting the properties of the geological model and the fluid model, respectively, the results of history matching can both be acceptable.

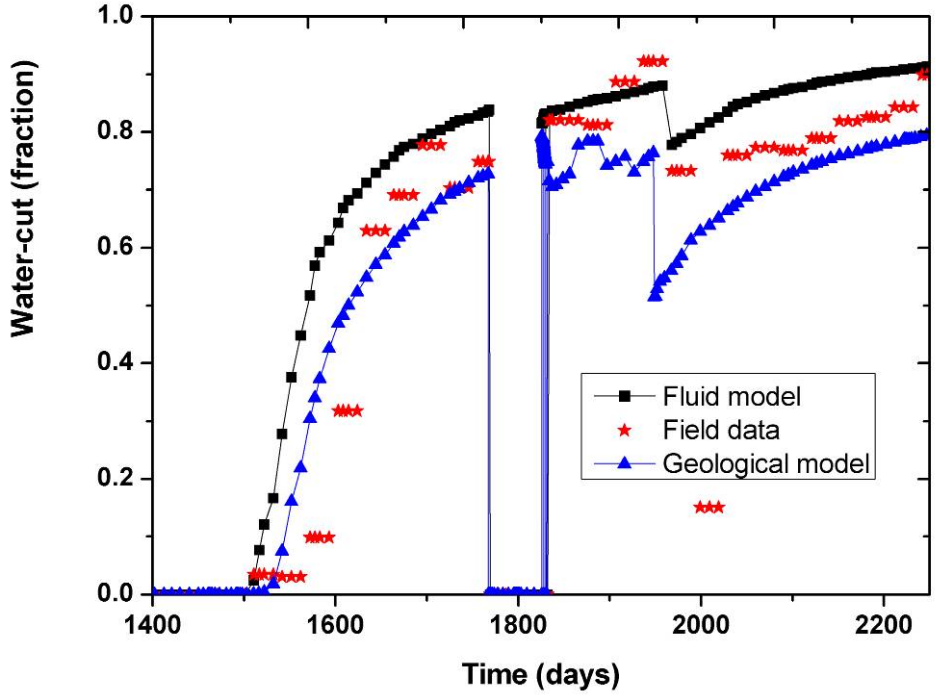

Figure 6.46 This figure is the comparison of water-cut under different matching conditions for well S-23. Through adjusting the properties of the geological model and the fluid model, respectively, the results of history matching can both be acceptable.

On the other hand, if reservoir engineers considered the changing of the fluid property at the down-structure location, the DD data of numerical simulation started to increase at some water-cut percentage and the effect of matching was very good. Comparing to changes of the geological properties, the results of matching were better.

As with the description above, there are two models that can be used to predict the performance of the field, and the results of both models can be accepted, but which model is better? Under multiphase flow conditions, transient well test data was very useful, in which the BHP curve went up. Using these data to update the reservoir model, the fluid model was close to the real fluid model.

6.4 Chapter Conclusion

The various case studies carried out on example 1 and example 2 have shown that it is not only possible to apply the new multiphase flow numerical well testing procedure to a real mature field, but there are also benefits of such a procedure over the conventional history matching method. Because more and more PDG are applied to the mature field to monitor the performance of well and field, these large multi-phase transient pressure data from permanent down-hole gauges contain a great deal of reservoir information. By applying these dynamic PDG data to update the reservoir model, management of mature fields in real time can be achieved. The key contribution is that a practicable workflow of history matching for well test data has been developed. Though this workflow, the uncertainties of the model will be reduced, and the updated reservoir model is more accurate and closer to the real reservoir model.

A further development in the history matching process is to define the fluid model, which includes the PVT data and the relative permeability data. These properties of fluid model can affect the trend of bottom-hole flowing pressure.

Chapter 7
Conclusion and Future Work

7.1 Overview

This chapter contains a summary of the key results of this thesis, presents main conclusions of the research and gives suggestions for future work. The total aim of the research was to prove the importance of multiphase flow well testing in future field management. Therefore, a number of case studies were developed to examine the following vital issues:

1. Modify the traditional multiphase flow well testing approach, which is only suitable for uniformly saturated reservoirs. The results from this modified approach can be directly used to update the reservoir model for reservoir management.

2. Demonstrate the effect of multiphase flow on well test interpretation in non-uniformly saturated reservoirs. The total mobility of fluid controls the trend of the BHP curve and pressure derivative curve.

3. Show the type curves of multiphase flow well testing for layered commingled reservoirs. According to multi-rate multi-zone production logging, a selective inflow performance (SIP) test was developed.

4. Because equations governing multiphase flow have no analytical solution, transient

pressure or PDG data can be dynamically used to update reservoir model through numerical solutions and history matching. A new multiphase flow numerical well testing procedure was developed, which is suitable for all fluids with multiphase flow.

Each chapter in the thesis deals with the different multiphase flow problems, as is illustrated in **Table 7.1**.

The case studies developed in chapters 1-3 and chapters 5 are all synthetic studies designed to research multiphase flow problems. The models in chapter 4 and chapter 6 are real field models.

Table 7.1 A summary of the various case studies carried out in this thesis and some contributions

Chapter	Geological Model			Fluid Model		Contribution to Thesis
	Structure	Geology		Multiphase	Saturation	
		horizontal	Vertical			
Chapter 1	Anticline	Homogeneous	Homogeneous	Oil-Water	Uniform or Low Water cut	Under uniform saturation reservoir or low water cut conditions, reconsider the application of the traditional multiphase flow well testing approach; systematically sum up the advantages and disadvantages of traditional approaches.
	Anticline	Homogeneous	Homogeneous	Oil-Gas	Uniform	
Chapter 2	Radial	Homogeneous	Homogeneous	Oil-Water	Uniform	For different ideal flow mechanisms, a modified P-M approach was developed, and the results from this modified approach are more accurate and practical.
Chapter 3	Anticline	Homogeneous	Homogeneous	Oil-Water	Non-uniform	Part 1: Theoretical analysis of the influence of the pressure behavior of transition zone in oil-water and gas-water reservoirs. Part 2: Theoretical analysis of the influence of water cut for bottom-hole flowing pressure curve.
	Anticline	Homogeneous	Homogeneous	Gas-Water	Non-uniform	
Chapter 4	Anticline	Homogeneous	heterogeneous	Oil-Water	Non-uniform	Provide the type curve of interlayer interference for different reservoir models and practicable analysis approach (SIP approach)
Chapter 5	Anticline	heterogeneous	heterogeneous	Oil-Water	Non-uniform	Develop a new multiphase flow numerical well testing procedure
Chapter 6	Anticline	heterogeneous	heterogeneous	Oil-Water	Non-uniform	Demonstrate the complete research outcomes on two real field examples, showing the procedure of mature field management through well test data or PDG data

Chapter 1 describes traditional the multiphase flow well testing approach and systematically sums up the advantages and disadvantages of the traditional approach.

- A nested grid technique was applied to the reservoir model in order to avoid numerical dispersion.
- Equations governing Multiphase flow have no analytical solutions, so traditional multiphase flow well testing approaches are only suitable for uniform saturation reservoirs or special reservoirs.
- From an application scope point of view, the P-M approach is suitable for all reservoir systems, but it is limited to a low saturation gradient The pressure-squared approach is only valid for low rate condition for an oil-water system and is better than the P-M approach in a gas-oil system. The pseudo-pressure approach can be used effectively in a gas-oil system.
- From the analysis precision and parameter point of view, because the treatment of inner boundary conditions for a pressure-squared approach is more reasonable than for a P-M approach, so the result from a pressure-squared approach is more precise than a P-M approach. P-M approach and pressure-squared approaches only estimate the phase permeability, but the pseudo-pressure approach can obtain the absolute permeability.
- From a practical point of view, the P-M approach is simple and has wide application. On the other hand the pressure-squared approach relies on a suitable α value, and the pseudo-pressure approach depends on an effective permeability curve, and so the latter two approaches are a little difficult to apply.
- From an analysis method point of view, the semi-log plots are suitable for all traditional approaches in simple reservoirs, but for complex reservoirs, these methods do not work.
- In practice, geological models and fluid models are very complex, so a numerical solution approach is the only way to study multiphase flow problems.

- For numerical models, the capillary pressure, multiphase flow effect, gravitational effect, complex geological structure, etc. should all be considered.

Chapter 2 describes a modified P-M approach. Its results are more accurate and can be directly used to update the reservoir model.

- Only the P-M approach can be used to interpret well tests for different flow mechanism. This method is simple and widely used, but it also has restrictions that limit its applicability or accuracy. A modified P-M approach was developed, which is consistent with simulation data. The interpretation resulting from this modified P-M approach can be directly used to update the reservoir model and for reservoir management.
- However the modified P-M method is quite sensitive to the error in the relative permeability data. It is therefore very important to ensure the quality of relative permeability data.
- Because multiphase flow governing equations are high nonlinear equations, the numerical well test is a good tool for studying multiphase flow well testing problems.

Chapter 3 describes new understandings of transient pressure response in the transition zone of oil-water and gas-water systems and the behavior of bottom-hole flowing pressure after water breakthrough.

- Based on a theoretical development by Thompson, a new expression is derived from Darcy's Law. According to this expression and the numerical well test results, the pressure behavior of transition zones in oil-water and gas-water reservoirs can be reasonably interpreted.
- Capillary pressure in the transition zone has a insignificant impact on pressure response.
- The derivative of bottom-hole pressure is a function of the integral of total mobility, which can be approximatively replaced by the average total effective mobility. It controls the trend of the pressure derivative.

- It is normal that the BHP curve goes up in multiphase flow situations. The trend of the BHP curve is controlled by the total mobility. Comparing the fluid property and the relative permeability curve, oil viscosity has more effect on the trend of the BHP curve.
- For a non-uniformly saturated reservoir, after water breakthrough, when the water cut is low or high, traditional multiphase well testing approaches (including transient well testing and stabilized well testing) can be used to interpret; but if the water-cut is more than 30% or less than 80%, there are two kinds of BHP data (including normal transient pressure and abnormal transient pressure), which cannot be analyzed by traditional multiphase flow well testing approaches. For this type of transient data or PDG data, by considering numerical well testing method and history matching approach to analyze, the data can be used to update the reservoir model.

Chapter 4 describes the behavior of bottom-hole flowing pressure in layered commingled reservoirs. A number of case studies were developed to generate the type curve of interlayer interference under multiphase flow conditions. Furthermore, a selective inflow performance (SIP) test approach was introduced to analyze the interlayer interference problem.

- According to synthetic studies, for multi-layered commingled reservoirs, the shapes of the buildup curve have a big variation under different conditions. Permeability, porosity, initial layer pressure and radius of each zone are very sensitive, but the thickness of each zone is insensitive.
- Comparing the single layer system and multi-layer systems, the late transient period in the multilayer system can be much longer than the late transient period for a single layer system, because during tests, it takes a very long time for the crossflow between layers to be completed and for the total system to reach a balance.
- Under some conditions, there is crossflow through wellbores in layered commingled systems. At the same time, another interlayer interference phenomena of “backflow” may take place, which is defined as front transient

period and back transient period from the type curve.

- Using transient well test data to calculate the average properties of a reservoir is not practicable. Currently, multi-rate multi-zone production logging and transient testing can be used to calculate the properties of each zone and evaluate the layer contribution to the total production. This method is the selective inflow performance (SIP) test approach.
- For multi-layered commingled reservoirs, under low flow rate, cross flow is very severe. Hence, for these reservoirs, the production rate for more layers perforated has a low or even negative value due to crossflow, but if selecting a reasonable production type, the crossflow effect can be avoided.

Chapter 5 describes a new multiphase flow numerical well testing procedure. It can integrate all available reservoir data to carry out the dynamic calibration of the reservoir model.

- Windowing, local grid refinement and local time-stepping techniques can be carried out through existing commercial reservoir simulation software. It can improve the CPU time and the accuracy of history matching.

- The new numerical well testing workflow can be readily used as well test data or PDG data to update the reservoir model. Through matching the well test data in a Cartesian plot and log-log plot, the VOI model or the window can be calibrated. Under multiphase flow conditions, modification of the fluid model (including the PVT data and effective permeability curve) is very important due to the strong influence of the multiphase effect on bottom hole flowing pressure.

- The new multiphase flow numerical well testing procedure can provide a systematic, practicable and integrated approach to improve the quality of the reservoir description, by combining all the available data (such as geology data, geophysics data, well test data, PDG data, dynamical data, production history, etc.). According to this new workflow, the ultimate objective of well

test–dynamic monitoring, continuous model calibration and real time reservoir management can be achieved.

Chapter 6 describes two real mature field studies. The study shows that transient well test data or PDG data can be readily used to improve history matching and update the reservoir model.

- The various case studies carried out in example 1 and example 2 show that it is not only possible to apply the new multiphase flow numerical well testing procedure to a real mature field, but that there are also benefits for such a procedure over the conventional history matching method. When the mature field enters middle-late development period, much of the dynamic monitoring data from the PDG contain a large amount of reservoir information. By applying this dynamic information to update reservoir model, modern reservoir management of a mature field in real time can be achieved. One key contribution is that a practicable workflow of history matching for well test data has been developed. Through this workflow, the uncertainties of the model will be reduced, and the updated reservoir model is more accurate and closer to the real reservoir model.
- A further development in the history matching process is to define the fluid model. Under multiphase flow conditions, the properties of the fluid, including the PVT data and the effective permeability curve, can affect the trend of the bottom-hole flowing pressure. Hence adjusting the parameters of the fluid model to match the well test data is very important in reservoir numerical simulation.

7.2 Key Findings

The key findings of this thesis can be divided into three groups:

(1) A modified multiphase well testing approach, designed to improve the accuracy and the practicability of interpretation results;

(2) New understandings or discoveries about multiphase flow rules;

(3) A new multiphase flow study workflow.

7.2.1 Modified Multiphase Well Testing Approach

The key contribution of this thesis is to provide modified methods to analyze multiphase flow well testing.

- In uniform saturation reservoirs, according to the effective permeability curve, normalized total mobility can be obtained. From the normalized total mobility curve, under different water cut conditions, absolute permeability can be derived.
- In segregated flow reservoirs, by considering saturation logging and the effective permeability curve, the traditional P-M approach can be modified to obtain more precise absolute permeability.
- In oil reservoirs with aquifer support, a modified empirical solution was developed. According to this modified P-M approach, the distance of movement for oil-water contact can be monitored.
- In layered commingled reservoirs, a selective inflow performance (SIP) test approach was introduced to analyze the productivity index for each zone.

7.2.2 New understandings or Discoveries

The following findings or discoveries are based on the results of **chapter 3 - 5**:

- Firstly, by systematically and theoretically studying the behavior of transient pressure response in the transition zone of oil-water and gas-water systems, a new equation was derived according to Darcy's Law, which shows that pressure response in the transition zone is a function of total effective mobility. For oil-water reservoirs, the pressure derivative of the transient zone first decreases and then increases due to the change of fluid total mobility in closed systems; but for gas-water reservoirs, the pressure derivative of the transient zone first increases and then decreases due to the change of fluid total mobility under

constant pressure boundary conditions. This new understanding can guide the identification of boundaries for real field cases.

- By systematically and theoretically studying the behavior of bottom-hole flowing pressure after water breakthrough, it is shown to be normal that the BHP curve goes up under multiphase flow situations, due to the change in fluid total mobility. According to Darcy's Law, a new theoretical expression was derived in this situation, in which the derivative of bottom-hole flowing pressure is a function of the integral of total mobility, which can be approximatively replaced by the average total effective mobility. From this equation, the reason for well bottom-hole pressure increasing with time may be reasonably explained. Although this type of data is invalid for well testing, it contains a lot of information about the fluid, and can be used to update the fluid model through a history matching approach.

- Through discovering the phenomena of backflow in layered commingled reservoirs, its type curves can be defined as front transient period and back transient period.

- In the course of history matching for transient data or PDG data, adjustment of the fluid model has a major influence on the bottom-hole flowing pressure.

7.2.3 New Multiphase Flow Study Procedure

Because of the limitation of multiphase flow governing equations, the numerical solution approach is the only way to study multiphase flow problems.

- A new numerical well testing workflow was developed to use well test data or PDG data to update the reservoir model.

- A new multiphase flow numerical well testing procedure can provide a systematic, practicable and integrated approach to improve the quality of reservoir description, through combining all available data (such as geology

data, geophysics data, well test data, PDG data, dynamical data, production history, etc.).

7.3 Contributions to Industry

With many reservoirs entering their mature development period, multiphase flow problems are increasing. A particular challenge is the application of PDG data where there is a multiphase flow effect. According to this thesis, some useful results have been discovered for the petroleum industry:

- The nested grid technique and cut-windows technique can improve CPU time.
- A modified P-M approach can easily used to interpret reservoir conditions
- These new findings and discoveries can provide guidance for real-case interpretations.
- Applying these new multiphase flow numerical well testing procedures to real mature fields is the best practice.

7.4 Recommendations for Future Work

The key issues that remain unaddressed in this thesis are:

- This thesis has focused on two phase flows for oil-water reservoirs with low GOR. However, oil-gas systems with normal to high GOR, oil-water reservoirs with different oil compressibilities, gas-condensate systems and gas-water systems need further study to discover their rules.
- For oil-gas-water reservoirs or more phase composite reservoirs, multiphase flow problems are more complex, and also require investigation.
- The study object of this thesis is the oil well, but for injection wells, multiphase flow problems are also important.

Based on these key points, for future work, the numerical well testing approach is a powerful tool, which can be used to solve multiphase flow problems.

References

[1] Institute of Petroleum Engineering, Heriot-Watt University, “Reservoir Simulation”, Course note of MSc.

[2] Perrine,R.L.,“Analysis of Pressure Buildup Curves”, Drill&Prod. Prac., API,Dallas(1956)482-509.

[3] Martin,J.C.,“Simplified Equations of Flow in Gas Drive Reservoirs and the Theoretical Foundation of Multiphase Pressure Buildup Analysis”,Trans., AIME(1959)216,309-11.

[4] Brons, F. and Marting, V.E.,“The Effect of Restricted Flow Entry on Well Productivity,” J.Pet.Tech., (Feb.1961),PP.172-174; AIME,222.

[5] Weller,W.T.,“Reservoir Performance During Two-phase Flow”, Shell Oil Co.., SPE 1334, 1966.

[6] Fetkovich,M.J., Phillips Petroleum Co.,“The Isochronal Testing of Oil Wells”, SPE 4529, 1973.

[7] Raghavan, R., U. of Tulsa,“Well Test Analysis: Wells Productiong by Solution Gas Drive”, SPE 5588, 1976.

[8] Raghavan, R., U. of Tulsa,“Well -Test Analysis for Multiphase Flow”, SPE 14098, 1989.

[9] A1-Khalifa, A, J., Aziz, K., and Horne, R.N., Stanford U,“A New Approach to

Multiphase Well Test Analysis", SPE 16743, 1987.

[10] A1-Khalifa, A, J., Aziz, K., and Horne, R.N., Stanford U,"In-Place Determination of Reservoir Relative Permeability Using Well Test Analysis," SPE 16774, 1987.

[11] A1-Khalifa, A, J., Saudi Aramco, Horne, R.N. and Aziz, K., Stanford U.,"Multiphase Well Test Analysis: Pressure and Pressure-Squared Methods", SPE 18803, 1989.

[12] A1-Khalifa, A, J., and Odeh, A.S., "Well Test Analysis in Gravity-Segregated Reservoirs"，SPE 18577, 1988.

[13] A1-Khalifa, A, J., APAMCO, and Odeh, A.S.,Mobil R&D,"Well Test Analysis in Oil Reservoirs with Gas Caps and/or Water Aquifers", SPE 19842,1989.

[14] Athichanagorn, Suwat., SPE, Stanford University, Horne, R.N., SPE, Stanford University, and Kikani, J., SPE, Chevron Petroleum Technology Company,"Processing and Interpretation of Long-term Data from Permanent Downhole Pressure Gauges", SPE 56419, 1999.

[15] Ouyang, Liang-Biao., and Kikani, J., SPE, ChevronTexaco Exploration & Production Technology Co.," Improving Permanent Downhole Gauge (PDG) Data Processing via Wavelet Analysis", SPE 78290, 2002.

[16] Pickup, G.E., Ringrose, P.S., Forrester, M.M., Jensen, J.L., and Sorbie, K.S., Heriot-Watt U., "The Geopseudo Atlas: Geologically Based Upscaling of Multiphase Flow", SPE 27565, 1994.

[17] Pickup, G.E., and Carruthers, D., Heroit-Watt U., "Effective Flow Parameters for 3D Reservoir Simulation", SPE 35496, 1996.

[18] Chorneyko, D.M.,ExxonMobil Upstream Research Co.,"Real-Time Reservoir Surveillance Utilizing Permanent Downhole Pressures—An Operator's Experience", SPE 103213, 2006.

[19] McCracken, M., and Chorneyko, D., ExxonMobil Upstream Research,"Rate Allocation Using Permanent Downhole Pressures", SPE 103222, 2006.

[20] Tibold, M.P., ExxonMobil Exploration Company, Simonian, S., Schlumberger-Riboud Product Centre, Chawla, M., Kuwait Oil Company, Akbar, M., Kuwait Oil Company,"Well Testing with a Permanent Monitoring System", SPE 63079, 2000.

[21] Queipo，N.V., SPE, Verde, A., SPE, Goicochea, J., Romero, D., Applied Computing Institute, University of Zulia, Venezuela; Zambrano, A., and Bracho, A., PDVSA Exploration and Production," Applications of Permanent Downhole Pressure, Temperature, and Flow Rate Measurements for Reservoir Description and Production Optimization: a Taxonomy, Processes, and Benefits", SPE 77897, 2002.

[22] Gringarten, A.C., Imperial College London, SPE, Schroeter, Thomas von, Imperial College London, Rolfsvaag, T., ConocoPhillips, SPE, and Bruner , J., ConocoPhillips, SPE," Use of Downhole Permanent Pressure Gauge Data to Diagnose Production Problems in a North Sea Horizontal Well", SPE 84470, 2003.

[23] Al-Mohannadi, N., SPE, Ozkan, E., SPE, and Kazemi, H., SPE, Colorado School of Mines, " Grid-System Requirements in Numerical Modeling of Pressure-Transient Tests in Horizontal Wells", SPE 92041, 2007.

[24] Evinger,H.H. and Muskat,M., "Calculation of Theoretical Productivity Factor," Trans, AIME(1942) Vol.146,126-139.

[25] Chu Wei-Chun, Reynolds,A.C., and Raghavan. R, U.of Tulsa,"Pressure Transient

Analysis of Two-phase Flow Problems" , SPE formation evalution, 1986.

[26] Dyung, T.Vo, SPE, Unocal Corp., and Raghavan. R, SPE, Texaa A&M U.,"An Approximate Multiphase Flow Analysis Data Method", SPE 18112, 1991.

[27] Bφe .A, Skjaeleland, S.M. and Whltson, C.H., SPE,"Two-phase Pressure Test Analysis" , SPE 10224, 1989.

[28] Horne, R.N., Modern Well Test Analysis.

[29] Lee, J., Rollins, J.B., and Spivey, J.P., Pressure Transient Testing.

[30] Roadifer,R.D.,"Pressure Behavior of Wells Completed in Multiphase Reservoirs Containing a Constant Pressure Boundary,"SPE 36555, 1996.

[31] Thompson,L.G., and Reynolds, A.C.,"Well Testing for Radially Heterogeneous Reservoirs Under Single and Multiphase Flow Conditions,"SPE Formation Evaluation, March 1997.

[32] Vogel, J.V., "Inflow Performance Relationships for Solution-Gas Drive Wells,", JPT (January 1968) 83; Trans., AIME, 243.

[33] Jones, L.G., Blount, E.M., and Glaze, O.H., "Use of Short Term Multiple Rate Flow Tests To Predict Performance of Wells Having Turbulence," paper SPE 6133 presented at the 1976 SPE Annual Technical Conference and Exhibition, New Orleans, 3–6 October.

[34] Klins, M.A. and Majcher, M.W., "Inflow Performance Relationships for Damaged or Improved Wells Producing Under Solution-Gas Drive," JPT (December 1992) 1357.

[35] Sukarno, P. and Wisnogroho, A., "Generalized Two-Phase IPR Curve Equation

under Influence of Non-linear Flow Efficiency," Proc., Soc.of Indonesian Petroleum Engineers Production Optimization Intl. Symposium, Bandung, Indonesia (1995) 31–43.

[36] Wiggins, M.L.,U.of Oklahoma.,"Generalized Inflow Performance Relationships for Three-Phase Flow,"SPE 25458, 1994.

[37] Wiggins, M.L., Russell, J.E., and Jennings, J.W., "Analytical Development of Vogel-Type Inflow Performance Relationships," SPEJ (December 1996) 355.

[38] Zhong, Haiquan and Li,YingChuan, Southwest Petroleum University; Wen,Yulian, Schlumberger.,"A New General Formula For Dimensionless Well Inflow Performance Relationship,"SPE 109113, 2007.

[39] Economies, M.J., and Ogbe, D.O., U. of Alaska.,"Single-Well and Multiwell Pressure Interference Analysis,"SPE 13665, 1985.

[40] Leaver, J.D., Grader, A. and Ramey, H.J., Stanford U.J.,"Multiple-Well Interference Testing in the Ohaaki Georhermal Field,"SPE 15122, 1988.

[41] Onur ,M., Serra ,K.V., and Reynolds ,A.C., U. of Tulsa.," Analysis of Pressure-Buildup Data From a Well in a Multiwell System,"SPE 18123, 1991.

[42] Grasman, T.J., and Grader, A.S., Pennsylvania State U.," Constant-Pressure Interference Testing: Detecting Double-Porosity Properties,"SPE 18835, 1990.

[43] Britt, L.K., Jones, J.R., Pardinl, R.E., and Plum, G.L., Amoco Production Co.,"Reservoir Description by Interference Testing of the Clayton Field,"SPE 19846, 1991.

[44] Hallford, D.L., GeoQuest, Hegeman, P.S., Schlumberger.," A Field Application of

Multiple-well Testing for Reservoir Characterization," SPE 30575, 1995.

[45] Erwin ,M.D., Phillips Alaska,Inc, Sander,L.Allen.s., Anadarko Petroleum Corp., Redman ,R.Scott., Phillips Alaska,Inc.," multiwell Interference Test in the Colville River Field, Alaska,"SPE 77453, 2002.

[46] Marhaendrajana, T., Ariadji, T., and Permadi, A.K., Institute Teknologi Bandung.,"Performance Prediction of a Well under Multiphase Flow Conditions," SPE 80534, 2003.

[47] Harper, T.R., British Petroleum Co., and Moftah, I., Suez Oil Co.,"Skin Effect and Completion Options in the Ras Budran Reservoir,"SPE 13708, 1985.

[48] Roadifer, R.D., Yeh,N.S., and Jones,J.R.,"Accurate Well Condition Estimates Under Multiphase Flow Conditions,"SPE 30579, 1995.

[49] Eigestad,Geir Terje., and Larsen, Johne Alex.,"Numerical Modelling of Capillary Transition Zones ,"SPE 64374, 2000.

[50] Fanchi,J.R, Christiansen,R.L, and Heymans,M.J.,"Estimating Oil Reserves of Fields With Oil/Water Transition Zones,"SPE 79210, 2002.

[51] Dahroug,A., Zheng, S. , and Baily, J.,"The Application of Transient Pressure Testing to Track Phase boundaries During Production-A One-Well Case Study from UKCS,"SPE 94446, 2005.

[52] Cobb,W.M.,SPE-AIME, Atlantic Richfield Co., H.J.Ramey,Jr., SPE-AIME, Stanford U.,"Well-Test Analysis for wells Producing Commingled Zones", SPE 3014,1972.

[53] Earlougher, R.C., Kersch, K.M.., Kunzman, W.J., SPE-AIME,Marathon Oil Co.,

Some Characteristics of pressure builduo behavior in bounded multiple-layered reservoir without crossflow, SPE 4499, 1974.

[54] Raghavan, R., SPE-AIME, Amoco Production Co., Topaloglu,H.N., Turkish Petroleum Corp., Cobb,W.M., SPE-AIME, Missisippi State U., Ramey, H.J., SPE-AIME, Stanford U., "Well-test analysis for wells producing from two commingled zones of unequal thickness", SPE 4559, 1974.

[55] Yeh, N., SPE, and Reynolds, A.c.,SPE, U. of Tulsa., "Analysis of pressure data from a restricted-entry well in a multiplayer reservoir", SPE 15584, 1989.

[56] Park, H. and Horne, R.N., Stanford U., "Well test analysis of a multilayered reservoir with formation crossflow", SPE 19800, 1989.

[57] Kato, E.T. and Serra, K.V., Petrobras., "Influence of multiphase flow in well test analysis of nonflowing wells", SPE 22721, 1991.

[58] Aly, A., and Lee, W.J., Texas A&M U.,"A new pre-production well test for analysis of multilayered commingled reservoirs woth unequal initial pressures", SPE 27730, 1994.

[59] Jatmiko, W.,SPE, Daltaban, T.S., Archer, J.S., Imperial College, London., "Multi-phase flow well test analysis in multi-layer reservoirs", SPE 36557, 1996.

[60] Almehaideb, R.A., UAE University," Application of an integrated single well model to drawdown and buildup analysis of production from commingled zones", SPE 36987, 1996.

[61] Lee, W.J., and Spivey, J.P., SPE, S.A.Holditch & Associates , Inc., "Numerical and analytical well test analysis: a case history", SPE 50946,1998.

[62] Jackson, R.R., SPE, and Banerjee.R., SPE, Schlumberger, "Advances in multiplayer reservoir testing and analysis using numerical well testing and reservoir simulation", SPE 62917, 2000.

[63] Al-Ajmi, N.M., SPE, Kazemi.H., SPE, and Ozkan.E., SPE, Colorado School of Mines, "Estimation of storativity ratio in a layered reservoir with crossflow", SPE 84294, 2003.

[64] Kamal, M.M., Pan.Y. and Landa, J.L., Chevron Corp., and Thomas, O.O., Stanford U, "Numerical well testing –A method to use transient testing results in reservoir simulation", SPE 95905, 2005.

[65] Weiland, J., Shell Exploration&Production; Azari.M., SPE, Suparman, "Case History Review of the Applocation of Pressure Transient Testing and Production Logging in Monitoring the Performance of the Mars Deepwater Gulf of Mexico Field", SPE 115591, 2008.

[66] Eissa, M., Joshi, S., and Singh, K., SPE, Schluberger, and Bahugna, A., and Elbadri, M., GNPOC, "Identifying Layer Permeabilityies and skin using a Multi-layer Transient Testing Approach in a Complex Reservoir Environment", SPE 116969, 2008.

[67] Al-Thawad, F.M., Issaka, M.B., Saudi Aramco, Dominic Agyapong and Banerjee.R, Schlumberger SPE members,"A Simple Approach to Numerical Analysis of Complex Well Tests", SPE 81514, 2003.

[68] Raghavan, R., SPE member, and Dixon,T.N., SPE member, Phillips Petroleum Co.; Phan, V.Q., SPE member, Stanford U.; and Robinson, S.W., Phillips Petroleum Co., "Integration of Geology, Geophysics, and Numerical Simulation in the interpretation of a Well Test in a Fluvial reservoir", SPE 72097, 2001.

[69] Puchyr, P.J., SIMTECH Consulting services Ltd., "A Numerical Well Test Model",

SPE 21815, 1991.

[70] He, Nanqun., SPE, Chambers, K.T., SPE, Chevron Petroleum Technology Company, "Calibrate Flow Simulation Models with Well Test Data to Improve History Matching",SPE 56681, 1999.

[71] Mlacnik, M.J., SPE and Heinemann,Z.E., SPE, Mining U. of Leoben,"Using Well Windows in Full-Field Reservoir simulation", SPE 85709, 2003.

[72] Landa, J.L., SPE, and Horne, R.N., SPE, Stanford U., Kamal, M.M., SPE and Jenkins, C.D., SPE, Arco Exploration and Production Technology, "Reservoir Characterization Constrained to Well-Test Data: A Field Example", SPE 65429, 2000.

[73] Nnadi.M., SPE, Laser Engineering and Resources Consultants Ltd., Port Harcourt; Onyekonwu.M., SPE, University of Port Harcourt., "Numerical Welltest Analysis", SPE 88876, 2004.

[74] Freddy, H.E., Universidad Surcolombiana, Juan Miguel Navarrete, Hydrocarbon services Ltd., Hernan Dario Losada, Hydrocarbon Services Ltd., "Evaluation of Pressure Derivative Algorithms for Well-Test Analysis", SPE 86936, 2004.

[75] Zakirov, S.N., Indrupskiy, I.M., Zakirov, E.S., SPE, Anikeev,D.P., Tarasov, A.I., and Bradulina, O.V., Inst. of the Russian Academy of Sciences, "New Approaches in well Testing", SPE 100136, 2006.

[76] Landa, J.L., SPE,Stanford University, Kamal, M.M., SPE, and Jenkins, C.D., SPE, ARCO Exploration and Production Technology, and Horne, R.N., SPE, Stanford University, "Reservoir Characterization Constrained to Well Test Data: A Field Example", SPE 36511, 1996.

[77] Zhang, P.G., SPE, BP Exploration; and Pickup, G.E., SPE, and Christie, M., SPE,

Heriot-Watt U., "A New Practical Method for Upscaling in Highly Heterogeneous Reservoir Models", SPE 103760, 2008.

[78] Archer, R.A., SPE, Texas A&M University, and Yildiz, T.T., SPE, Texas A&M University, "Transient Well Index for numerical Well Test analysis", SPE 71572, 2001.

[79] Yao Jun, China university of Petroleum, and Zheng, S.Y., SPE, Heriot-Watt University,"New Advance in Numerical well Testing through Streamline simulation", SPE 122409, 2009.

[80] Raghavan R., SPE, U. of Tulsa,"Behavior of Wells Completed in multiple producing Zones", SPE 14111, 1989.

[81] Kucuk, F., Karakas, M., Ayestaran L., SPE, Schlumberger Well Services, "Well Testing and Analysis Techniques for Layered Reservoirs", SPE 13081, 1986.

[82] Ehlig-Economides, C.A., Joseph, J., SPE, Schlumberger Perforating and Testing Center, "A New Test for Determination of Individual Layer Properties in a Multilayered Reservoir", SPE 14167, 1987.

[83] Lefkovits, H.C., Hazebroek, P., Allen, E.E., Matthews, C.S., AIME, Shell Development Co., "A Study of the Behavior of Bounded Reservoirs Composed of Stratified Layers", paper presented at 34th Annual Fall Meeting of SPE, Oct. 4-7, 1959, in Dallas.

[84] Kuchuk, F.J., Schlumberger Doll Research; Shah, P.C., and Ayestaran L., Schlumberger Well Services; and Nicholson B., Schlumberger Inland Services, "Application of Multilayer Testing and Analysis: A Field Case", SPE 15419, 1986.

[85] Veeken, C.A.M., Chin, H.-V., Ross, R.W., and Newell, M.D., Sarawak Shell Berhad, "Monitoring and Control of Water Influx in Strong Aquifer Driver Gas Fields

Offshore Sarawak", SPE 64402, 2000.

[86] Dubost, F.X., Zheng, S.Y., Corbett, P.W.M., Institute of Petroleum Engineering, Heriot-Watt University, "Analysis and Numerical Modelling of Wireline Pressure Tests in Thin-Bedded Turbidites", Journal of Petroleum Science and Engineering 45(2004) 247-261.

[87] Yin, Hongjun., Zhai, Yunfang., SPE, and Fu, Chunquan., Daqing Institute of Petroleum, Ma, Shuilong., and Li, Zhongchen., Daqing Petroleum Administration Burea, "Well Test Analysis for Multiphase Displacement Reservoir", SPE 57312, 1999.

[88] Kamal, M.M., SPE-AIME, Amoco Production Co., "The Use of Pressure Transients to Describe Reservoir Heterogeneity", Journal of Petroleum Technology, 1979.

[89] Zheng, S.Y., Li, X.G., Institute of Petroleum Engineering, Heriot-Watt University, "Transient pressure analysis of 4D reservoir system response from permanent down hole gauges(PDG) for reservoir monitoring, testing and management", SPE 109112, 2007.

[90] Verga, F.M., SPE, and Griffa, G.L., SPE, Politecnico di Torino, Aldegheri A., SPE, Division, ENI-Agip," Advanced Well Simulation in a Multilayered Reservoir", SPE 68821, 2001.

[91] Bensadok, A., Sonatrach and Djebbar Tiab, The University of Oklahoma, "Pressure Behaviour of a Well Between Two Intersecting Leaky Faults", SPE 88873, 2004.

[92] Corbett, P.W.M., Heriot-Watt U., Mesmari, A., Agip Oil Co., and Stewart, G., Edinburgh Petroleum Services Ltd.,"A Method for Using the Naturally-Occurring Negative Geoskin in the Description of Fluvial Reservoirs", SPE 36882, 1996.

[93] Zheng, S.Y., and Corbett, P.W.M., Heriot-Watt U., Stewart, G., Edinburgh Petroleum Services Ltd.,“ The Impact of Variable Formation Thickness on Pressure Transient Behavior and Well Test Permeability in Fluvial Meander Loop Reservoirs”, SPE 36552, 1996.

[94] Buckley, S.E., and Leverett, M.C., AIME, “Mechanism of Fluid Displacement in Sands”, Petroleum Technology, 1941.

[95] Buckley, S.E., and Craze, R.C., AIME, “The Development and Control of Oil Reservoirs”,paper presented at spring meeting, Southwestern District Division of Production, Houston, Texas, Apr 29-30,1943.

[96] Umnuayponwiwat, S., SPE, and Ozkan, E., SPE, Colorado School of Mines, and Raghavan R., SPE, Phillips Petroleum Co.,“ Pressure Transient Behavior and Inflow Performance of Multiple Wells in Closed Systems”, SPE 62988, 2000.

[97] Sahni, A., Hatzignatiou, D.G., SPE; and Ogbe, D.O., SPE, University of Alaska Fairbanks Mow with Stanfourd., “Interference Pressure Behavior in Multi-layered Faulted Reservoirs”, SPE 35719, 1996.

[98] Hatzignatiou, D.G., Ogbe, D.O., U. of Alaska Fairbanks, “Interference Pressure Behavior in Dtratified Reservoirs”, SPE 26051, 1993.

[99] Britt, L.K., SPE, Jones, J.R., SPE, Pardinl, R.E., SPE and Plum, G.L., SPE, Amoco Production Co., “Reservoir Description by Interference Testing of the Calyton Field”, SPE 19846, 1991.

[100] Hatzignatiou, D.G., U. of Tulsa, Ogbe, D.O., and dehghani, K., U. of Alaska, and Economides, M.J., Dowell Schlumberger, “Interference Pressure Behavior in Multilayered Composite Reservoirs”, SPE 16766, 1987.

[101] Onur, M., SPE, and Reynolds, A.C., SPE, U. of Tulsa, "Interference Testing of a Two-Layer Commingled Reservoir", SPE 15132, 1989.

[102] Lakovlev, S.V., SPE, Global Consultants Inc., Lee, W.J., SPE, Texas A&M University, "Multi-phase Flow in Several Layers Limits the Applicability of Conventional Buildup Analysis", SPE 62854, 2000.

[103] Kamal, M.M., SPE, Freyder, D.G., SPE, and Nurray, M.A., SPE, Arco E&P Technology, "Use of Transient Testing in Reservoir Management", SPE 28008,1995.

[104] Gunasekera, D., SPE, Cox, J., Lindsey, P., GeoQuest., "The Generation and Application of K-Orthogonal Grid Systems", SPE 37998, 1997.

[105] Mlacnik, M.J., SPE, Heinemann, Z.E., SPE, U. of Leoben, Austria, "Using Well Windows in Full Field Reservoir Simulation", SPE 66371, 2001.

[106] Sinha, S.P., SPE, and Al-Qattan, R., Kuwait Oil Co., "Numerical Simulation to Design and Analyze Pressure Transient Tests in a Shaly, Interbedded Reservoir", SPE 93491, 2005.

[107] Zheng, S.Y., and Corbett, P., Inst. of Petroleum Engineering, Heriot-Watt U., "Well Testing Best Practice", SPE 93984, 2005.

[108] Kamal, M., Chevron Texaco, "Well Testing: Where We Are and Where We Go From Here", SPE 101641, 2004.

[109] Al-Thawad, F.M., SPE,and Liu, J.S., SPE, Saudi Aramco, and Banerjee, R., SPE, and Agyapong, D., SPE, Schlumberger,"Linking Well-Test Interpretation to Full Field Simulations", SPE 105271, 2007.

[110] Sahni, A., SPE, Kelsch, K., SPE, Samorn, H., and Boonmeelapprasert, C., SPE, Chevron, "Integrating Pressure Transient Test Data with Seismic Attribute Analysis to Characterize an Offshore Fluvial Reservoir", SPE 110272, 2007.

[111] Bui, T., SPE, Schlumberger; Bandal, M., SPE, and Hutamin, N., SPE, Petronas; and Gajraj, A., SPE, Golden Eagle Inti., "Material Balance Analysis in Complex Mature Reservoirs-Experience in Samarang Field, Malaysia", SPE 101138, 2006.

[112] Meddaugh, W.S., SPE, Chevron Energy Technology Co., "Reservoir Modeling for Mature Fields- Impact of Work Flow and Upscaling on Fluid-Flow Response", SPE 99833, 2006.

[113] Bischoff, R., OMV E&P Gmbh, and Bejaoui,R., Enterprise Tunisienne d'Activites Petrolieres, "Integrated Modeling of the Mature Ashtart Field, Tunisia",SPE 94007, 2005.

[114] Babadagli, T., SPE, U. of Alberta, "Mature Field Development- A Review", SPE 93884, 2005.

[115] Larsen, L., Rogaland Research Inst., "Wells Producing Commingled Zones with Unequal Initial Pressures and Reservoir Properties", SPE 10325, 1981.

[116] Jatmiko, W., Daltaban, T.S., and Archer, J.S., Imperial College, "Determination of Relative Permeability from Well Testing in Multi-layer Reservoirs"SPE 28752, 1994.

[117] Agarwal, B., Phillips Petroleum Co., Chen, H.Y., Texas A&M U., and Raghavan, R., Phillips Petroleum Co., "Buildup Behaviors in Commingled Reservoir Systems with Unequal Initial Pressure Distributions: Interpretation", SPE 24680, 1992.

[118] Aly, A., Texas A&M U/ Schlumberger; Chen, H.Y., New Mexico Inst. of Mining

& Technology; and Lee, W.J., Texas A&M U., "A New Technique for Analysis of Wellbore Pressure from Multi-layered Reservoirs With Unequal Initial Pressures to Determine Individual Layer Properties", SPE 29176, 1994.

[119] Chen, C.C., SPE, Halliburton Energy Services, Chu, W.C., SPE, and Sadighi, S., SPE, Marathon Oil Co., "Pressure Transient Testing of Gas Reservoirs With Edge-water drive", paper presented Formation Evaluation, December 1996.

[120] Khalaf, A.A., and Emam, M.E., ADMA-OPCO, and Mahmoud, Y., and Saeedi, J., Schlumberger Middle East S.A., "Successful Applications of the Multilayer Transient Testing Technique: Arab-C Members of the Umm Shalf Reservoir", SPE 25666, 1993.

[121] Ayan, C., and Lee, W.J., Texas A&td U.,"Multiphase Pressure Buildup Analysis: Field Examples", SPE17412, 1988.

[122] Nabor, G.W., Barham, R.H., AIME, Socony Mobile Oil Co., INC., Dallas, TEX.,"Linear Aquifer Behavior", SPE 791, 1964.

[123] Gomas, E.E., Standard Oil Company of California, SPE-AIME, "Evaluating Effective Properties of Linear Aquifers", SPE 5360, 1975.

[124] Miller, R.T., Shell Oil Co., and Rogers, W.L., Shell Development Co., AIME," Performance of Oil Wells in Bottom Water Driver Reservoirs", SPE 4633, 1973.

[125] Sabet, M.A., Well Test Analysis.

[126] W.A. Nestlerode, "The Use of Pressure Data from Permanently Installed Bottomhole Pressure Gauges", Paper SPE 590 presented at the SPE Rocky Mountain Joint Regional Meeting, Denver, 27–28 May 1963